DOCTOR OF PHILOSOPHY

Development and investigation of a novel thermochemical energy storage reactor for residential use

Zeng, Cheng

Award date:
2020

Awarding institution:
Coventry University

Development and investigation of a novel thermochemical energy storage reactor for residential use

By

Cheng Zeng

June 2020

A thesis submitted in partial fulfilment of the University's requirements

for the Degree of Doctor of Philosophy

Content removed on data protection grounds

Certificate of Ethical Approval

Applicant:

Cheng Zeng

Project Title:

Thermochemical energy storage applied in high solar radiation and low temperature/pressure climate

This is to certify that the above named applicant has completed the Coventry University Ethical Approval process and their project has been confirmed and approved as Low Risk

Date of approval:

06 November 2018

Project Reference Number:

P76791

Content removed on data protection grounds

Abstract

Thermochemical energy storage is an important technology to increase the share of renewable energy use in buildings. It has advantages over sensible and latent heat storage in terms of energy density and the ability of seasonal storage.

The main aim of the study is to investigate a thermochemical reactor for residential building applications. The research conducted in the thesis includes an extensive literature review, reactor theoretical study, experimental testing and numerical simulation of the reactor. The study has proposed a three-phase thermochemical reactor, which innovates in trapezoidal containers, side gaps and added fins, featuring air and water outlet in discharging. Experimental testing has shown that integration of fins improves the reactor performance in both charging and discharging. Comparing to the reactor without fins, in charging it presents a significant increase in the thermochemical material temperature and nearly 10 °C increase in the outlet air temperature in discharging. It also achieves a higher water temperature lift ranging from 1.8 °C to 4 °C.

The study has developed and validated a numerical reactor model to investigate the reactor performance under varying operation and configuration conditions. In charging, the critical parameters to the charging performance are charging temperature, air mass flow rate, reactor bed porosity and charging duration. Their effect to achieve an optimal charging performance has been investigated. In discharging, a smaller particle diameter and inlet relative humidity at around 40% are desirable. Additionally, the varying reactor geometrical parameters to the reactor performance have been obtained. The reactor with a smaller air travel path shows superior charging and discharging performance. According to the results, the study provides a decision-making tool for achieving a three-phase reactor design with superior performance.

Acknowledgements

Foremost, I would like to express my sincere gratitude to Prof. Shuli Liu and Dr. Ashish Shukla. I thank them for their guidance and encouragement throughout the research work. They always clarified my doubts with their immense knowledge and enthusiastic motivations.

The colleagues and doctorates, Dr. John Karadelis, Dr. Abdur Rehman Mazhar, Mr. Obiajulu Iweka, Mr. Mamatniyaz Bake, Mr. Hao Mu, Dr. Muriel Iten, Dr. Yongcai Li and Mr. Steve Hutton have given their support. I have learned and gained from their suggestions. I am sincerely thankful to Dr. Abdur Rehman Mazhar who helped me substantially with my work and English writing.

A special thanks to Beijing Institute of Technology for supporting me to use the laboratory facilities to conduct the experimental work. I would like to extend sincere gratitude to my colleagues Mrs. Liu Yang, Miss Xiaojing Han, Mr. Ming Song, Mr. Yanjun Zhang and Miss Xiue Yang. Their support, efforts and excellence have impressed and inspired me. I am sincerely grateful to Mr. Ian Breakwell, Mr. Jia Li and Mr. Zuzheng Li for their suggestions and efforts in the experimental work.

A special thanks to Dr. Abdullahi Ahmed and Dr. Yongliang Li for being the examiners of the work and making it better.

Words cannot express my gratefulness to my family for all their support and unconditional love.

Table of Contents

Nomenclature

Symbol	Term	Unit
A	contact area	m^2
A_{ad}	adsorption potential	kJ/kg
a	specific transfer area of adsorbent	m^2/ m^3
c_p	specific heat capacity at constant pressure	kJ/(kg·K)
D	diameter of water pipe	m
D_e	equivalent diffusivity of adsorbent particles	m^2/s
D_0	reference diffusivity	m^2/s
d	diameter of adsorbent particle	m
E_{act}	activation energy in linear driving force model	kJ/mol
E_{ad}	characteristic energy in adsorption equilibrium	kJ/kg
e	emissivity	-
H	heat of adsorption	kJ/kg_{H2O}
h	convection heat transfer coefficient	$kW/(m^2·K)$
K	permeability of adsorbent	m^2
k_m	mass transfer coefficient	s^{-1}
L	length	m
m	mass	kg
Nu	Nusselt number	-
n	heterogeneity parameter in Dubinin-Astakhov equation	-
P	pressure	Pa
Pe	Peclet Number	-
Pr	Prandtl number	-
Q	thermal energy	kW
q	heat transfer rate	kW
R	ideal gas constant	kJ/(K·mol)
R_{cond}	conductive thermal resistance	$(m^2·K)/kW$
R_{conv}	convective thermal resistance	$(m^2·K)/kW$
Re	Reynolds number	-

R_w	specific gas constant of water vapour	kJ/(kg·K)
r	radius	m
T	temperature	K
t	time	s
u	velocity	m/s
W	adsorption volume	m^3/kg
X	water uptake of adsorbent	$kg_{H2O}/kg_{adsorbent}$
y	distance	m

Greek symbols

β	thermal expansion coefficient of air	1/K
δ	thickness	m
ε	porosity	-
μ	dynamic viscosity	kg/(s·m)
ρ	density	kg/m^3
σ	Stefan-Boltzmann constant	$kW/(m^2 \cdot K^4)$
λ	thermal conductivity	kW/(m·K)
ν	kinematic viscosity	m^2/s
ϕ	specific humidity of air	g/kg

Subscriptions and superscriptions

0	reference point
a	air
ads	adsorption
amb	ambient
bed	reactor bed
$char$	charging
$dischar$	discharging
eq	equilibrium
fin	pipe fin
hs	heat source

in	inlet
m	metal tube
out	outlet
$particle$	zeolite particle
rct	reactor
s	solid adsorbent
sen	sensible
st	storage section
w	water

Abbreviations

IEA	International Energy Agency
DA	Dubinin-Astakhov
DSC	Differential scanning calorimetry
ECE	Energy conversion efficiency
EOA	Extent of adsorption
TGA	Thermogravimetric analyser
LDF	Linear driving force
RMSPE	Root mean square of percent error

List of Figures

List of Tables

CHAPTER 1: INTRODUCTION

1.1 Research Background

Growth in the world's population, technological developments, robust global economy and higher heating along with cooling needs have led to a sharp increase in worldwide energy consumption. According to the International Energy Agency (IEA), global energy consumption has nearly doubled the average growth rate since 2010 (IEA 2019). Under the current and planned policies, the IEA (2018) estimates that the global energy demand will grow by 25% in 2040. The increasing growth of energy consumption, especially for fossil fuels, has been causing severe challenges of global climate, posing a risk of human health, ecosystem and the economy. For instance, air pollution, the major public health crisis, is closely linked to energy use. Coal is responsible for about 60% of global SO_2 emissions, causing acid rain and respiratory illness (IEA 2016).

In response to mitigating climate change, countries around the world have set sustainability targets. Under the United Nations Framework Convention on Climate Change, 193 nations provided Nationally Determined Contributions (NDCs) to achieve reductions in greenhouse gas emissions by 2017. Within this context, 101 nations explicitly mentioned the building sector and 49 countries committed to applying renewable energy sources in buildings (UN Environment and International Energy Agency 2017). The EU's 2030 climate and energy framework aims to achieve at least 40% reduction in greenhouse gas emissions from the 1990 levels (Comissão Europeia 2019). In the UK, the Climate Change Act has set a legally binding target to cut the greenhouse gas emissions by at least 100% by 2050 of the 1990 levels (Committee on Climate Change 2019, Climate Change Act 2008). In China, the government aims to reduce CO_2 emissions by 65% based on the 2005 level (Xunzhang et al. 2017).

Buildings contribute significantly to global emissions. It is essential to reduce greenhouse gas emissions from buildings. In 2015, fossil fuels supplied 82% of

final energy consumption in buildings (UN Environment and International Energy Agency 2017). By 2018, buildings and construction account for 36% of global final energy consumption and 39% of CO_2 emissions. In the EU, buildings take up about 40% of energy consumption and 36% of CO_2 emissions (European Commission 2019). The operation and maintenance of buildings can take up about 40% of global energy consumption, as reported by the Intergovernmental Panel on Climate Change (Chenari et al. 2016, IPCC 2013). It shows that the space heating takes 32% of the total energy use in residential buildings (Ürge-Vorsatz et al. 2015). Domestic hot water accounts for about 24% and 12% energy use in residential buildings and commercial buildings, respectively. According to the IEA (2017) space heating, water heating and cooking account for 46% of global energy consumption. Only 10% of the energy was produced by renewables.

Renewables such as biomass, solar thermal and geothermal are considered as being the key technologies for heating and cooling in building application. A substantial increase in the share of renewables should take place to address building energy consumption and greenhouse gas emissions. Along with other technologies, solar heating technologies have been of significant importance. According to the International Renewable Energy Agency (2018), solar thermal systems would increase with a total collector area projected to be 10 times higher by 2050, from around 600 million m^2 to over 6000 million m^2. Between 2010 to 2050, solar collectors for space heating and hot water can increase by an average 7.1% annually and reach an installed capacity of 500 GW to meet the annual energy demand in the buildings sector at around 8.9 EJ by 2050 (International Energy Agency 2012). Solar energy, as a sustainable and clean source of energy, is one of the most promising renewable energy resources. In the domestic sector, the energy consumed in space heating/cooling and domestic hot water accounts for over 50% of its total energy consumption (Parameshwaran et al. 2012). As a diurnal cyclic resource, solar energy can be stored and utilised efficiently with energy storage technologies. Within this context, related technologies in supporting the development of solar heating in buildings play an influential role. Energy storage, especially thermal energy storage, is one of the critical

technologies requiring research and development. Because of the dynamic nature of solar energy, there is a mismatch between the energy generation of the solar energy source and the demand of buildings, being one barrier in improving the share of solar thermal systems (Garg et al. 2012). Thermal energy storage is to store the energy from the side of generation and provides supply when the demand is high, improving the share of solar energy in buildings. Although large scale sensible heat storage using water has already been applied, such as district heating systems, the volume requirement makes it difficult to expand the application in residential use. Therefore, development of a novel, compact and cost-effective solar thermal energy storage technology is crucial for the development of solar thermal systems to achieve the greenhouse emission goals.

1.2 Energy storage technologies and thermochemical energy storage

There are a variety of energy storage systems including electricity storage, heat storage and mechanical energy storage, as shown in Figure 1 - 1 (Dincer and Rosen 2011, Gil et al. 2010, Gondre 2017). Regarding thermal energy storage, there are three types of technologies including sensible heat storage, latent heat storage and thermochemical energy storage. For sensible heat storage, thermal energy is stored through the temperature change of a storage medium such as water. For latent heat storage, thermal energy is stored in phase change materials as latent heat. The solid-liquid transition is the most used phase change approach (Kuznik et al. 2011). For thermochemical energy storage, however, energy is stored by a reversible physical or chemical sorption mechanism.

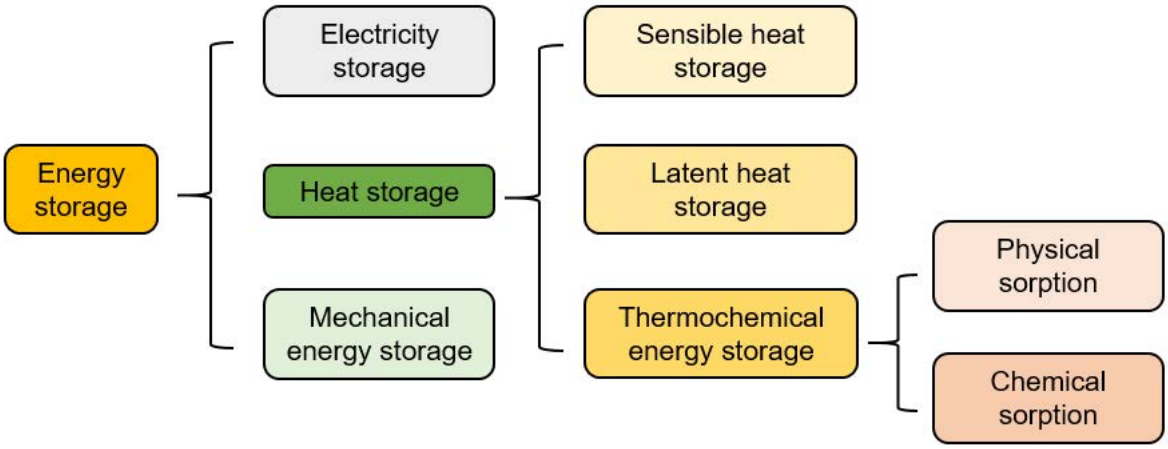

Figure 1 - 1 Classification of energy storage technologies (Dincer and Rosen 2011, Gil et al. 2010, Gondre 2017)

Table 1 - 1 illustrates the differences in the three types of thermal energy storage methods. Thermochemical energy storage stands out in the high energy storage density. Depending on the materials, it offers 2 to 10 times higher energy storage densities compared to sensible heat storage and latent heat storage, respectively (Casey et al. 2014). The relatively high energy density of thermochemical energy storage materials is because of the high energetic processes involved in the destruction and reformation of chemical bonds (Garg et al. 2012). The high volumetric energy density permits more compactness of the related systems, giving it an advantage in building application where space is a premium consideration. Additionally, in the energy storage period, thermochemical energy storage materials can be stored at ambient temperature for a theoretically unlimited time with little thermal loss to the environment.

Table 1 - 1 Main advantages and disadvantages of thermal energy storage technologies (Gil et al. 2010, Pardo et al. 2014)

	Sensible heat storage	Latent heat storage	Thermochemical energy storage
Temperature range	• 50 - 95 °C (water tank) • 10 - 80 °C (aquifer/ground storage) • 300 - 400 °C (concrete)	• 50 - 60 °C (paraffin) • 30 - 50 °C (salt hydrate) • Over 100 °C (inorganic eutectics, organic materials, molten salt, etc.)	• 20 - 800 °C or higher
Volumetric energy density	~ 50 kWh/m^3 (Low)	~ 100 kWh/m^3 (Medium)	~ 500 kWh/m^3 (High)
Gravimetric energy density	~ 0.02 - 0.03 kWh/kg (Low)	~ 0.05 - 0.1 kWh/kg (Medium)	~ 0.5 - 1 kWh/kg (High)
Temperature of the materials in storage period	Charging temperature	Charging temperature	Ambient temperature
Storage length	Limited	Limited	Theoretically unlimited
Transport	Short distance	Short distance	Theoretically unlimited
Technical complexity	Simple	Medium	Complex

1.3 Opportunities and challenges of thermochemical energy storage in residential buildings

Using thermal energy storage in residential buildings is key to reducing fossil fuel consumption. Currently, the development is facing a few issues which can be tackled by applying the thermochemical energy storage technique (Kuznik et al. 2015, Eames et al. 2014, Lizana et al. 2017). Sensible heat storage leads to large volume requirements due to the low energy density. There is limited time of heat availability for both sensible and latent heat storage. The stored heat is released in a short time due to heat loss. The volume requirements and short term availability make the integration of the systems to buildings difficult, while increasing the initial costs. Additionally, gas boilers provide heat rapidly in residential buildings including space heating and domestic hot water, making the end users have limited experience of the benefits from heat storage systems.

Thermochemical energy storage is a promising thermal energy storage technology for residential applications. It has gained increasing attention in residential buildings for high energy storage density and long term storage potential. The advantages are significant to residential applications since they lead to a number of opportunities including seasonal heat storage, conversion of excess heat from renewable sources such as solar PVs, waste heat storage and integration of off-peak electricity (Pinel et al. 2011, Li et al. 2016). Additionally, since the technology involves destruction and reformation of chemical bonds, there are numerous material pairs available with output temperature ranging from 40 ºC to 70 ºC, matching to the space heating and domestic hot water applications in residential buildings (Abedin and Rosen 2012, Pardo et al. 2014, Dincer and Rosen 2011).

Thermochemical materials can be found in gas, liquid and solid phases. A large share of relevant studies in building application employs the solid-gas material pair (Clark et al. 2020, Scapino et al. 2017). Because gas-gas and gas-liquid pairs involve pressurisation and depressurisation of a system, this poses safety risks for long term applications and increases the complexity of the system (Kuznik et

al. 2018). Besides, water vapour can be used as the gas pair which is widely accessible in built environments. Furthermore, for the solid pair, there are a number of materials suitable for different temperatures and applications in building including chemical reaction, solid adsorption and composites (Jarimi et al. 2019). Therefore, this study focuses on the solid-gas pairs.

Since thermochemical energy storage is a relatively new technique for residential application, there are some challenges requiring further research and development including the materials, systems design and reactor. Within this context, the thermochemical reactor is a critical component. It is where the energy storage and release take place. This study focuses on the thermochemical reactor and related performance. Currently, the hurdles for the thermochemical reactor are reduced heat and mass transfer, pressure drop, cost, etc. (Solé et al. 2015a, Zeng et al. 2019). For instance, according to an experimental test of a solar heating system using thermochemical energy storage, the output heating power is about 2.5 kW with the designed output of 40 kW (Mauran et al. 2008). Limited mass transfer and a relatively high pressure drop are caused by the difficulty in providing a uniform heat transfer fluid through the thermochemical material (Aydin et al. 2016). According to an experiment of a thermochemical system with 0.017 m^3 sorption material, the pressure drop of the entire system is about 220 Pa (Zondag et al. 2013). Gartler et al. (2004) developed a seasonal solar energy storage system using the technology for domestic hot water and heating of a single-family house in Austria. The authors reported that to reach the theoretical storage capacity would require a too large reactor setup to be economically feasible.

1.4 Aim and objectives

The project aims to develop a thermochemical reactor applied to residential buildings. The aim is accomplished by completing the following objectives:

1. Conduct an extensive literature review on thermochemical energy storage reactors and materials;
2. Determine suitable thermochemical energy storage materials for residential application in solar thermal energy storage;
3. Propose a novel thermochemical reactor with an improvement in heat and mass transfer;
4. Investigate the reactor performance in charging and discharging processes; and
5. Evaluate the reactor performance under critical parameters and configurations.

1.5 Research methodology

- Approach to objective 1 – Comprehensive literature review on the thermochemical reactor and materials

This approach is designed to provide a state-of-the-art thermochemical energy storage reactor in building application and to present the opportunities in the reactor development. The steps leading towards this include (1) presenting the fundamental principles of the thermochemical energy storage technique; (2) reviewing the current status and characteristics of thermochemical materials for building application; and (3) reviewing the development status and the related thermochemical reactors and systems.

- Approach to objective 2 – The selection of suitable thermochemical material

This approach is to select suitable thermochemical materials for the study with rationales and also provide guidance for material selection. It includes the following approaches: (1) review the material characteristics in thermochemical energy storage applications based on material types and reaction mechanisms. The material characteristics include but are not limited to the theoretical energy

storage density, reaction pairs, reaction temperature, cost, etc.; (2) highlight issues and advantages of the materials; and (3) propose a material selection framework and identify the suitable material for the study.

- Approach to objective 3 – Design of a novel thermochemical energy storage reactor

This approach is to design and develop a novel thermochemical energy storage reactor that tackles the drawbacks of current reactors in the literature. The steps to achieve this are (1) conducting a theoretical study of a thermochemical reactor and presenting its heat and mass transfer processes; (2) designing the reactor with improvements in heat and mass transfer and completing the reactor sketch drawings; and (3) building a numerical model of the reactor for numerical simulation.

- Approach to objective 4 – Design, construction and testing of the thermochemical reactor

The approach is to evaluate the performance of the reactor. The steps in the approach include (1) designing and building an experimental test rig of the thermochemical reactor; and (2) conducting charging and discharging tests to investigate the operational characteristics under the laboratory conditions.

- Approach to objective 5 – Investigate the thermochemical reactor with the validated numerical model

The approach is to evaluate the thermochemical reactor performance with a validated numerical model and also contribute to achieving a reactor with desirable performance. The steps in the approach include (1) validating the numerical model to illustrate the accuracy of the model; (2) conducting a parametric study of the reactor to represent how the critical parameters affect the reactor in charging and discharging; and (3) proposing schemes, steps and considerations for a designer in designing a thermochemical reactor to achieve the desirable performance.

1.6 Thesis Structure

The thesis contains 7 chapters presented in Figure 1 - 2.

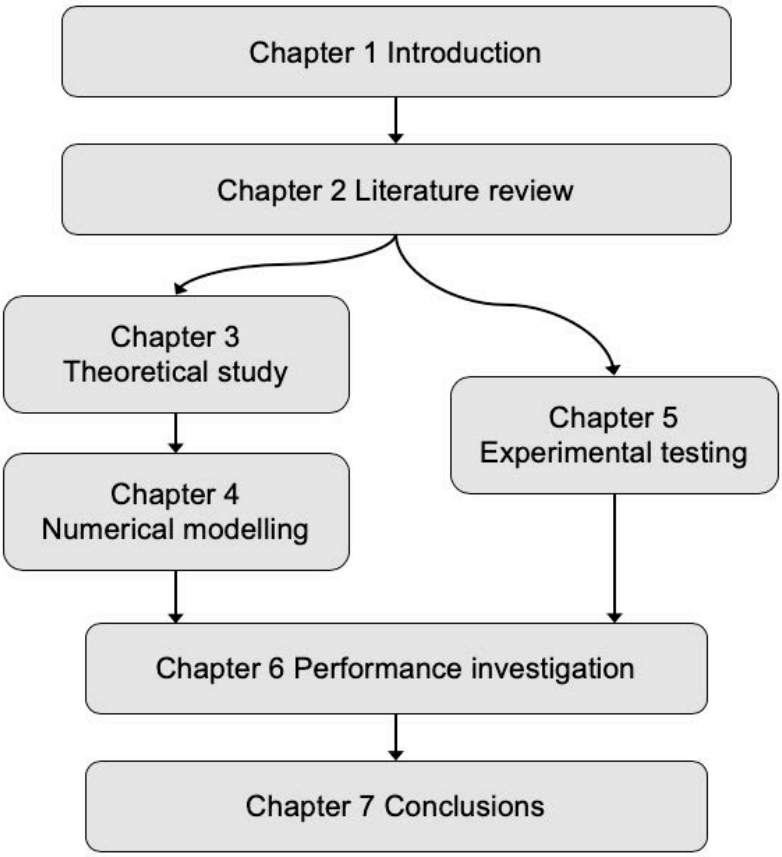

Figure 1 - 2 Flow chart of the thesis structure

Following chapter 1 which introduced the research background, chapter 2 presents a comprehensive literature review of the thermochemical energy storage, especially on the reactor and material. It presents the development of thermochemical reactors and materials to interpret the opportunities for further research and development. It proposes a thermochemical material selection scheme and selects a suitable thermochemical material for this study. Objectives 1 and 2 are completed in the chapter. Chapters 3 and 4 complete objective 3. Chapter 3 presents the theoretical study of a thermochemical reactor. Chapter 4 proposes a three-phase thermochemical reactor and conducts numerical modelling of the reactor. For objective 4, chapter 5 details the laboratory testing of the proposed thermochemical reactor. It illustrates the construction of the experimental rig and presents the experimental testing of the reactor. For

objective 5, chapter 6 presents the reactor performance investigation using the validated numerical modelling. It investigates the reactor configurations and operational parameters on the reactor performance. It provides a reactor design scheme with steps for a designer to achieve a reactor with key considerations. Chapter 7 gives conclusions of the study and provides further works and recommendations in the field.

CHAPTER 2: LITERATURE REVIEW ON THERMOCHEMICAL ENERGY STORAGE IN BUILDING APPLICATION

2.1 Overview

Researchers have been conducting a wide range of research and development on thermochemical energy storage for its significant potential in building application. This chapter carries out a comprehensive literature review of the technology, especially for the thermochemical reactor and materials. It also identifies research gaps and suggests future research opportunities. The major work and approaches in this chapter are given as follows.

- Demonstrate the fundamental principles of thermochemical energy storage.
- Illustrate a comprehensive literature review on thermochemical energy storage reactor in building application.
- Present the current development status of thermochemical energy storage materials.
- Identify the thermochemical material for this study with rationales.

2.2 Fundamentals of thermochemical energy storage

2.2.1 Classification and basic terminology

Thermochemical energy storage can be divided as thermochemical without sorption, chemical adsorption and chemical absorption. Figure 2 - 1 shows the relationship between chemical storage and sorption storage (Aveyard and Haydon 1973, Ding and Riffat 2013). The expressions ‘chemical storage’, ‘thermochemical storage’ and ‘sorption storage’ differ in some studies (Boer et al. 2004, Iammak, Wongsuwan and Kiatsiriroj 2004, Kuznik and Johannes 2014, Mugnier and Goetz 2001).

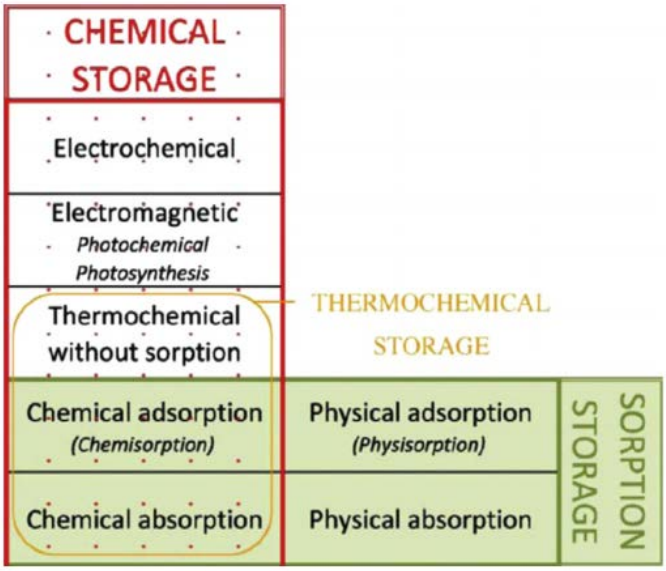

Figure 2 - 1 A classification of chemical storage and sorption storage (Aveyard and Haydon 1973, Ding and Riffat 2013)

Table 2 - 1 summaries the definition of terms used in studies of thermochemical energy storage (Hauer 2007, Wang et al. 2009, Srivastava and Eames 1998, N'Tsoukpoe et al. 2009).

Table 2 - 1 Definition of different thermochemical terms (Hauer 2007, Wang et al. 2009, Srivastava and Eames 1998, N'Tsoukpoe et al. 2009)

Term	Definition
Sorption	A phenomenon of fixation or capture of a gas or a vapour (sorbate) by a substance in condensed state (sorbent)
Sorbate	Substance in the adsorbed/absorbed state
Sorbent	Solid material on which adsorption/absorption occurs
Adsorption	A surface phenomenon: an attachment of a liquid or gas to the surface of another substance
Absorption	A liquid or gas enters a solid or liquid
Adsorptive	Adsorbate substance in the fluid phase

The term 'sorption' is the phenomenon to capture a gas or a vapour (sorbate) by a substance in solid or liquid state (sorbent) (Hauer 2007). Sorption can include both adsorption and absorption (Ding and Riffat 2013). In terms of adsorption, it

is usually used to describe the phenomenon of binding of a gas on a surface of a solid or porous material (Poulopoulos and Inglezakis 2006). Figure 2 - 2 shows the process schematically (Letcher 2016). During the charging step, heat is added to the sample. This breaks the binding forces and removes the adsorbates from the inner surface by raising them to a higher energy level. The adsorption step is to add adsorbates to the adsorbent and release the adsorption energy (Paksoy 2007).

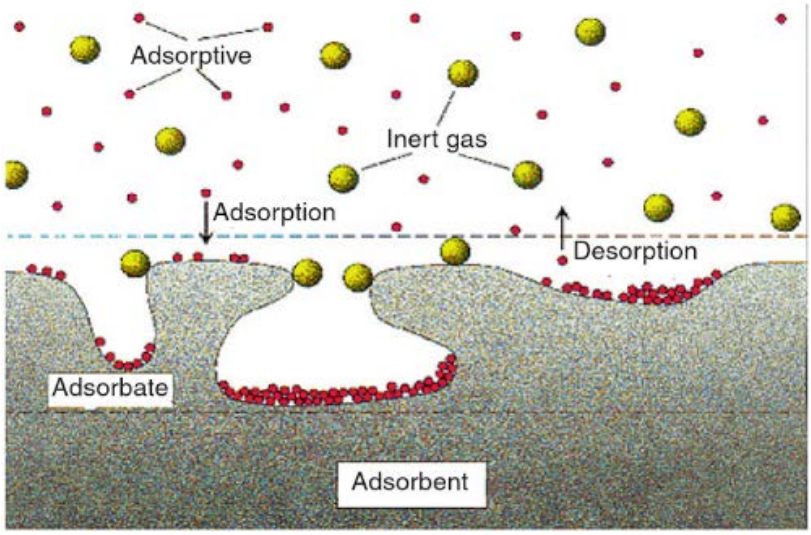

Figure 2 - 2 Schematic presentation of adsorption and desorption (Letcher 2016)

According to the cohesive force between the two phases, adsorption can be divided into two types: physical adsorption (physisorption) and chemical adsorption (chemisorption). Physisorption is the behaviour of atoms on weakly attracting surfaces of bulk liquids and solids (Dash 1975). It occurs at the surface of the adsorbent. A thin layer of atoms or molecules will be formed on the adsorbent surface, while leaving the adsorbent structure unaltered. In this process, no expansion occurs and it requires no activation energy (Scapino et al. 2017). The forces involved are intermolecular forces (Van der Waal forces) and hydrogen bonding, The Van der Waal forces are the same forces for the imperfection of gases and condensation of vapours. The interaction is

characterised by low heat of adsorption, less than 40 kJ/mol (Otterstedt and Brandreth 1998).

These interactions contrast with the stronger bonding in chemical adsorption. Covalent forces lead to the formation of chemical compounds. Specifically, due to the surface valency requirements, the sharing of electrons and atoms of the adsorbent and adsorbate is involved. A form of chemical bonding occurs with the heat of adsorption between 40 kJ/mol to 400 kJ/mol (Wang et al. 2009, Srivastava and Eames 1998, Otterstedt and Brandreth 1998). Chemical adsorption requires an activation energy. It requires a certain temperature. It usually leads to a change in the adsorbent surface. However, some chemical adsorption processes could be irreversible (Poulopoulos and Inglezakis 2006). It is worth mentioning that both physical and chemical adsorption can simultaneously take place and a clear interpretation of data is often complicated.

In terms of absorption, it is a phenomenon in which the molecules of absorbate penetrate the surface layer and enter the structure of the bulk solid or liquid. It occurs at the sorbent molecule level and alters the composition and morphological structure of the absorbent (Nic et al. 2014). Therefore, a material expansion occurs in absorption and it requires higher activation energy than adsorption. The energy is mainly the covalent forces of atoms and molecules. Absorbates can be gases or liquids, leading to a difference of the binding energy released as heat of reaction (Scapino et al. 2017). If the absorbents are gases, all binding energy is released as the heat of reaction. If the absorbents are liquids, however, part of the binding energy is to break the bonds within the liquid, leaving only part of it as heat of reaction. When the absorbent is a liquid and the absorbate is a gas, in literature, the process is named liquid gas absorption or liquid absorption. The most used liquid absorption pairs are LiBr/H_2O (Zhai et al. 2011, Siddiqui and Said 2014) and H_2O/ammonia (Hassan and Mohamad 2012).

2.2.2 Principles of operation

The mechanism of the thermochemical energy storage can be described as the following reversible equation and Figure 2 - 3 (Yu et al. 2017, Abedin and Rosen 2012).

$$C + Heat \leftrightharpoons A + B$$

A thermochemical energy storage cycle includes three main processes, charging, storing and discharging. In a charging process, thermal energy is absorbed from a heat source in an endothermic reaction which breaks the binding force of the substance C. Thermochemical material dissociates into two substances, A and B. In the storage process, the substances A and B are stored separately. The substances are stored at ambient temperatures with theoretically no thermal losses, expect for the cooling of the materials after the charging process. The energy is stored based on the chemical potential with the mass fraction of A and B. When it requires to release the energy, in a discharging process, substance A reacts with substance B. The exothermic reaction releases the heat and forms substance C.

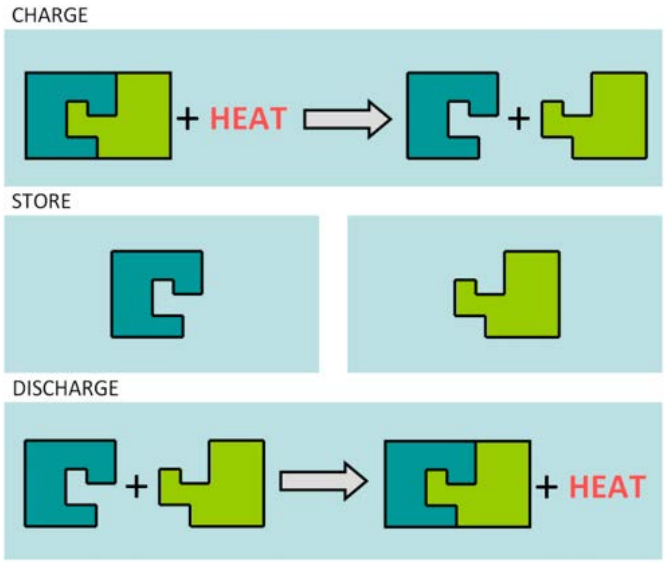

Figure 2 - 3 Processes of thermochemical energy storage (Abedin and Rosen 2012)

In sensible and latent heat storage systems, heat is transferred directly to the storage medium, i.e. direct heat storage media (Hauer 2007). The capacity of

thermal energy storage is at a temperature of the heat source depending on the capacity of the entropy uptake. The energy density is limited by the entropy storage capacity of the material (Gartler et al. 2004). Thermochemical energy storage is a reversible physic-chemical reaction to store heat indirectly (Hauer 2007). During the charging step, heat from the heat source is used to overcome the bonding between the working fluid molecules and the molecules of thermochemical energy storage material. The gaseous product is then released to the environment or condensed. The associated entropy of the gaseous product is released to the environment. Thus, the energy and entropy flow are separated in the storage process. During the discharging process, the entropy is taken up from the environment or the condenser to combine again energy and entropy flow (Bales et al. 2005). This leads to the high thermal energy storage capacity because the entropy is separated from the storage media and released to the environment (Gartler et al. 2004, Bales et al. 2005).

2.2.3 Reversible reaction and equilibrium in thermochemical energy storage

When a reversible reaction reaches equilibrium, the rate of the forward reaction equals the rate of the reverse reaction. There is no observable change in this phase but both directions of reaction are occurring (Jim Clark 2002). The balance point, i.e. the position of equilibrium, can be affected by adjusting:

- The concentration of the reacting substances if solutions are involved;
- The pressure of reacting gases; and
- The temperature.

According to Le Chatelier's principle (Jenkins 2008), if applying a change to a system at equilibrium, the system adjusts the position of equilibrium to counteract the change as much as possible. In such case, the position of equilibrium shifts to counteract the change in concentration, pressure and temperature (Burton 2000). In terms of concentration, the increasing of reactant concentration causes the position of equilibrium to move to the product side. Similarly, decreasing the product concentration leads the equilibrium to move to the same side. In terms of

pressure, increasing the pressure moves the equilibrium to the side of the equation with fewer gas molecules as this reduces the pressure. Decreasing the pressure moves the equilibrium to the side of the equation with more gas molecules as this increases the pressure. In terms of temperature, heating the reversible reaction at equilibrium shifts the reaction to the direction of the endothermic reaction. In turn, cooling a reversible reaction at equilibrium shifts the reaction to the direction of the exothermic reaction.

2.2.4 The scale and representation

For thermochemical storage with water vapour and solid sorbent, how to treat the air flow through the reactor is mainly a question of distance. Adsorption is in molecular level which can be treated as macroscopic or microscopic scale. As illustrated in Figure 2 - 4, when the distance is at the adsorbent bed scale, mass transfer occurs to the space between the adsorbent particles. The large distance leads to complications with numerous channels and cavities in the problem (Donald A. and Adrian 2013). When the distance is short, for instance at the microscale scale (molecular level), the configuration of pore structure may be irregular and complex. The microscopic level description of heat and mass transfer is not practical in view of the effort for mathematical formulation (Civan et al. 2011). Within this limit, a macroscopic volume is defined that the volume length is much larger than the pore scale of microparticles, but significantly smaller than the scale of the reactor (Donald A. and Adrian 2013). The macroscopic volume is named as representative elementary volume. It can be considered as all averaged geometrical characteristics and applying global measurements such as permeability and conductivity to study equilibrium states in the porous medium (Brown et al. 2000), since the equilibrium is based on the statistical balance of momentum at a large number of molecules (Daïan 2014a). In this project, a macroscopic scale will be applied, and heat and mass transfer accounted in a macroscopic way.

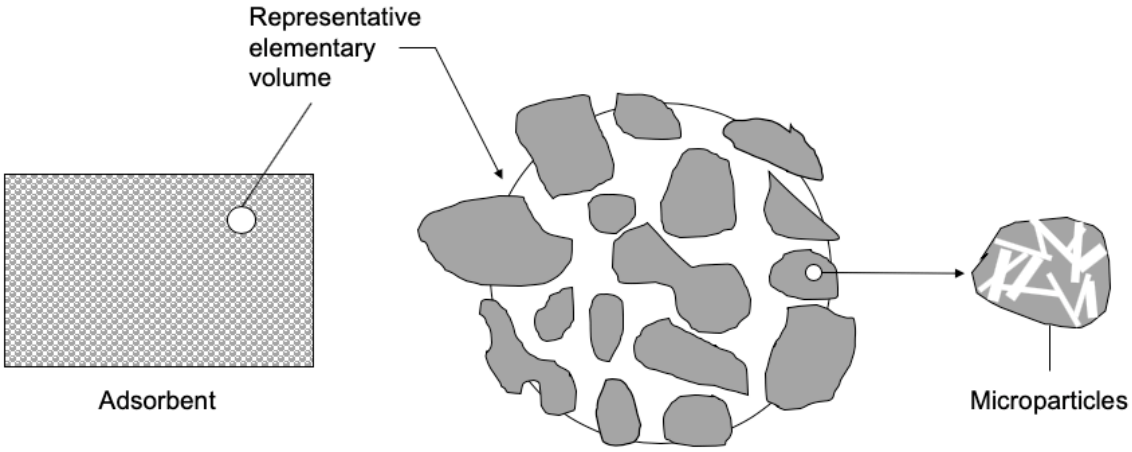

Figure 2 - 4 Relative size illustration of the reactor, the representative elementary volume and microparticles

2.2.5 Heat and mass transfer in the macroscopic scale

Heat and mass transfer occurs between adsorbent particles and also inside particles. As shown in Figure 2 - 5, when air flows through the adsorbent bed, it travels between the adsorbent particles and also penetrates into a particle. For fluid molecules to be adsorbed, they pass through the fluid film and particle skin and move into the micropores where the molecules are adsorbed (Thomas and Crittenden 1998).

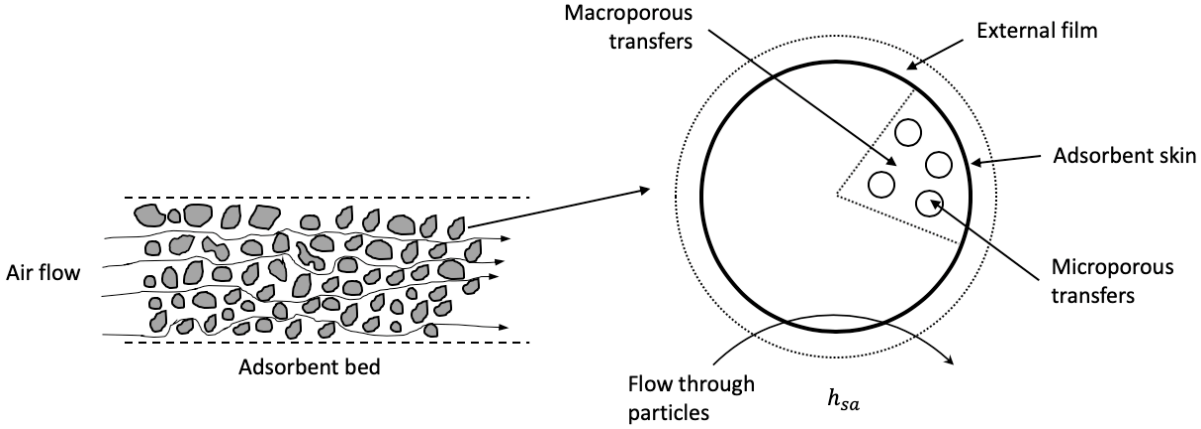

Figure 2 - 5 Details of heat and mass transfer in the solid adsorbent (Thomas and Crittenden 1998)

With respect to a charging process, heat transfers from the air flow to the particles due to temperature difference. The convective heat transfer coefficient between air and adsorbent particle can be defined as $h_{s,a}$. The rise of adsorbent

temperature has created a relatively higher internal energy so the adsorbed moisture becomes relatively more active to desorb from the adsorbent. The equilibrium between the solid adsorbent and ambient environment has been pushed to the side determined by the air flow conditions. Since the vapour pressure of adsorbent exceeds that of air flow, the moisture of the adsorbent desorbs from the adsorbent particles and joins the air flow.

For a discharging process, the release of charged energy from the adsorbent requires a supply of moisture. Air, with added moisture from the humidification device, flows through the adsorbent in the discharging process. Due to the vapour pressure difference between air and adsorbent, the moisture travels from the air across the adsorbent particle surface to its pores. The process of moisture transfer increases the water uptake of adsorbent as well as initiating the exothermic reaction. The charged energy releases from the adsorbent. This energy heats up the hydrated adsorbent and increases its temperature. Meanwhile, the adsorbent loses heat to the air flow due to the temperature difference between the two substances.

2.3 Thermochemical energy storage reactors in buildings

2.3.1 Reactor types

Thermochemical reactor can be classified into several categories. According to Trambouze and Euzen (2004), the main objectives of the classification are volume, type, operating mode and flow pattern of working fluids. In terms of the operating mode, the reactor can be classified as continuous, semi-batch and batch reactor. Batch reactors work in non-steady state conditions while continuous reactors work in steady state conditions (Su et al. 2014). Based on the flow pattern of working fluids, the reactors can also be classified as counter current, concurrent and crosscurrent reactor. In literature, the most used classification is based on the status of sorbent, namely fixed bed, moving bed and fluidised bed reactor. Table 2 - 2 lists the reactor types along with the advantages and challenges.

Table 2 - 2 The comparison of thermochemical reactors based on the material status (Solé et al. 2015a, Zondag et al. 2013)

Reactor type	Pictures	Advantages	Challenges
Fixed bed	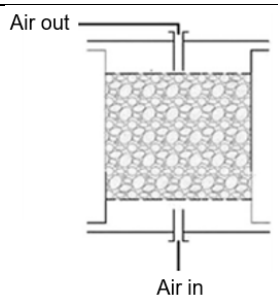	• Simple for design and modelling	• Low heat and mass transfer in large diameter fixed bed • High pressure drop
Moving bed	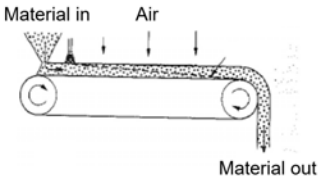	• Direct heat transfer between sorbate and sorbent	• Complex in hydrodynamics
Fluidised bed	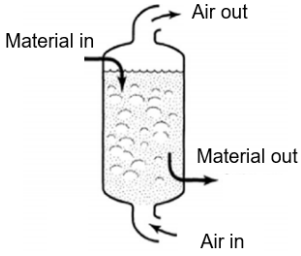	• The risk of hotspots and thermal instability • High heat transfer coefficients	• Complex in modelling • Erosion of internal components

In a fixed bed reactor, the material must be regenerated when the full conversion of the material has been achieved. The fixed bed reactor is simple in design and manufacture, and besides low heat and mass transfer, it can also lead to varying thermal power output with increasing conversion of the material (Mette et al. 2011). For the moving bed and fluidised bed reactor, the thermochemical material runs from one side to the other, providing a stationary reaction process. However, the challenge is to ensure a uniform material flow. The mass flows of the material and the working fluid/air should be adjusted with each other (Mette et al. 2011). For the operation pressure, the reactor can be classified into closed and open reactors. An open reactor operates in the ambient pressure. A closed reactor is isolated from the ambient pressure. The working fluid circulates in the closed loop with the condensation/evaporation in the condenser/evaporator. Table 2 - 3 gives a comparison between the open and closed reactors.

Table 2 - 3 Advantages and challenges of open and closed thermochemical reactors (Edem N'Tsoukpoe et al. 2014, Michel et al. 2014b)

	Advantages	Challenges
Open reactor	• Operate under atmospheric pressure; • No sorbate is stored, being favourable for storage density; • In some cases, one flow acts as heat transfer fluid and reactive gas; no internal heat exchanger is needed; and • Through forced circulation, the flow rate can be adjusted for the desired temperature output.	• Usually a fan is needed for gas circulation; • A humidifier is needed in most cases; • Only water can be used as the reaction gas due to safety and cost concerns; and • In a fixed bed reactor, the size of the storage system results in relatively high pressure drop and relatively high flow rate is needed due to the low thermal capacity of the gas.
Closed reactor	• No mass exchanger with the environment; • The pressure and the mass transfer can be better controlled; and • It can be used as a sorption heat pump for cooling and heating with a range of pressure (Chua et al. 2010).	• A heat exchanger is usually needed and generates technological constraints for evaporator/condenser design; • The sorbate should be stored within the system; • To maintain a good mass transfer within the reactor, vacuum condition is created at about 1000 Pa; but it is difficult to managing vacuum in large reactors (N'Tsoukpoe et al. 2009); and • A heat source is needed at the discharging step (a geothermal source for example).

2.3.2 Selected studies on open thermochemical reactors

Michel et al. (2016, 2014a) have conducted experimental tests on a segmented reactor as shown in Figure 2 - 6(a). To increase the energy density of the adsorption bed and create air paths, rectangular modules have been stacked in parallel. Both the top and bottom of each module are supported by perforated sheets so that the air flow can contact the thermochemical materials. Key parameters and the changes of reactive bed during charging and discharging processes have been investigated by the authors. The study has found that an increase in bed density and energy storage density can significantly reduce bed permeability (Michel et al. 2016). This shows that a high bed density, as a key parameter, can lead to a high energy storage density but reduces bed porosity and slows mass transfer. Bed permeability also decreases within a discharging process because of the change in the porous bed texture.

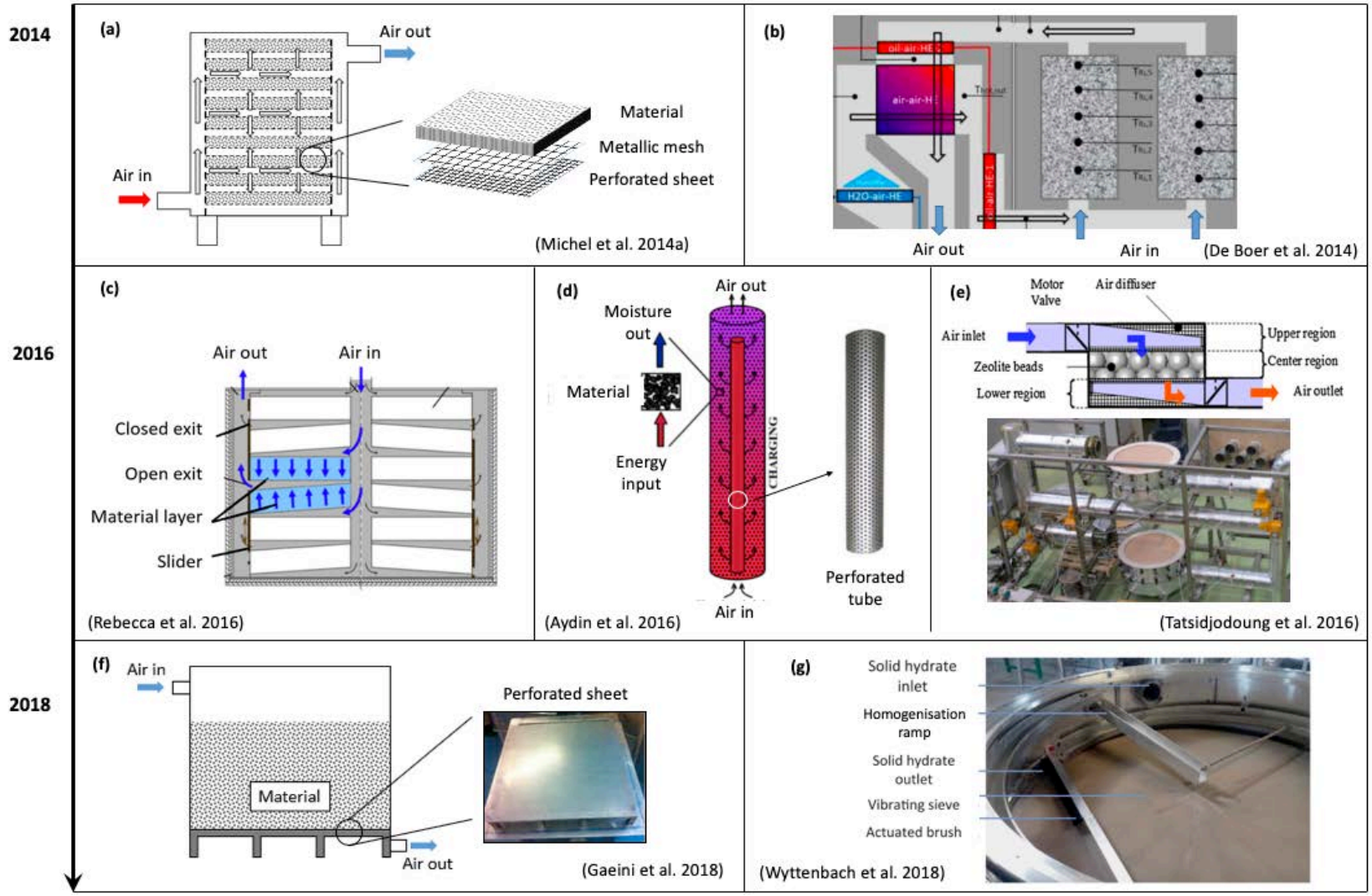

Figure 2 - 6 Overview of the open reactors in the selected studies

De Boer et al. (2014) have developed a laboratory prototype of a two segmented reactor as shown in Figure 2 - 6(b). There is a valve at each segment air inlet to switch the air flow on and off to control the charging or discharging of the segments. An air-to-air heat exchanger has been integrated into the air flow channel to preheat the intake air. According to the experiment's tests, in discharging, the intake air can be preheated to 40 °C. The preheated air flow then contributes to the output air reaching up to 70 °C, showing the importance of intake air temperature to reach a desirable output air temperature level. Moreover, the experimental data has revealed relatively low energy efficiency in a cycle of reactor charging, storage and discharging. The thermal storage efficiency is 15% with 117 MJ heat input in charging, but only 17 MJ delivered to air in discharging. Statistically, in terms of total heat input to the reactor system, in charging, 52% of the input heat has been lost to the environment, excluding the sensible heat accumulated in the reactor. During the storage, 16% of the input heat has been lost to the environment as the reactor cools down. In discharging, 17% of the input heat has been used to heat thermochemical material and reactor facilities, ultimately being transferred to the environment. Overall, the data has emphasised the significance of charging efficiency optimisation and reactor heat loss reduction in a whole energy storage cycle.

Rebecca et al. (2016) have developed and tested a segmented reactor as shown in Figure 2 - 6(c). Using zeolite 13X as the thermochemical material, the reactor configuration allows the material to be separated into 4 sub-sectors. Additionally, each sub-sector is vertically divided into 6 layers. The layers contain the thermochemical material and form gaps among any two layers as an air flow path. In this configuration, the segmentation and air flow control enable the reactor segments to be charged and discharged separately. To control the air flow path, sliders have been assembled at exits of the air flow path. By using the slider, air path exit opening can be opened and closed, adjusting the air flow path through required material layers. Reported by the authors, in the charging experiment, the temperature of some material locations are lower than other locations (Henner et al. 2014). This can result from non-uniform air flow distribution along the material

layers. According to the simulations, when discharging the two closing material layers, the upper side layer would reach complete discharging while discharging of the lower side layer is not yet complete. This shows that the adsorption front has moved faster than the lower layer. The non-uniform air flow can reduce the output air temperature since the lower side material layer cannot be hydrated as the condition of the upper side. Therefore, by optimising the segment and layer geometry, it can achieve a better air flow distribution and uniform charging or discharging in the material layers.

Aydin et al. (2016) developed a modular thermochemical reactor with internal air input as shown in Figure 2 - 6(d). A pipe shaped reactor comprises an internal perforated diffuser pipe and thermochemical material is filled between the diffuser pipe and the reactor wall. Different from other reactors where the air flow path starts from one side of the material, the internal diffuser pipe enables air diffuses through its holes to the material. Using this configuration, the authors have reported a relatively high adsorption and desorption rate at over 10 g/min in experimental tests. Additionally, the authors have integrated the reactor into concentrated solar collectors as shown in Figure 2 - 7. In a charging process, rather than heating the intake air, the thermochemical material is heated with the concentrated solar collectors. Intake air flow through the material is to extract the evaporated water from the material. In a discharging process, intake ambient air is humidified by a water spray nozzle and then travels through the reactor via the internal perforated pipe. The output heated air is then supplied to the end user. According to the experimental tests of a test room in Cyprus (floor area at 12.4 m^2), the integrated reactor and collect system can provide sufficient heat at 2.85 kWh with 0.013 m^3 of vermiculite $CaCl_2$ to meet the heat load. However, the issue of charging has been found in decline of the material. As reported, 60% drying ratio is achieved in charging processes using solar energy. Further improvement in reactor pipe and solar collector dimensions have been called to achieve a higher material temperature in charging.

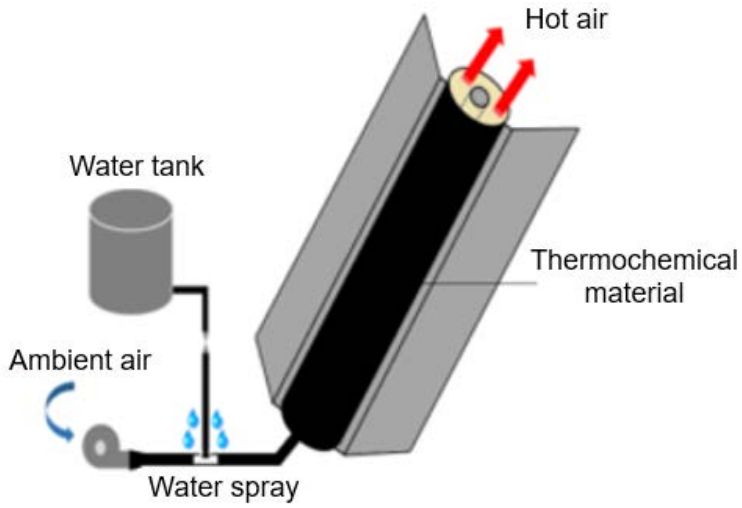

Figure 2 - 7 illustration of reactor in a concentrated solar collector in discharging

Tatsidjodoung et al. (2016) have investigated a thermochemical energy storage system with two segmented reactors as shown in Figure 2 - 6(e). Each reactor segment is a sandwich configuration with an upper region, a central region and a lower region. Air diffusers have been applied at the upper and lower regions to allow uniform distribution of the air flow. The thermochemical material zeolite 13X is located in the central region, which is supported by an oval shaped perforated grating. The two segments are connected by air ducts, which allows the segments to be charged and discharged in sequence and parallel mode. According to the experimental tests, the authors have reported an average temperature lift of 38 °C at each segment outlet for about 8 hours in a discharging phase. The output air temperature is significantly influenced by the intake air humidity.

Gaeini et al. (2018) designed and tested a four segmented reactor for seasonal heat storage and hot tap water production at a household scale. The thermochemical material zeolite 13X has been used in 4 parallel adsorption sub-systems. Each sub-system is comprised of a reactor core (Figure 2 - 6(f)), a bubble column as a humidification facility and an electric heater to lift the intake air temperature. This configuration allows the authors the control of the charging and discharging sequence of the segmented reactor. According to the study, each reactor segment achieves a maximum power of 0.9 kW (43 kg Zeolite per

segment). Air output from one segment is directed into an air-to-water heat exchanger to produce hot tap water. The results have shown that one reactor can heat 100 litre water up to 75 °C when using a heat exchanger to recover the heat from the output air.

Despite the material bulk structure, moving bed reactors have been investigated by some researchers. Wyttenbach et al. (2018) have developed a circular moving bed thermochemical reactor for seasonal storage in buildings (see Figure 2 - 6(g)). The study has integrated a vibrating sieve into the reactor to move the solid material constantly, increasing turbulence in the air flow. The thermochemical material is a composite developed from a silica gel matrix impregnated with 43 wt% $CaCl_2$. According to the experimental tests, the reactor has achieved an average 356 W heating power with air temperature lift at around 6 °C. The energy density is 200.4 Wh per kg of the hydrated solid composite. However, the authors have highlighted the issue of reducing the electrical consumption of the reactor. The vibration unit has taken electrical consumption for about 70 W and air circulation for 10 W.

Zettl et al. (2014) have developed and tested a rotating reactor as show in Figure 2 - 8. Driven by a motor, the reactor and its contained material zeolite 4A can maintain rotation while air is travelling through the reactor. Air travels through a fixed pipe in pipe configuration through the material. The main feature of the reactor is that the whole material can contribute to the adsorption and desorption processes because of the rotation movement, while in fixed bed reactors, a sorption front is normally formed. The authors reported that, in discharging, the material can reach 60 °C with intake saturated air at 20 °C. The maximum thermal power peaks at 30 W/kg with the average figure from 13 W/kg to 20 W/kg. Additionally, the control of reaction temperature and thermal power in discharging can be achieved by adjusting the humidity supply. However, the reactor requires air flow pressure at 500 Pa to 700 Pa. Also, fan noise has been reported by the authors.

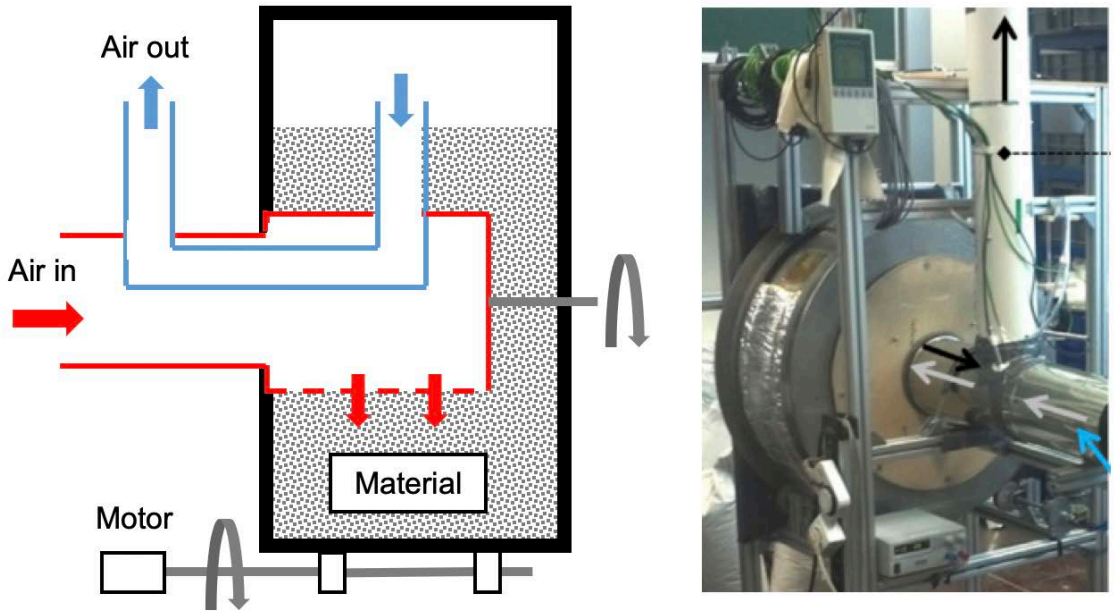

Figure 2 - 8 Rotating bed with pipe in pipe construction (Zettl et al. 2014)

Jiao et al. (2010) have reported a cross-flow rotating bed for a liquid and gas system (NaOH and CO_2). As depicted in Figure 2 - 9, the liquid enters the reactor from the bottom and gas enters from the left side. The liquid is distributed from the reactor centre. The distributor irrigates the liquid to the porous plates packed in the reactor. When the motor rotates the plates, liquid flows along the radial direction and spreads the plates because of centrifugal force. It is then collected at the reactor walls and leaves the reactor. Corrugated and smooth plates have been used and compared in experimental tests. The authors reported that, under similar measurement conditions, the gas pressure drop of the cross flow reactor (10 Pa to 260 Pa) is substantially lower than counter current flow reactor (100 Pa to 5000 Pa). Additionally, corrugated plate configuration has shown a better performance than the smooth plates with the volumetric mass transfer coefficient improved by around 25%. This is because of the improved wettability of the corrugated plate.

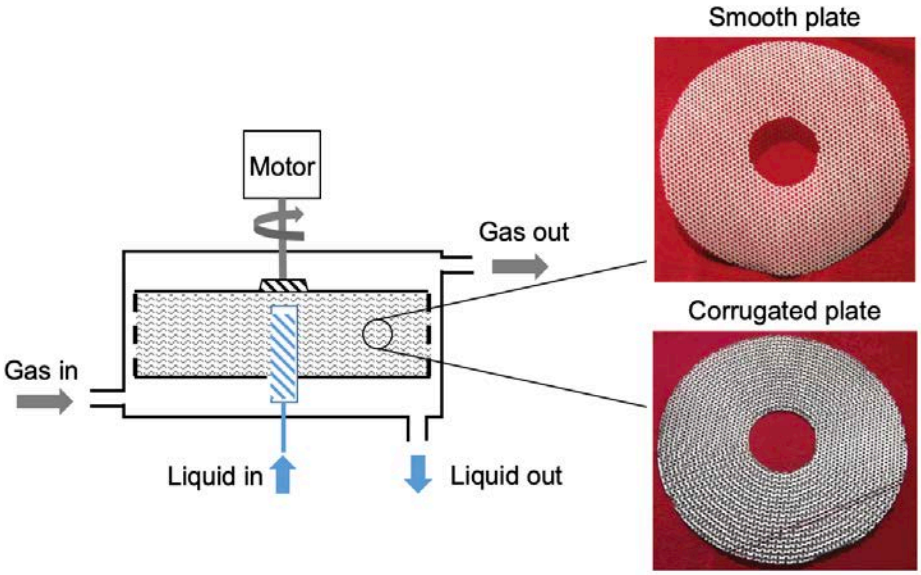

Figure 2 - 9 Cross flow rotating bed packed with corrugated porous plate or smooth porous plate (Jiao et al. 2010)

A reactor with external thermochemical material storage and supply has been developed and experimentally tested (Mette et al. 2014a). As shown in Figure 2 - 10, a thermochemical material reservoir is separated from the reaction chamber. To achieve a relatively homogenous air distribution, a cross flow section (0.53*0.53 m^2) has been used at the entrance and exit of the air flow path. In discharging, hydrated thermochemical material is supplied to the reaction chamber by gravity. Then, humid air flows through the reactor and supplies moisture to the thermochemical material. The air is heated by the material in the exothermic reaction. The air then flows through an air to liquid heat exchanger where the air transfers heat to the liquid, thermal oil. In this process, the heat of adsorption is transported to the air and then to the thermal oil. In terms of the thermochemical material, in a charging process, however, the air flow direction is reversed. When air flows through the air to the oil heat exchanger, it is heated by the circulated thermal oil, which has been heated by an electric heater. The heated air then regenerates the material in the regeneration chamber. To support the material transportation, a vacuum exhauster with an electrical power of 1600 W has been used. According to the experimental tests, a thermal power of about 500 W has been transferred to the thermal oil which is 60% of the thermal power

released by the thermochemical material. Due to the uninsulated reactor, about 37% of the released heat is lost to the environment.

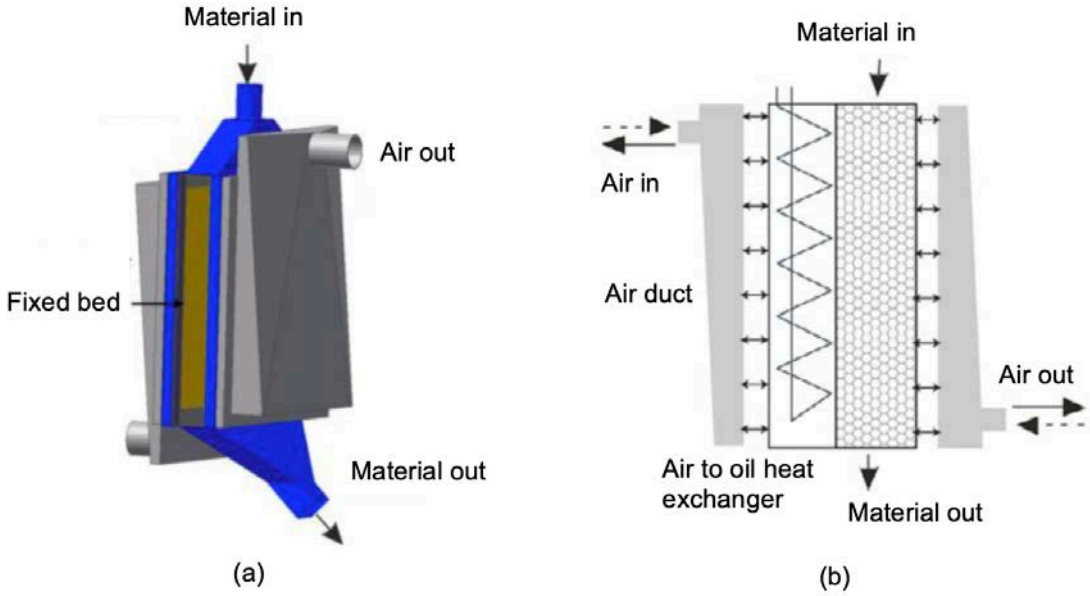

Figure 2 - 10 View of an external thermochemical reactor (Mette et al. 2014a)

Additionally, some studies have been focusing on specialising the structure and texture of thermochemical material instead of using conventional thermochemical material as beads or granules. This has been motivated by maintaining a relatively high reactor material density and reducing air flow pressure drop. Gantenbein et al. (2008) have developed a structured zeolite bulk as reactor core in experimental tests (see Figure 2 - 11(a)). The shaped body contains a number of small and straight channels, leading to the advantages of reducing pressure drop and better adsorption properties. The authors have reported that the structured zeolite bulk can achieve material energy storage density at 160 kWh/m^3 and provide thermal output power from 14 W/kg to 21 W/kg, depending on the intake air humidity and reactor's insulation. Janchen et al. (2015) have tested the thermochemical performance of a honeycomb structured zeolite reactor (see Figure 2 - 11(b)). According to the simulation analysis, it has been found that compared with a zeolite granule reactor, the structured reactor can provide a more homogeneously distributed moisture concentration in the outlet air stream. Additionally, according to a discharging experiment, the structured

zeolite reactor shows a significant impact on dynamic adsorption properties. Compared to a zeolite granule reactor, the developed honeycomb reactor can speed up adsorbent temperature increase by nearly 50%. In addition to the tested honeycomb zeolite reactor, the authors have developed different shapes of textured zeolite like cylinder and multi-channel ones as shown in Figure 2 - 11(c) (Schumann et al. 2014).

Figure 2 - 11 Developed thermochemical material textures in recent studies (Gantenbein et al. 2008, Janchen et al. 2015, Schumann et al. 2014)

Table 2 - 4 shows an overview of the status of open thermochemical reactors applied in buildings. It summarises the materials, methodologies, performance and related issues. According to the review, the characteristics in the open thermochemical reactor in building application can be listed as follows.

- Researchers have made efforts to maximise energy storage density and maintain heat and mass transfer in compact reactors. The utilised heat and mass transfer methods are: (1) separate thermochemical material into modular stacks supported by a perforated sheet; (2) apply binders and diffusers; (3) change texture of thermochemical material such as creating air gaps; (4) induce air flow into thermochemical material; and (4) maintain continuous movement of thermochemical material grains.
- Perforated gratings have been used in most of the studies. It aims to support the solid thermochemical beads or granules to stay in the reactor and ensure the continuity of the air flow through the reactor and materials. When using a perforated grating, the size of the holes is smaller than the size of the

thermochemical material. The general grating shapes are rectangular (Michel et al. 2016) and oval (Tatsidjodoung et al. 2016).

- Regarding the air flow used in charging and discharging, reactor segmentation can help reduce pressure drop. Blowing an air stream through an entire storage section causes a relatively high pressure drop.
- Thermochemical energy storage systems usually operate under transient conditions like solar energy applications. Reactor segmentation features flexibility in both charging and discharging operations. For example, in discharging, only a part of the whole reactor may need to be discharged, leading to reduced heat losses. The entire reactor does not have to be heated in discharging. The flexibility also provides the potential of a fast response to changing energy demand, such as dynamic heating demand in buildings. Additionally, reactor segments can be controlled to discharge in sequence or in parallel according to the end user heating demand.
- Heat loss and air leakage during charging and discharging cannot be ignored (Rebecca et al. 2016, Mette et al. 2012). De Boer et al. (2014) have reported 52% heat from heat source had been lost for convection and air leakage. Similarly, in discharging, Weber et al. (2014) have stated 54% heat lost for pipe and duct connections, improper insulation and outlet air flow in charging.
- Evaluation of charging and discharging cycles especially short-term charging and discharging has been missing in some studies (Tatsidjodoung et al. 2016, Janchen et al. 2015, Casey et al. 2015, 2017). Through testing charging and discharging cycles, evaluations can be made in thermochemical material's cyclability and reactor's performance over the cycles. Investigating the performance of short-term cycles is also of significance, since in practice thermochemical material may not reach complete dehydration.

Table 2 - 4 Selected studies of open reactors for building applications

Studies	Heat and mass transfer enhancement method	Materials	Storage energy density (kWh/m^3)	Charging temperature (°C)	Output power (W/kg)	Total input energy sources in operation
(Reichl et al. 2016, Zettl et al. 2014)	• Create movement of material	Zeolite 4A and Na-MSX(50 kg spheres, diameter 1.6 - 2.5 mm)	96	180	20	Motor and fan at 100 W
(Jiao et al. 2010)	• Rotate reactor material • Cross flow of air and liquid inlet	$NaOH/CO_2$ pair	-	-	-	Motor
(Kerskes et al. 2012, Mette et al. 2014a)	• External reactor to supply thermochemical material • Cross flow of air and material supply	Zeolite 13X	-	180	34	Vacuum and fan
(Rebecca et al. 2016, Henner et al. 2014)	• Reactor segmentation • Air flow path switch	Zeolite 13X	163	165	9	Fan
(Michel et al. 2016, 2014a)	• Reactor segmentation	$SrBr_2$/ H_2O, (400 kg hydrated salt)		80		Fan

(Johannes et al. 2015, Tatsidjodoung et al. 2016)	• Reactor segmentation • Air diffuser for uniform intake air distribution	Zeolite 13X	-	120 and 180	28	Fan
(De Boer et al. 2014)	• Reactor segmentation	Zeolite 13X	-	150	10	Fan
(Aydin et al. 2016, Casey et al. 2017)	• Reactor segmentation • Internal air diffusion	Vermiculite $CaCl_2$	290	80	-	
(Gantenbein et al. 2008)	• Multichannel material bulk	Zeolite 4A	160	150	21	Fan
(Janchen et al. 2015)	• Multichannel material bulk	Zeolite 4A	-	120 - 180	-	

2.3.3 Selected studies on closed thermochemical reactors

This section reviews the selected studies of closed thermochemical reactors. Reactor designs, performance in experiment and reported issues have been presented. Followed by the review, discussions of the closed reaction studies have been conducted with the comparison of open reactors.

Gantenbein et al. (2008) have developed a closed adsorption reactor using silica gel for a single-family house in Austria. A pilot plant has been built and tested, as shown in Figure 2 - 12. The reactor features a compact design with an adsorber, evaporator, and heat exchanger in one container (350 litres). Rather than connecting evaporator and adsorber through ducts or pipes, the one container design allows a relatively short vapour path from the evaporator/condenser to the adsorber, reducing pressure losses. In terms of the experimental tests, however, the main issue is the low energy storage density of silica gel, requiring a large volume and being expensive for energy storage purposes. To overcome the issue, zeolite 13X has been used in the study (Helden et al. 2014). By using zeolite 13X, the volumetric energy density of the material is 77 kWh/m^3 and the maximum output power is 1.08 kW. The authors have reported that the evaporator performance has a significant impact on the system, which requires further investigation.

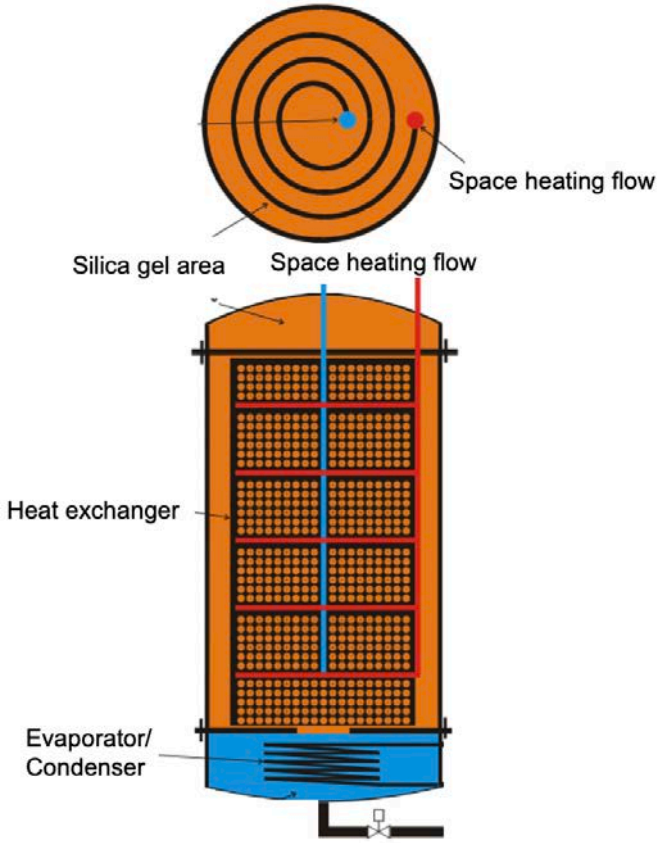

Figure 2 - 12 Prototype of a closed silica gel/H_2O reactor (Gantenbein et al. 2008)

Mauran et al. (2008) have developed and tested a closed thermochemical reactor with $SrBr_2$/natural graphite composite. The reactor is a modular concept stacking of heat exchanger plate (5 - 6 mm thick), thermochemical materials (12 mm thick), and gas diffusers (5 - 6 mm thick), as shown in Figure 2 - 13. The reactor has a volume of 1 m^3. According to experiment, the reactor achieves 60 kWh heating (at 70 - 80 °C) and 40 kWh cooling (at 18 °C). The limitations are the transfer of vapour through the composite and the limited conductive heat transfer between the thermochemical material and the wall of the heat exchanger, lowering the heating and cooling powers of the prototype. The conductive heat transfer coefficient has been measured at 5 - 30 W/(m^2·K) but was expected at over 500 W/(m^2·K).

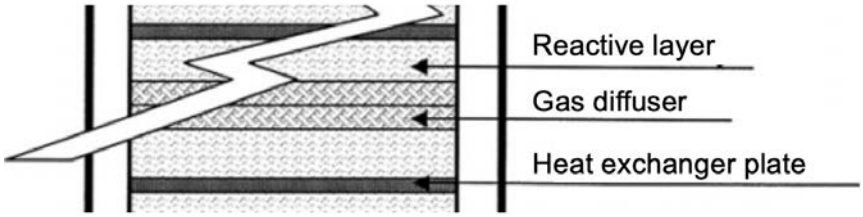

Figure 2 - 13 Cross section of a module in the reactor (Mauran et al. 2008)

To enhance water vapour transfer, investigations have been made on a heat exchanger with glued on zeolite spheres (Cuypers et al. 2012). Showing in Figure 2 - 14, the reactor consists of a 400-mm long heat exchanger with a water accessible cross section at 40 mm^2. Adsorption experiments of the reactor have suggested that the energy output reached 60% of the theoretical value. The maximum specific output power is 0.6 kW/kg. Focusing on the water vapour transfer to the zeolite, apart from the mass resistance of zeolite layers, rate of evaporation has also been reported as a crucial factor for fast adsorption and sufficient subsequent mass transfer.

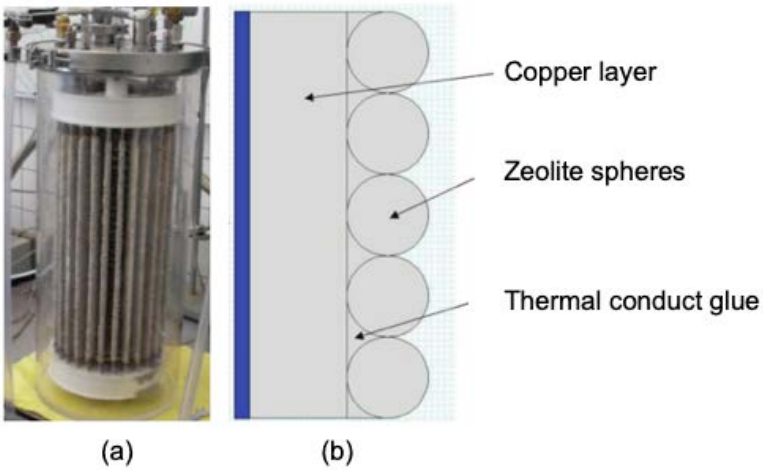

Figure 2 - 14 (a) Reactor with zeolite glued heat exchanger; (b) schematic of copper layer, zeolite and thermally conducting glue (Cuypers et al. 2012)

In another study, Richter et al. (2016) have proposed a tube bundle heat exchanger as a closed reactor. There are 31 tubes with a length of 400 mm and a diameter of 9 mm. Thermochemical material $CaCl_2$ (700 g) is filled inside the tubes (Figure 2 - 15). A thinner air channel (diameter of 1 mm) is embedded in

each tube. The air channel is rolled from a wire mesh filter with the mesh size at 100 μm. Water vapour is supplied from the top of the tube bundle. This arrangement allows a long and thin thermochemical material bed and aims to maintain good permeability of material to the water vapour along the tube. However, because of the characteristics of $CaCl_2$, after 3 cycles of charging and discharging experiments, agglomerates form, limiting the distribution of absorption heat.

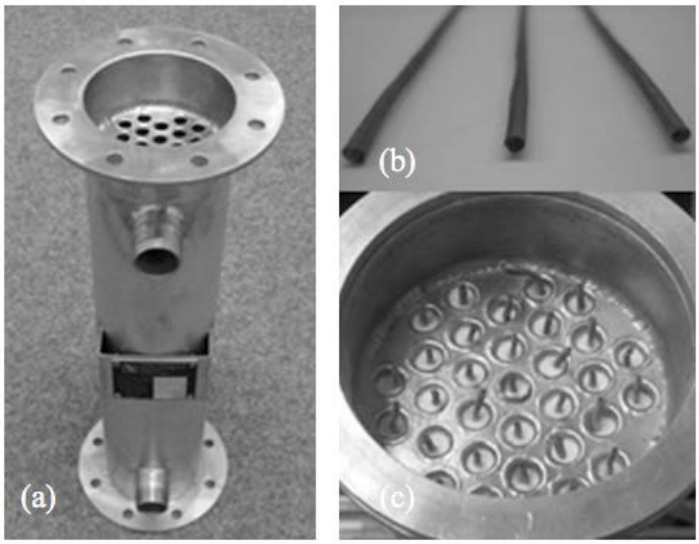

Figure 2 - 15 (a) Tube bundle exchanger; (b) air channels: (c) tube bundle filled with $CaCl_2$ and inserted air channels (Richter et al. 2016)

To tackle agglomeration problems and enhance water vapour and heat transfer, a honeycomb structured exchanger has been developed and tested (Fopah-Lele et al. 2016b). The heat exchanger consists of a bundle tube and a honeycomb bed structure (Figure 2 - 16). The bundle tube contains heat transfer fluid and the honeycomb structure contains thermochemical material. The two parts are welded and a thermal conductive adhesive has been applied between the two parts. Additionally, a diffusive mesh has been bolted on the honeycomb surface to maintain the material being fixed. The thermochemical material is 1 kg $SrBr_2$. According to 13 charging and discharging experiment cycles, thermal capacity of 65 kWh and energy storage density of 213 kWh/m^3 have been achieved. Discharging temperature from 30 °C to 52 °C has been recorded with water

vapour pressure ranging from 10 mbar to 20 mbar. However, issues noted by the authors are corrosion to the exchanger material aluminium and the salt loss from the honeycomb structure during charging/discharging cycles because of reactor position and orientation.

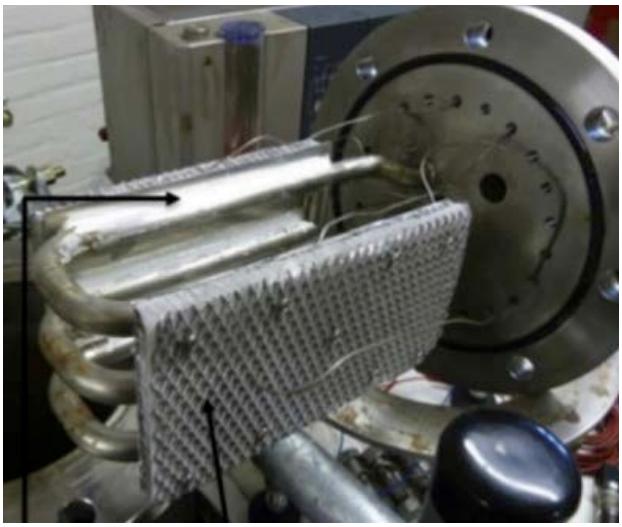

Figure 2 - 16 The honeycomb structure reactor with bundle tubes (Fopah-Lele et al. 2016b)

Similar to open reactor, for closed reactor studies, to achieve desirable energy storage performance the target is to maintain vapour transmission and not sacrifice the energy storage density of the reactor. In a closed reactor, besides reactor geometry, experimental conditions in reactors can be more accurately controlled. It provides opportunities of wider thermochemical material selections, minimising the related material issues, and improving charging and discharging performance with desired temperature and pressure. Salt hydrates are with relatively higher theoretical energy storage density than adsorption materials such as zeolites. However, material issues should be addressed such as multi-step reactions, overhydration and producing toxic products. In closed reactor studies, these issues can be solved by adjusting and maintaining charging and discharging temperature and pressure (Fopah-Lele et al. 2016b, Richter et al. 2016). Additionally, charging can be chosen at low vapour pressure (2 - 3 kPa) to decrease the required charging temperature; In reverse, to discharge at a higher temperature, higher pressures can be applied (about 100 kPa).

Furthermore, in discharging, rate of evaporation can also be adjusted and increased with a higher evaporation temperature. This leads to sufficient water vapour supply, a larger pressure difference between the evaporator and reactor, and higher temperature in discharging.

2.3.4 Potential opportunities in the reactor development

The literature review on the thermochemical reactor helps to identify the opportunities for developing a better thermochemical reactor.

2.3.4.1 Reactor structure optimisation

In the reviewed studies, perforated mesh has been placed at the bottom of a reactor to support thermochemical materials, as shown in Figure 2 - 6. The mesh opening size ranges from 1 mm to 5 mm depending on the size of the thermochemical material. In addition to the mesh, for the reactor structure strength, supporting structures such as metallic mesh is used since the density of the thermochemical material is over 500 kg/m^3. The perforate mesh and supporting structures have created a tiny air travel path, increasing flow resistance, and deteriorating system efficiency. Improvements shall be made on the reactor structure with the optimisation goals listed as follows.

- Ensure relatively large air flow opening area to reduce flow resistance;
- Provide robust support of the thermochemical material; and
- Maximise material compactness and reduce reactor volume.

2.3.4.2 Heat and mass transfer enhancement

The performance of a thermochemical energy storage system is closely linked to the heat and mass transfer performance of its reactor. In literature, thermal conductivity of thermochemical material is relatively low. When the heat transfer is reduced, relatively more energy and time is used in a charging process. Similarly, in discharging, this leads to relatively large heat loss and less energy is transferred to end users. Additionally, for mass transfer, when reactors operate under ambient pressure, the density of water vapour or reactant gas is relatively low, limiting the mass transfer inside the reactor, especially for a large dimension reactor. Poor mass transfer can lead to small adsorbed or desorbed quantities,

decreasing the reactor kinetics and making the charging and discharging process ineffective. To promote heat and mass transfer inside the reactor, efforts should be made in reactor structure, packing configuration, material particle shapes and the movement of the materials.

2.3.4.3 Improving the reactor flexibility

Improvements can be made in a reactor to cope with various application demands. Reactor design should be simple and easy to scale depending on the application scenarios. Some recent reactor designs in literature have focused on the segmentation for flexibility in charging and discharging (see Figure 2 - 6). However, complexity has been increased in the air travel path and system components. Additionally, in discharging, most of the studies have been using air as the energy supply media. The advantage of the process is simple and effective. However, in some studies, the heat loss takes up about 20% of the energy stored (van Alebeek et al. 2018). It comes from the sensible heat loss during a discharging process and between charging and discharging. The reactor has to be isolated from the air flow between charging and discharging, leaving part of the input energy from charging lost to the environment. Some applications also require heated water supply from the reactor. Some studies have used air-to-water heat exchanger to extract heat from the reactor outlet air to heat the water stream (Gaeini et al. 2018, De Boer et al. 2014). Other studies have applied a heat exchanger inside of the reactor, but the studies are currently limited to closed systems (Schreiber et al. 2015, Fopah-Lele et al. 2016a). The applications led to the development opportunity of extracting the discharging energy from inside the reactor.

2.4 Thermochemical energy storage materials in building applications

Thermochemical energy storage materials are involved with several fields and disciplines. The focus of this section is to assist in material selection, characterisation and enhancement. With regards to the building applications, in literature, the main requirements of the materials are listed as follows (van Essen et al. 2009b, Pardo et al. 2014, Kuznik et al. 2015):

- High energy storage density;
- High affinity for the sorbent by the sorbate;
- Reachable temperature reaction by a solar collector;
- Stable after several hydration/dehydration reactions;
- Easy to handle with low environmental impact, non-toxic and non-flammable of the material, non-corrosive at storage or reaction;
- Low cost of the material; and
- Moderate operating pressure range with no excessive pressure conditions and especially no vacuum requirement.

Considering these criteria, a suitable thermochemical material should be able to store a relatively large amount of energy and release energy efficiently when it is needed. Additionally, application background and climate conditions should be considered when selecting suitable thermochemical materials. Currently, there are numerous materials that can be used in thermochemical energy storage. However, for classification, the use of ‘chemical storage’, ‘chemical reaction’, ‘sorption storage’ and ‘thermochemical storage’ differs from one study to another. One study (Abedin and Rosen 2012) reports the entire category as chemical energy storage and can be divided into sorption and thermochemical reactions. Salt hydrates have been considered in the chemical reaction group. However, (Tatsidjodoung et al. 2013) thermochemical materials have been classified into sorption phenomena materials and chemical reaction materials. Similarly, salt hydrates are classified as a group of chemical reaction materials. In another study (Yu et al. 2013), the entire category is called sorption thermal storage. It has been divided into liquid absorption, solid adsorption, chemical reaction and composite materials. Different types of classification have been made based on the mechanism of the sorption process. In this paper, as shown in Figure 2 - 17, thermochemical materials are divided into chemical reaction/solid absorption, solid adsorption, composites and liquid sorption thermochemical energy storage materials.

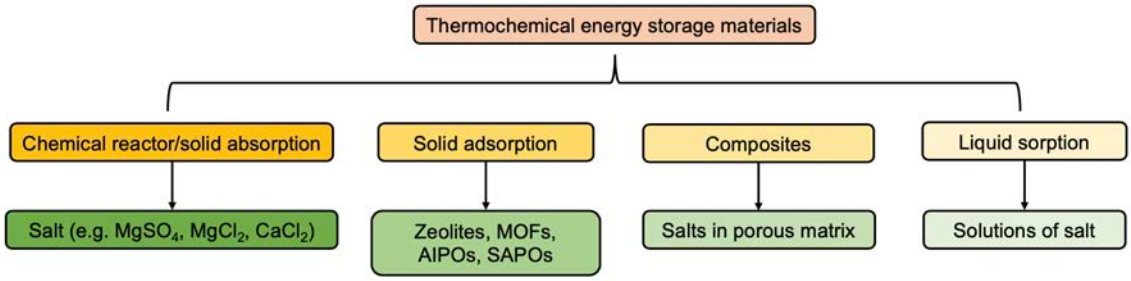

Figure 2 - 17 Classification of thermochemical energy storage (Scapino et al. 2017, Yu et al. 2013)

2.4.1 Chemical reaction/solid absorption materials

This section reviews reported promising chemical reaction/solid absorption materials for building applications. Specific attention has been paid on the energy storage density, absorption/desorption temperature, cyclic stability and related issues in applications. Table 2 - 6 summarises the reviewed materials and remarks.

2.4.1.1 Magnesium sulphate ($MgSO_4$)

Magnesium sulphate heptahydrate, $MgSO_4 \cdot 7H_2O$, is gaining attention in thermochemical energy storage for buildings (Bales et al. 2008, Okhrimenko et al. 2017). Apart from being non-toxic and non-corrosive, it attracts researchers with relatively high theoretical energy storage density of 780 kWh/m^3 when charging at 122 °C (Gantenbein et al. 2008). However, some issues have been reported including melting in dehydration at around 50 °C (Paulik et al. 1981, van Essen et al. 2009a, 2008). As a result, the melting limits the water uptake capacity of the material since it reduces the vapour transport.

2.4.1.2 Magnesium chloride ($MgCl_2$)

Magnesium chloride hexahydrate, $MgCl_2 \cdot 6H_2O$, has shown appealing characteristics in theoretical energy storage density at 694.4 kWh/m^3 and up to 85 °C temperature in hydration (van Essen et al. 2009b). Shown in Figure 2 - 18, the dehydration of $MgCl_2 \cdot 6H_2O$ starts at about 50 °C and forms monohydrate

$MgCl_2$ at around 150 °C (Zondag et al. 2010). This shows that a relatively large mass change can be achieved with solar thermal collectors.

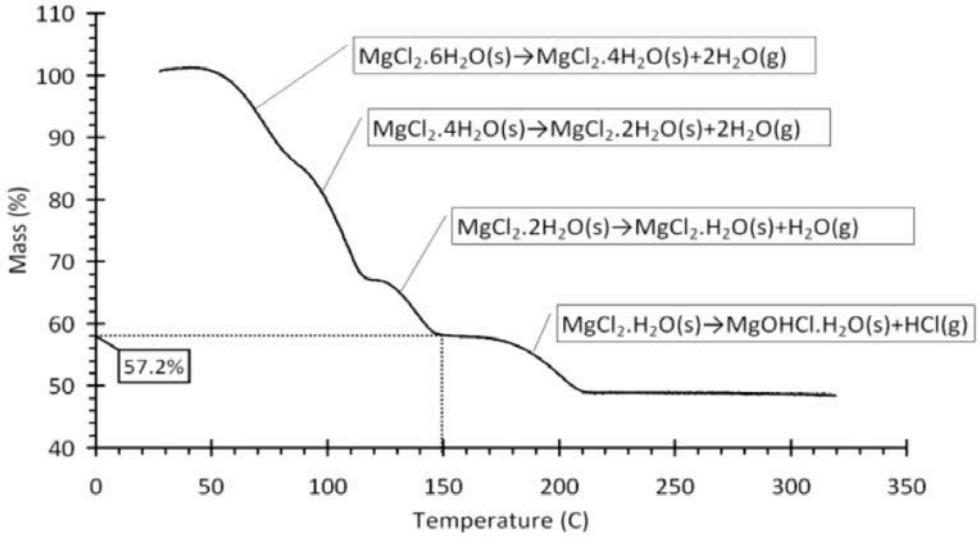

Figure 2 - 18 Water loss during the dehydration at 1 °C/min (Zondag et al. 2010)

However, the stability of the material in both low and high temperatures is problematic. Overhydration with the appearance of deliquescence has been found at the relative humidity between 22 - 33% and the temperature of 20 °C to 100 °C (Ferchaud et al. 2012). It causes structural changes, blocking the vapour transport, and reducing hydration performance. Figure 2 - 19 shows the overhydration in closed and open reactor experiment (Zondag et al. 2010).

(a) (b)

Figure 2 - 19 (a) Overhydration in a closed reactor; (b) formation of a hard layer due to overhydration in an open reactor (Zondag et al. 2010)

Additionally, for the high temperature at 140 °C to 150 °C, decomposition of the material occurs, forming hydrogen chloride HCl vapours and non-reactive $Mg_3Cl_2(OH)_4 \cdot 2H_2O$. The decomposition reaction can be given as the following equation.

$$MgCl_2 \cdot 6H_2O \rightarrow 1/3\, Mg_3Cl_2(OH)_4 \cdot 2H_2O + 4H_2O + 4/3\, HCl \qquad 2.1$$

This leads to safety issues and corrosion and the reduction of the energy storage capacity.

2.4.1.3 Sodium sulphide (Na_2S)

Sodium sulphide Na_2S is another material with a relatively high theoretical energy storage density at about 750 kWh/m^3 (De Jong et al. 2014). There have been a few studies reporting the utilisation of Na_2S for heat storage in buildings (De Boer et al. 2004, Ucar and Pounder 1982, Brunberg EA 1980). However, the material may produce toxic H_2S gas during hydration (Trausel et al. 2014, Ucar and Pounder 1982). Also, Na_2S is corrosive to carbon steel, aluminium and copper since it reacts with metals including carbon steel, copper, aluminium and zinc (Solé et al. 2015b).

2.4.1.4 Copper sulphate ($CuSO_4$)

The theoretical energy storage density from monohydrate ($CuSO_4 \cdot H_2O$) to pentahydrate ($CuSO_4 \cdot 5H_2O$) is reaching 574 kWh/m^3. Based on the hydration experiment, the material remains stable during hydration and dehydration cycles (Bertsch, F., Mette, B., Asenbeck, S., Kerskes, H. Müller-Steinhagen 2009). However, reaction kinetics reduction during hydration and dehydration cycles, and toxicity are the issues of $CuSO_4$ (Bertsch, F., Mette, B., Asenbeck, S., Kerskes, H. Müller-Steinhagen 2009). Also, toxicity is a drawback of $CuSO_4$ (University of Nebraska 2012, Vrdoljak and Erfanifar 2016).

2.4.1.5 Calcium chloride ($CaCl_2$)

The application of $CaCl_2$ as thermochemical material has been reported in several literatures (van Essen et al. 2009a, Molenda et al. 2013, Zondag et al. 2008). Main advantages are relatively high theoretical energy storage density, availability and environmental compatibility. The reported theoretical energy storage density can be reached at 750 kWh/m^3 (Trausel et al. 2014, N'Tsoukpoe et al. 2014). However, only a part of the reported energy storage density can be used depending on temperature and pressure conditions.

Table 2 - 5 summarises the stable crystalline structures of $CaCl_2$ having 2, 4 or 6 coordination water during a sorption stage with the related sorption temperature and enthalpy (Edem N'Tsoukpoe et al. 2015). There is a temperature gap of over 120 °C between $CaCl_2 \cdot 4H_2O$ and $CaCl_2 \cdot 2H_2O$. For the storage application at around 40 °C, $CaCl_2 \cdot 4H_2O$ and $CaCl_2 \cdot 6H_2O$ would occur in hydration. Within the sorption temperature range, however, $CaCl_2 \cdot 4H_2O$ and $CaCl_2 \cdot 6H_2O$ are liquid. As stated in the hydration experiments (Zondag et al. 2008, van Essen et al. 2009a), this can cause agglomeration and the presence of liquid during the hydration of $CaCl_2$, consequently reducing bed porosity and rehydration performance.

Table 2 - 5 The relevant temperature and reaction enthalpy of $CaCl_2$ and H_2O reactions (Trausel et al. 2014, Edem N'Tsoukpoe et al. 2015, Molenda et al. 2013)

$CaCl_2$ and H_2O sorption	Desorption temperature (°C)	Reaction enthalpy (kJ/mol)
$CaCl_2 \cdot 6H_2O \leftrightarrows CaCl_2 \cdot 4H_2O + 2H_2O$	29.8	117 - 236
$CaCl_2 \cdot 4H_2O \leftrightarrows CaCl_2 \cdot 2H_2O + 2H_2O$	45.3	118 - 124
$CaCl_2 \cdot 2H_2O \leftrightarrows CaCl_2 \cdot H_2O + H_2O$	175	101 - 114
$CaCl_2 \cdot H_2O \leftrightarrows CaCl_2 + H_2O$	200	70

2.4.1.6 Lanthanum chloride ($LaCl_3$)

In a systematic evaluation of 125 salt hydration (N'Tsoukpoe et al. 2014), $LaCl_3$ has reported to be promising from the thermodynamic perspective. The hydration temperature under 12 mbar vapour pressure is 66 °C. An almost complete dehydration has been reached with the dehydration temperature at 73 °C under 20 mbar vapour pressure (Donkers et al. 2017, N'Tsoukpoe et al. 2014). However, the main drawback is a relatively low energy storage density, at 133 kWh/m^3 (N'Tsoukpoe et al. 2014, Sahoo et al. 2014). Lanthanum is a rare earth metal, causing a high price of $LaCl_3$ of up to £37/kg.

2.4.1.7 Strontium bromide ($SrBr_2$)

$SrBr_2$ has been investigated as a possible thermochemical material in several studies (Michel et al. 2014a, Mauran et al. 2008, Lahmidi et al. 2006, Michel et al. 2012). The temperature of 80 °C is used to charge the material. The temperature lift ranging from 20 °C to 40 °C has been reported based on the experiment conditions. According to the measurements, compared with $LaCl_3$ and $MgSO_4$, the $SrBr_2$ shows the highest theoretical energy storage density at 628 kWh/m^3 (N'Tsoukpoe et al. 2014). For the stability of $SrBr_2$, 7 cycles in open systems (Michel et al. 2012, 2014a) and 13 - 14 cycles in a closed system have been successfully performed (Courbon et al. 2017). However, $SrBr_2$ can cause eyes or skin irritation (Fopah-Lele and Tamba 2017).

Table 2 - 6 A summary of the reviewed material properties and remarks

Hydrated material	Dehydrated material	Theoretical energy density (kWh/m^3)	Desorption temperature (°C)	Cost (£/kg) (1 U.S. $ = £ 0.76)	Remarks	References
$MgSO_4 \cdot 7H_2O$	$MgSO_4$	780	22 - 150	0.06 - 0.16	• Melting was found at a low temperature 48 - 52 °C. Slow kinetics occurs in hydration.	(Glasser 2014)
$MgCl_2 \cdot 7H_2O$	$MgCl_2 \cdot 2H_2O$	694	68 - 150	0.07 - 0.10	• Deliquescence found at a low temperature 20 - 100 °C. Decomposition and formation of HCl gas reported at 140 - 150 °C.	
$CuSO_4 \cdot 5H_2O$	$CuSO_4$	574	28 - 150	0.59 - 1.78	• Being toxic and reaction kinetics drop over cycles	
$CaCl_2 \cdot 6H_2O$	$CaCl_2$	750	32 - 147	0.37 - 0.97	• Being toxic and overhydration is likely to occur. The temperature gap between $CaCl_2 \cdot 4H_2O$ and $CaCl_2 \cdot 2H_2O$ is over 120 °C.	(Glasser 2014, Druskea et al. 2014)

$Na_2S·9H_2O$	$Na_2S·2H_2O$	750	66 - 75	0.24 - 0.32	• Formation of toxic gas H_2S in hydration. Severe corrosion of Na_2S to carbon steel, aluminium and copper.	(Donkers et al. 2017)
$SrBr_2·6H_2O$	$SrBr_2$	628	45 - 52	0.76 - 1.53	• Hydration can be affected by agglomeration. $SrBr_2$ can cause skin and eye irritation.	(N'Tsoukpoe et al. 2014)
$LaCl_3·7H_2O$	$LaCl_3$	133	66 - 73	0.75 - 37	• Low energy density compared to the other salt hydrates and relatively highly priced.	(Donkers et al. 2017)
$CuCl_2·2H_2O$	$CuCl_2$	483	53	3.05 - 3.64	• Being toxic.	(National Library of Medicine 2015)
$KAl(SO_4)_2·12H_2O$	$KAl(SO_4)_2·3H_2O$	517	33 - 57	0.15 - 0.52	• Reaction kinetics limitation.	(Marias et al. 2014)

2.4.2 Solid adsorption materials

2.4.2.1 Aluminophosphates (AlPOs) and silicoaluminophosphates (SAPOs)

A recent development of thermochemical materials is aluminophosphates (AlPOs) and silicoaluminophosphates (SAPOs). AlPOs and SAPOs are solids that pose a neutral framework (Wright 2008). Some exhibit structural types close to zeolites such as zeolite A and Y. Thus, they have been considered as zeolite-like materials (Jänchen et al. 2005). Different from zeolites, they often show S-shape isotherms (Figure 2 - 20) (Henninger et al. 2012). The S-shape isotherm emphasises a sharp increase of the isotherm within a narrow relative pressure range. The driving force is that highly ordered water clusters can be formed in the pores (Ristić et al. 2012). The coordination of water molecules to aluminium atoms locally increases the aluminium coordination from four- to six-fold, therefore, making the material become more hydrophilic and leading to the sudden increase in the water uptake. Table 2 - 7 summarises the water uptake and adsorption heat of AlPOs and SAPOs.

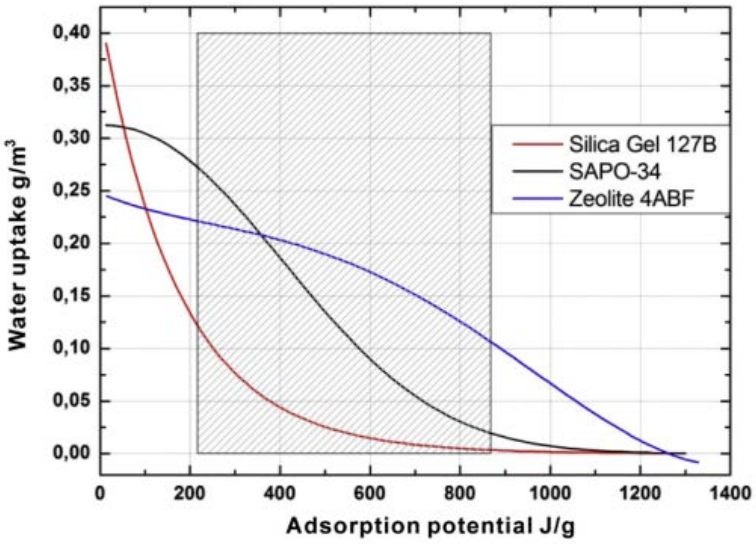

Figure 2 - 20 S-shape isotherm of SAPO-34 and the comparison with silica gel 127B and zeolite 4ABF (Henninger et al. 2012)

Table 2 - 7 An overview of AIPOs and SAPOs properties

Material	Maximum water uptake ($kg_{H2O}/kg_{material}$)	Heat of adsorption (kJ/mol)	References
SAPO-34	0.20	55.5	(Henninger et al. 2010, 2012)
AlPO-5	0.24	53.4	(Jänchen et al. 2005)
AlPO-17	0.28	55.4	
AlPO-18	0.25	55.1	(Henninger et al. 2010)
APO-Tric	0.31	53.6	(Ristić et al. 2012)

2.4.2.2 Metal Organic Frameworks (MOFs)

Besides AlPOs and SAPOs, a class of microporous materials known as Metal Organic Frameworks (MOFs) has been receiving attention for their promising porosity and chemical variability (Küsgens et al. 2009). They are crystalline porous materials, made by linking inorganic and organic clusters and metal icons with strong bonds (Furukawa et al. 2013). They are interconnected by organic ligand molecules with a modular principle. This principle defines the precise pore system of the MOFs compared with less ordered materials such as activated carbons, porous metal oxides and silica gel (Bon 2017). The potential application of MOFs in solar cells, super capacitors, adsorbent chillers, heat pumps and thermal energy storage have been reported in several studies (Henninger et al. 2010, Canivet et al. 2014, Elsayed et al. 2017, Bon 2017). Table 2 - 8 provides some MOFs with the characteristic values including pore volume and maximum water uptake.

Table 2 - 8 Schematic structure and characteristic values of MOFs

MOFs	Schematic structure	Metal nodes	Pore volume (cm^3/g)	Maximum water uptake (kg_{H2O}/kg)	References
MIL-100 (Al/Fe)	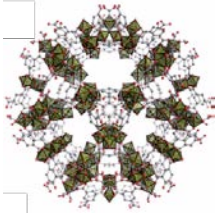	Al^{3+}/Fe^{2+}	1.14	0.75	(Jeremias et al. 2012)
Al-fumarate	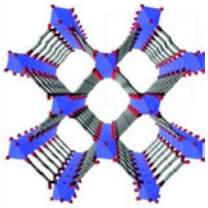	Al^{3+}	0.48	0.45	(Jeremias et al. 2014a, 2014b, Henninger et al. 2017)
MIL-101Cr	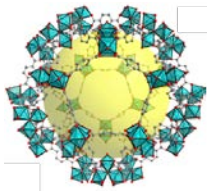	Cr^{3+}	2.02	1.43	(Tanh Jeazet et al. 2013, Ehrenmann et al. 2011)
HKUST-1	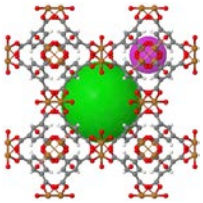	Cu^{2+}	0.72	0.55	(ChemTube3D 2017)
CPO-27(Ni)	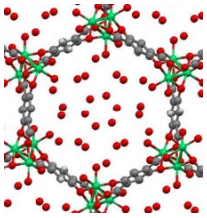	Ni^{+}	0.21	0.47	(Elsayed et al. 2017, Gallo et al. 2013)

Jeremias et al. (2012) reported the appealing characteristic of MIL100(Al, Fe). It presents the ability of absorbing up to 0.75 g water vapour per 1 g material. Additionally, relatively high hydrothermal cyclic stability has been found with the capacity reduced about 2% and 6% after 20 and 40 cycles, respectively. Interesting results have been reported in an experimental study on the water

adsorption and cyclic performance of the MOFs, HKUST-1 and MIL-100Fe (Rezk et al. 2012). Utilising a gravimetric dynamic vapour sorption analyser, HKUST-1 has shown a 93.2% increase in water vapour uptake compared with that of silica gel (evaporating temperature at 5 °C). However, HKUST-1 has exhibited significant thermal instability with the hysteresis between adsorption and desorption. Additionally, MIL-100Fe has shown a 33% reduction in water uptake compared with that of silica gel at the evaporating temperature of 5 °C but an improved performance at the evaporating temperature of 12 °C. In a recent simulation study (ul Qadir et al. 2017), a multi-walled carbon nanotube/MIL-100Fe composite adsorbent has been applied in a solar adsorption chiller. A maximum cooling power of 455 W/kg and coefficient of performance of 3.9 have been reported for the chiller with the composite adsorbent. The findings can serve as a potential support for the replacement of the adsorbents such as silica gels, activated carbons and zeolites.

According to the current studies, MOFs are still on a material and laboratory scale but have shown promising potential. The advantages and challenges of MOFs are stated as follows.

The advantages of MOFs are:

- MOFs have an exceptionally high porosity, uniform pore geometry and large surface area (up to 5500 m^2/g) (Basdogan and Keskin 2015); and
- High water adsorption capacity reported from 0.45 to 1.43 $kg_{H2O}/kg_{material}$ (Huo and Yan 2012, Rezk et al. 2012).

The challenges of MOFs are:

- Some MOFs such as HKUST-1 and Zr-MOF have shown thermal instability with significant hysteresis between the adsorption and desorption (Rezk et al. 2012); and other studies have reported a significant decrease in water uptake capacity after adsorption (Küsgens et al. 2009, Janiak and Henninger 2013, Canivet et al. 2014);

- To achieve higher heat and mass transport in heat pumps or chillers, MOFs adsorbents require to be shaped into 100 - 200 μm thickness; but the preparation procedures are scarce (Jeremias et al. 2014a).
- Thermal properties of MOFs are limited such as thermal conductivity, heat capacity, thermal stability; and
- There is limited study on the performance of MOFs in thermal energy storage technologies.

2.4.2.3 Zeolites

Zeolites, commonly used as commercial adsorbents and catalysts, are microporous aluminosilicate minerals. The general formula of a zeolite is (Wright 2008, Yang 2003):

$$M_{x/n}^{n+} Al_x Si_{1-x} O_2 \cdot yY$$

In the formula, M is the extra-framework charging-balancing cation and Y is the species such as water molecules in each unit cell. The structure of zeolite can be considered as the frameworks comprising corner-sharing silicate and aluminate tetrahedra.

Zeolites either naturally exist in nature or can be synthesised. There are about 40 types of natural zeolites and 150 types of artificially synthesised zeolites (Cabeza et al. 2017). Due to molecular sieve properties and cation-exchange ability, natural zeolites have been used as adsorbents in separation and purification including removing hardness and heavy metals of acid waters, high cation exchange, water retention, etc. (Sun et al. 2016, Motsi et al. 2009, Wang and Peng 2010). Regarding artificially synthesised zeolites, different arrangements have led to numerous possibilities. Zeolites created by ion replacement with different sizes and charges can improve their storage properties. For thermal storage applications studies are normally focused on synthesised zeolites. The major zeolites are 4A, 5A, 10X, 13X and Y (Yu et al. 2013). Figure 2 - 21 depicts the framework structure of zeolite A and Y (Wang et al. 2009).

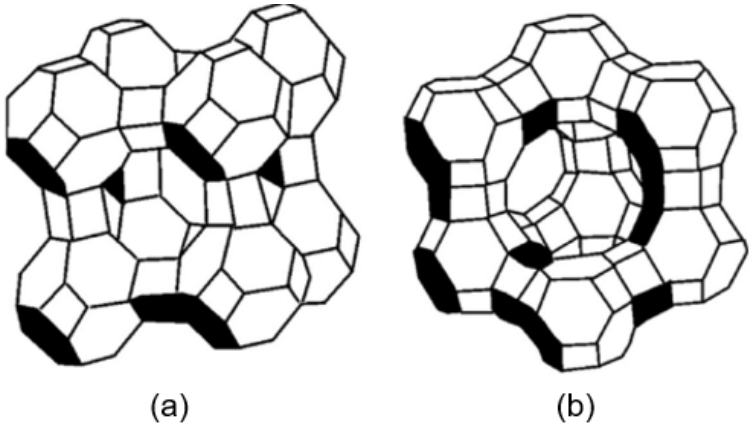

Figure 2 - 21 (a) Crystal cell of zeolite A and (b) zeolite X/Y (Wang et al. 2009)

Zeolites, especially types 13X and 4A, have been receiving interest in heat storage purposes due to the relatively high water uptake, promising adsorption temperature, fast reaction kinetics and cyclic stability (Jänchen et al. 2012, Mette et al. 2014b). Table 2 - 9 summaries some key characteristics of zeolites types investigated. The water uptake of the zeolite types can achieve over 0.20 kg_{H2O}/kg. For the adsorption temperature, Mette et al. (2014b) have reported that the maximum discharge temperature lift is dependent on the humidity of the air flow. During the experiment, zeolite 13X has achieved adsorption temperature at 68 °C with inlet air flow at 35 °C and a water vapour pressure at 15 mbar. Similar results have also been reported in other studies (Jänchen et al. 2004, Gantenbein et al. 2008).

Table 2 - 9 A summary of characteristics of zeolite types

Zeolite types	Maximum water uptake (kg_{H2O}/kg)	Average heat of adsorption (kJ/kg_{H2O})	Specific heat (kJ/(kg·K)	Energy density (kJ/kg)	References
4A	0.22	4400	1.05	1250	(Demir et al. 2008)
	0.21	4000	n.a.	530	(Zettl et al. 2014)
5A	0.22	4180	1.05	1200	(Demir et
10A	0.20	4000	n.a.	897	al. 2008)
13X	0.32	5000	0.88	n.a.	(Mette et al. 2014b)

However, relatively lower energy density of zeolites has been reported in several studies, ranging from 100 kWh/m^3 to 163 kWh/m^3 depending on the study conditions (N'Tsoukpoe et al. 2009, Rebecca et al. 2016). Figure 2 - 22 gives a comparison of zeolites, SAPOs, AlPOs and MOFs with regards to water uptake and different desorption temperature (Henninger et al. 2010). Noticeably, zeolites with different cations require a relatively high charging temperature to achieve a desired water uptake. For a low charging temperature less than 95 °C, zeolites have shown no increase or even smaller amount of water uptake compared with silica gel. When increasing the desorption temperature to 140 °C, the water uptake of zeolite Li-Y and zeolite LaNa-Y has been increased by 71%. With regards to AlPO-18 and SAPO-34, they have shown great potential in water uptake performance. At the low desorption temperature, water uptake of SAPO-34 and AlPO-18 is about 2 and 4 times higher respectively than silica gel. For the Cu-BTC, as a class of MOFs, a sample shows the highest water uptake capacity at about 324 $g_{H2O}/kg_{material}$ for desorption temperature at 140 °C.

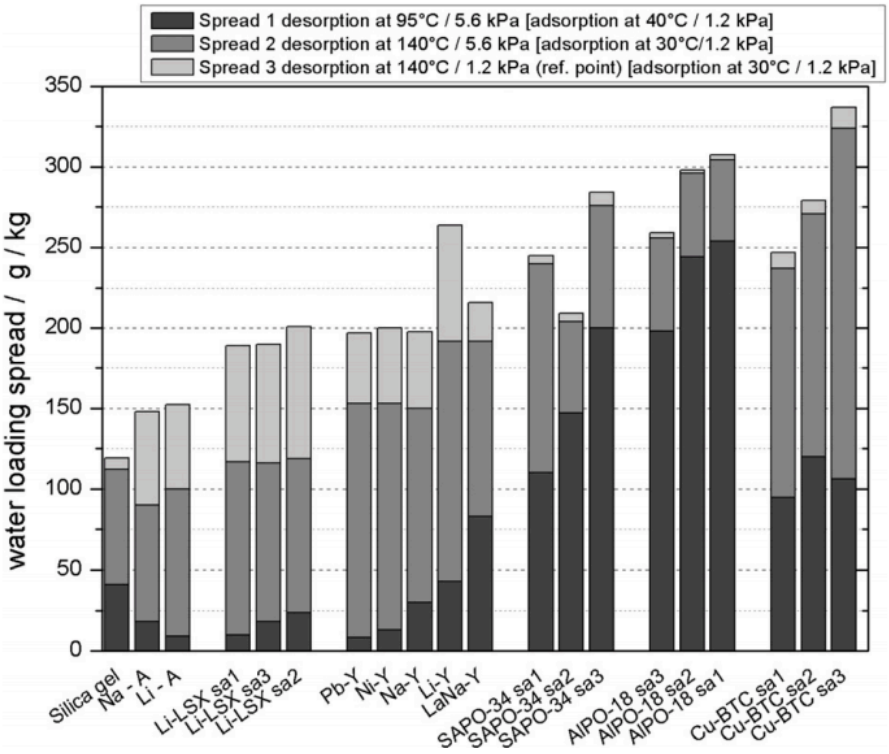

Figure 2 - 22 Water uptake of thermochemical materials (Henninger et al. 2010)

2.4.3 Composite thermochemical materials

To improve the performance of solid absorption materials, recent research in thermochemical material has led to composite materials. In literature, the composite materials are called composite salt porous matrix (CSPM) or salt in matrix (SIM) (Aristov 2007). It is called selective water sorbets (SWS) when the sorbate is water (Henninger et al. 2012, Freni et al. 2012, Aristov et al. 2000). Figure 2 - 23 illustrates the interaction between water and a composite material. A composite material consists of at least two materials of which one is a host matrix (such as silica gel, zeolite, alumina, aerogel, expanded natural graphite and expanded vermiculite); the other can be an inorganic salt (such as LiCl, $CaCl_2$, $MgCl_2$, $MgSO_4$, and $LiNO_3$). The inorganic salt is placed inside the pores of the host matrix (Okunev et al. 2008). The approaches to producing composite materials can be mixture, impregnation, and consolidation (Wang et al. 2009, Tian et al. 2012). There are three mechanisms taking place when water contacts the host matrix (Gordeeva et al. 2009). The first is the chemical reaction between

the salt and water. The second is the liquid absorption and sorbate transport. The third is the liquid adsorption on the surface of the host matrix.

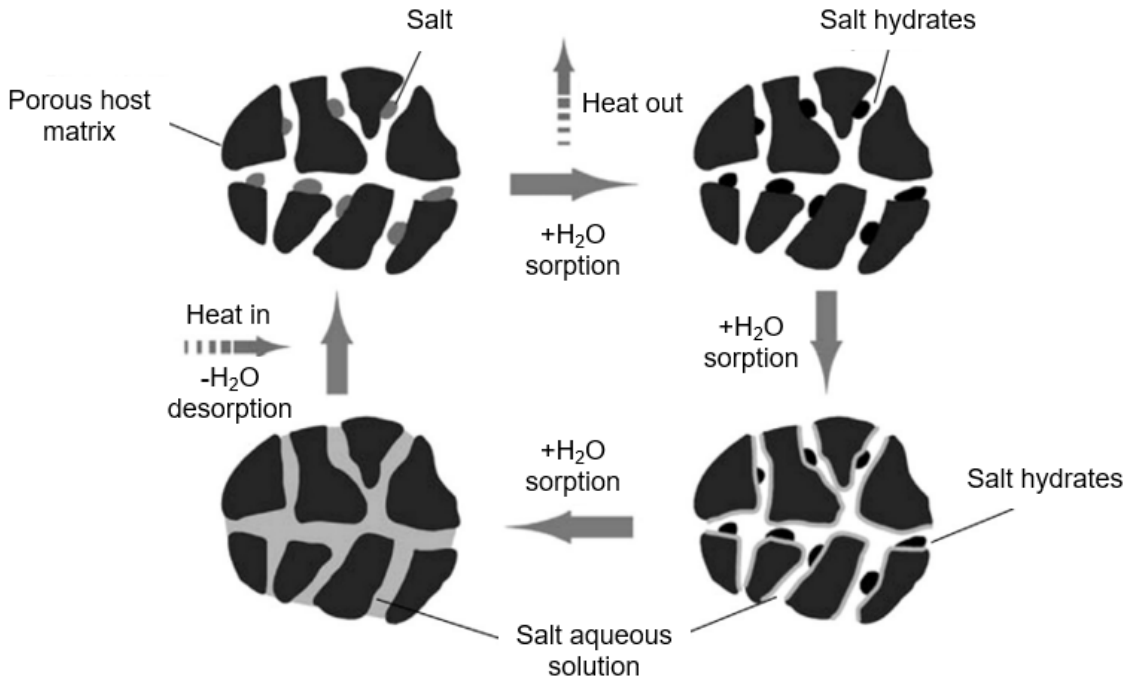

Figure 2 - 23 Water absorption mechanism on salt (Aristov 2007)

Advantages of the composites in comparison with the pure salt hydrates and solid adsorption are:

- Thermal conductivity improvement compared to pure salt hydrate;
- Theoretical energy storage density improvement compared to solid adsorption materials such as zeolites and silica gel;
- Stability enhancement in hydration/dehydration cycles; and
- Create the potential for matching targeted system operating conditions and perform optimum performance.

The improvement in thermal conductivity is because of the increase in surface area (Fopah Lele et al. 2015, Aydin et al. 2015). Table 2 - 10 gives the properties of some promising matrices (Aydin et al. 2015). Noticeability, the specific surface area of activated carbon is superior to the other materials, about twice that of silica gel. However, the required charging temperature of active carbon is over

150 °C. For the composites, an experiment on expanded natural graphite with $CaCl_2 \cdot nNH_3$ shows the thermal conductivity can increase to over 7 W/(m·K) (Wang et al. 2006). Thermal conductivity at 7.65 W/(m·K) has been reported in the study of a composite formed by $SrBr_2$ and expanded natural graphite (Zhao et al. 2016). In terms of metal form, in an experiment, the thermal conductivity of a composite has increased from 1 W/(m·K) to about 20 W/(m·K) by using 20% aluminium of the total composite mass (Askalany et al. 2017).

Table 2 - 10 Comparison of some host matrix (Aydin et al. 2015)

	Specific surface area (m^2/g)	Pore volume (cm^3/g)	Charging temperature (°C)	Thermal conductivity (W/m·K)	Cost (£/kg)
Vermiculite	8 - 10	2.8	50 - 80	0.064	0.16 - 33
Silica gel	750 - 850	1	130 - 150	0.174	0.67 - 1.01
Zeolite	550 - 600	0.17	> 200	0.2 - 0.4	1.25 - 1.67
Activated carbon	1500 - 1700	2	150 - 180	0.15 - 0.5	0.38 - 3.8
Expanded natural graphite	18 - 22	0.073	100 - 200	24 - 470	1.37 - 1.9
Activated alumina	150 - 300	44	160 - 220	1.4 - 2.5	0.74 - 1.25

Table 2 - 11 summarises some latest studies in composite materials for thermochemical energy storage. The composite shows improvement in energy density, stability and adaptability in system operating conditions. Hongois et al. (2011) have tested the hydration and dehydration cycles of a composite, $MgSO_4$ 15 - 25 wt% integrated in zeolite 13X, for long-term thermal storage. The results from thermogravimetric analysis (TGA) and differential scanning calorimetry (DSC) have shown that almost 80% of the water content in the composite can be dehydrated at 150 °C. During sorption, the temperature lift at 30 °C has been

reached. A volumetric energy density of the composite has been measured at 0.6 GJ/m^3 which is 47% more than that of zeolite 13X. For the cyclic stability, micro-calorimetry measurements have shown that the energy density remains at this level for 3 hydration/dehydration cycles. In another study conducted by Yu et al. (2015), a composite is developed by using activated carbon as host matrix, mixing with expanded natural graphite to improve heat transfer and adding silica solution to enhance mechanical strength. Additionally, to integrate the energy storage in variable heat sources (Jiang et al. 2017), a multilevel composite combined with $MnCl_2$, $CaCl_2$ and NH_4Cl has been investigated. Apart from the improvements in pure solid absorption materials, however, research in composite thermochemical materials is currently at the material level. The current studies are to find suitable composite materials for suitable application temperature, hydrothermal stability, energy density, reaction kinetics, etc.

Table 2 - 11 A summary of the latest studies on composite thermochemical energy storage materials

Studies	Study aim	Matrix	Salt	Energy storage density (kWh/m^3)	Hydration, dehydration temperature (°C)	Findings
(Hongois et al. 2011)	Characterisation of zeolite/$MgSO_4$ composite	Zeolite 13X	$MgSO_4$ 15 - 25 wt%	166	20, 150	• Optimum percentage of $MgSO_4$ is 15 wt%. • Energy density remains at the reported level for over 3 cycles.
(Zamengo et al. 2013)	Enhance thermal conductivity of $Mg(OH)_2$	Expanded graphite	$Mg(OH)_2$	n.a.	120, 400	• Thermal conductivity has been improved from 0.2 to 0.4 W/(m·K). • The composite has shown a constant performance for 24 cycles.
(Zhang et al. 2016)	Characterisation the hydration and dehydration of $SrBr_2$/Vermiculite	Vermiculite	$SrBr_2$, 10 - 40 wt%	105.36	50, 211	• Water uptake has been improved from 0.3 kg_{H2O}/kg of $SrBr_2$ to 0.53 kg_{H2O}/kg of the composite.
(Courbon et al. 2017)		Silica gel	$SrBr_2$ 58 wt%	203	20 - 80, 170	• The composite provides relatively high energy density storage at 203 kWh/m^3. • It performs stable for over 14 cycles.

(Jabbari-Hichri et al. 2017)	Hydrothermal characteristics of $CaCl_2$ in the three host matrices.	Silica gel, alumina, and bentonite	$CaCl_2$	576 - 746 kJ/kg	n.a., 150	• Silica gel/$CaCl_2$ has shown the best performance in water uptake (0.27 kg_{H2O}/kg) and energy storage density (746 kJ/kg). • Silica gel is suggested as a better host matrix compared with alumina and bentonite.
(Yu et al. 2015)	Search and prepare the suitable matrix for LiCl as heat storage purposes	Activated carbon as host matrix, expanded graphite and silica solution as binders	LiCl	n.a.	n.a., 180	• Activated carbon has been reported as a better choice of host matrix for LiCl compared with silica gel. • The thermal conductivity of the composite has been reached at 2.83 W/m·K, 14 times higher than that of loose packed activated carbon/LiCl.
(Jiang et al. 2017)	Investigate the sorption characteristics of bi-salt and tri-salt composites	Expanded graphite	$MnCl_2$+$CaCl_2$+NH_4Cl, $CaCl_2$+NH_4Cl	1802 - 1949 kJ/kg	n.a., 180	• The multilevel composites have shown the potential for energy storage of variable heat sources.

2.4.4 Liquid sorption thermochemical materials

Table 2 - 12 illustrates the theoretical energy storage density, required charging temperature and price of some liquid/gas thermochemical materials (Hui et al. 2011, N'Tsoukpoe et al. 2009, N'Tsoukpoe, KE Edem et al. 2012). The LiCl, LiBr and KOH solutions stand out in their high energy storage density. However, the price of the LiCl and LiBr solutions are 14 times higher than that of the $CaCl_2$ solution. For $CaCl_2$ solution, the energy storage density is relatively low at 119 kWh/m^3. Additionally, for the NH_3/H_2O, the energy storage system should operate at high pressure (610 kPa) compared with the that of the $LiCl/H_2O$, $LiBr/H_2O$, $NaOH/H_2O$ and KOH/H_2O (Hui et al. 2011). Considering the relatively high pressure, the design of NH_3/H_2O system should be conducted properly to avoid leakage. In addition to solar energy storage, the working pair NH_3/H_2O has also been applied in electricity load shifting with a diurnal energy storage system for cooling in summer, heating in winter or providing with domestic hot water (Xu et al. 2007). However, a low energy density has been calculated at 34.8 kWh/m^3.

It is hard to achieve the temperature required for residential application, being one major drawback of liquid sorption. The main reasons are relatively low energy output and low concentration difference of solution between sorption and desorption. For energy output, it is closely linked to the solution flow rate. According to a numerical study of a solar heat storage system using LiBr (N'Tsoukpoe, KE Edem et al. 2012), a low solution flow rate in desorption can lead to insufficient regeneration of the solution; however, when the flow rate is too high, the heat provided to the solution mainly contributes to the increase of solution temperature rather than the desorption process. An optimum flow rate at 0.006 L/s has been identified in the study. For the absorption process, the solution flow rate should be as low as possible with sufficient distribution to the heat exchange. In terms of solution concentration difference between sorption and desorption, it should be maintained below 10% to avoid crystallisation in strong solution (Yu et al. 2014). However, energy storage ability of liquid sorption technology owes to the solution concentration difference of sorbate attached to sorbent in sorption and desorption processes. In the absorption experiment

(N'Tsoukpoe, Kokouvi Edem et al. 2012), low concentration difference at only 1% to 1.7 wt% solution concentration change has been achieved; the achieved absorption temperature has been recorded at around 30 °C. Additionally, to improve the energy storage density, crystallisation in salt solutions during the storage phase has been suggested (Yu et al. 2014). N'Tsoukpoe et al. (2013) have developed and investigated a closed system that allows crystallisation within the salt solution storage tank. However, the crystallisation management in desorption and solution flow is key which increases the system complexity and requires further investigation.

Table 2 - 12 Theoretical energy storage density and reaction temperature of liquid/gas thermochemical materials (Hui et al. 2011)

Thermochemical materials	Theoretical energy density (kWh/m^3)	Charging temperature (°C)	Price (£/kg, purity ≥ 99%)
$LiCl(solution)/H_2O$	400	154	5.06
$LiBr(solution)/H_2O$	313	72	4.22
$KOH(solution)/H_2O$	313	63	1.01
$NaOH(solution)/H_2O$	154	50	2.53
$CaCl_2(solution)/H_2O$	119	44.8	0.29
$H_2O(solution)/NH_3$	98	155.5	0.34

2.4.5 Conclusions for the review on thermochemical energy storage materials

A review of thermochemical energy storage materials has been conducted. These materials have been reported as promising in thermochemical energy storage, such as $SrBr_2$ (N'Tsoukpoe et al. 2016, Lele 2015), $MgCl_2$ (Zondag et al. 2010) and $CaCl_2$ (Edem N'Tsoukpoe et al. 2015. In the review, characteristics of the materials have been presented including theoretical energy storage density, water uptake capability, adsorption and desorption temperature, cyclic stability and related issues in applications.

With regards to chemical reaction/solid absorption materials, the main advantage is the relatively high theoretical energy density, ranging from 480 - 780 kWh/m^3. However, drawbacks of the materials can limit their performance in hydration/dehydration cycles, including melting at 48 - 52 °C ($MgSO_4$), overhydration ($CaCl_2$ and $MgCl_2$), slow reaction kinetics ($CuSO_4$ and $MgSO_4$), and toxicity or formation of toxic products (Na_2S, $MgCl_2$, and $CuSO_4$).

Adsorption materials are more hydrothermally stable. However, the energy density is relatively lower ranging from 100 - 280 kWh/m^3. The energy density is closely linked to water uptake capacity and desorption temperature (Henninger et al. 2010). AlPOs, SAPOs and MOFs have a promising water uptake capacity and require lower desorption temperature than zeolites. However, research on these materials is at the material level and system cost can be significant. Zeolites are commercially available and, especially for zeolite 13X and 4A, have been investigated as promising thermochemical materials (Janchen et al. 2015, Kerskes et al. 2012, Mette et al. 2014a).

When it comes to composite materials, finding a suitable host matrix and salt hydrate pairs is critical. To solve the issues of salt hydrates, improvements have been reported in thermal conductivity, stability and adaptability of application conditions. However, the research on composites is at the material scale. Investigation of composites performance in system level under practical climate conditions should be conducted.

For liquid sorption materials, the main issue is that with the desorption temperature it is hard to achieve the required temperature for domestic heating. Energy density can be increased by allowing solution crystallisation in the storage step, whilst investigation is due to be conducted in the increased system complexity and crystallisation management in desorption and fluid flow.

In total, different thermochemical energy storage materials have advantages and drawbacks. To find the most suitable material for the current study,

considerations should be made on material characteristics and background of the application including climate conditions and achieving target.

2.5 Selection of a thermochemical energy storage material

According to the review of the currently used thermochemical energy storage materials, this section illustrates the selection of the most suitable material for this study. This study formulates a 2 step selection to achieve the goal. The first step focuses on the safety, price and availability of a potential material. The second step is to further locate the most suitable thermochemical material according to the intended application and available resources. In this study, targeting the building application, especially space heating, it covers energy density of a material, application charging and discharging temperatures, and considers durability in charging and discharging operation cycles.

In order to illustrate the selection clearly, Table 2 - 13 presents the selection criteria and three-point score principle. Scores from 1 to 3 have been given to the potential materials according to their characteristics illustrated in the review. A score of 3 shows that a material meets the criteria. A score of 2 means that a material meets the criteria, but it may perform inferior to another material in that aspect. Whilst a score of 1 is for a material that cannot meet the criteria unless taking significant measures to mitigate a risk. Figure 2 - 24 presents the material selection using the criteria and scores.

In the first step of the selection, the materials such as $SrBr_2$, $MgCl_2$, Na_2S and $CuSO_4$ have been eliminated since toxic products (H_2S or HCl) can be formed in sorption/desorption cycles or the material can cause skin irritation. SAPOs, MOFs and composites have been excluded because of their low availability and high price. Composites aim to overcome the issues of salt hydrates, but most of the studies has been focusing on the materials. Researches are ongoing to find a suitable host matrix and salt hydrates pairs for different conditions. When it comes to the second step, considerations have been taken on the factors including energy storage density, applicable charging and discharging temperature, and

other issues in the applications such as cyclability and reliability. Specifically, with respect to energy storage density, Figure 2 - 25 shows the desorption temperature with the energy density as reported in literature. Salt hydrates provide relatively high theoretical energy density ranging from 600 kWh/m^3 to 800 kWh/m^3. However, partly due to their own issues and inconveniences as stated, the achieved energy density in some studies significantly falls from the theoretical values to about 230 kWh/m^3 (N'Tsoukpoe et al. 2009). With regards to liquid sorption materials, although allowing solution crystallisation in the storage step can be developed (Yu et al. 2014, N'Tsoukpoe et al. 2013), crystallisation management requires in-depth investigation, adding to the system complexity. For solid adsorption materials like zeolites, energy density around 200 kWh/m^3 has been achieved in some experiments (Rebecca et al. 2016, Tatsidjodoung et al. 2016), and a relatively higher desorption temperature from 150 °C to 180 °C is applicable (Henninger et al. 2010). Zeolites also show fast reaction kinetics, good cyclic stability and suitable adsorption temperature for domestic heating. Therefore, according to the considerations, zeolites are the most promising materials for the current study.

Table 2 - 13 Thermochemical material selection criteria and scores

Note: The selection criteria are conducted according to Table 2 - 6, Table 2 - 11, Section 2.4.2, and Section 2.4.4.

Thermochemical materials	1st material selection criteria		2nd material selection criteria		
	Safety	Price and availability	Energy density	Applicable charging and discharging temperature	Durability
$MgSO_4$	1	3	3	3	1
$MgCl_2$	1	3	3	3	1
Na_2S	1	2	3	3	1
$CuSO_4$	1	2	3	3	1
$CaCl_2$	1	2	3	3	1
Na_2S	1	3	3	3	1
$SrBr_2$	1	2	3	3	1
$LaCl_3$	1	1	2	3	1
AlPOs, SAPOs, MOFs	-	1	2	3	-
Zeolites	3	3	2	3	3
Composites	3	1	2	3	2
Liquid materials like LiCl solution	1	1	2	2	2

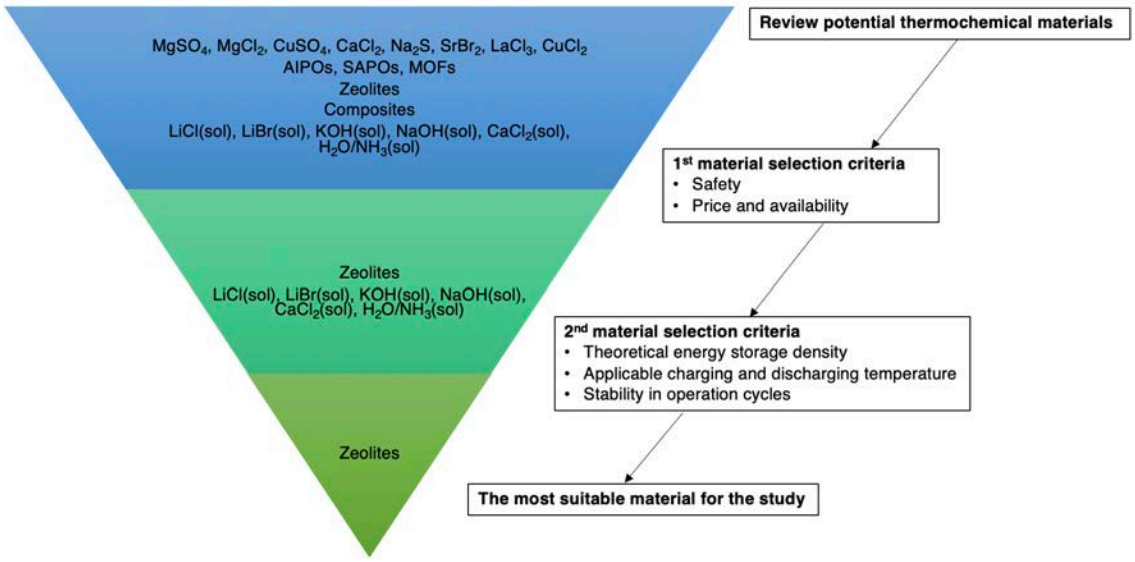

Figure 2 - 24 Thermochemical energy storage material selection framework

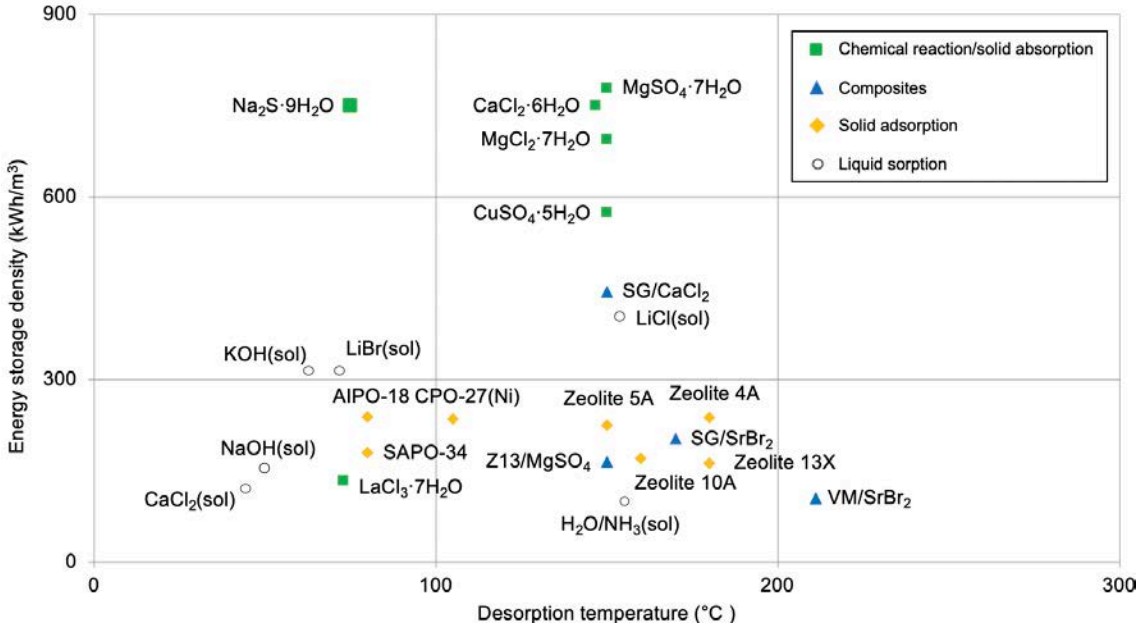

Figure 2 - 25 Comparison of the reviewed materials with regards to energy density and desorption temperature

2.6 Chapter summary

This chapter has presented the current status of thermochemical energy storage as applied in buildings. With respect to the thermochemical reactor, researchers aim to develop a reactor with high energy storage density along with effective heat and mass transfer. For the open reactors, it is seen that the novel geometry design, effective interaction between reactants, and reactor segmentations are the effective methods to improve the reactor performance. For the closed reactors, the reviewed studies have shown a wider selection of thermochemical materials and variable operation conditions. However, the reactor studies have revealed the challenges in heat losses, inadequate heat and mass transfer, and charging and discharging performance.

The chapter has also reviewed the thermochemical materials including chemical reaction, solid adsorbents, composites and liquid sorption materials. Different thermochemical energy storage materials have advantages and drawbacks. It has found that the chemical reaction materials such as $MgSO_4$ stand out in the theoretical energy density ranging from 480 kWh/m^3 to 780 kWh/m^3. However, the issues are overhydration ($CaCl_2$ and $MgCl_2$), producing toxic gases (Na_2S and $MgCl_2$), and melting at a low temperature ($MgSO_4$). With the liquid sorption materials such as $CaCl_2$ solutions it is difficult to achieve the required domestic heating temperature. The composite materials have been presenting some promising results, but the research is to develop the suitable host matrix and salt hydrate pairs. Adsorption materials are hydrothermally stable with a relatively smaller energy density from 100 kWh/m^3 to 280 kWh/m^3. To select the suitable material, the study has formulated the material selection criteria from being easy to handle to the charging and discharging temperatures. It has selected zeolites as the thermochemical material for the study.

With the conducted review, this study is to carry out a theoretical study of a thermochemical reactor.

CHAPTER 3: THEORETICAL STUDY OF A THERMOCHEMICAL REACTOR

3.1 Overview

This chapter presents the theoretical study of a thermochemical reactor applied in residential buildings. It starts with a thermochemical energy storage system with a heat source, energy storage section, and heat and moisture supply section. Then it goes deeper into the reactor and presents the mathematical conversation equations and theoretical foundations of the heat and mass transfer.

3.2 Thermochemical energy storage as applied in residential buildings

Figure 3 - 1 presents an open thermochemical energy storage system applied in residential buildings. There are three components in the system including heat source, storage and moisture supply, and heat supply. The heat source is comprised of solar collectors such as parabolic troughs. For the storage sector, the main component is the thermochemical reactor. For the heat supply sector, air and water supply are integrated in the system.

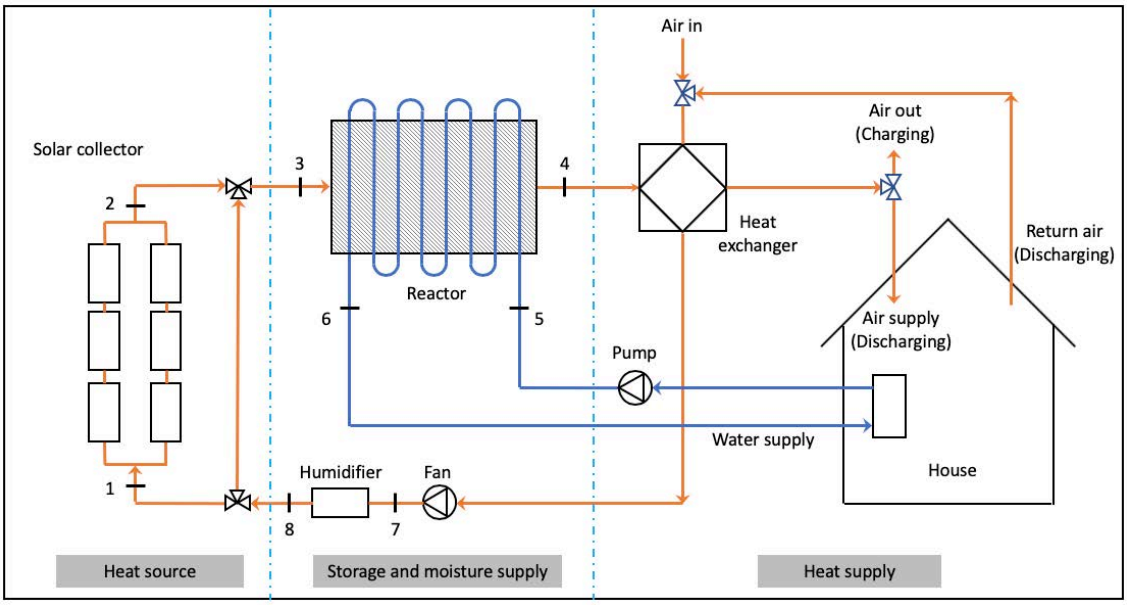

Figure 3 - 1 Schematic of the proposed thermochemical energy storage system

With respect to the operation, in charging, the adsorbent dehydrates with the assist of the solar collectors. In sunny times, the solar collectors heat the air by absorbing solar radiation (Bellos et al. 2016, Good et al. 2014). The air then flows to the reactor when it reaches to the charging temperature. The adsorbent increases temperature and releases water vapour which is extracted by the air flow. The air from the reactor flows through a heat exchanger where it preheats the inlet air before it leaves to the environment. The process is endothermic and allows energy to be stored in the reactor.

In this case, the solar collectors generate thermal energy $\dot{Q_{hs}}$ to the air flow. A part of the energy losses in the distribution to the reactor $\dot{Q_{loss,2\to3}}$. A part of the energy transfers to the storage section $\dot{Q_{st}}$. A part is the energy loss through the reactor air outlet $\dot{Q_{loss,outlet}}$. The equation can be given as follows:

$$\dot{Q_{hs}} = \dot{Q_{loss,2\to3}} + \dot{Q_{st}} + \dot{Q_{loss,outlet}} \qquad 3.\ 1$$

where the energy generated by the heat source is:

$$\dot{Q_{hs}} = \dot{m_a} \cdot c_{p,a} \cdot \left(T_{a,2} - T_{a,1}\right) \qquad 3.\ 2$$

The distribution energy loss involves conduction and convection through duct walls, which reduces the air flow temperature. The energy loss is given as follows:

$$\dot{Q}_{loss,2\to3} = \dot{m}_a \cdot c_{p,a} \cdot \left(T_{a,2} - T_{a,3}\right) \quad 3.\ 3$$

For the energy transferred to the storage section $\dot{Q}_{st}$, in charging, it includes the energy stored by the adsorbent, sensible heat gain and energy loss of the storage section.

$$\begin{aligned} \underbrace{\dot{Q}_{st}}_{Energy\ transferred\ to\ reactor} &= \underbrace{Q_{sen}}_{Sensible\ heat\ transfer\ to\ reactor} \\ &+ \underbrace{\dot{Q}_{loss,char}}_{Energy\ loss\ through\ reactor\ to\ ambient\ in\ charging} \\ &+ \underbrace{\dot{Q}_{ads}}_{Adsorption\ energy\ stored\ by\ the\ adsorbent} \end{aligned} \quad 3.\ 4$$

The sensible heat transfer of the storage section is the sensible energy accumulated in the reactor, adsorbent and water.

$$Q_{sen} = Q_{rct} + Q_s + Q_w \quad 3.\ 5$$

The Q_{rct} is the sensible energy accumulated in the reactor components such as the reactor containers, metal water pipes and adsorbent. It can be calculated by the relevant mass, specific heat capacity, and the temperature difference between the component and the ambient.

$$\begin{aligned} Q_{sen} = m_{rct} \cdot c_{p,rct} \cdot \left(T_{rct,char} - T_{amb}\right) + m_s \cdot c_{p,s} \cdot \left(T_{s,char} - T_{amb}\right) \\ + m_w \cdot c_{p,w} \cdot \left(T_{w,char} - T_{amb}\right) \end{aligned} \quad 3.\ 6$$

For energy loss from the reactor to ambient $\dot{Q}_{loss,char}$, convection and radiation heat transfer are considered.

$$\underbrace{\dot{Q}_{loss,char}}_{Energy\ loss\ from\ the\ reactor\ to\ ambient\ in\ charging} = \underbrace{h_{rct} \cdot A_{rct} \cdot \left(T_{rct,char} - T_{amb}\right)}_{Energy\ loss\ of\ reactor\ \ via\ convection} + \underbrace{e \cdot \sigma \cdot A_{rct} \cdot \left({T_{rct,char}}^4 - {T_{amb}}^4\right)}_{Energy\ loss\ of\ reactor\ via\ radiation} \quad 3.7$$

For the adsorbents, the energy transferred to the adsorbent leads to the removal of water from the adsorbent to the air flow. The energy stored in the adsorbent $\dot{Q_{ads}}$ can be calculated by the multiplication of the enthalpy of adsorption ΔH, the rate of water uptake $\dot{X}$, and the adsorbent mass.

$$\dot{Q_{ads}} = \left(\underbrace{H_{X=X_0-\dot{X_{char}}\cdot t,\ \ t=t_{char}} - H_{X=X_0,\ \ t=0}}_{Enthalpy\ of\ adsorption}\right) \cdot \underbrace{\dot{X_{char}}}_{rate\ of\ water\ uptake} \cdot \underbrace{m_s}_{Adsorbent\ mass} \quad 3.8$$

The enthalpy of adsorption of the adsorbent is a function of water uptake. Relatively more energy is stored in the adsorbent material when it becomes dry. $H_{X=X_0,t=0}$ represents the thermodynamic potential at the initial charging state when $t = 0$ and the adsorbent water uptake is $X = X_0$. When the charging time increases to $t = t_{char}$, the water uptake reduces to $X = X - \dot{X_{char}} \cdot t_{char}$ with the rate of water uptake at $\dot{X}_{char}$. The corresponding thermodynamic potential becomes $H_{X=X_0-\dot{X}_{char}\cdot t,\ \ t=t_{char}}$. The change in thermodynamic potential or enthalpy is the enthalpy of adsorption. The fundamentals enthalpy of adsorption is illustrated in section 3.4.5.

With respect to the air taken out the water vapour from the adsorbent, the absolute humidity ϕ increases with the removal of water from adsorbent,

$$\underbrace{\dot{X} \cdot m_s}_{Rate\ of\ water\ removed\ from\ the\ adsorbent} = \underbrace{\left(\phi_{a,4} - \phi_{a,3}\right)}_{Change\ of\ absolute\ humidity\ of\ air\ flow} \cdot \underbrace{\dot{m}_a}_{Mass\ flow\ rate\ of\ air} \cdot 0.001 \quad 3.\ 9$$

where the absolute humidity of air at the inlet of the reactor equals to the ambient.

$$\phi_{a,3} = \phi_{a,amb} \quad 3.\ 10$$

Therefore, the absolute humidity of air flow leaving the reactor is

$$\phi_{a,4} = \phi_{a,3} + \frac{\dot{X} \cdot m_s}{\dot{m}_a} \cdot 1000 \quad 3.\ 11$$

Once a charging process reaches to a final state, the reactor is isolated from the ambient except for the heat transfer to the ambient. The heat loss in between a charging and discharging process can be considered as heat loss $Q_{loss,char \rightarrow dischar}$.

$$\dot{Q}_{loss,char \rightarrow ddischar} = \underbrace{h_{rct} \cdot A_{rct} \cdot \left(T_{rct,char} - T_{amb}\right)}_{Energy\ loss\ of\ reactor\ via\ convection} + \underbrace{e \cdot \sigma \cdot A_{rct} \cdot \left({T_{rct,char}}^4 - {T_{amb}}^4\right)}_{Energy\ loss\ of\ reactor\ via\ radiation} \quad 3.\ 12$$

where $T_{rct,char}$ is the temperature at the end of the charging process.

In cold times, when the end user requires space heating, the stored energy can be released through the rehydration of the thermochemical material using the water vapour of the air flow passing through the reactor. Shown in Figure 3 - 2, moisture can be provided by the humidifier and added into the air flow. The humid air flows to the reactor where the exothermic reaction takes place. The released adsorption heat is extracted from the reactor by the air and water flow depending on the operational strategy. Additionally, the air from the house can be taken to the system to achieve relatively higher reactor inlet air temperature.

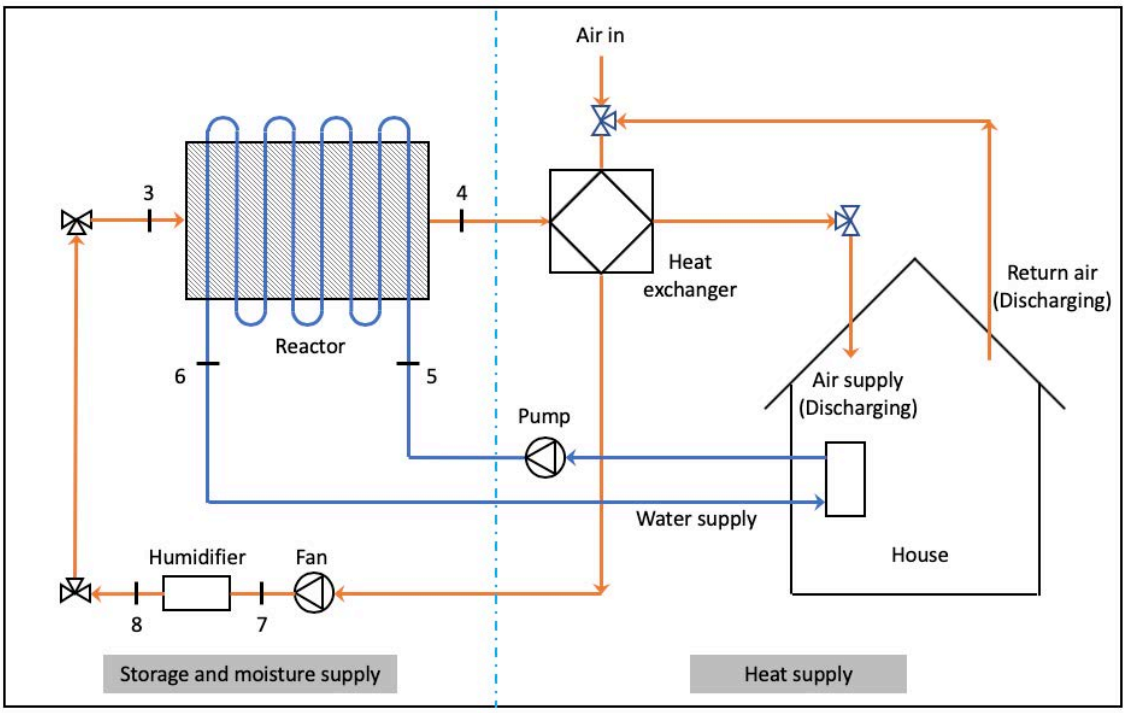

Figure 3 - 2 The thermochemical energy storage system in discharging

The adsorption process takes place where adsorption energy is released from the adsorbent material. The energy can be transferred to the air flow, water flow, the reactor, and energy loss to the ambient, given as the following equation:

$$\dot{Q_{ads}} = \dot{Q_a} + \dot{Q_w} + Q_s + Q_{rct} + \dot{Q_{loss,dischar}} \qquad 3.\ 13$$

where the adsorption energy release Q_{ads} is because of the change of enthalpy of adsorption. It can be described by using the enthalpy of adsorption, rate of water uptake in discharging, and the adsorbent mass in equation.

$$\dot{Q_{ads}} = \underbrace{\left[H_{X=X_0-\dot{X}_{char}\cdot t_{char},\ t=0} - H_{X=X_0-\dot{X}_{char}\cdot t_{char}+\dot{X}_{dischar}\cdot t,\ t=t_{dischar}}\right]}_{Enthalpy\ of\ adsorption} \cdot \underbrace{\dot{X_{dischar}}}_{Rate\ of\ water\ uptake} \cdot \underbrace{m_s}_{Adsorbent\ mass} \qquad 3.\ 14$$

Theoretically, the water uptake remains constant between charging and discharging. Thus, the water uptake is $X = X_0 - \dot{X}_{char} \cdot t_{char}$ at the beginning of the discharging when $t = 0$. During discharging, the water uptake of the adsorbent increases with the rate at $\dot{X_{dischar}}$. At discharging time $t = t_{dischar}$, the water uptake has increased to $X = X_0 - \dot{X}_{char} \cdot t_{char} + \dot{X}_{dischar} \cdot t$.

The adsorption energy transfers to the air flow, solid adsorbent, water, and reactor components flow via heat conduction and convection, which can be expressed as follows.

$$\dot{Q_a} = \dot{m_a} \cdot c_{p,a} \cdot \left(T_{a,4} - T_{a,3}\right) \quad 3.\ 15$$

$$Q_s = m_s \cdot c_{p,s} \cdot \left(T_{s,dischar} - T_{amb}\right) \quad 3.\ 16$$

$$Q_{rct} = m_{rct} \cdot c_{p,rct} \cdot \left(T_{rct,dischar} - T_{amb}\right) \quad 3.\ 17$$

Regarding the water flow, when switching on the water pump, the adsorption heat transfers to water, via the water metal pipe, and can be expressed as follows.

$$\dot{Q_w} = \dot{m_w} \cdot c_{p,w} \cdot \left(T_{w,6} - T_{w,5}\right) \quad 3.\ 18$$

Additionally, convection and radiation heat transfer are considered for the energy loss from the reactor to the ambient.

$$\dot{Q_{loss,d}} = h_{rct} \cdot A_{rct} \cdot \left(T_{rct,dischar} - T_{amb}\right) + e \cdot \sigma \cdot A_{rct} \cdot \left({T_{rct,dischar}}^4 - {T_{amb}}^4\right) \quad 3.\ 19$$

For the mass transfer, the humidifier supplies the moisture to the air flow which then transfers to the adsorbent.

$$\Delta\phi_{humidifier} = \phi_{a,3} - \phi_{amb}$$
$$\left(\phi_{a,3} - \phi_{a,4}\right) \cdot \dot{m_a} \cdot 0.001 = \dot{X_{dischar}} \cdot m_s \quad 3.\ 20$$

Therefore, the absolute humidity of air flow leaving the reactor $\phi_{a,4}$ is

$$\phi_{a,4} = \phi_{a,3} - \frac{\dot{X_{dischar}} \cdot m_s}{\dot{m_a}} \cdot 1000 \quad 3.\ 21$$

3.3 Reactor evaluation parameters

The reactor can be evaluated by various indicators in literature depending on the facilities and operational conditions (Aydin 2016). In literature, reactor evaluation parameters are in various aspects to describe the suitability for a specific application such as energy density, achieved temperature in discharging, cost, thermal power, system size and scalability (Scapino et al. 2017). Since this

project focuses on the reactor in charging and discharging, the conversion of heat and mass are of significance. For the heat conversion, in both charging and discharging, the stored adsorption heat and released useful heat are supplied by the heat source in charging. In terms of mass conversion, the actual moisture transfer is initiated by the tendency to reaching the equilibrium. Therefore, this project applies energy conversion efficiency (ECE) and extent of adsorption (EOA) to evaluate the heat and mass transfer for the charging and discharging of the reactor.

With respect to the heat transfer, in charging, part of the energy from the heat source converts to the adsorption energy stored in the adsorbent. For a charging process, the energy conversion efficiency (ECE_{char}) is defined as the ratio of adsorption energy to the energy provided by the heat source.

$$ECE_{char} = \frac{\dot{Q_{ads}}}{\dot{Q_{hs}}} \times 100\% \qquad 3.\ 22$$

In discharging, part of the energy from the adsorption energy is supplied to the end user as useful heat, represented by the sum of $\dot{Q_w}$ and $\dot{Q_a}$. In a discharging process, the energy conversion efficiency ($ECE_{dischar}$) is defined as the ratio of the useful heat to the energy provided by the heat source.

$$ECE_{dischar} = \frac{\dot{Q_a} + \dot{Q_w}}{\dot{Q_{hs}}} \times 100\% \qquad 3.\ 23$$

The ratio $ECE_{dischar}$ is more inclusive than using the ratio of useful heat to the stored adsorption heat as it involves the heat conversion starting from the heat source (Kuznik et al. 2019, Gondre 2017).

Regarding the mass transfer, the extent of adsorption (EOA) is used to describe the adsorption advancement. As shown in Figure 3 - 3, when the adsorbent is in a complete hydration state, the EOA is defined as 100%. At the other end of the process, the EOA is 0% when the adsorbent is in dehydration.

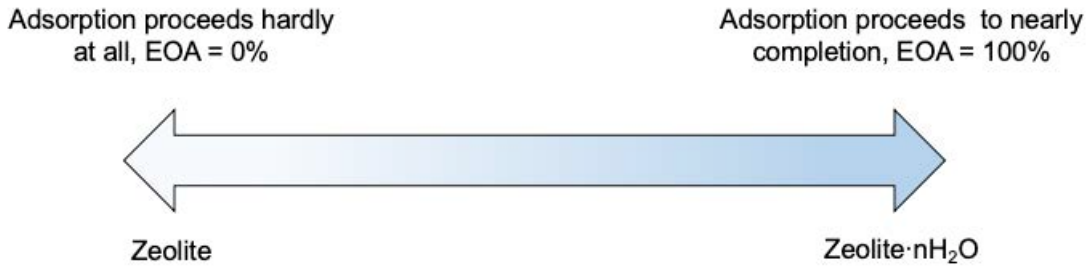

Figure 3 - 3 Illustration of the extent of adsorption

The EOA can be calculated by the actual amount of mass transfer to the charging equilibrium and the maximum mass transfer that can be achieved, as given in 3. 24.

$$EOA = \frac{\left(X_t - X_{eq,char}\right) \cdot m_s}{\left(X_{eq,dischar} - X_{eq,char}\right) \cdot m_s} \times 100\% \qquad 3.\ 24$$

The maximum amount of mass transfer is determined by the water uptake at EOA 100% and EOA 0%. For the adsorbent in equilibrium with discharging and charging conditions, the water uptake is $X_{eq,dischar}$ and $X_{eq,char}$, respectively. The maximum amount of mass transfer for the adsorbent mass m_s is $\left(X_{eq,dischar} - X_{eq,char}\right) \cdot m_s$. For a charging or discharging process, the actual water uptake X_t can be obtained and the amount of mass transfer to the charging equilibrium is $\left(X_t - X_{eq,char}\right) \cdot m_s$.

3.4 Fundamental elements of the reactor theoretical study

This section presents definitions of key elements in the reactor theoretical study, including porosity, effectively fluid velocity, adsorption kinetics, adsorption equilibrium and enthalpy of adsorption of zeolite 13X.

3.4.1 Porosity

The porosity ε of a porous media is the fraction of the volume of voids over the total volume of the medium. ε_{bed} is the bed macroscopic porosity. It represents

the fraction of the volume of voids outside of zeolite particles over the volume of adsorbent bed (Tatsidjodoung et al. 2016).

$$\varepsilon_{bed} = 0.39 \qquad 3.\ 25$$

Different from the bed macroscopic porosity, $\varepsilon_{particle}$ is the particle mesoscopic porosity. Generally, an adsorbent particle consists of relatively smaller primary particles. The mesoscopic porosity is focused on the volume of voids inside the zeolite particles (Ergun 1952).

$$\varepsilon_{particle} = 0.32 \qquad 3.\ 26$$

The total volume which can be occupied by air flow is the total porosity ε (Solmus et al. 2012).

$$\varepsilon = \varepsilon_{bed} + (1 - \varepsilon_{bed}) \cdot \varepsilon_{particle} \qquad 3.\ 27$$

3.4.2 Effective fluid velocity

For a porous medium, the effective fluid velocity can be considered as the volumetric flow rate divided by the cross-sectional area. The effective fluid velocity is also called superficial velocity. It can be determined by Darcy's equation (Daïan 2014b).

$$\overrightarrow{u_a} = -\frac{K}{\mu} \cdot \overrightarrow{grad}(P) \qquad 3.\ 28$$

Here, $\overrightarrow{grad}(P)$ is the pressure gradient in the air flow direction, K is the permeability of the adsorbent bed, and μ is the dynamic viscosity of the air flow.

Darcy's equation is valid when the Reynolds number of the fluid is in the range of 10 (Fanchi 2002). The Reynolds number is calculated by the fluid density ρ_a (1.2 kg/m^3), dynamic viscosity μ (1.8E-5 N·s/m^2), superficial velocity and characteristic length l.

$$Re = \frac{\rho_a \cdot u_a \cdot l}{\mu} \qquad 3.\ 29$$

Although it is complicated to calculate the velocity and characteristic length, an estimation of this can be given to calculate the range of the Reynolds number. With respect to the porous medium, the fluid air flows through the interstices between the adsorbent particles and also flows into a particle. The Reynolds number achieves maximum for the flow between particles since both the velocity and characteristic length are larger than the flow within a particle. The estimated Reynolds number is around 11, which is suitable for using Darcy's equation.

The permeability depends on the geometry of the porous medium. Kozeny and Carman have presented the following equation to calculate the permeability of porous media (Daïan 2014b).

$$K = \frac{d^2 \cdot {\varepsilon_{bed}}^3}{180 \cdot (1 - \varepsilon_{bed})^2} \qquad 3.\ 30$$

where ε_{bed} is the bed porosity and d is the average adsorbent particle diameter. The constant 180 has been obtained to provide the best fit with experimental tests. According to the studies, the Carman-Kozeny equation provides reasonable permeability estimates for periodic packs of spheres (Kärger 1996) and random packing of spheres (Valdes-Parada et al. 2009).

The dynamic viscosity of air μ represents its resistance to shearing flows. Since the dynamic viscosity of air at 180 °C is 40% higher than that of 20 °C, its dependence to air temperature cannot be assumed to be negligible. The correlation in equation 3. 31 has been used to calculate the value (Kuznik et al. 2019).

$$\mu(T_a) = 4.564 \times 10^{-8} \times T_a + 4.745 \times 10^{-6} \qquad 3.\ 31$$

3.4.3 Adsorption kinetics

As presented earlier, during an adsorption process, adsorbate molecules attach to the external surface of the adsorbent, followed by the internal diffusion of the adsorbate moving into the micropores. Adsorption kinetics is used to describe the rate of the adsorption (Largitte and Pasquier 2016), which can be achieved

through different mathematical expressions such diffusion model and linear driving force (LDF) model.

Compared to the linear driving force (LDF) model, the diffusion model is more rigorous to describe adsorbate transport within the adsorbent particle (Sircar and Hufton 2000). It is able to describe the local rates of adsorption at the particle level. However, it is complex and requires more computing resources (Gondre 2017). The LDF model is simple and analytical for the adsorption process. Although the LDF model cannot describe the local rates of adsorption at particle level, the investigation in the microscopic scale is beyond the scope of the project. The LDF model is used in this project for adsorption kinetics since it provides physical consistency and it is frequently used for practical analysis (Sircar and Hufton 2000).

The LDF model, originally proposed by Glueckauf and Coates (1947), gives the rate of water uptake in equation 3. 32,

$$\frac{dX}{dt} = k_m \cdot (X_{eq} - X_t) \qquad 3.\ 32$$

where X_{eq} is the equilibrium water uptake of adsorbent at time t in terms of air water vapour pressure and adsorbent temperature T_s; X_t is the actual water uptake of zeolite at time t. The coefficient k_m is the effective LDF mass transfer coefficient which is obtained from experimental data (Glueckauf 1955) with a function of adsorbent particle radius r and diffusivity D_e.

$$k_m = 15\frac{D_e}{r^2} \qquad 3.\ 33$$

The equivalent diffusivity can be expressed as (Gondre 2017):

$$D_e = D_0 \cdot exp\left(-\frac{E_{act}}{RT_s}\right) \qquad 3.\ 34$$

where D_0 is the reference diffusivity and E_{act} is the activation energy (Tatsidjodoung et al. 2016).

3.4.4 Adsorption equilibrium

Adsorption data is commonly presented in the form of adsorption isotherms. An adsorption isotherm is used to describe when a quantity of gas or vapour is adsorbed by a porous media under a constant temperature and adsorbate pressure. Isotherms can be divided into 5 forms, known as Types I to V, as given in Figure 3 - 4 (Brunauer et al. 1940).

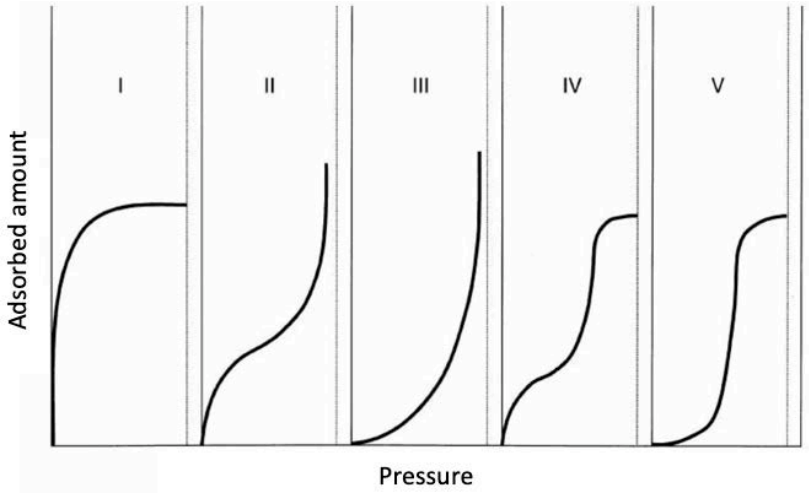

Figure 3 - 4 Types of equilibrium isotherms (Brunauer et al. 1940)

Type I isotherm is applicable to the formation of a single monolayer of adsorbate on the adsorbent surface (Thomas and Crittenden 1998). The isotherm is observed when the pore sizes of adsorbent are not much larger than the adsorbate molecule diameter. Types II and III isotherms are observed when adsorbents have a wide range of pore sizes (Gondre 2017). They do not exhibit a saturation limit. Adsorbate forms successive layers leading to capillary condensation in the large pores which displays a higher adsorption capacity. For Type III isotherm, adsorbate and adsorbent are relatively weak and it shows a convex curve with respect to the partial pressure axis (Donohue and Aranovich 1998). Type IV isotherm is similar to Type II isotherm, but the adsorption completes near to the relative pressure of unity. Type V isotherm is similar to Type III isotherm and saturation is observed at a point when the relative pressure is increased.

Corresponding to the adsorption isotherm, a variety of isotherm equations have been proposed such as the Langmuir isotherm (Liu 2006), the Freundlich isotherm (Foo and Hameed 2010), the BET theory (Brunauer et al. 1938), Polanyi's potential theory (Hutson and Yang 1997), etc. For the application of zeolite and water vapour, the Dubinin-Astakhov (DA) equation has been used and validated in a number of studies (Mette et al. 2014b, Semprini et al. 2017, Oh et al. 2017, Wu et al. 2009).

The Dubinin-Astakhov (DA) equation has been adopted from Polanyi's potential theory where an essential parameter is A_{ad}, given by (Hutson and Yang 1997):

$$A_{ad} = R_w T_s ln\left(\frac{P_0}{P_w}\right) \qquad 3.\ 35$$

where P_w is the partial water vapour pressure, P_0 is the saturation pressure, and R_w is the specific gas constant of water vapour.

The equation is built on the adsorption to be a process of volume filling, arriving at the following expression:

$$W = W_0 exp\left[-\left(\frac{A_{ad}}{E_{ad}}\right)^n\right] \qquad 3.\ 36$$

where W_0 is the maximum adsorption volume and W is the volume that can be filled when the relative pressure is P_w/P_0. E_{ad} is the characteristic energy of adsorption; n is heterogeneity factor related to pore distribution.

The water uptake at equilibrium state, defined as the ratio of the mass of the adsorbate water adsorbed to the mass of the dry adsorbent zeolite at an equilibrium state, is calculated by the equation:

$$X_{eq} = \rho_{H2O} \cdot W \qquad 3.\ 37$$

where ρ_{H2O} is the density of the adsorbed water and W is the specific volume to be adsorbed.

The water density calculation has been reported by several equations in literature (Nikolaev and Dubinin 1958, Semprini et al. 2017, Cook and Basmadjian 1964,

Krese et al. 2018). In selection of the density equation, Nagel et al. (2015) have reported that for energy storage application, a general mathematical expression for an accurate fit of experimentally observed curve should be applied. For this study, the density model is given as the equation 3. 38 (Mugele 2005) since it has been observed experimentally (Mette et al. 2014b) and reported to perform well in the comparative analysis study of different adsorbate density models (Nagel et al. 2015).

$$\rho_{H2O} = \frac{\rho_{20C}}{1 + \beta_{20C} \cdot (T_s - 293.15)} \qquad 3.\ 38$$

where the ρ_{20C} is the moisture density at 20 °C and β_{20C} is the thermal expansion coefficient of water vapour at 20 °C.

3.4.5 Enthalpy of adsorption

The surface of most adsorbent material, including zeolites, is heterogeneous which leads to the variable adsorption energy (Chiou 2003). The adsorption starts from the highest-energy sites to the lowest-energy sites. The force field within an adsorption site that attracts a water molecule varies significantly with the location. Thus, the net enthalpy of adsorption decreases with the increasing water uptake in the adsorbent. According to Chiou (2003), a vapour will condense to form a liquid adsorbate when the porous adsorbent is exposed to increasing partial pressure of a vapour. As shown in Figure 3 - 5, the condensation takes place at the highest potential sites until the adsorption potential becomes zero and the adsorption space is filled as the ambient pressure becomes saturated.

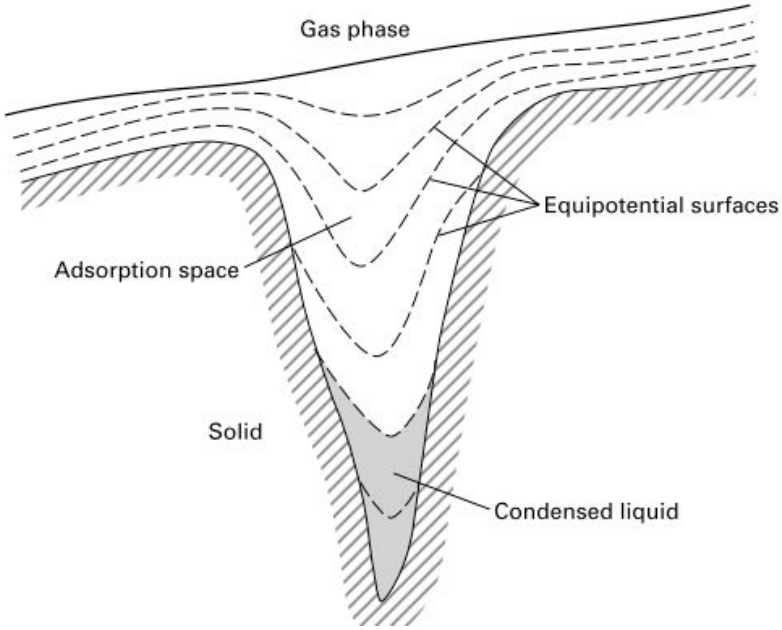

Figure 3 - 5 Schematic illustration of a porous region (Chiou 2003)

An adsorption process can involve the formation of intermolecular forces, hydrogen bonding and covalent forces (Beta et al. 2004, Ooms et al. 1988). For a vapour at a given equilibrium, when the vapour is condensed as a liquid adsorbate, the net enthalpy of adsorption is the sum of heat of evaporation of the liquid and the heat of adsorption due to the potential energy change of adsorption (Kim et al. 2016, Rahman et al. 2013). When the adsorption reaches the maximum of the adsorbent, the adsorption heat is zero and the enthalpy of adsorption equals to the heat of adsorbate condensation. Using the differential scanning calorimetry (DSC) and thermogravimetric analyser (TGA), Kim et al. (2016) have obtained the enthalpies of adsorption of various adsorbents including zeolite 13X. Figure 3 - 6 depicts the correlation between the enthalpy of adsorption and water uptake of zeolite 13X. Using the polynomial fitting of the study (Kim et al. 2016), enthalpy of adsorption can be given in the following equation.

$$H = 7 \times 10^7 X^6 - 7 \times 10^7 X + 3 \times 10^7 X^4 - 7 \times 10^6 X^3 + 899951 X^2 - 69983 X + 6491.3 \quad 3.\ 39$$

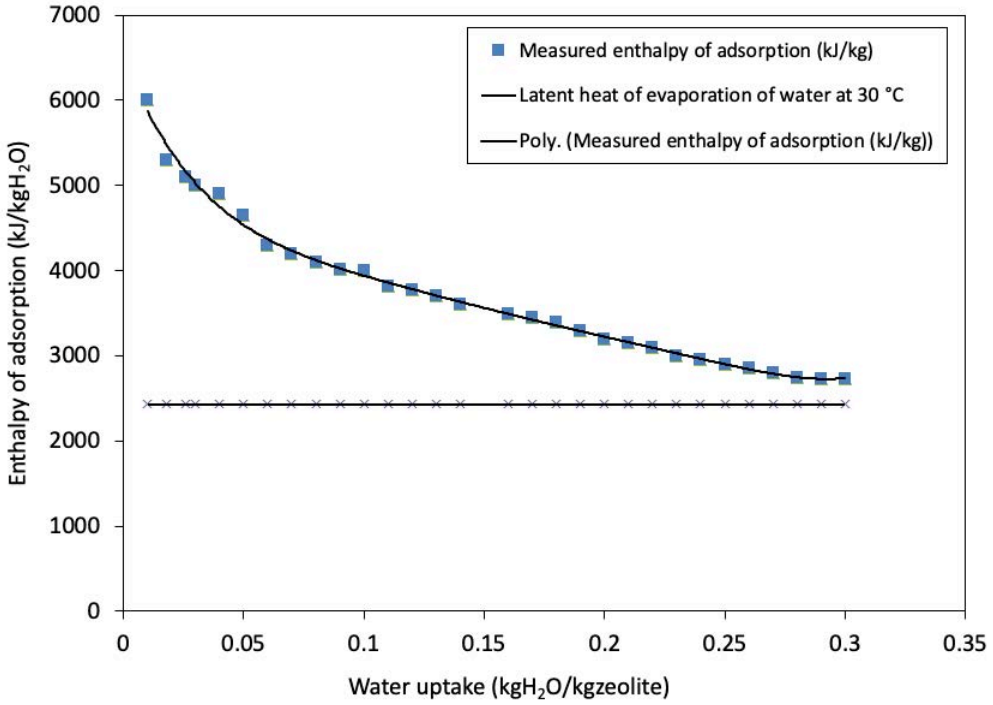

Figure 3 - 6 Enthalpy of adsorption as a function of water uptake of the adsorbent zeolite 13X (latent heat of evaporation of water at 30 °C at 2430 kJ/kg) (Kim et al. 2016)

3.5 Chapter summary

This chapter covers the theoretical overview of the reactor for heating applications in residential uses. Focusing on the reactor of the thermochemical energy storage system, it illustrates heat and mass transfer conversation equations of the reactor in charging and discharging processes. For the reactor evaluation, the chapter defines energy conversion efficiency (ECE) and extent of adsorption (EOA) as the key evaluation parameters. From the point of view of macroscopic volume, the chapter presents the expressions of adsorption kinetics where the LDF model is used for the physical consistency and simplicity. This chapter has also presented the types of adsorption isotherm and the application of the Dubinin-Astakhov (DA) equation for zeolite 13X and vapour adsorption. It has illustrated the theoretical basis of enthalpy of adsorption and gives a correlation of enthalpy of adsorption as a function of water uptake for zeolite 13X. The chapter provides theoretical foundation for developing a numerical model of a thermochemical reactor which is presented in the next chapter.

CHAPTER 4: DESIGN AND NUMERICAL MODEL OF A THREE-PHASE THERMOCHEMICAL REACTOR

4.1 Overview

Thermochemical reactor is a vital component in a thermochemical energy storage system. This chapter proposes a three-phase thermochemical reactor and develops a numerical model of the reactor. The major work of the chapter includes the design of the three-phase thermochemical reactor development of a reactor numerical model.

4.2 Design of a three-phase thermochemical reactor

4.2.1 Structure and dimensions

With the reactor development opportunities presented in chapter 2, this study proposes a thermochemical reactor named three-phase thermochemical reactor. The critical components are thermochemical material container, water pipe and thermochemical material. Figure 4 - 1 presents illustrations of the reactor container. As shown in Figure 4 - 1(a), the container is in the trapezoid shape. To increase the hollow area for the air flowing to the container, a number of gaps have been created on the left and right side of the trapezoid container. The gaps and trapezoid shape provide a robust material support and removes the application of perforated mesh. To improve the flexibility, multiple containers can be aligned in a row or scaled up to layers according to the thermochemical material capacity. Additionally, a water pipe has been integrated in the container and immersed in the thermochemical material, as shown in Figure 4 - 1(c). The water pipe travels through the material containers from one to the other.

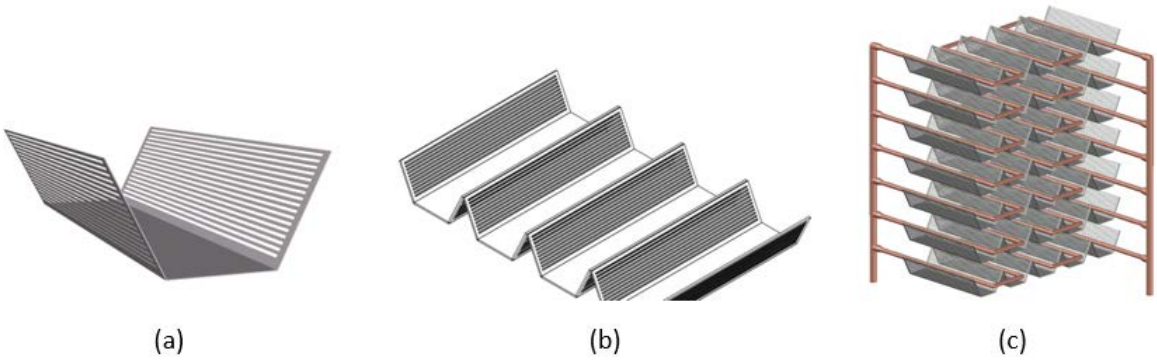

Figure 4 - 1 The reactor design: (a) the container, (b) multiple containers, (c) integration with water pipe

The dimensions of the reactor have been presented in Figure 4 - 2. The reactor container is 480 mm (length) × 100 mm (width) × 100 mm (height). The water pipe diameter is 16 mm located at the centre of the container cross section. The gap is 4 mm and the distance between any two gaps is 4 mm. The 4 mm gap is determined by the available zeolite 13X particle diameter at 5 mm to ensure the zeolite particles stay inside of the container. The distance between any two gaps is 4 mm to ensure the accuracy of the gaps during manufacturing.

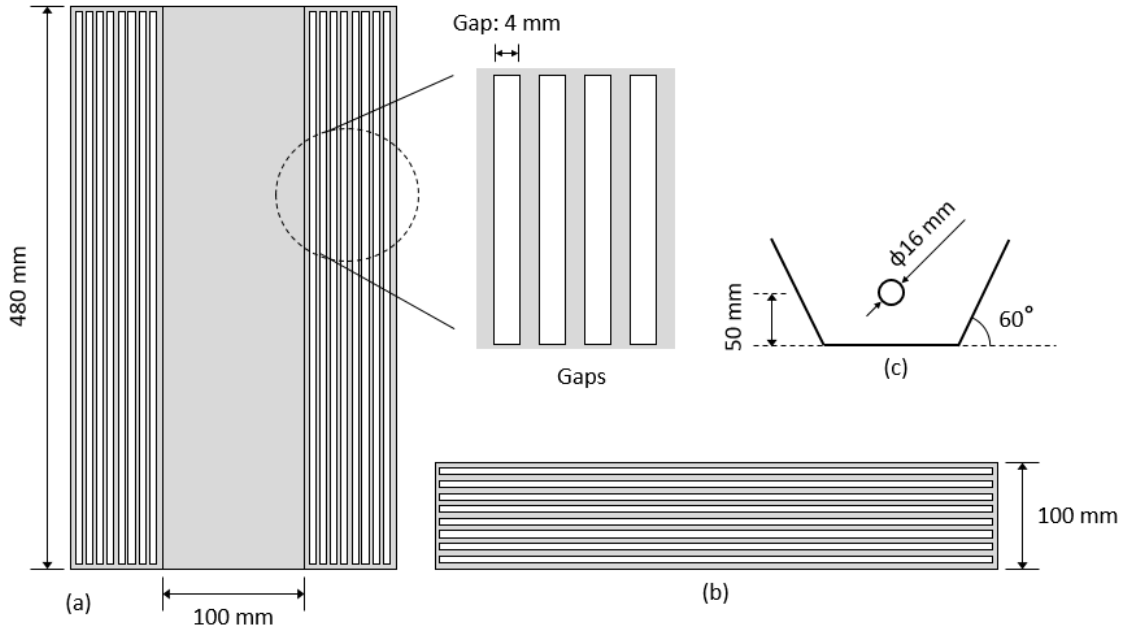

Figure 4 - 2 Reactor dimensions: (a) top view, (b) side view, (c) cross section view

To enhance the heat transfer within the reactor, fins are integrated with the water pipe, as the illustration and diameters shown in Figure 4 - 3. In the project, the reactor with and without fins are named as fin pipe reactor and smooth pipe reactor, respectively.

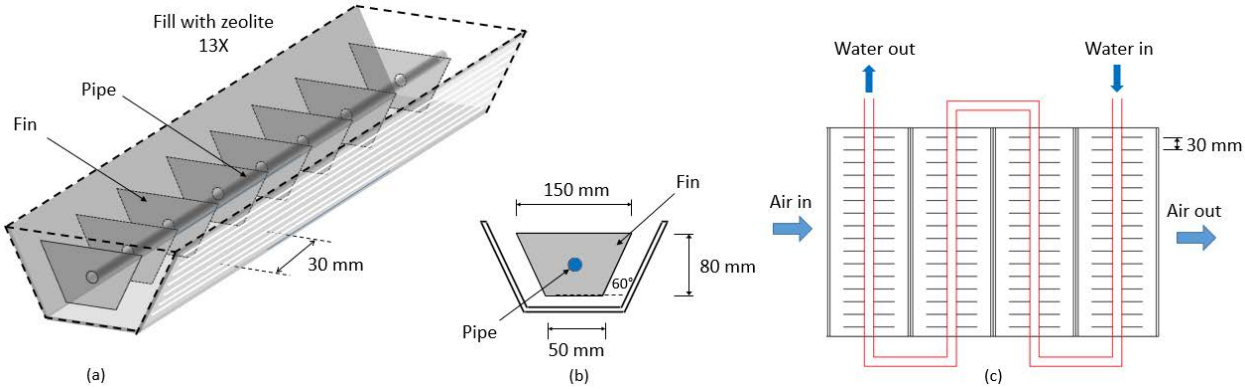

Figure 4 - 3 Illustration of the fin pipe reactor: (a) the fin pipe reactor, (b) cross section view, (c) air flow and water flow

4.2.2 Charging and discharging processes

Figure 4 - 4 depicts the air and water flow within the reactor. With respect to a charging process, when the solid adsorbent is saturated, heat is required to regenerate the material by extracting its moisture. The heated air from a heat source can be introduced to the reactor. The thermochemical material temperature dehydrates gradually as the air travels across the reactor.

In a discharging process, the air flow is to supply moisture to the material, initiating to the adsorption process. Meanwhile, the fluid pipe acts as the heat sink to extract the adsorption energy out of the reactor. As shown in Figure 4 - 4, when air flows through the reactor, moisture transfers from the air to the thermochemical material, initiating the adsorption process with adsorption energy being released from the thermochemical material. The material and air will be heated by the released adsorption energy. The air then travels to the next container. Since the air has been heated to a relatively higher temperature than that of the inlet air, in the next container the heat transfers to the solid adsorbent. The adsorbent temperature is improved due to the temperature difference

between the solid and inlet air. This leads to an improvement in the mass transfer coefficient of the solid, boosting the adsorption process. The water flow circulates through the containers, extracting the released heat. The water can either flow through the reactor containers at a certain flow rate or be stationary depending on the discharging control strategy.

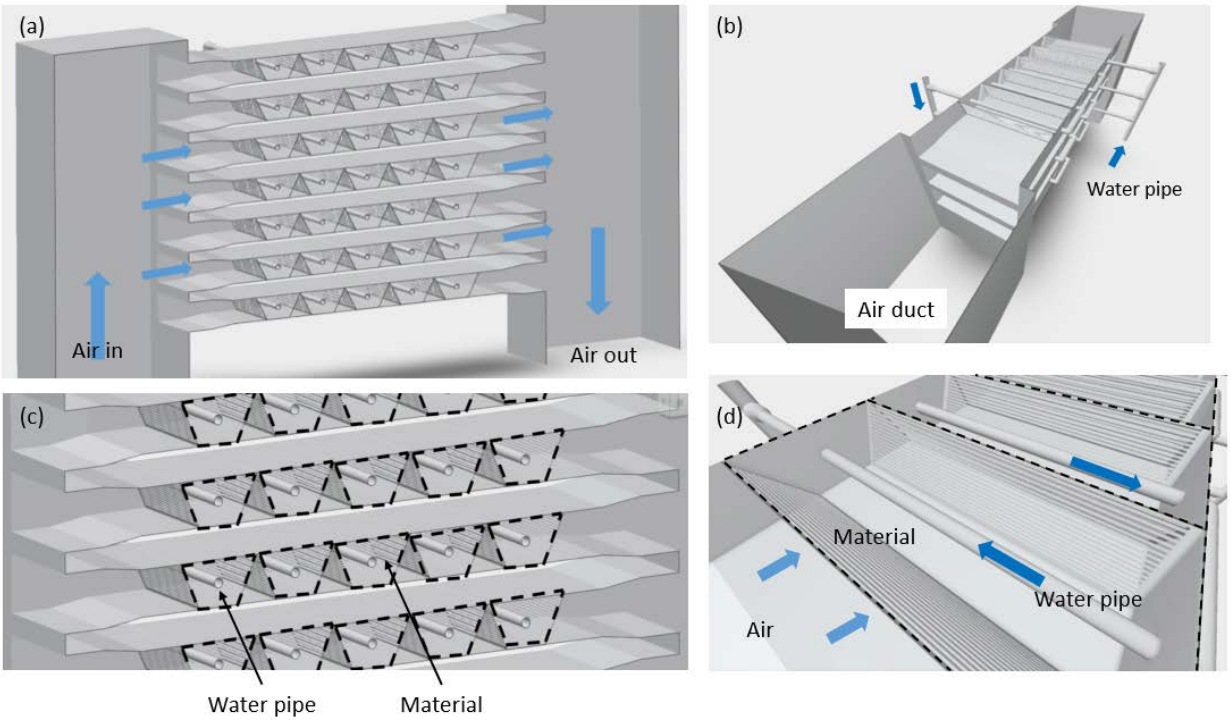

Figure 4 - 4 Cross section of the three-phase thermochemical reactor without insulation and thermochemical materials

4.2.3 Innovations and advantages of the design

The proposed reactor features several advantages which can be summarised as follows.

- The reactor container provides robust thermochemical material support and also contributes to reducing the air flow resistance.
- Fins have been integrated into the reactor to improve the heat and mass transfer within the reactor.
- The three-phase design enables the water flow to extract heat from inside of the reactor in a discharging process. The air flow can also be used as the heat sink in discharging. This enhances feasibility of the reactor.

- In between charging and discharging processes, sensible heat of the reactor can be extracted by the water flow to the end user while the thermochemical material retains the chemical potential. This contributes to reducing heat losses in a charging and discharging cycle.
- Due to the segmentation design, the reactor can be scaled up depending on the required thermochemical material volume and thermal power.

4.3 Numerical modelling

4.3.1 Calculation method

Figure 4 - 5 illustrates the calculation method of the three-phase reactor model. It consists of air flow, water flow and solid thermochemical material. “Finite element” is used to transfer the reactor into numerous “differential” divisions where equations of heat and mass balance are applied to each calculation element. As presented in Figure 4 - 5(b), the whole calculation can be assumed to be integrated with unlimited elements with respect to the water flow direction, such as i-1, i, and i+1. Then to take the air flow into consideration, the element is further divided into sub-elements, such as the j-1, j, and j+1. The size of each element is width L_1, length L_2, and height H_1. Newton iteration is used to achieve the equilibrium state of heat and mass transfer process. The equations provided in the numerical model are to be solved by using the software Matlab.

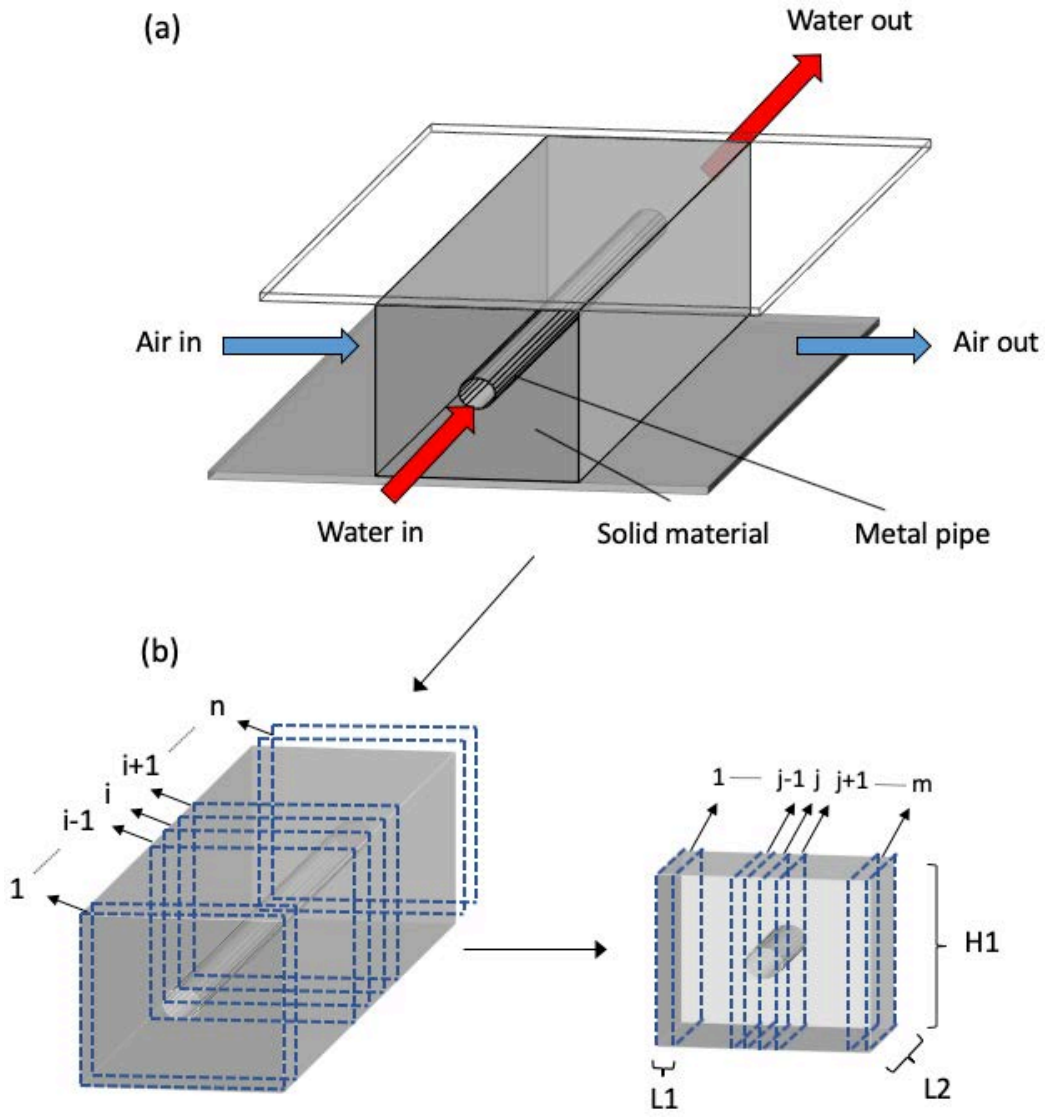

Figure 4 - 5 Illustration of the calculation method: (a) reactor illustrations (b) divisions in the calculation method

The heat transfer within the reactor is induced by temperature difference of water, air flow, and solid adsorbent. For instance, if the water temperature is higher than the adsorbent and air, heat is transferred from water to the adsorbent and air flow, as presented in Figure 4 - 6. When there is temperature difference between air flow and adsorbent, the heat transfer between the two is considered.

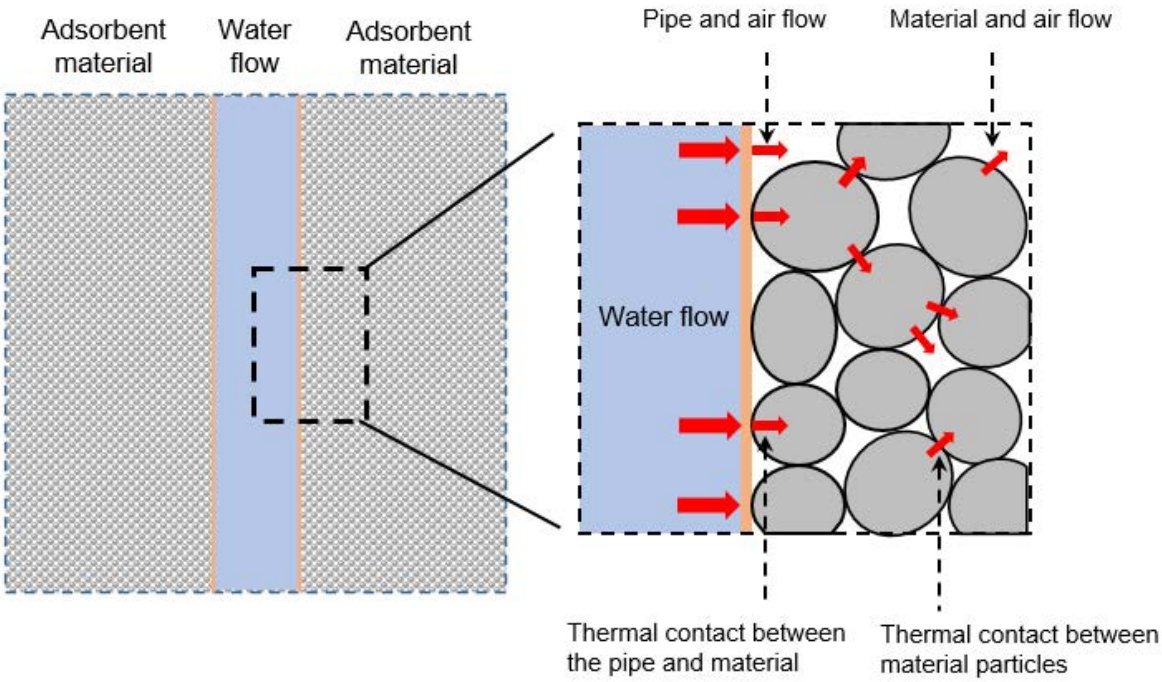

Figure 4 - 6 Heat transfer details in the reactor

To simplify the numerical simulation process, the following assumptions have been made:

- Zeolite particles share the same property in the reactor and a unique bed porosity is used in the model;
- Physical properties of zeolite such as thermal conductivity and specific heat capacity do not vary with temperature;
- Radiative heat transfer, conductive heat transfer between adsorbent particles, work done by pressure changes and viscous dissipation are neglected;
- The humid air is assumed to be ideal gas with the composition of dry air and vapour;
- The external wall of the reactor is assumed adiabatic; and
- Thermal resistance of the metal water pipe is neglected.

4.3.2 Heat transfer between solid adsorbent and air

Regarding convective heat transfer between solid adsorbent and air flow, the heat transfer rate can be written as:

$$dq_{s\to a} = \left(T_s - T_{a,in}\right)/(R_{cond} + R_{conv}) \cdot dA_{s,a} \qquad 4.\ 1$$

The thermal resistance takes account of the conductive heat transfer within an adsorbent particle and convective heat transfer between the adsorbent particle and air flow at its adsorbent surface.

An adsorbent particle, as presented in Figure 4 - 7, is covered by the adsorbent skin. Under the skin, it contains numerous microparticles shown in Figure 4 - 7(a) and (b). Any microparticle presents a distance to the adsorbent skin. Since the conductive resistance R_{cond} is determined by the microparticle conductivity λ and the distance between the microparticle and adsorbent skin, the microparticles are simplified into a mean microparticles with internal radius r and distance between the microparticle and skin y (Figure 4 - 7(c)).

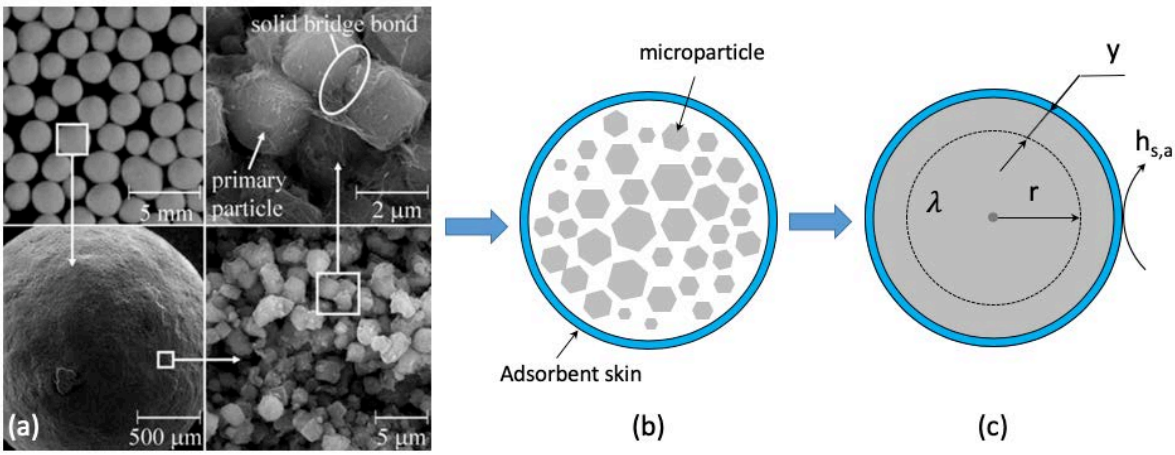

Figure 4 - 7 (a) SEM images of zeolite particles; (b) schematic of an adsorbent particle; (c) a simplified adsorbent particle with a microparticle (adopted from (Akhtar et al. 2014, Gondre 2017))

The mean distance y is calculated by assuming that the total volume of microparticles equals the space between the microparticles and the particle skin (Gondre 2017). The equation of the volume is given in equation 4. 2.

$$\frac{4}{3}\pi r^3 = \frac{4}{3}\pi\left(\frac{d}{2}\right)^3 - \frac{4}{3}\pi r^3 \qquad 4.\ 2$$

where the mean microparticles radius r can be calculated by using adsorbent particle diameter d and the distance y, i.e. $r = \frac{d}{2} - y$, therefore, the distance y can be written in the equation 4. 3.

$$y = \frac{d}{2}\left(1 - \frac{1}{\sqrt[3]{2}}\right) \quad 4.3$$

The conductive heat transfer resistance within the adsorbent particle can be written as equation 4. 4.

$$R_{cond} = \frac{y}{\lambda} = \frac{d}{2\lambda}\left(1 - \frac{1}{\sqrt[3]{2}}\right) \quad 4.4$$

In terms of the convective heat transfer coefficient $h_{s,a} = 1/R_{conv}$ for solid adsorbent and air flow. It depends on adsorbent particle diameter and air flow velocity. When the bed porosity is around 0.4, Wakao and Kagei (1982) have presented a correlation for the convective heat transfer, given in equation 4. 5.

$$\frac{h_{s,a}d}{\lambda_a} = \left(2 + 1.1Pr^{1/3}Re^{0.6}\right) \quad 4.5$$

With respect to the bed porosity ranging from 0.2 to 0.9, Kuwahara et al. (2001) have proposed a correlation which has been reported to agree well with available experiment data. The correlation has been given in equation 4. 6. Considering the relatively wider application range of bed porosity, this correlation is used in the present study.

$$\frac{h_{s,a}d}{\lambda_a} = \left(1 + \frac{4(1-\varepsilon_{bed})}{\varepsilon_{bed}}\right) + \frac{1}{2}(1-\varepsilon_{bed})^{1/2}Re^{0.6}Pr^{1/3} \quad 4.6$$

Thus the convective heat transfer resistance can be obtained and written in equation 4. 7.

$$R_{conv} = \frac{1}{h_{s,a}} = \frac{d}{\lambda_a\left(\left(1 + \frac{4(1-\varepsilon_{bed})}{\varepsilon_{bed}}\right) + \frac{1}{2}(1-\varepsilon_{bed})^{1/2}Re^{0.6}Pr^{1/3}\right)} \quad 4.7$$

Therefore the thermal resistance between air and adsorbent is written in equation 4. 8.

$$R_{cond} + R_{conv} = \frac{d}{2\lambda}\left(1 - \frac{1}{\sqrt[3]{2}}\right) + \frac{d}{\lambda_a\left(\left(1 + \frac{4(1-\varepsilon_{bed})}{\varepsilon_{bed}}\right) + \frac{1}{2}(1-\varepsilon_{bed})^{1/2} Re^{0.6} Pr^{1/3}\right)} \quad 4.\ 8$$

The contact area for the air and solid adsorbent in the calculation elementary cell $dA_{s,a}$ can be calculated by the multiplication of the volume of the elementary cell and specific surface area of air and solid adsorbent. The specific surface area $a_{a,s}$ (m^2/m^3) for spherical particles can be evaluated by equation 4. 9 (Mhimid 1998).

$$a_{a,s} = \frac{6(1-\varepsilon)}{d} \quad 4.\ 9$$

Thus

$$dA_{s,a} = a_{a,s} \cdot L_1 \cdot L_2 \cdot H_1 \quad 4.\ 10$$

4.3.3 Heat transfer between air and water flow

When water is heated by the reactor, the heat transfer from the air, via metal pipe, to water can be written as:

$$dq_{a\to w} = \left(T_{a,in} - T_{w,in}\right) / \left(\frac{1}{h_{w,m} \cdot dA_w} + \frac{\delta}{\lambda_m \cdot dA_w} + \frac{1}{h_{m,a} \cdot dA_{m,a}}\right) \quad 4.\ 11$$

where the contact area of water and the metal tube is dA_w and the contact area of metal tube and air flow is $dA_{m,a}$. The term $\frac{\delta}{\lambda_m \cdot dA_w}$ is the conductive thermal resistance of the metal pipe. Considering the pipe thickness is minimum and the thermal conductivity of the pipe is much larger than the adsorbent, the thermal resistance of the pipe is negligible. Thus, the heat transfer rate can be expressed as:

$$dq_{a\to w} = \left(T_{a,in} - T_{w,in}\right) / \left(\frac{1}{h_{w,m} \cdot dA_w} + \frac{1}{h_{m,a} \cdot dA_{m,a}}\right) \quad 4.\ 12$$

where $h_{w,m}$ and $h_{m,a}$ are the heat transfer coefficient of water flow within the metal pipe and heat transfer coefficient of air flow across the metal pipe, respectively. The two terms can be evaluated by their Nusselt number.

Nusselt number of water flow

The equations for calculating the Nusselt number of water flow is determined by whether it is laminar flow or turbulent flow. To identify the status, the critical Reynolds number is 2300. In terms of laminar flow, Sieder and Tate have given the equation according to their experimental data (R. Welty et al. 1970), expressed as:

$$Nu_w = 1.86\left(Pe\frac{D}{L}\right)^{1/3}\left(\frac{\mu_w}{\mu_m}\right)^{0.14} \quad 4.\ 13$$

where the Peclet Number Pe can be calculated with the Reynolds and Prandtl number.

$$Pe = Re \cdot Pr \quad 4.\ 14$$

When the water flow is turbulent flow, the Nusselt number can be calculated by the equation proposed by Dittus and Boelter (R. Welty et al. 1970), expressed as:

$$Nu_w = 0.023Re^{0.8}Pr^n \; with \begin{cases} n = 0.3 \; for \; charging \; the \; adsorbent \\ n = 0.4 \; for \; discharging \; the \; adsorbent \end{cases} \quad 4.\ 15$$

where the Reynolds, Prandtl and Nusselt number is referred to:

$$Re = \left(\frac{uD}{\nu}\right)_w \quad 4.\ 16$$

$$Pr = \left(\frac{\mu_{\ p}}{\lambda}\right)_w \quad 4.\ 17$$

$$Nu_w = \left(\frac{hD}{\lambda}\right)_w \quad 4.\ 18$$

Therefore, the heat transfer coefficient of water flow is calculated by:

$$h_{w,m} = \frac{0.023\lambda_w \left(\frac{uD}{\nu}\right)_w^{0.8} \left(\frac{\mu c_p}{\lambda}\right)_w^n}{D} \; with \begin{cases} n = 0.3 \; for \; charging \; process \\ n = 0.4 \; for \; discharging \; process \end{cases} \quad 4.\,19$$

Nusselt number of air flow through the metal pipe

Considering air flowing over the metal pipe embedded in porous medium, as shown in Figure 4 - 8, the Nusselt number can be expressed as (Donald A. and Adrian B. 2013):

$$Nu_D = 1.015(RePr)_D^{1/2} \quad 4.\,20$$

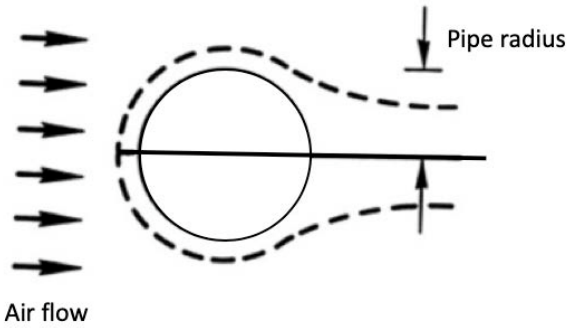

Figure 4 - 8 Illustration of air flow over the pipe embedded in porous medium

Therefore, the convective heat transfer coefficient $h_{m,a}$ can be calculated with the equation 4. 21.

$$h_{m,a} = \frac{\lambda_a \cdot 1.015 \left(\frac{\rho_a u_a D c_{p,a}}{\lambda_a}\right)^{1/2}}{D} \quad 4.\,21$$

4.3.4 Heat transfer between water and solid adsorbent

Since the adsorbent particles contact with the metal pipe, considerations should be given to the conductive heat transfer between the metal pipe and adsorbent and the convective heat transfer of the water. Similar to the heat transfer between air and water, thermal resistance of the pipe is negligible. The heat transfer can be written as:

$$dq_{s\to w} = \left(T_s - T_{w,in}\right) / \left(\frac{1}{h_{w,m} \cdot dA_w} + \frac{y}{\lambda \cdot dA_{m,s}}\right) \quad 4.\,22$$

where the contact area of solid adsorbent and metal tube is $dA_{m,s}$.

4.3.5 Heat transfer between air and fin

With respect to air and fin, the Nusselt number is given by (Donald A. and Adrian B. 2013):

$$Nu_{fin} = 1.329(RePr)_{fin}^{1/2} \quad 4.\ 23$$

$$Re = \frac{\rho_a u_a L_f}{\mu_a} \quad 4.\ 24$$

$$Pr = \frac{\mu_a \ _{p,a}}{\lambda_a} \quad 4.\ 25$$

The convective heat transfer coefficient can be calculated with equation 4. 26.

$$h_{fin,a} = \frac{\lambda_a 1.329 \left(\frac{\rho_a u_a L_f c_{p,a}}{\lambda_a}\right)^{1/2}}{L_{fin}} \quad 4.\ 26$$

It is noted that there is similarity between Nu_D and Nu_{fin}. But in each case, it is the dimension that is aligned with the flow direction which is used as the length scale of the Nusselt and Peclet number. The length scale used in the equation 4. 21 is the pipe diameter and the length scale used in the equation 4. 24 is the fin length.

4.3.6 Mass balance between solid adsorbent and air

For both charging and discharging process, moisture transfers between the adsorbent zeolite and the air flow. The change of mass for the adsorbent can be obtained from the LDF model, as given in equation 3. 32. The change of mass for air can be calculated by the specific humidity of the inlet and outlet air for a calculation element.

$$\underbrace{\dot{m}_a \cdot \left(\phi_{a,out} - \phi_{a,in}\right) \cdot 0.001}_{Change\ of\ mass\ for\ air} = \underbrace{-\frac{dX}{dt} \cdot m_s}_{Change\ of\ mass\ for\ zeolite} \quad 4.\ 27$$

4.4 Chapter summary

The chapter has proposed a three-phase thermochemical reactor to address the current research gaps of the reactors. It has presented the reactor illustrations and operations in charging and discharging. The reactor features trapezoidal containers with gaps to allow air flow and provides robust support for the thermochemical material. It is also integrated with water pipes to provide heat output from air and water in discharging. Fins are also integrated in the reactor to enhance the heat transfer. According to the proposed design, the chapter develops a numerical model to describe the heat and mass transfer of the reactor in charging and discharging. Considerations have been made on the heat and mass conservation of the air, water and solid thermochemical material. The numerical model is to be validated in Chapter 6 which serves as the tool for the reactor configuration study and investigations. The following Chapter 5 is the experimentation of the proposed reactor, which provides the original data for the numerical model validation.

CHAPTER 5: EXPERIMENTATION OF THE THREE-PHASE THERMOCHEMICAL REACTOR

5.1 Overview

Using zeolite 13X as the thermochemical material, the study has carried out experimental tests to investigate the reactor's charging and discharging performance. The experimentation has been conducted at the School of Mechanical Engineering, Beijing Institute of Technology from December 2018 to March 2019. We thank the Beijing Institute of Technology for their support of the project.

According to the established conceptual design of the thermochemical reactor, this chapter illustrates the development of the experimental rig and the experimentation of the reactor. The performance of the reactor in charging and discharging processes has been presented. Additionally, the chapter has tested the effect of some key parameters on the reactor performance.

5.2 Design of the experimental rig

To evaluate the reactor, an experimental rig has been developed. The schematic illustration of the experimental rig is depicted in Figure 5 - 1. Air from the environment, can be pumped by the fan and driven through the platform. First, it travels across the heat exchanger where the ambient air can be heated by the air leaving the system. Then air travels through the air duct heater. Upon the reactor entrance, the air flow is directed into the reactor. When the air leaves the reactors, it heads to the air-to-air heat exchanger where the sensible heat of the exhaust air transfers to the intake air. Driven by a water pump, the copper pipes direct the water through the material container and then circulate it to a water tank.

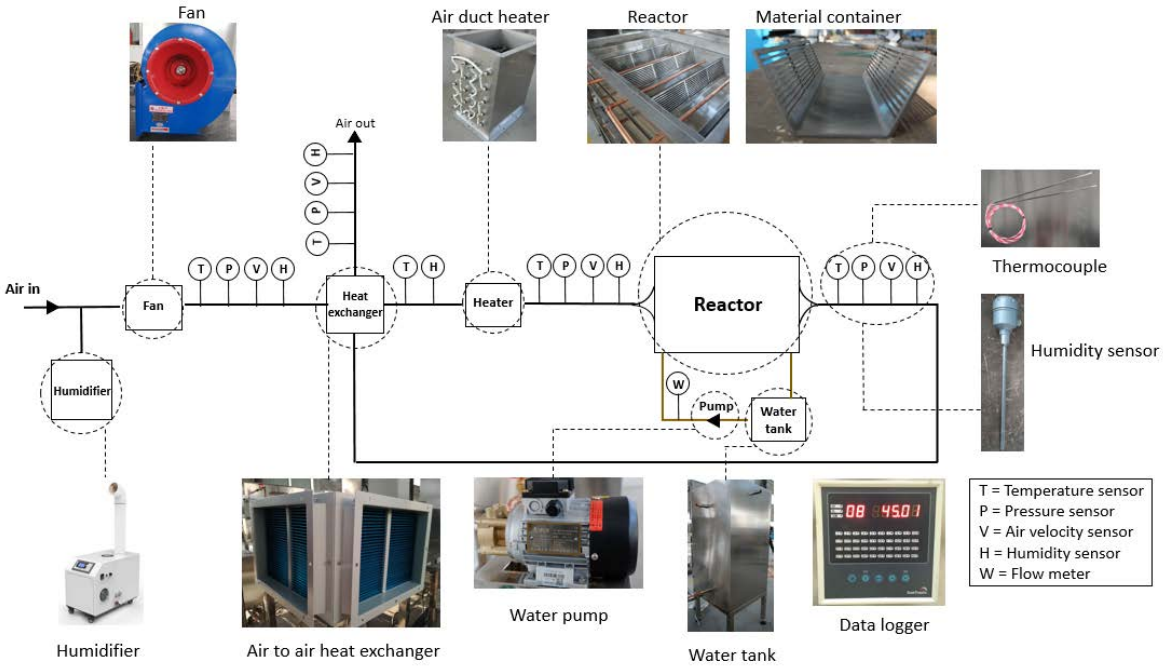

Figure 5 - 1 Schematic illustration of the developed experimental platform

The layout of experimental setup in a 60.12 m^2 laboratory is presented in Figure 5 - 2. The air inlet and outlet of the setup are placed next to the windows to get a relatively constant inlet air temperature and to release the heated exhaust air out of the laboratory during a charging test. Considering the safety risks, the control cabinet is placed at the far side of the electric heater so a person cannot approach the heater during an operation.

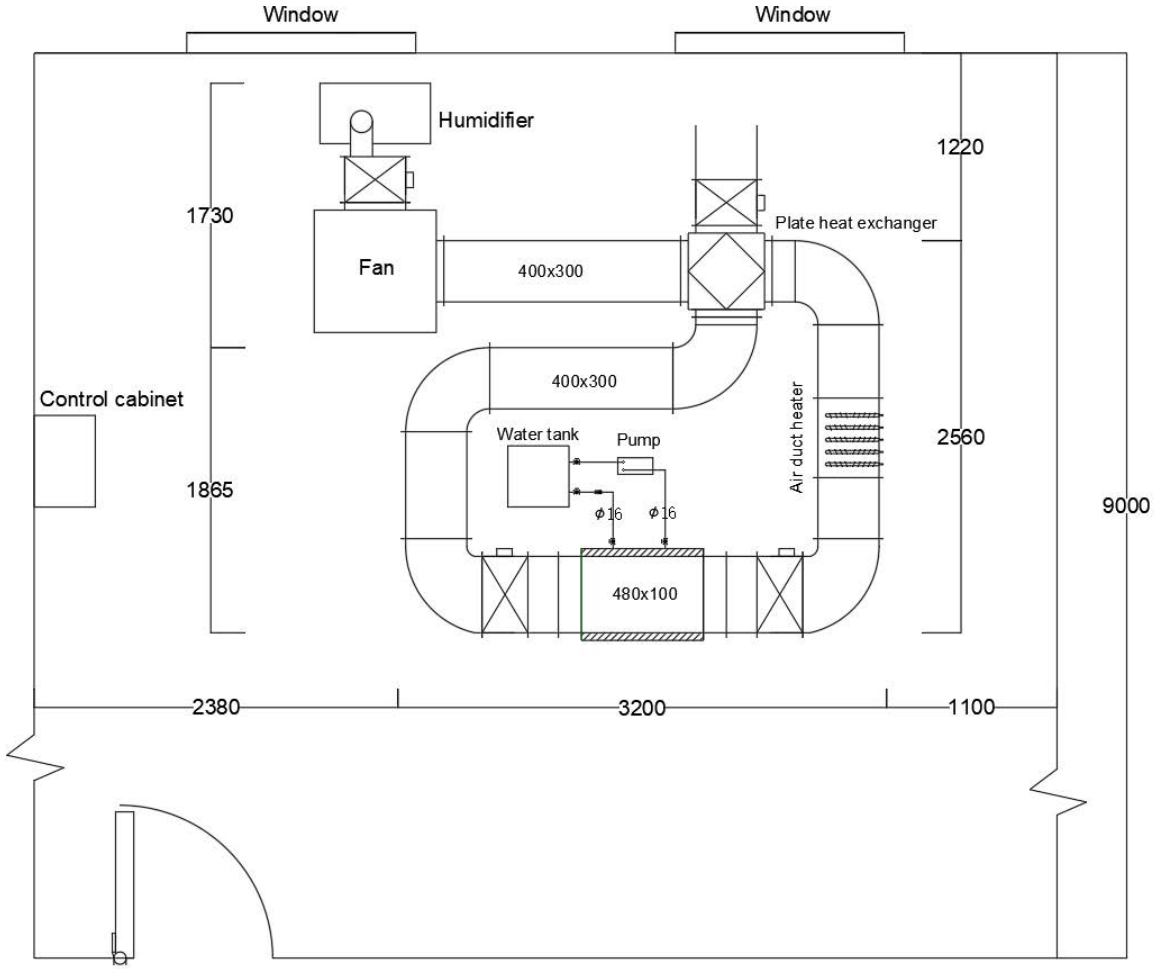

Figure 5 - 2 Layout of the experimental rig in the laboratory

5.3 Specifications of the reactor, experimental rig and instrumentation

5.3.1 The reactor

The reactor container has been built according to the design, as shown in Figure 5 - 3. The study selects 5 mm thick stainless steel plates to guarantee structural stability during the experiment. The manufacturing applies a laser cutting machine to cut out the gaps before bending the plate to the trapezoid shape. To maintain gap accuracy during the cutting, each gap has been separated into 3 sections with a 4 mm distance between any sections.

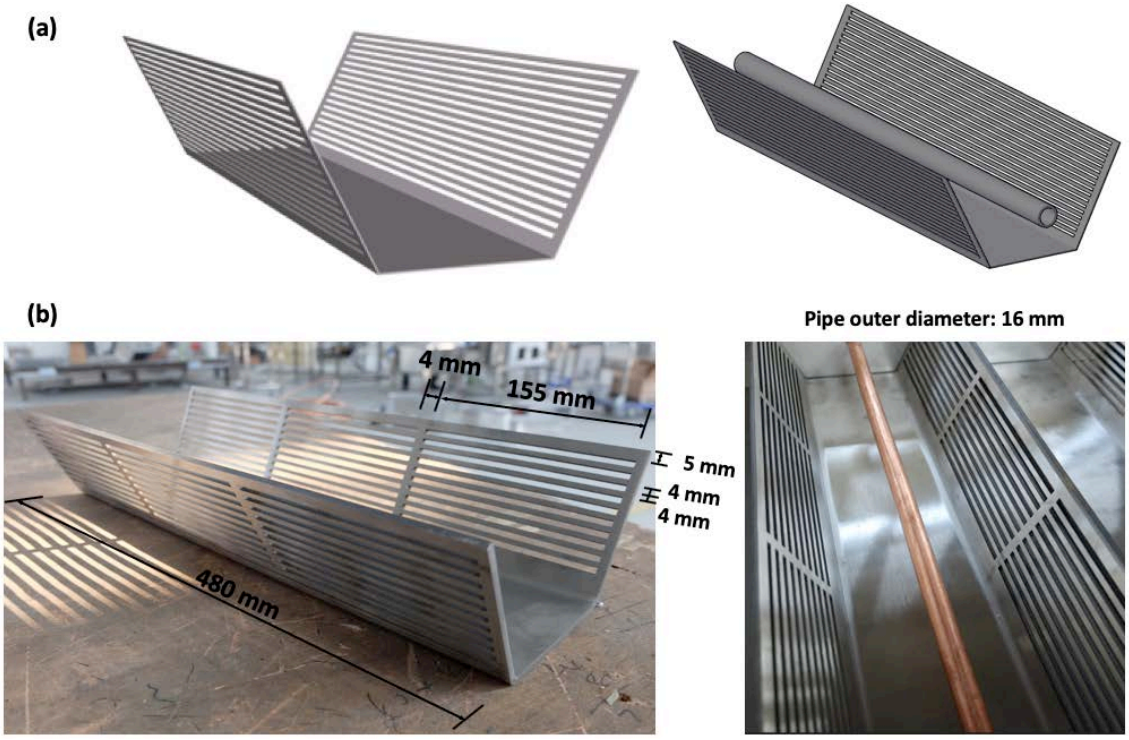

Figure 5 - 3 Pictures of the reactor: (a) the reactor design, (b) the built reactor

The study has constructed 8 containers and divided them into 2 reactor segments, one for smooth pipe and another for fin pipe, as shown in Figure 5 - 4. It also presents the air flow direction. The containers of smooth pipe reactor with the air flow direction are named as ‘S1’, ‘S2’, ‘S3’, and ‘S4’. Similarly, ‘F1’, F2’, ‘F3’, and ‘F4’ represents the containers of fin pipe reactor in line with the air flow direction. Additionally, glass wool insulation at 50 mm thickness is embedded into the external structure.

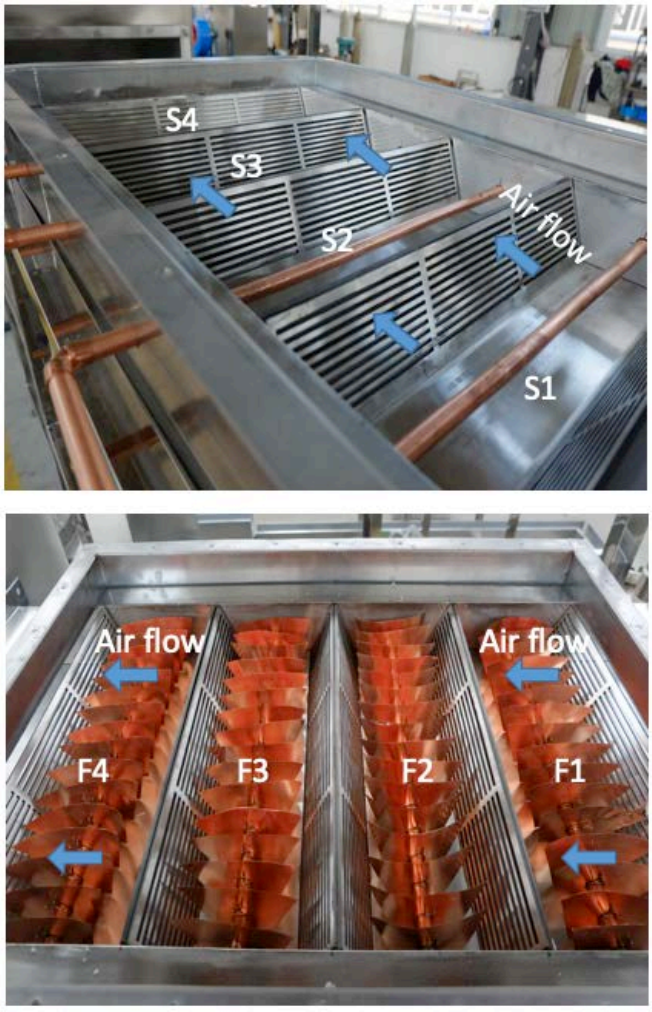

Figure 5 - 4 Containers without zeolite 13X in the smooth pipe and fin pipe reactor

5.3.2 Environment simulation system

To conduct parametrical measurement of the reactor in charging and discharging processes, an environment simulation system has been constructed, as shown in Figure 5 - 5. It consists of an ultrasonic humidifier, a fan, an electric heater, a plate heat exchanger and air duct valves.

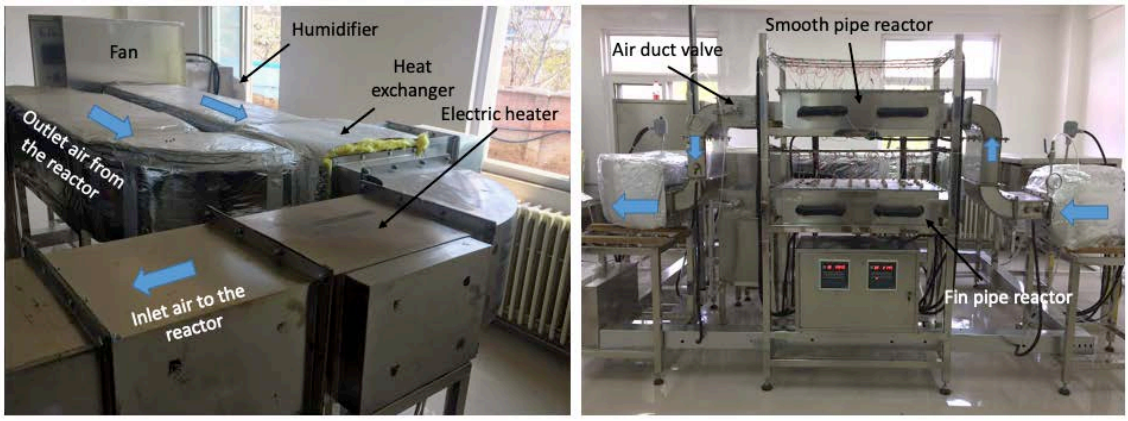

Figure 5 - 5 An overview of the environment simulation system in the experimental rig: (a) air intake and exhaust, (b) front view with embedded smooth and fin pipe reactor

The selection of the components has considered the experimental test conditions and the zeolite used in the experiment. For instance, to achieve a relatively high temperature in charging, the electric heater can achieve a maximum 300 °C output air with 15 kW. Considering the amount of zeolite 13X used in the reactor, the humidifier capacity is 6 kg/hour. The details and specifications of the key components are listed in Table 5 - 1.

Table 5 - 1 Specifications of the environment simulation system

Component	Specifications	Quantity
Ultrasonic humidifier	Type: DRS-06A, humidification capacity: 6 kg/hour, Power: 0.6 kW	1
Fan	Airflow rate: 2000 m^3/h, Pressure: 2000 Pa, Power: 2.2 kW, 3.2 amps, 380 V	1
Air duct heater	Power: 15 kW	1
Plate heat exchanger	Dimensions: 500(W)*500(L)*360(H) Plate distance: 5 mm	1
Duct/ fittings	Galvanised steel duct 400 mm*300 mm, 90-degree elbows	15 m
Air duct valve	Dimensions: 500 mm*150 mm, 400 mm*300 mm	4

5.3.3 Water pipes and fin pipes

Figure 5 - 6 presents the water flow system built in the testing rig. Driven by a pump, water flows from the water tank to the smooth or fin pipe reactor before returning to the tank. To control the water flow to one reactor, isolation valves have been installed at the inlet and outlet of each reactor. The water flow is in indirect contact with the air flow and thermochemical material. Table 5 - 2 gives the main components and specification of the water flow system. The water tank has been designed and built with an internal float valve to maintain the water level.

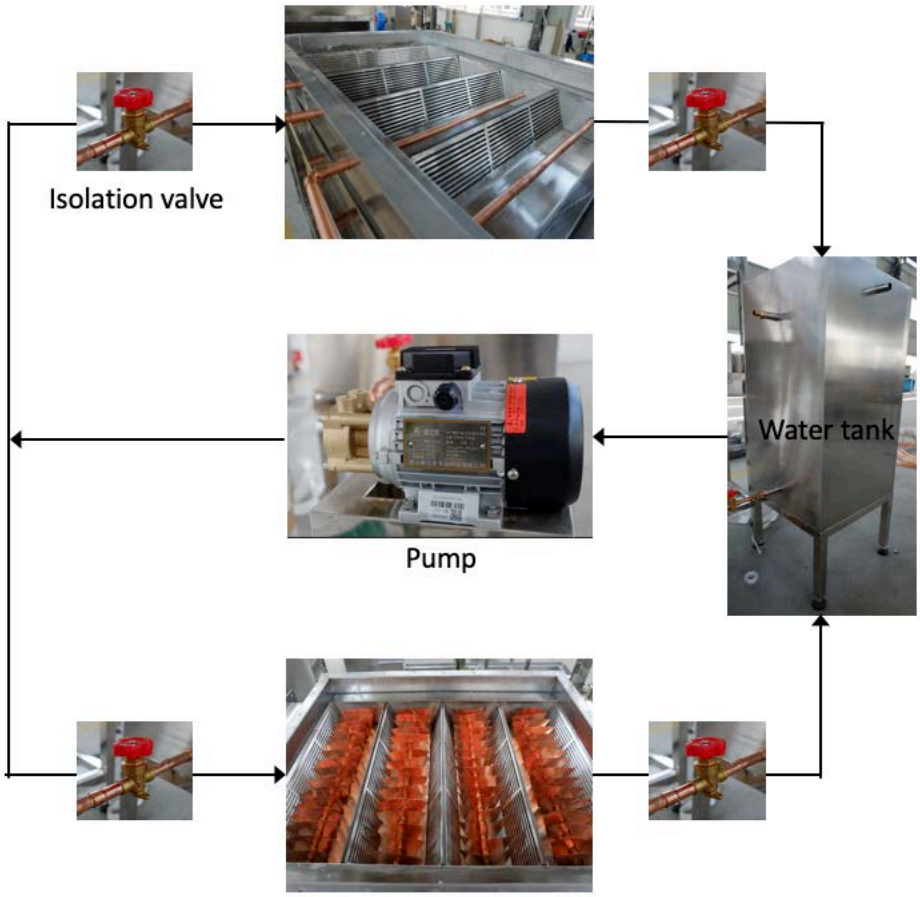

Figure 5 - 6 Illustration of water flow in the experimental rig

Table 5 - 2 Specifications of the components in the water flow

Component	Specifications	Quantity
Pump	Aulank WD-016, head: 36 m, maximum flow rate: 10 L/min	1
Water tank	Dimension: 500 mm * 500 mm * 900 mm, insulation: 50 mm glass wool	1
Isolation valve	Yongheng valve 22 mm	6
Copper pipe	Outer diameter: 22 mm, total length: 15 m	1
Copper solder ring	Straight coupling 22 mm, equal 90°C elbow 22 mm	20
Copper sheet	Dimension: 0.8 mm * 300 mm * 300 mm	5

Additionally, the study has built the fin pipe reactor. Fins have been cut out from copper sheets according to the fin dimensions in Figure 4 - 3. Then using a punch die tool, a hole is punched at the centre of the fin according to the pipe diameter. Specifically, as shown in Figure 5 - 7(a), an extended contact area has been created around the hole to increase the contact between the fin the pipe. After inserting the pipe through the fin, a clip has been used to secure the fin location (see Figure 5 - 7(b)). The distance between any two fins is 30 mm.

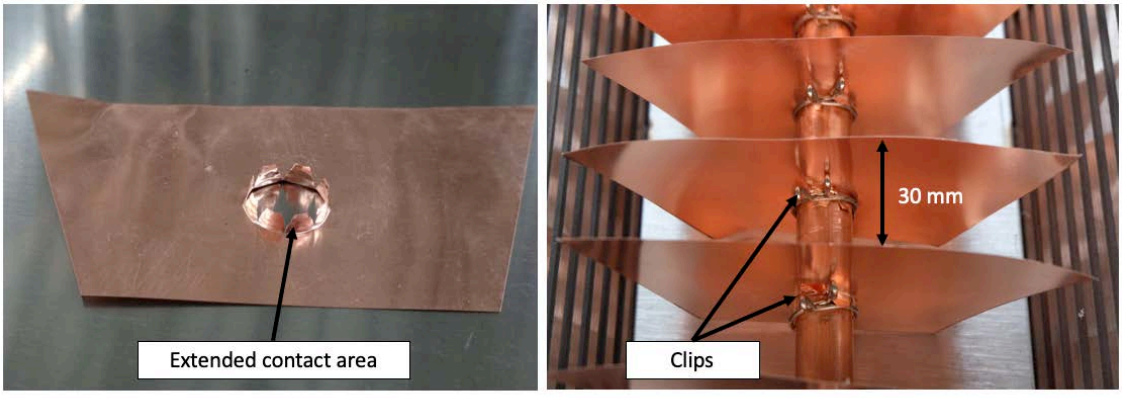

Figure 5 - 7 Picture of the fin and fin pipe: (a) fin with extended contact area, (b) fin pipe with clips to secure the position

5.3.4 Parameter measurement, instrumentation, and data acquisition

The parameters recorded in the experiment are air temperature, air flow rate, air humidity and air pressure with respect to the ambient and material temperature. Figure 5 - 8 presents the instrumentation in the air duct.

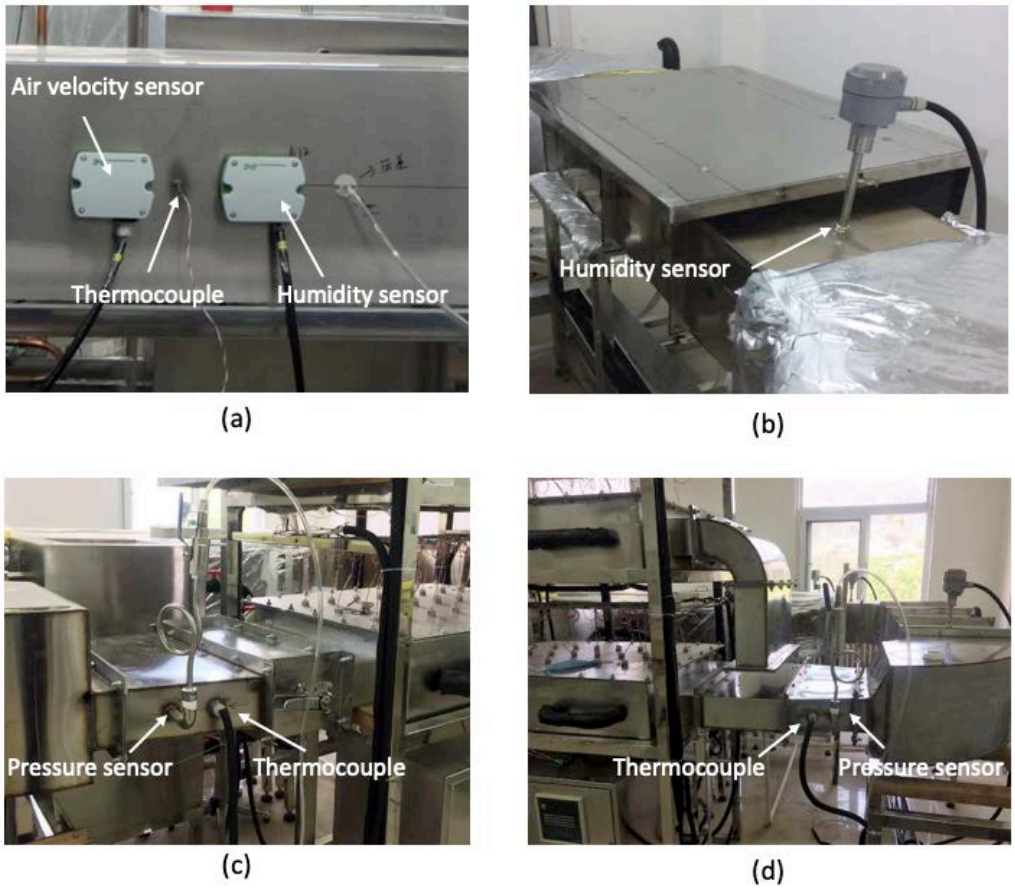

Figure 5 - 8 Instrumentation in the air duct: (a) air velocity, humidity and thermocouple at the system inlet, (b) humidity sensor at the reactor inlet, (c) thermocouple at the reactor inlet, (d) thermocouple at the reactor outlet

The installation positions have been selected at the centre of the air duct to ensure the measurement of the stabilised air flow. Figure 5 - 9 gives an example of the instrumentation positions in the air duct.

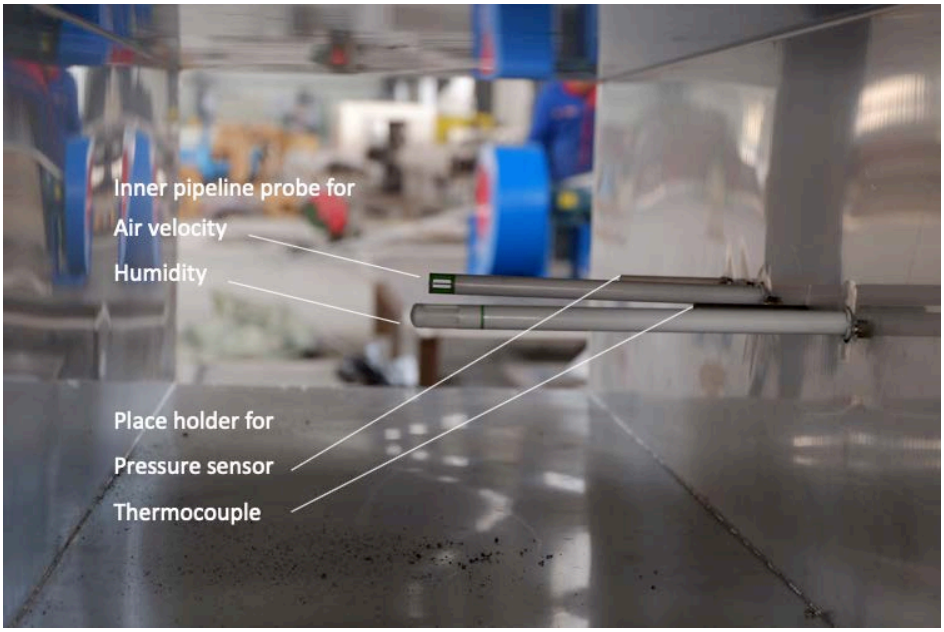

Figure 5 - 9 Picture of the instrumentations in the air duct

To measure the zeolite temperature, each reactor container has been integrated with 6 thermocouples. The locations have been depicted in Figure 5 - 10. Since the air and water can flow through the reactor, temperature sensor locations have been separated along the air and water travel paths. Besides the temperature sensors inserted in the zeolite, thermocouples have been attached to the metal water pipe at the water inlet and outlet of each container. The thermocouples record the water pipe temperature and partly represent the water temperature. When constructing the reactor, the resources were limited to integrate thermocouples into the water pipe without leakages. The thermocouples have been fixed on the exterior of the water pipe.

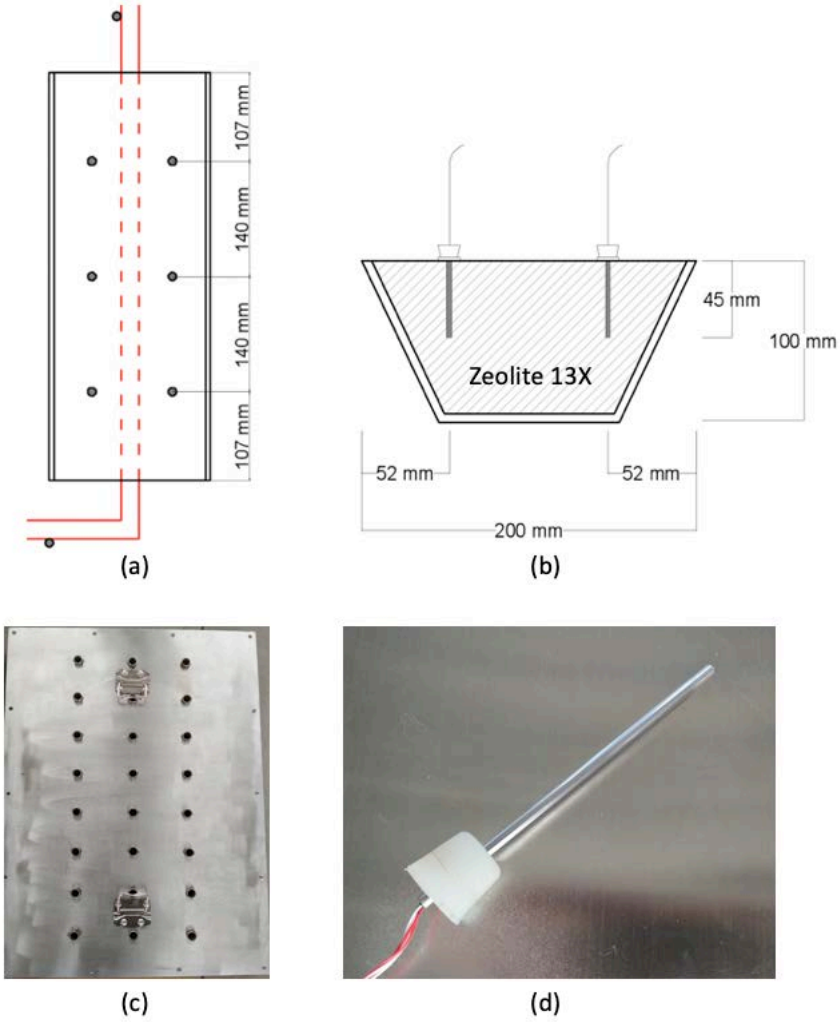

Figure 5 - 10 Illustration of thermocouples in the reactor: location of thermocouples for a reactor container (a) and cross section view (b), (c) reactor cover with thermocouple holes, (d) thermocouple with rubber stopper

The applied sensors in the experiment have been carefully selected to meet the operation conditions in the tests such as a relatively high temperature at 180 °C and air relative humidity above 90%. Table 5 - 3 summarises the specifications of the measurement instruments. To achieve accurate measurement of air, zeolite 13X and water, all the measurement instruments have been calibrated prior to the experimental tests.

Table 5 - 3 Specification of the instrumentations

Instrument	Specifications	Quantity
Thermocouple	Manufacture: Sailing Technology, China	64
	Model: PT100	
	Range: - 200-500 °C	
	Accuracy: 3%	
Humidity sensor	Manufacture: E+E, Engerwitzdorf, Austria	5
	Model: EM1900	
	Range: 0-100 %	
	Accuracy: 3%	
Pressure sensor	Manufacture: Setra System, Boxborough, US	2
	Range: 0-1000 Pa	
	Accuracy: 1%	
Air velocity sensor	Manufacture: E+E, Engerwitzdorf, Austria	4
	Model: EE660	
	Range: 0-100 m/s	
	Accuracy: 3%	
Water flow meter	Manufacture: Sailing Technology, China	1
	Accuracy: 3%	

The communication of control and data acquisition is shown in Figure 5 - 11. To adjust the operation status of fan and water pump, two frequency inverters have been installed. To achieve a target air temperature, a proportional integral derivative (PID) controller has been used which links the electric heater and a specific thermocouple located at the inlet of the reactor. During a test, the PID control maintains the temperature of the inlet air at the target value. Regarding the data acquisition, 2 data loggers, Kunlun Tianchen TPC1061Ti, have been used to record the data from the instrumentations such as thermocouples, pressure sensors, humidity sensors and air velocity sensors. All the controls and communication is fed back to the primary monitor located at the control cabinet. Additionally, the data is sent to the computer for data recording and system control such as adjusting air flow rate, target temperature of the electric heater and water flow rate.

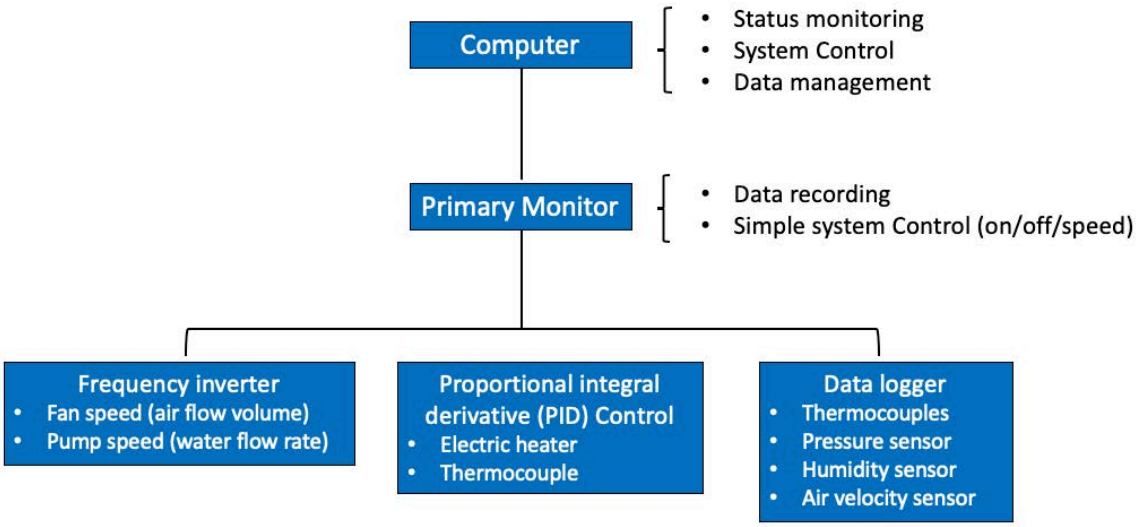

Figure 5 - 11 Diagram for experimental rig control and data acquisition

5.3.5 Reactor performance evaluation indicators

In the experiment, energetic and hydrothermal performance of the reactor has been investigated.

In charging process, the thermal energy transferred to the adsorbent can be expressed as:

$$\dot{Q_{char,a}} = \dot{m}_a \cdot c_{p,a} \cdot \left(T_{a,in} - T_{a,out}\right) \quad 5.\ 1$$

The cumulative thermal energy input over a charging duration t_c is calculated with the equation 5. 2.

$$Q_{total,in} = \int_0^{t_c} \dot{m}_a c_{p,a} \left(T_{a,in} - T_{a,out}\right) dt \quad 5.\ 2$$

Similar to a charging process, in discharging, the thermal energy of air can be expressed as:

$$\dot{Q_{dischar,a}} = \dot{m}_a \cdot c_{p,a} \cdot \left(T_{a,out} - T_{a,in}\right) \quad 5.\ 3$$

For air and water output in discharging, the cumulative thermal energy over a discharging process $t_{dischar}$ is calculated with the equation 5. 4.

$$Q_{total,out} = \int_0^{t_{dischar}} \dot{m}_a c_{p,a} \left(T_{a,out} - T_{a,in}\right) dt + \int_0^{t_{dischar}} \dot{m}_w c_{p,w} \left(T_{w,out} - T_{w,in}\right) dt \quad 5.4$$

5.4 Evaluation and results discussions

The study has conducted charging and discharging tests to investigate the performance of the reactor. A total of 9 tests of 5 hours each have been carried out. As given in Table 5 - 4, the tests investigate the reactor performance under different charging temperature, the effect of inlet air flow rate and the comparison between smooth and fin pipe reactor. Table 5 - 5 presents a summary of the experimental results.

Table 5 - 4 Operating conditions for charging and discharging tests

Test No.	Charging/ Discharging	Duration (hour)	Inlet air temperature (°C)	Air mass flow rate (kg/s)	Relative humidity of inlet air (%)
Test 1	Charging	5	120	0.045	Ambient
Test 2	Discharging		20	0.02	95%
Test 3	Charging		140	0.045	Ambient
Test 4	Discharging		20	0.02	95%
Test 5	Charging		180	0.045	Ambient
Test 6	Discharging		20	0.024	95%
Test 7	Discharging		25	0.015	95%
Test 8	Discharging		25	0.018	95%
Test 9	Discharging		25	0.02	95%

Table 5 - 5 Overall summary of the results of the experimental tests

Test No.	Reactor type	Outlet air temperature $T_{a,out}$ (°C)		Inlet and outlet air temperature difference ΔT (°C)		Instantaneous heat input in charging and heat output of air in discharging $Q_{d,a}$ (W)		Cumulative energy Q_{total} (Wh)	Energy density (Wh/g)
		Peak	Average	Peak	Average	Peak	Average		
Test 1	Smooth	96.23	68.99	88.16	46.35	1332.93	700.82	3504.12	0.18
	Fin	89.56	68.17	89.04	47.17	1346.26	713.27	3566.38	0.18
Test 2	Smooth	54.04	45.99	33.73	26.31	707.79	304.27	1523.87	0.07
	Fin	51.35	42.45	31.14	22.77	509.945	397.84	1989.21	0.10
Test 3	Smooth	108.80	74.53	96.30	56.33	1456.08	851.74	4265.83	0.21
	Fin	103.63	76.39	94.54	54.47	1429.37	823.51	4124.45	0.21
Test 4	Smooth	56.72	48.31	42.67	34.27	645.17	518.09	2594.77	0.13
	Fin	39.26	30.33	39.26	29.55	593.56	458.58	2296.71	0.12
Test 5	Smooth	172.43	149.44	91.44	8.89	1382.55	134.46	672.315	0.03
	Fin	171.27	142.40	114.24	15.94	1727.26	240.97	1204.86	0.06
Test 6	Smooth	67.65	42.37	46.81	20.12	1415.58	608.54	3047.75	0.15
	Fin	77.23	45.61	52.15	21.15	1577.07	639.46	3197.29	0.16
Test 7	Smooth	72.04	43.18	44.62	16.13	674.70	243.88	1219.41	0.06
	Fin	74.75	47.69	47.28	20.65	714.87	312.16	1560.79	0.08
Test 8	Smooth	76.29	46.70	52.20	20.95	947.15	380.14	1900.68	0.10
	Fin	64.32	40.73	40.87	17.32	741.52	314.26	1571.31	0.08
Test 9	Smooth	67.65	42.40	46.81	20.15	943.72	406.31	2031.57	0.10
	Fin	77.23	45.61	52.15	21.15	1051.38	426.31	2131.52	0.11

5.4.1 The charging tests under different charging temperature

The reactor has been charged with inlet air temperature at 120 °C (Test 1) and at 140 °C (Test 3). Figure 5 - 12 gives the temperature profiles of zeolite 13X in the smooth pipe reactor and the inlet air temperature during charging. The containers are named according to the indications in Figure 5 - 4.

With respect to the zeolite temperature, it increases gradually during charging (see Figure 5 - 12). When charging the reactor at 120 °C, container 1 reaches 120 °C in 4.5 hours, container 2 reaches 115.3 °C, container 3 at 105.5 °C and container 4 at 93.6 °C. When charging the reactor at 140 °C, container 1 reaches 140 °C in 4.6 hours with container 2 at 133.4 °C, container 3 at 120.8 °C and container 4 at 106.08 °C. For both cases, container 4 achieves the lowest temperature in the reactor. For charging at 140 °C, the temperature of container 4 surpasses that of container 3 in charging at 120 °C in 4.58 hours at 105.9 °C. Similarly, for charging at 140 °C, the temperature of containers 3 and 2 surpass that of containers 2 and 1 in 3.28 hours at 110.7 °C and in 1.78 hours at 108.8 °C.

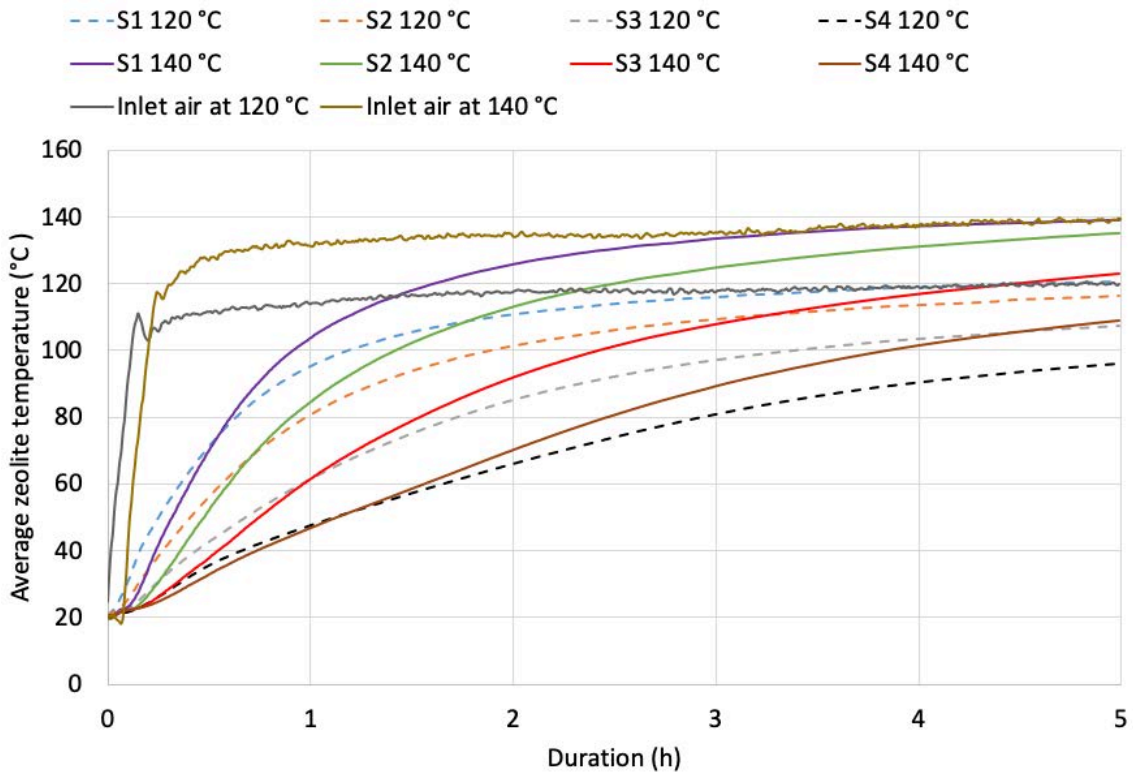

Figure 5 - 12 Temperature of zeolite 13X in the smooth pipe reactor in charging with inlet air at 120 °C (Test 1) and 140 °C (Test 3)

Figure 5 - 13 depicts the thermal energy of the containers in the smooth pipe reactor under charging at 120 °C and 140 °C. Container 1 achieves the peak thermal energy at around 1094 W at 120 °C and 1181 W at 140 °C. The thermal energy of the other containers reach to 400 W. At the beginning of the charging process, for Container 1, the thermal energy at 140 °C is relatively lower than that of the 120 °C for the inlet air temperature difference of the two cases. For the 140 °C case, the inlet temperature fluctuates at the beginning of the charging process, causing delay for the inlet air temperature reaching its target value.

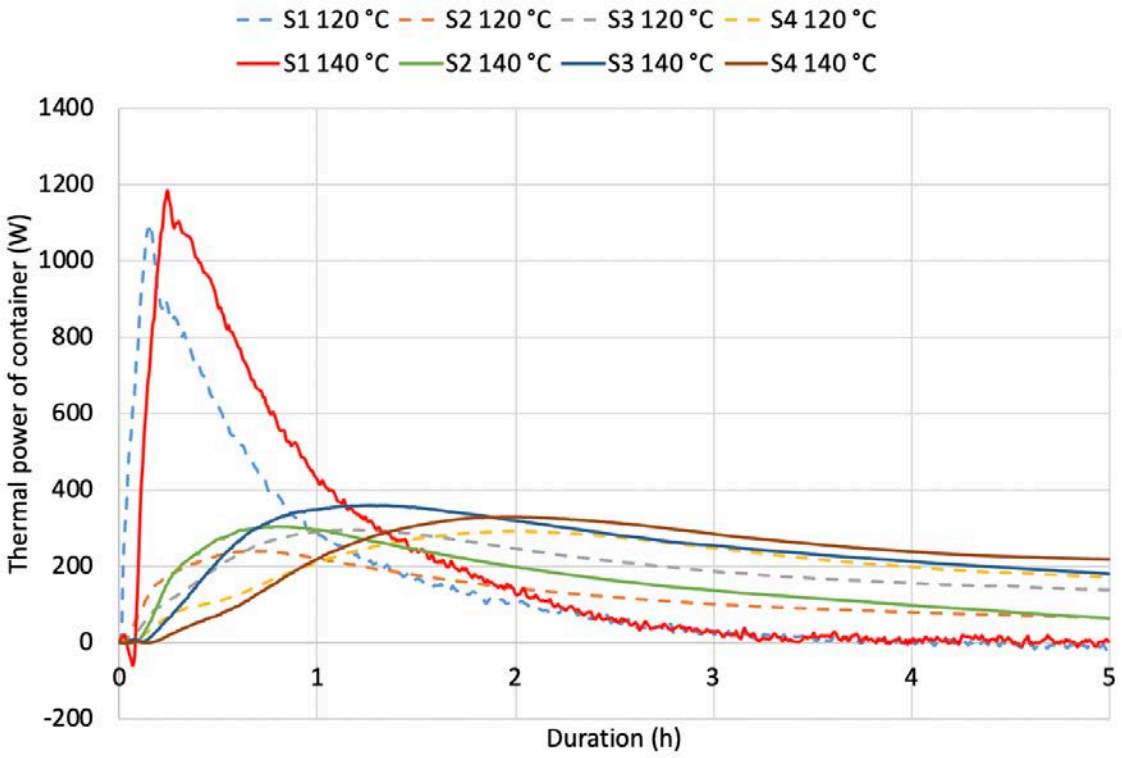

Figure 5 - 13 Comparison of the thermal energy of the smooth pipe reactor in charging at 120 °C (Test 1) and 140 °C (Test 3)

5.4.2 The discharging tests with different charging temperature

The reactor discharging performance under different charging temperature has been presented in Figure 5 - 14. This figure shows the peak reactor outlet air temperature in Test 2, Test 4 and Test 6. The tests are the discharging cases when the reactors have been charged with inlet air at 120 °C, 140 °C and 180 °C. Noticeably, increasing the charging temperature leads to relatively higher reactor outlet air temperature in discharging. With the reactor being charged with 180 °C inlet air, for Test 6, the smooth pipe and fin pipe reactor achieves the peak outlet air temperature at 67.65 °C and 77.23 °C, respectively, over 20 °C higher than charging with inlet air at 120 °C. The increase in charging temperature has improved the outlet air temperature in discharging, regardless of the integration of fins. Higher charging temperature contributes to removing relatively more moisture from the zeolites, increasing the energy release in discharging. However, the fin pipe reactor at Test 4 shows the lowest peak outlet temperature at 39.26 °C. This is due to air leakage in the air flow system where air leakage has

reduced the reactor moisture intake. The air leakage issue has been fixed before conducting Test 5 and Test 6. For Test 6, the fin pipe reactor achieves a superior performance with the reactor outlet air temperature at 7 °C higher than the smooth pipe reactor. The integration of fins enhances the reactor heat transfer, increasing the overall reactor temperature in discharging. Thus the fin pipe reactor has achieved a higher outlet air temperature than the smooth pipe reactor.

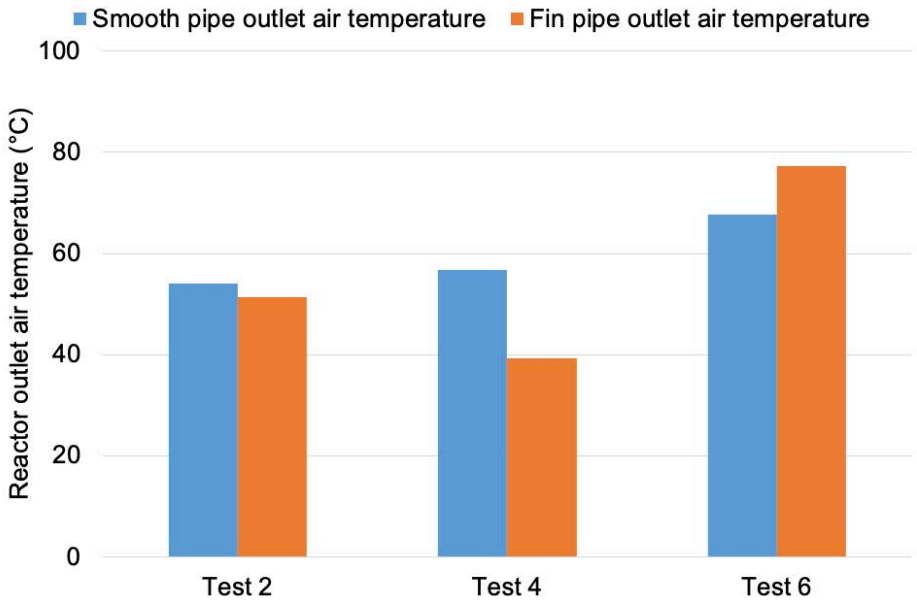

Figure 5 - 14 The peak reactor outlet air temperature in the discharging cases with different charging temperature

5.4.3 The comparison of fin and smooth pipe reactor in charging

Figure 5 - 15 gives a comparison of the average zeolite temperature of fin and smooth pipe reactor under the inlet air temperature at 180 °C in charging (Test 5). Obviously, Container 1 and Container 2 of the fin pipe reactor achieve relatively higher temperature levels than that of the smooth pipe reactor. The temperature profile of Container 3 in both reactors is comparable. In 1 hour, Container 1, Container 2, Container 3 and Container 4 of the fin pipe reactor reach to 180.9 °C, 166.5 °C, 144.2 °C and 116.8 °C respectively. For the smooth pipe reactor, Container 1, Container 2, Container 3 and Container 4 reach to 173.7 °C, 155.3 °C, 137.2 °C and 128.8 °C respectively. Fins direct the heat

across the containers and help the zeolite 13X reach a relatively higher temperature level, improving the reactor charging performance.

The relatively higher temperature in the fin pipe reactor improves the desorption process in the charging process, causing relatively more energy being stored in the zeolite 13X. This can be reflected from the relatively smaller temperature increases of Container 3 and Container 4 in the fin pipe reactor. Container 4 in the fin pipe reactor has shown a relatively smaller temperature than that of the smooth pipe reactor. Additionally, Figure 5 - 16 gives a comparison of the temperature gradient. Container 3 and Container 4 of fin pipe reactor present a relatively lower temperature gradient than the smooth pipe reactor in 0.3 hours.

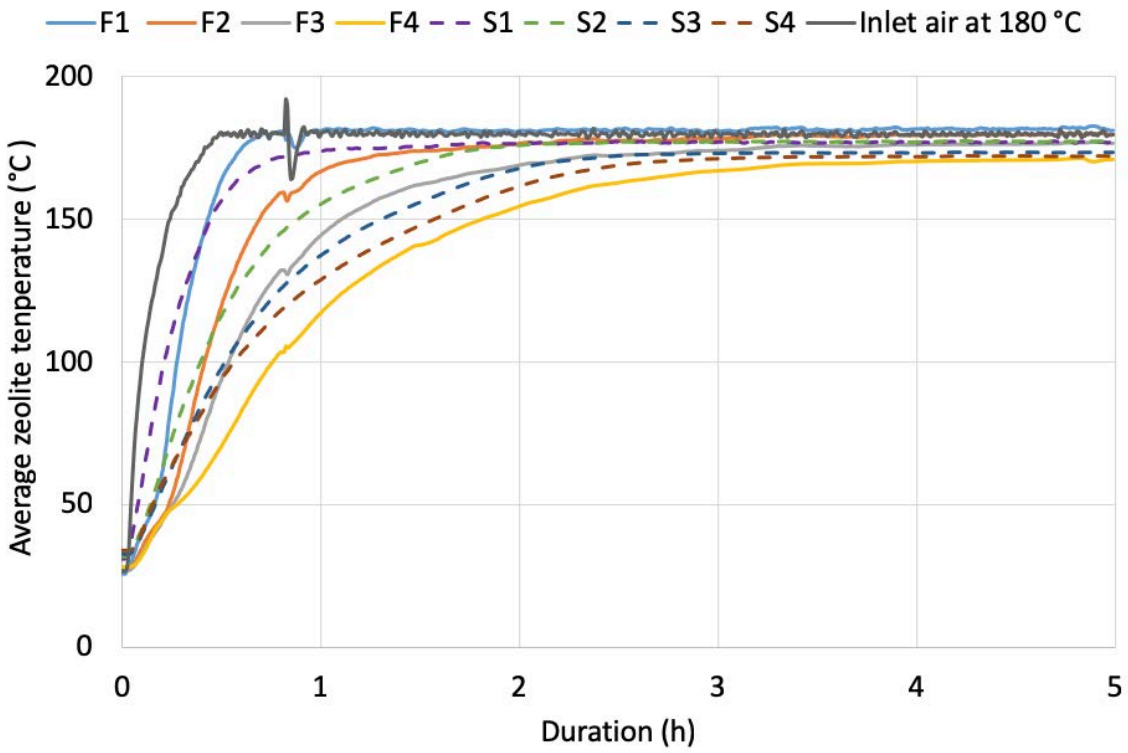

Figure 5 - 15 Comparison of the average zeolite temperature in the fin pipe and smooth pipe reactor in charging (Test 5)

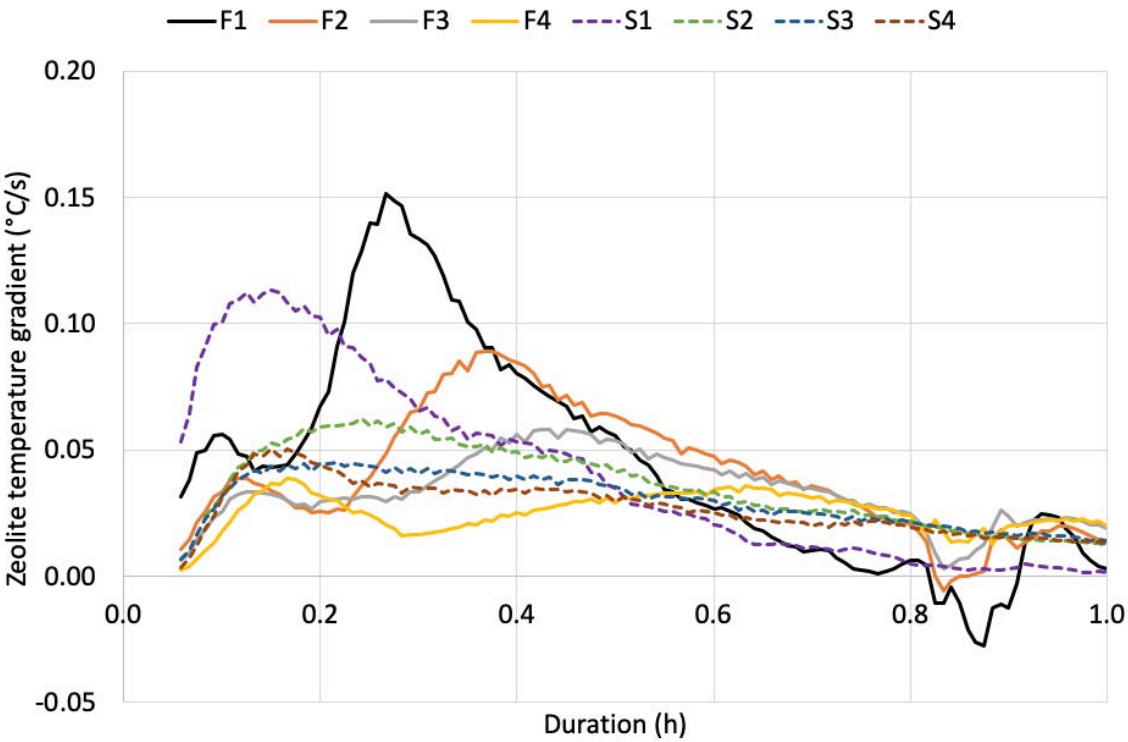

Figure 5 - 16 Temperature gradient from 0 to 1 hour

5.4.4 Discharging performance under different inlet air mass flow rate

Figure 5 - 17 illustrates the average zeolite temperature and outlet air temperature of the smooth pipe reactor in discharging under different inlet air mass flow rate at 0.015 kg/s, 0.018 kg/s, and 0.02 kg/s (Test 7, Test 8 and Test 9). The relatively larger inlet air mass flow rate increases the zeolite temperature in discharging. When the air mass flowrate is increased from 0.015 kg/s to 0.018 kg/s, the peak zeolite temperature in container 4 has been lifted by 4 °C and the average thermal power of the reactor has been increased by 56%. However, when the air mass flow rate increases to 0.02 kg/s, the peak reactor outlet air temperature reduces to 67.65 °C, 4.39 °C reduction based on the 0.015 kg/s value.

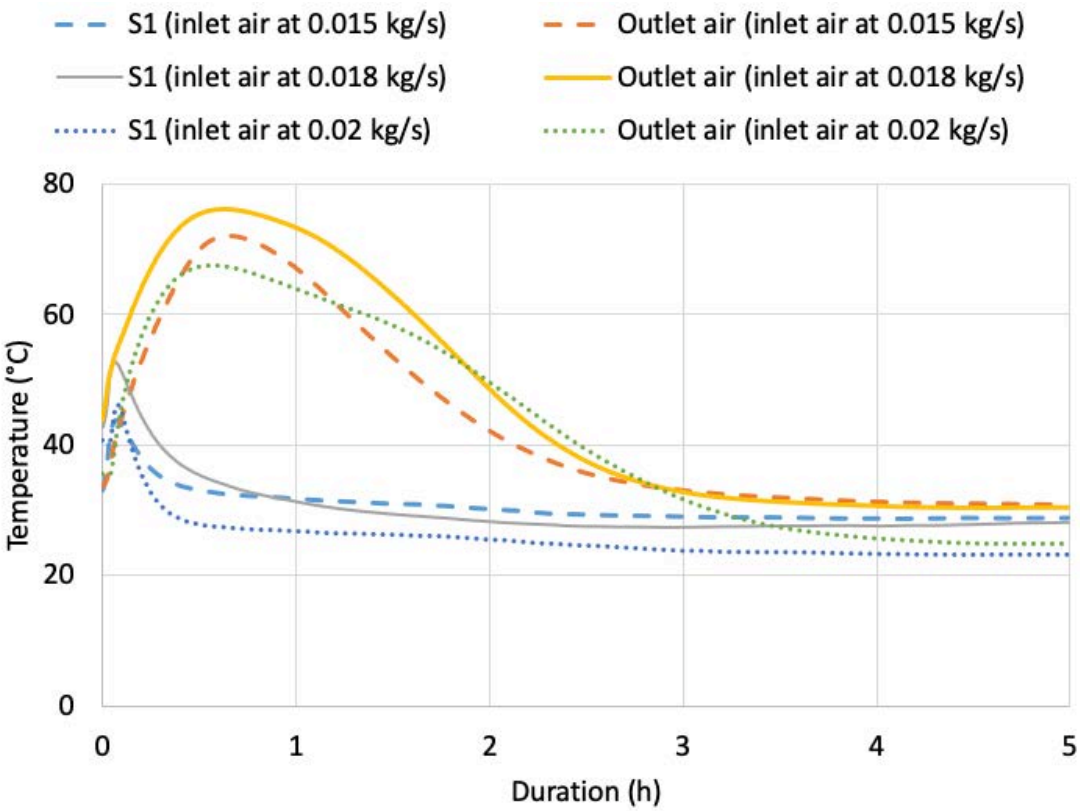

Figure 5 - 17 Zeolite and outlet air temperature of the smooth pipe reactor at different inlet air mass flow rate (Test 7, Test 8, and Test 9)

5.4.5 Water pipe temperature in discharging tests

The water pump can be switched on to use water for heat extraction in the discharging processes. To investigate the water temperature lift, discharging tests have been conducted for the smooth and fin pipe reactors with the water flow rate at 0.12 L/min. Figure 5 - 18 illustrates the water pipe temperature lift profiles of the smooth and fin pipe reactors under different inlet air mass flow rate. The water pipe temperature lift is the water pipe temperature difference between the outlet and inlet of a reactor.

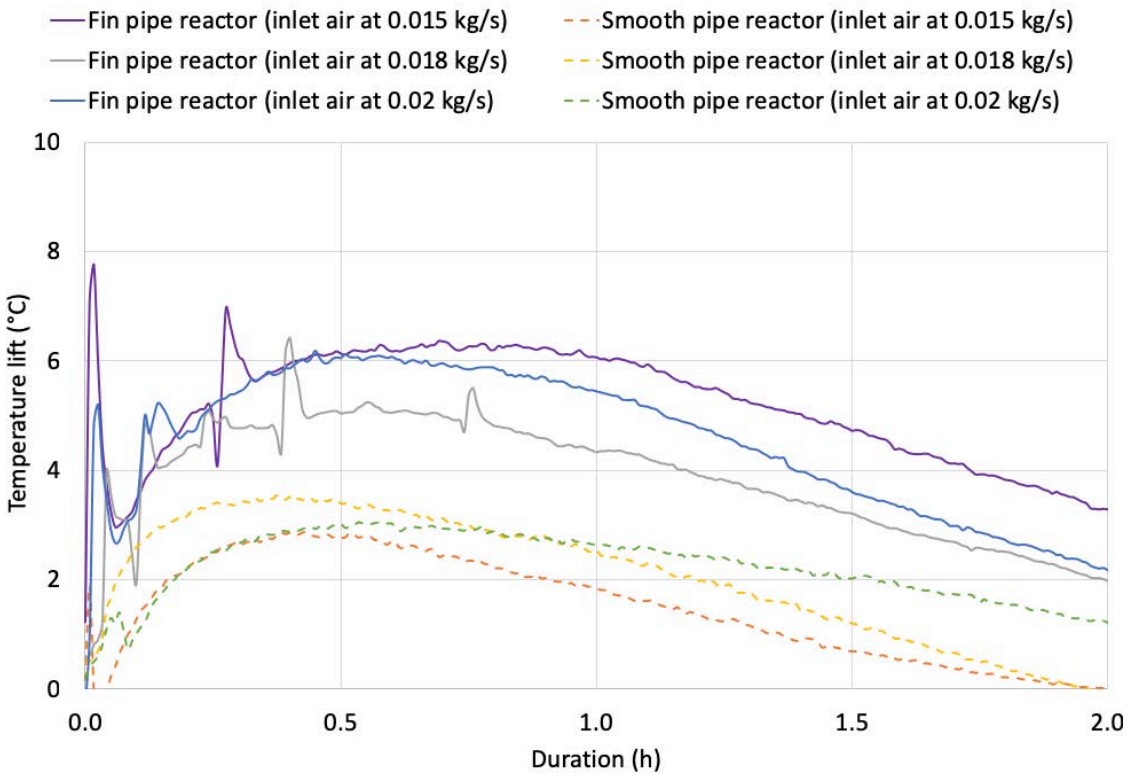

Figure 5 - 18 Water pipe temperature lift for smooth and fin pipe reactor under different inlet air mass flow rate

The fin pipe reactor has shown a superior performance in water temperature lift with 1.8 °C to 4 °C higher than that of the smooth pipe reactor. Specifically, the fin pipe reactor achieves the peak water temperature lift at 6.3 °C in 0.7 hours with inlet air mass flow rate at 0.015 kg/s. However, the peak water temperature lift for the smooth pipe reactor is 3.5 °C in 0.4 hours with inlet air mass flow rate at 0.018 kg/s. The value is relatively lower than the level for residential building application, indicating the potential in optimising the reactor operation strategy.

5.5 Limitations of the experimental tests

The limitations and sources of possible errors in the experimental tests are highlighted as follows.

- The water temperature increment is relatively small in the experimental tests. This may be caused by the water pipe thermocouple positions which are fixed

to the water pipe exterior. Also, the reactor temperature and water flow rate in discharging should be justified.

- The fins are tightly fitted on the water pipes rather than casting or extrusion, which introduces thermal contact resistance at the interface.
- No humidity measurement is presented in the study since the humidity sensors require further calibration to produce reliable data.
- The experimental conditions may experience the fluctuation of ambient temperature, which causes a difference between the experiment and simulation results.
- Errors in measuring and interpolation of the data.
- The thermocouples in the reactor may not represent the temperature developed above or under the location of the thermocouples.

5.6 Chapter summary

This chapter has illustrated the experimental rig and experimental tests of the proposed reactor. According to the experimental tests, the results are highlighted as follows.

- The increase in the charging temperature lifts the outlet air temperature in discharging. After charging the reactor at 180 °C, the following discharging process has achieved the peak outlet air temperature at 67.65 °C and 77.23 °C for smooth and fin pipe reactors respectively, which is over 20 °C higher than the reactor charging at 120 °C. For the smooth pipe reactor, the corresponding thermal energy generation has been lifted from 1523.8 Wh with charging temperature at 120 °C to 3047.7 Wh with charging temperature at 180 °C. The fin pipe reactor has achieved a slightly higher thermal energy generation from 1989.2 Wh with charging temperature at 120 °C to 3197.3 Wh with charging temperature at 180 °C.
- The fin pipe reactor has shown superior performance than the smooth pipe reactor in both charging and discharging processes. In charging, under the inlet air temperature at 180 °C, the fin pipe reactor has shown a significant increase in the zeolite temperature gradient of the thermochemical material.

For instance, Container 1 achieves the temperature gradient at 0.15 °C/s for fin pipe reactor and 0.11 °C/s for smooth pipe reactor. In discharging, the fin pipe reactor achieves relatively larger water temperature lift. With inlet water at around 20 °C at 0.015 kg/s, the fin pipe reactor provides water temperature lift at 1.8 °C to 4 °C higher than that of the smooth pipe reactor. For the outlet air temperature in Test 6, the fin pipe reactor has achieved the peak value at 77.2 °C with nearly 10 °C higher than that of the smooth pipe reactor.

- Increasing the inlet air mass flow rate can improve the reactor outlet air temperature. However, an excessive inlet air mass flow rate will reduce the outlet air temperature. For the smooth pipe reactor, for instance, the peak outlet air temperature has been increased from 71.9 °C to 75.6 °C when increasing the air mass flow rate from 0.015 kg/s to 0.018 kg/s. However, it reduces to 67.6 °C when the air mass flow rate increases to 0.02 kg/s.

CHAPTER 6: NUMERICAL PERFORMANCE INVESTIGATION OF THE THREE-PHASE THERMOCHEMICAL REACTOR

6.1 Overview

This chapter investigates a three-phase thermochemical reactor through an experimentally validated numerical model. According to the investigations, this chapter also provides the reactor configuration suggestions. The main work in the chapter includes:

- Validation of the two dimensional thermochemical reactor numerical model;
- Evaluating the sensitive parameters in the numerical model that affects the results;
- Investigating the effect of air and adsorbent parameters on the reactor charging and discharging processes;
- Evaluating the reactor configuration effect on the charging and discharging processes; and
- Provide suggestions in design a thermochemical reactor with considerations.

6.2 Numerical model validation

To illustrate the degree of which the numerical model represents the actual world for the intended applicability, numerical model validation is conducted. This section compares the computed results with the experimental values in charging and discharging cases. Figure 6 - 1 illustrates the flow chart of the numerical simulation and validation. It presents the input parameters and calculation methods in the numerical modelling. For the validation, 7 comparison cases are conducted. The conditions of the cases are presented in
Table 6 - 1. For charging, Case 1 and Case 2 are the charging experiment of the smooth pipe reactor and fin pipe reactor, respectively. For the smooth pipe reactor, Case 3 is the discharging with humidified ambient inlet air; and Case 4 is the discharging under the conditions of Case 3 with water circulation. For the fin pipe reactor, Case 5 is the discharging with humidified ambient inlet air; Case

6 is the discharging with humidified and preheated air at 50 °C; and Case 7 is the discharging under the conditions of Case 6, but it turns on water circulation when the reactor achieves peak temperature. It is noted that during a charging process, the zeolite temperature is used for both the experimental and numerical results. During a discharging process, the outlet air temperature is used as the results.

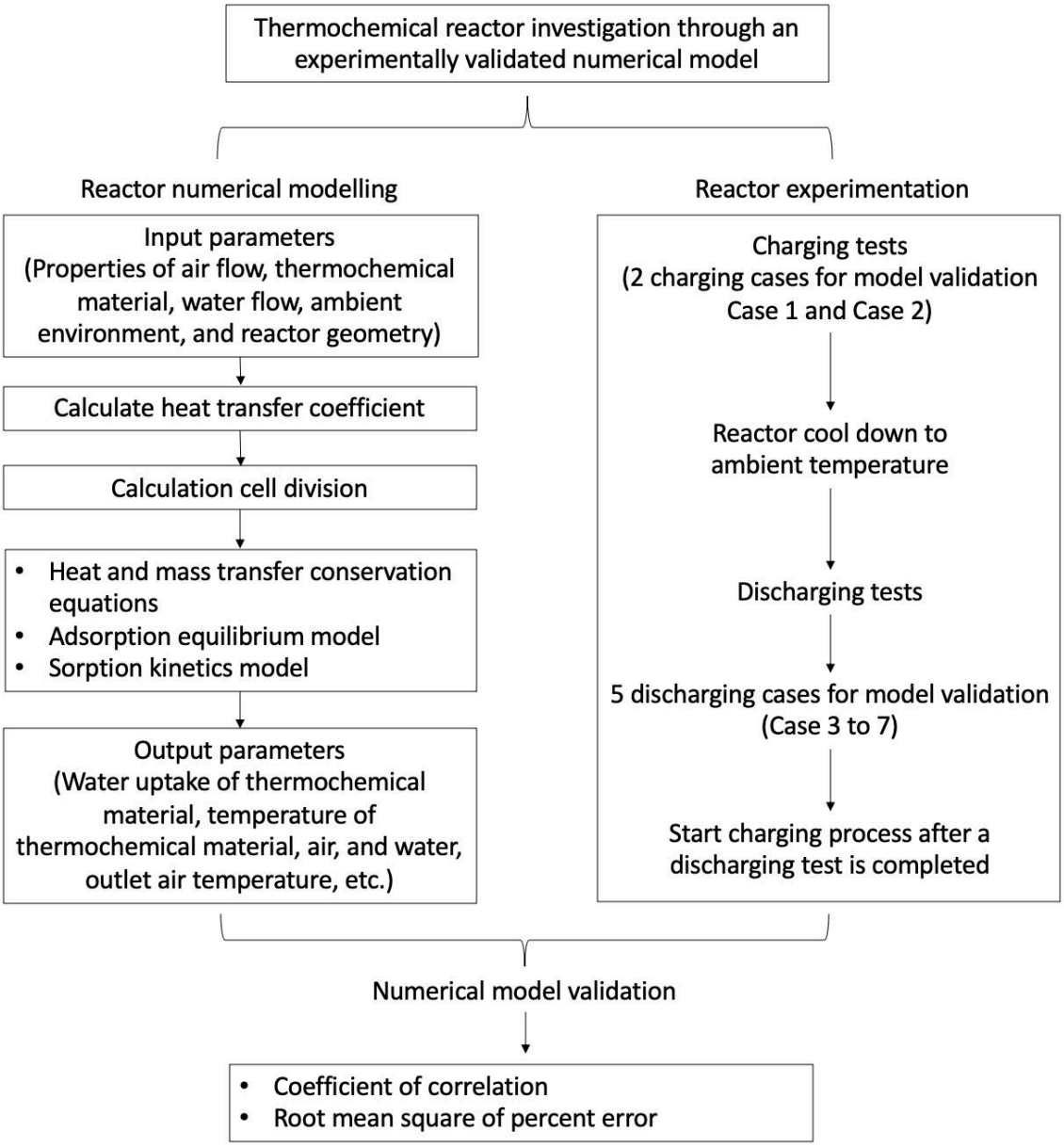

Figure 6 - 1 Flow chart of the simulation model and validation

Table 6 - 1 Operating conditions for charging and discharging the reactor

Parameter	Charging		Discharging				
	Case 1	Case 2	Case 3	Case 4	Case 5	Case 6	Case 7
Reactor type	Smooth	Fin	Smooth			Fin	
Ambient temperature	21.33	23.62	18.52	22.75	13.08	13.21	21.18
Air flow rate (kg/s)	0.045	0.024	0.024	0.024	0.045	0.045	0.045
Charging inlet air temperature (°C)	110.7	180.4	-	-	-	-	-
Discharging inlet temperature (°C)	-	-	18.52	22.75	25.23	50	50
Duration (h)	6	5	2	4	2	6	2
Water flow rate (L/min)	-	-	-	0.12	-	-	0.12

6.2.1 Numerical model validation in charging

Case 1 and Case 2

Figure 6 - 2 and Figure 6 - 3 show the comparison between the experimental and numerical results for the reactor outlet temperature during the charging study of the smooth and fin pipe reactor, respectively. The discrepancy between the experimental and numerical results of the cases is seen when the temperature is rising to the charging inlet temperature. For Case 1, the maximum temperature discrepancy during this stage reaches 25 °C. After the reactor temperature increases to 72 °C, a good agreement is obtained. For Case 2, the maximum temperature difference reaches 21.9 °C and a good agreement is achieved with the increasing of the reactor temperature. The temperature discrepancy can be attributed to the following.

- Heat loss from the reactor components to the environment has not been considered in the numerical model.

- Initial water content of zeolite in the charging test has not been identified. The difference in initial water content leads to different adsorption kinetics in the linear driving force model.

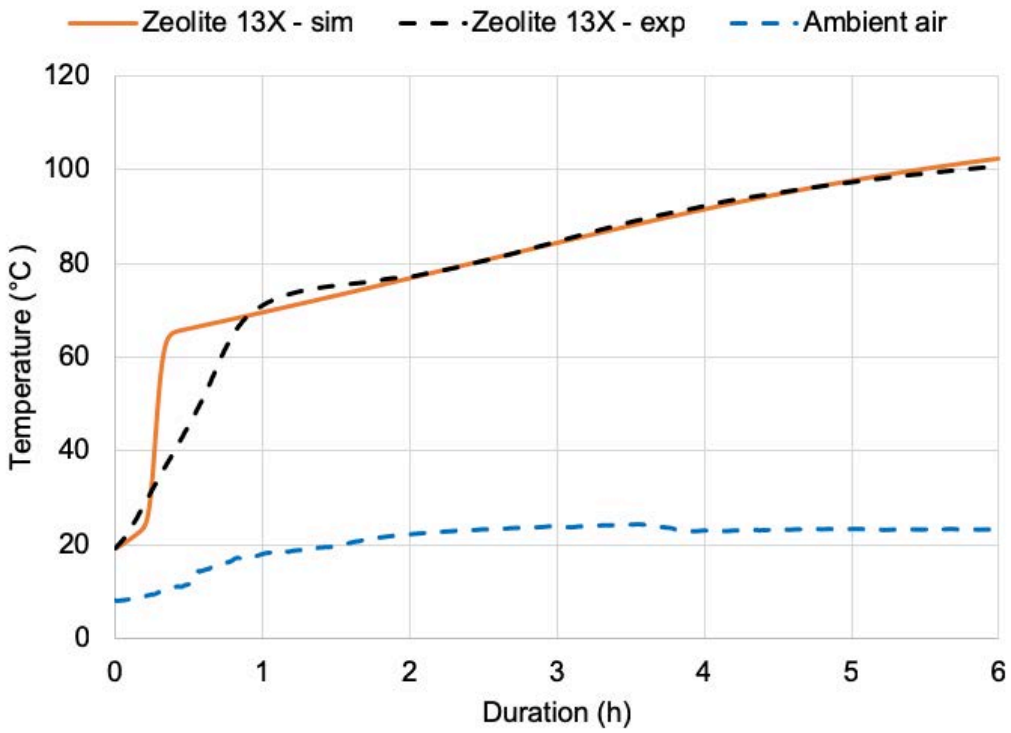

Figure 6 - 2 Measured and simulated adsorbent temperature of the smooth pipe reactor in charging (Case 1)

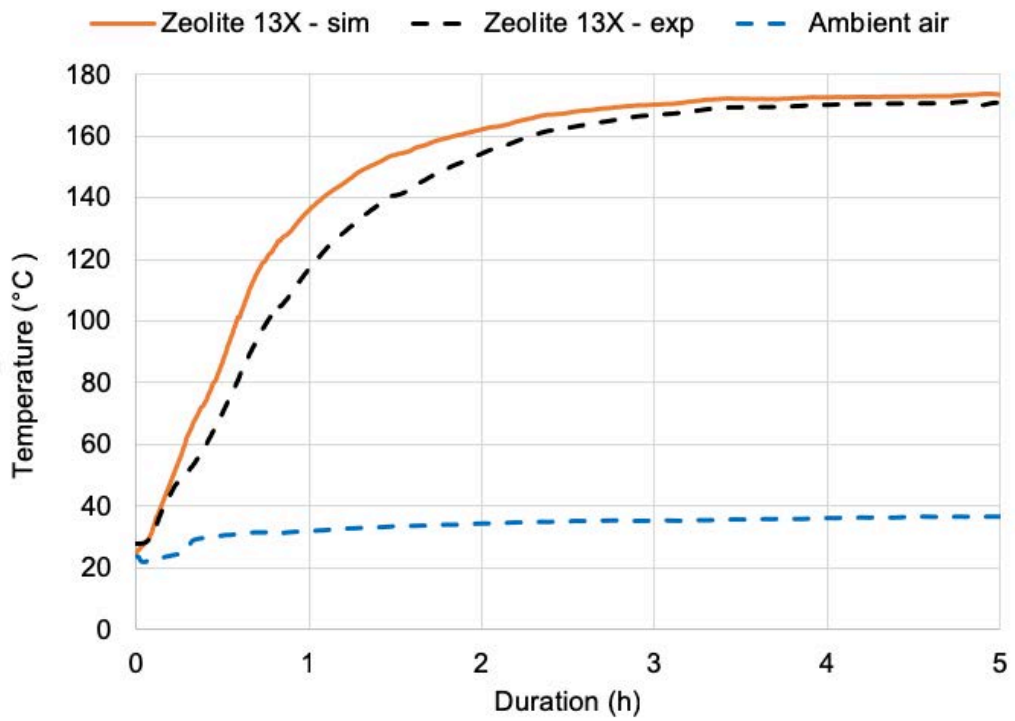

Figure 6 - 3 Measured and simulated adsorbent temperature of the fin pipe reactor in charging (Case 2)

6.2.2 Numerical model validation in discharging

Case 3 and Case 4

Regarding discharging, for the smooth pipe reactor, the comparison between computing values and experimental measurements are presented in Figure 6 - 4 and Figure 6 - 5. Figure 6 - 4 is Case 3 where the reactor has been discharging with the air at ambient temperature without water output. Figure 6 - 5 is the reactor with water supply and it shows the water temperature (Case 4). Both figures show good agreement between simulation results and experimental measurements. The maximum temperature discrepancy for Case 3 is 8 °C and for Case 4 is 1.8 °C during the temperature rising stage. For Case 4, the experimental water data shows fluctuations in the beginning of the discharging. The water has been turned off and the water pipes have directed heat from the adsorbent.

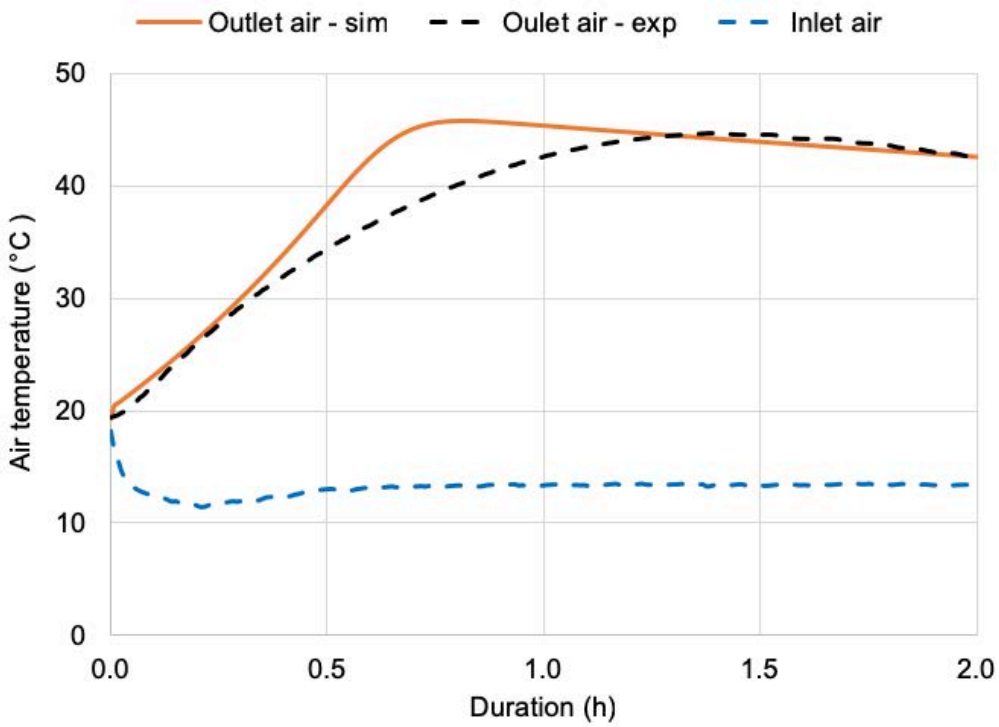

Figure 6 - 4 Measured and simulated smooth pipe reactor outlet air temperature in discharging with humidified ambient air (Case 3)

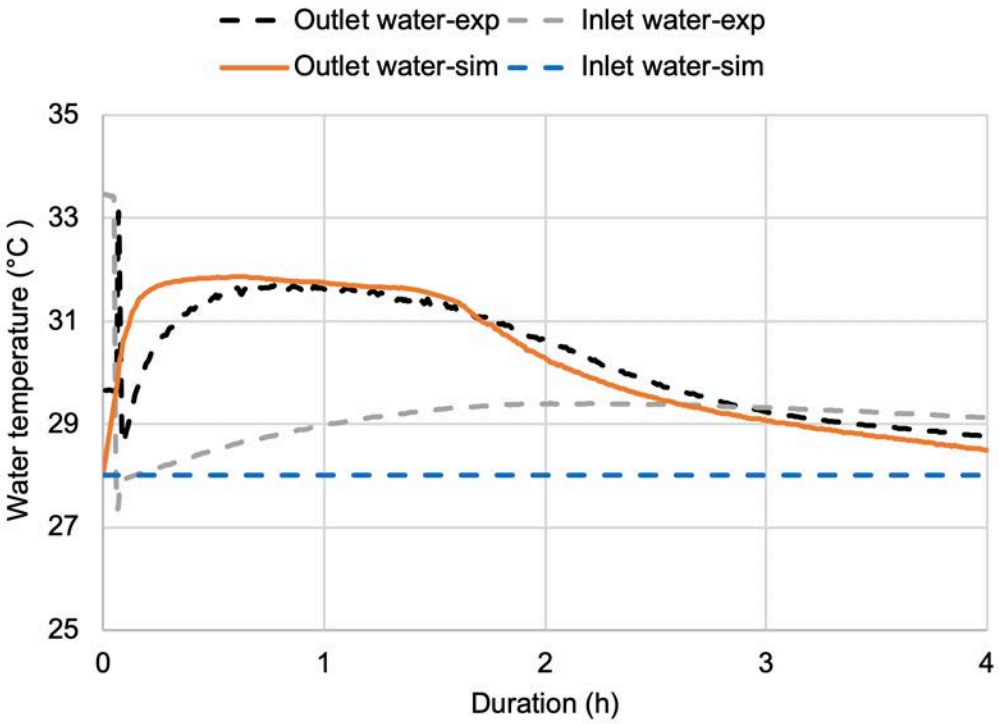

Figure 6 - 5 Measured and simulated smooth pipe reactor outlet water temperature (Case 4)

Case 5 and Case 6

Figure 6 - 6 is case 5 where the fin pipe reactor has been discharged with air at ambient temperature, while Figure 6 - 7 is for discharging with preheated air at 50 °C. Both figures have shown good agreement between the experimental and numerical results. For the numerical data, the reactor outlet temperature achieves the peak discharging temperature faster than the values obtained in the experiment. The maximum temperature discrepancy has been observed during the temperature rising stage at 10 °C and 7 °C, respectively. Specifically, in Figure 6 - 7, the temperature profile presents a noticeable difference for the discharging after 4.3 hours, because the air duct heater has been switched off after 4.3 hours. In experimental tests, the residual heat from the heater continues to preheat the air. While in the numerical model, the transitional stage has not been considered.

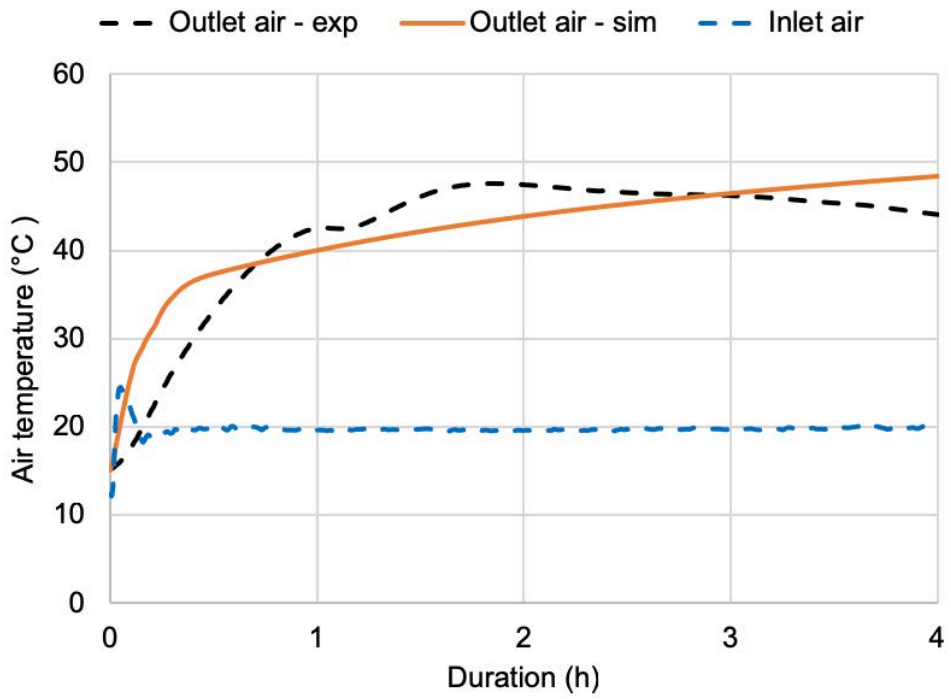

Figure 6 - 6 Measured and simulated fin pipe reactor outlet air temperature in discharging with humidified ambient air (Case 5)

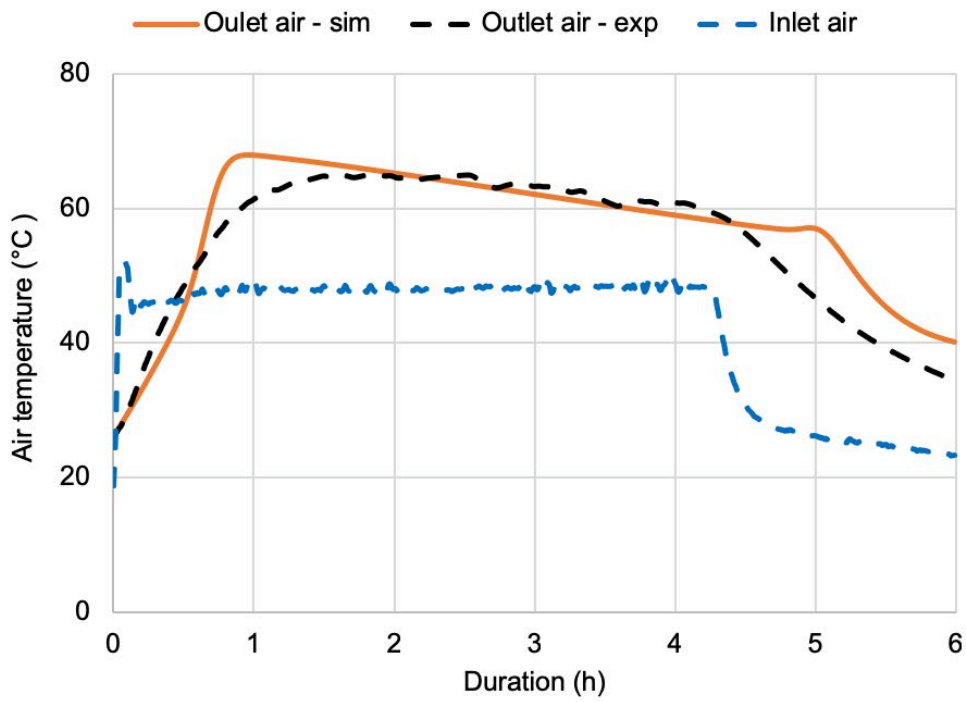

Figure 6 - 7 Measured and simulated fin pipe reactor outlet air temperature in discharging with heated air (Case 6)

Case 7

Under the conditions of Case 6, water circulation has been switched on when the zeolite temperature reaches the peak value at 68 °C. Figure 6 - 8 illustrates the comparison between the measured and computing values of water temperature at the inlet and outlet of the reactor. An unstable temperature profile in the measurement has been witnessed, because the heat from zeolite has been transferred to the metal pipe and water before 0.55 hours when the water circulation has been switched off. The transitional stage in the experiment has not been taken into the validation. After this stage, the water circulation pump has been switched on and the inlet and outlet temperature profiles become stable at 25 °C and 30 °C, respectively. The simulation outlet water temperature is relatively stable because of the axis scale and the relatively constant adsorbent temperature backed by the inlet air. When comparing the experimental data with the computing values, the maximum temperature difference is 9.6 °C during 0.6 to 0.8 hours when the measurements are reducing to a relatively stable value at

around 30 °C. After 0.8 hours, the temperature discrepancy drops to 1.1°C. The contributions to the discrepancy can be:

- The metal pipe energy accumulation has not been considered in the numerical model.
- In the experiment, thermocouples are attached to the outside of the metal pipe. The measured pipe temperature has been considered to be the water temperature.

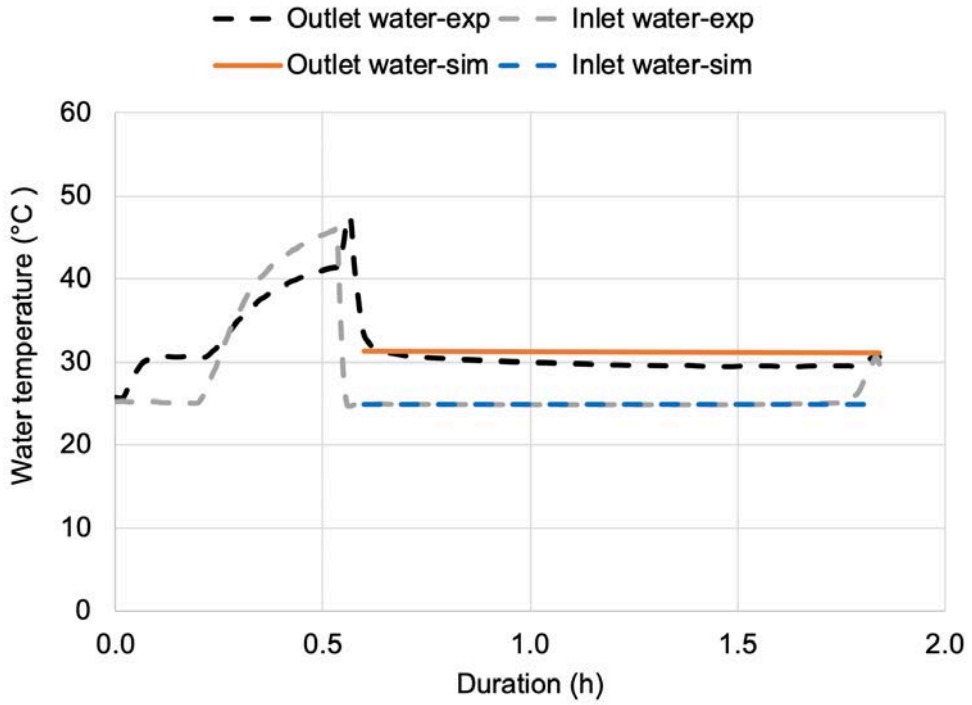

Figure 6 - 8 Measured and simulated fin pipe reactor inlet and outlet water temperature (Case 7)

6.2.3 Statistical analysis of the model validation

When validating the numerical model by the experimental results, the correlation between the numerical and experimental data is presented with the coefficient of correlation. It measures how well the two sets of data are related and can be calculated with the following equation (Shukla et al. 2008):

$$r' = \frac{N\sum_{i=1}^{i=N} F_i O_i - \sum_{i=1}^{i=N}(F_i)\sum_{i=1}^{i=N}(O_i)}{\sqrt{N\sum_{i=1}^{i=N} {F_i}^2 - \left(\sum_{i=1}^{i=N} F_i\right)^2}\sqrt{N\sum_{i=1}^{i=N} {O_i}^2 - \left(\sum_{i=1}^{i=N} O_i\right)^2}} \qquad 6.\ 1$$

Where there are N observations and forecast data F_i represents one of the forecast data obtained from the numerical model, O_i represents an observed experimental data.

Additionally, the root mean square of percent error (RMSPE) has been applied to the model validation which measures the percentage difference between the forecast data and observed values, given in the following expression (Guarino et al. 2017):

$$RMSPE = \sqrt{\frac{1}{N}\sum_{i=1}^{i=N}\left(\frac{O_i - F_i}{O_i}\right)^2} \times 100 \qquad 6.\ 2$$

The numerical model has been validated by comparing the computing values with the experimental results. Detailed statistical analysis is given in Table 6 - 2. The values of the coefficient of correlation and root mean square percentage error have been calculated for validating the model for the three-phase thermochemical reactor. The maximum root mean square percent error is for Case 2 at 12.78%. As reported in literature, the acceptable error is 14% (Shukla et al. 2008, Allouche et al. 2016) or the average error of less than 12% (Dolado et al. 2011). Therefore, there is a good agreement between the computed and measured results in both the charging and discharging processes.

Table 6 - 2 Statistical analysis in the model validation

Parameter	Value						
	Charging			Discharging			
	Case 1	Case 2	Case 3	Case 4	Case 5	Case 6	Case 7
Coefficient of correlation	0.96	0.98	0.94	0.93	0.91	0.95	-
Root mean square percent error (RMSPE)	12.29%	12.78%	7.64%	3.67%	12.79%	10.53%	6.02%

6.3 Parameters sensitivity analysis

Three parameters have been identified as sensible on the reactor temperature profile, the reference diffusivity D_0, heterogeneity factor n and initial water uptake X_0. These parameters are critical to adsorption isotherm and adsorption kinetics which affect the amount of heat charged or discharged from the adsorbent. The literature has reported uncertainty of the parameters. For instance, for the heterogeneity factor, in general, value of $n < 2$ are for heterogeneous carbons and value of $n > 2$ are for highly homogeneous carbons. However, Dubinin and Astakhov (1971), the suggested approximate value for zeolites is 4 to 6. While other literatures suggest the value ranging from 0.5 to 2 (Cortés et al. 2010). With respect to the reference diffusivity D_0, variations occur in different calculation method (Sircar and Hufton 2000) and molar fraction (Gorbach et al. 2004). For the initial water uptake, different experiment tests may start from different initial water uptake, affecting the adsorption kinetics and mass transfer scenario. This section presents how these parameters influence the reactor temperature profiles. The reactor outlet temperature is the zeolite temperature in charging, and the outlet air temperature in discharging. The base conditions can be referred to Table 6 - 3.

6.3.1 Effect of reference diffusivity

In charging, as shown in Figure 6 - 9(a), the reference diffusivity influences the elevation of temperature profile with respect to the charging time. Relatively larger reference diffusivity reduces the time required for the reactor reaching the charging inlet temperature. With the charging duration from 0 to 1 hour, the reactor outlet temperature increases to 80 °C ~ 95 °C for diffusivity from 2e-6 m^2/s to 4e-6 m^2/s while it increases to around 60 °C for diffusivity from 2e-7 m^2/s to 4e-7 m^2/s. In discharging, as shown in Figure 6 - 9(b), reference diffusivity ranging from 2e-7 m^2/s to 4e-7 m^2/s leads to less than 5 °C increase in reactor outlet temperature. When the diffusivity increases from 2e-6 m^2/s to 4e-6 m^2/s, the reactor temperature outlet increases significantly. Additionally, the steepness of the temperature profiles has been influenced by the diffusivity. According to the linear driving force model, the mass transfer coefficient increases with the rise

of diffusivity. Therefore, relatively larger amount of adsorption energy has been released, increasing the reactor outlet air temperature. The reference diffusivity used in the numerical modelling of the study is 2e-6 m^2/s.

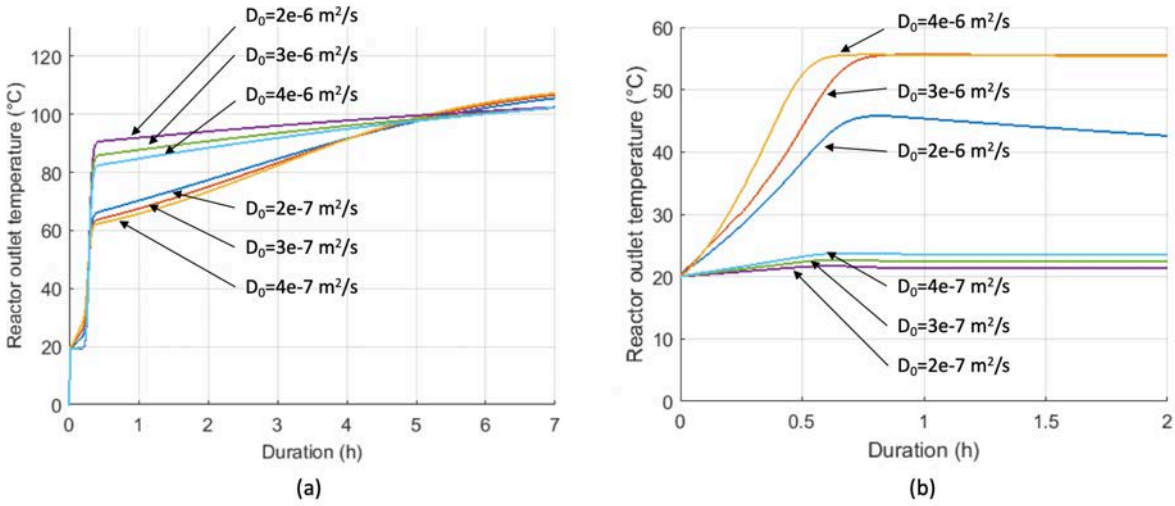

Figure 6 - 9 Influence of reference diffusivity to the temperature profile in (a) charging and (b) discharging

6.3.2 Effect of heterogeneity factor

Different heterogeneity factors for zeolite 13X have been reported in literatures (Dubinin and Astakhov 1971, Cortés et al. 2010). The results presented below illustrate the effect of the heterogeneity factor to the reactor outlet temperature (Figure 6 - 10). The heterogeneity factor n has been investigated from 0.5 to 6. At the beginning of the charging duration, there is a steep lift in the temperature profiles. The steepness has been enhanced by the increase of the heterogeneity factor. At relatively larger heterogeneity factor, the reactor outlet temperature reaches to the heat source temperature in a reduced amount of time. In terms of discharging, heterogeneity factor affects the level of peak outlet air temperature and the slope of the temperature profiles. The heterogeneity factor used in the numerical modelling of the study is 1.55.

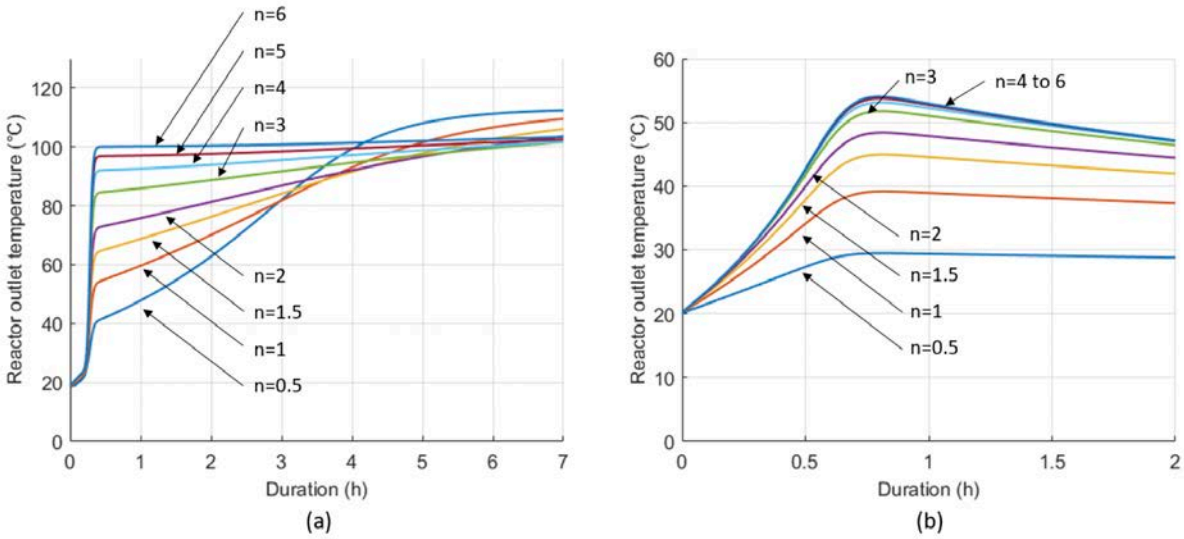

Figure 6 - 10 Influence of heterogeneity factor to the temperature profile in (a) charging and (b) discharging

6.3.3 Effect of initial water uptake

The effect of initial water uptake of zeolite 13X has been evaluated, as shown in Figure 6 - 11. In terms of charging, a relatively smaller initial water uptake increases the steepness of the outlet temperature profile and leads to a relatively higher temperature level within the first hour of charging. During the process, the margins among the reached temperature levels are reducing. However, when the initial water uptake is larger than 0.20 $kg_{H2O}/kg_{zeolite}$, the outlet temperature profile starts dropping significantly in the first hour of charging. When the charging duration goes up to the 7^{th} hour, all temperature profiles increase to the target charging temperature. Therefore, the initial water uptake is critical for the reactor temperature increasing at the start of a charging process. With respect to discharging, however, a relatively larger initial water uptake reduces the reactor outlet air temperature drastically from around 55 °C to less than 20 °C, as shown in Figure 6 - 11(b). The initial water uptake at 0.15 $kg_{H2O}/kg_{zeolite}$ can reach the peak discharging temperature under the current simulation conditions. The straight temperature profile indicates the adsorption energy is continuously transferring to the reactor within the 2 hours discharging session. However, when the initial water uptake increases to 0.30 $kg_{H2O}/kg_{zeolite}$, the temperature profile has been reaching the ambient temperature. The initial water uptake used in the

charging simulation is 0.33 $kg_{H2O}/kg_{zeolite}$ and in the discharging is 0.17 $kg_{H2O}/kg_{zeolite}$.

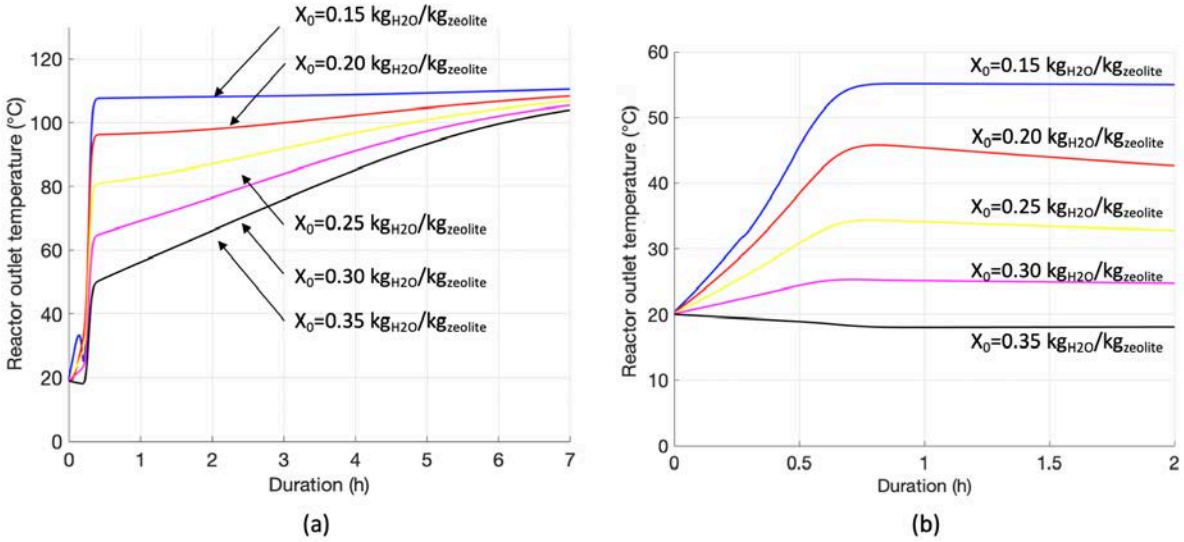

Figure 6 - 11 Influence of initial water uptake to the temperature profile in (a) charging and (b) discharging

6.4 The effect of air and adsorbent parameters on the reactor

The adsorption process takes place between the air and adsorbent. The parameters of air and adsorbent affect the reactor evaluation parameters, energy conversion efficiency (ECE) and extent of adsorption (EOA). According to the validated numerical model, this section investigates how a parameter of air and adsorbent affects the reactor's charging and discharging processes. The investigated parameters are inlet air temperature, air flow rate, inlet air relative humidity, adsorbent particle diameter, reactor bed porosity, and charging and discharging duration. The numerical model of the smooth pipe reactor has been applied in the investigation. The effect of the pipe on the reactor's charging and discharging is minimum since the size of the water pipe is relatively small and the water is unmoving.

Table 6 - 3 presents the initial and operative conditions of the analysis. The base conditions are referred to the validated zeolite adsorption models (Tatsidjodoung et al. 2016, Mette et al. 2014b). The discharging base conditions are inlet air temperature at 20 °C, air flow rate at 0.045 kg/s, relative humidity at 95%. The

discharging base conditions led to the adsorbent water uptake of 0.33 $kg_{H2O}/kg_{zeolite}$ when EOA reaches 100%. The water uptake is the initial water uptake of a charging process. The base conditions of a charging process are the air flow rate at 0.045 kg/s and inlet air temperature at 180 °C. Each charging duration is 4 hours. The charging base conditions lead to the adsorbent water uptake reducing to 0.19 $kg_{H2O}/kg_{zeolite}$. The water uptake is the initial water uptake for a discharging process. Then a discharging evolution is conducted with the discharging base conditions. Each discharging duration is 4 hours.

Table 6 - 3 Initial and operative conditions in the numerical analysis

Parameter	Symbol	Value	Unit	Reference
Bed porosity	ε_{bed}	0.39	-	(Tatsidjodoung et al. 2016)
Zeolite particle conductivity	$\lambda_{particle}$	0.20	W/(m·K)	
Activation energy	E_{act}	29.5	kJ/mol	
Reference diffusivity	D_0	2e-6	m^2/s	
Maximum adsorption volume	W_0	0.34e-3	$m^3/kg_{adsorbent}$	(Mette et al. 2014b)
Characteristic energy of adsorption in adsorption equilibrium	E_{ad}	1.1923e3	kJ/kg_{H2O}	
Zeolite particle diameter	d	4.0e-3	m	(Hengyi Chemical 2018)
Particle Porosity	$\varepsilon_{particle}$	0.32	-	(Sun et al. 1995)
Dry air density	ρ_a	1.177	kg/m^3	(R. Welty et al. 1970)
Air thermal conductivity	λ_a	2.62e-2	W/(m·K)	
Operative base conditions				
Ambient temperature		20	°C	
Inlet air temperature in charging		180	°C	
Inlet air mass flowrate in charging and discharging		0.045	kg/s	
Initial water uptake of zeolite 13X in charging	-	0.33	$kg_{H2O}/kg_{zeolite}$	
Initial temperature of zeolite 13X in charging and discharging		20	°C	
Inlet air relative humidity		95	%	

6.4.1 Impact of inlet air temperature

To evaluate impact of the intake air temperature, simulations have been conducted with intake air temperature ranging from 60 °C to 200 °C while other parameters remain as the base conditions. Figure 6 - 12 illustrates the evaluation parameters with the varying inlet air temperature in charging.

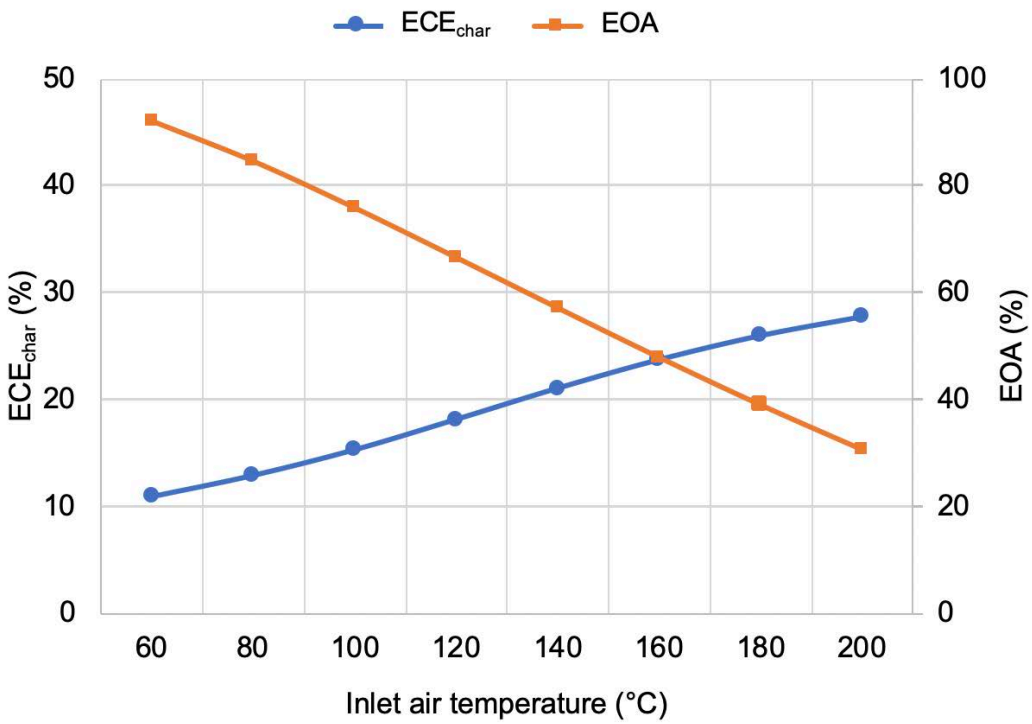

Figure 6 - 12 The reactor evaluation parameters with varying inlet air temperature in charging

The ECE_{char} increases and the EOA decreases with the increasing inlet air temperature. It shows that a higher inlet air temperature reaches a lower adsorbent water uptake. When the adsorbent reaches a higher temperature, the adsorption potential A_{ad} and equivalent diffusivity D_e increases, which leads to a larger mass transfer coefficient k_m. According to the linear driving force model, the increase in mass transfer coefficient leads to a larger rate of water uptake dX/dt. Therefore, increasing the inlet air temperature contributes to relatively larger amount of energy storage in the adsorbent. However, the relatively low inlet air temperature below 100 °C can be ineffective in a charging process. According to the analysis, the inlet air temperature at 100 °C has led to the

ECE_{char} and EOA at 15.3% and 75.9%, respectively. The relatively high EOA from a charging process can be unfavourable for the following discharging.

Figure 6 - 13 gives the reactor evaluation parameters with the varying inlet temperature in discharging. The inlet air temperature has been increasing from 20 °C to 70 °C with the other parameters remaining as base conditions.

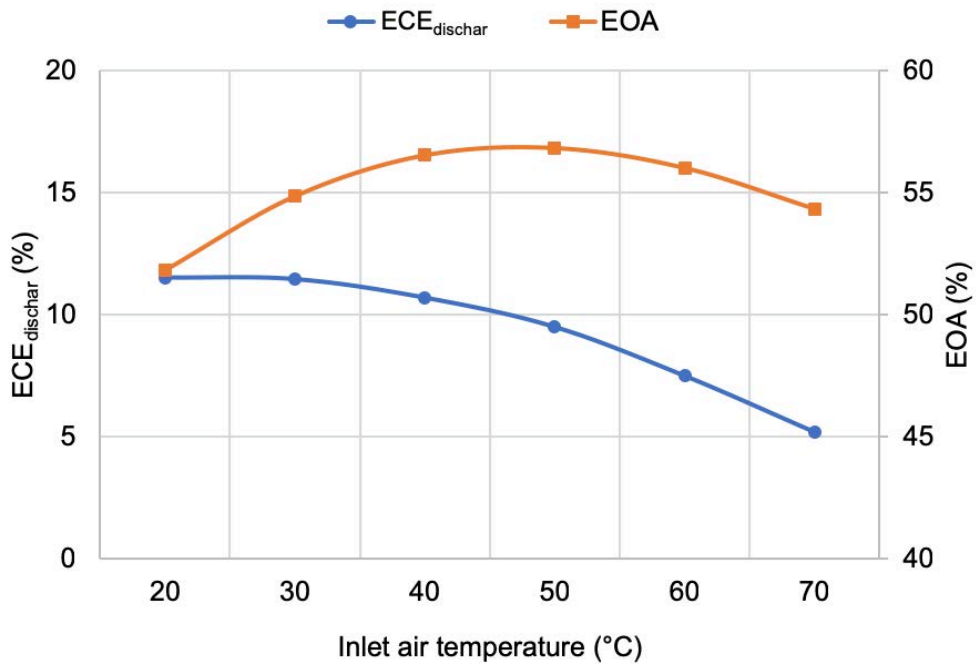

Figure 6 - 13 The reactor evaluation parameters with varying inlet air temperature in discharging

The $ECE_{dischar}$ decreases with the increasing inlet air temperature because relatively smaller air temperature lift has been achieved. When increasing the inlet air temperature, relatively more heat transfers to the adsorbent due to the temperature difference between the air and the adsorbent. It reduces the air temperature lift from the reactor. However, raising the inlet air temperature increases adsorbent temperature, which leads to a larger mass transfer coefficient k_m. According to the LDF model, it increases the rate of water uptake and contributes to the increase of EOA. In this evaluation, the EOA has increased from 51.8% to 56.6% with the inlet air temperature increasing from 20 °C to 40 °C. However, the EOA reduces with the inlet air at over 50 °C. This is because

the increase of adsorbent temperature constrains the discharging capability by reducing the equilibrium water uptake X_{eq}. The equilibrium water uptake X_{eq} reduced at a higher temperature. Thus, relatively less moisture is adsorbed in the reactor.

6.4.2 Impact of air flow rate

In addition to intake air temperature, the effect of air flow rate has been conducted. As shown in Figure 6 - 14, ECE_{char} and EOA reduce with the increasing air mass flow rate. With the air mass flow rate increasing to 0.19 kg/s, ECE_{char} and EOA reduces to 9.6% to 11.2%, respectively. It shows that an increase in moisture transfer has been achieved at a larger air mass flow rate. Since the moisture transfer is initiated by the vapour pressure difference between the air flow and solid adsorbent, the vapour pressure difference remains at a relatively higher level when there is relatively larger amount of air mass flow.

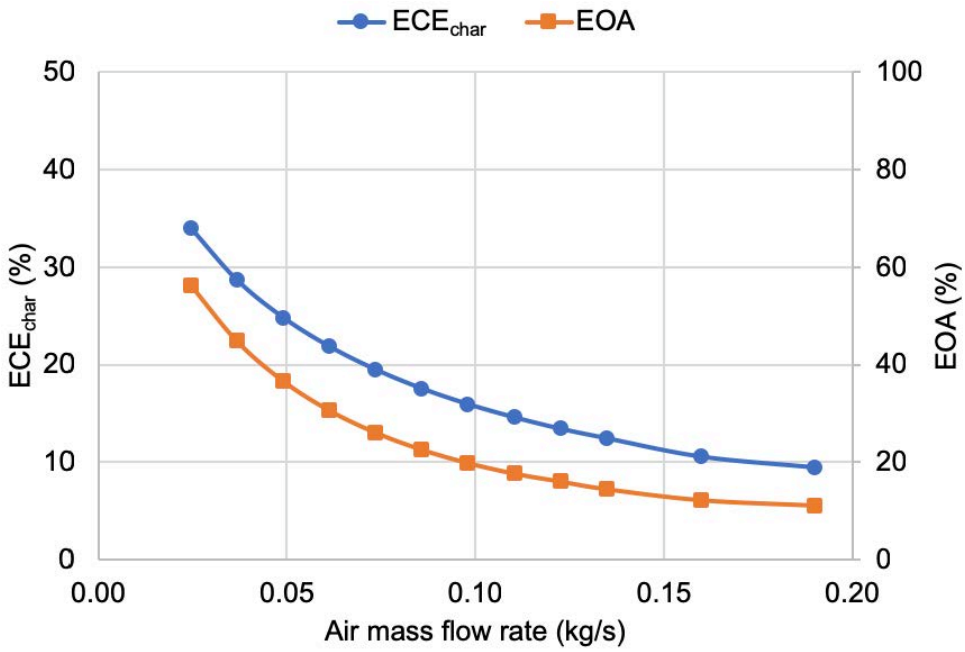

Figure 6 - 14 The reactor evaluation parameters with varying air mass flow rate in charging

Figure 6 - 15 shows the $ECE_{dischar}$ and EOA with the increasing air mass flow rate in discharging. Both profiles remain relatively stable with the average $ECE_{dischar}$

at 11.8% and the average EOA at 51.1%. This shows that, in discharging, increasing the air flow rate may not have a strong effect in increasing the amount of moisture absorbed in the reactor. This has resulted from the reduction of adsorbent temperature. Although increasing the air mass flow rate leads to an increasing amount of moisture supply, it reduces the adsorbent temperature since the inlet air temperature is lower than the adsorbent temperature. In this analysis, when increasing the air mass flow rate from 0.19 kg/s to 0.3 kg/s, the peak and average adsorbent temperature has been reduced by 33 °C and 12 °C, respectively. It leads to the decrease of mass transfer coefficient k_m and rate of water uptake dX/dt.

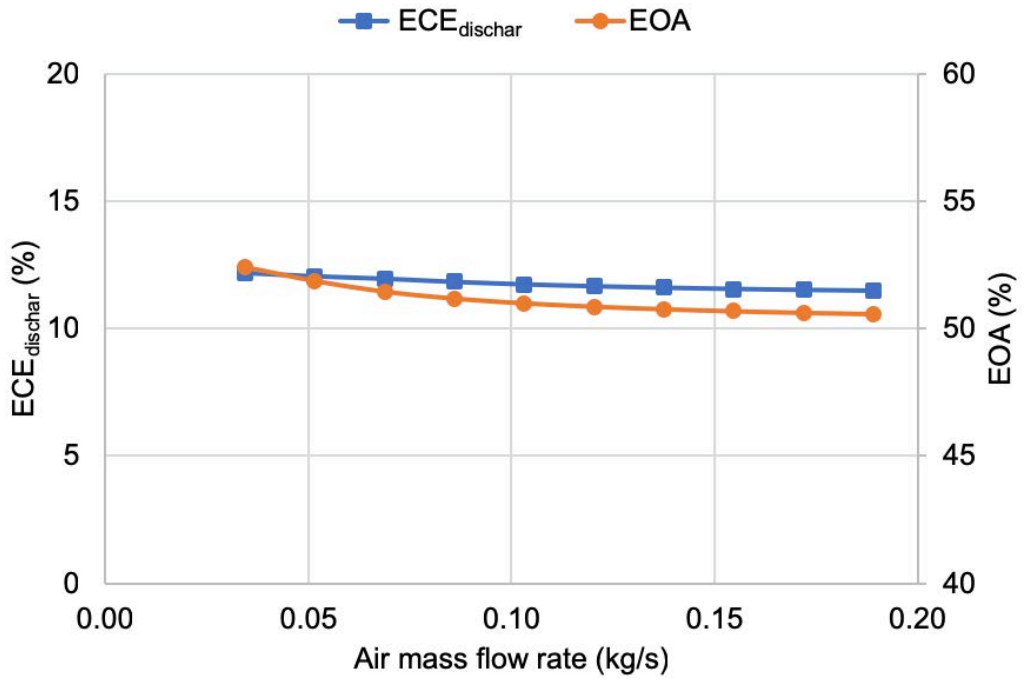

Figure 6 - 15 The reactor evaluation parameters with varying air mass flow rate in discharging

6.4.3 Impact of inlet air relative humidity

Since moisture transfers between air flow and solid adsorbent, the inlet air relative humidity can affect the reactor performance. Figure 6 - 16 illustrates the simulation results where the inlet air relative humidity varies from 10% to 90% with other parameters remaining as the base conditions.

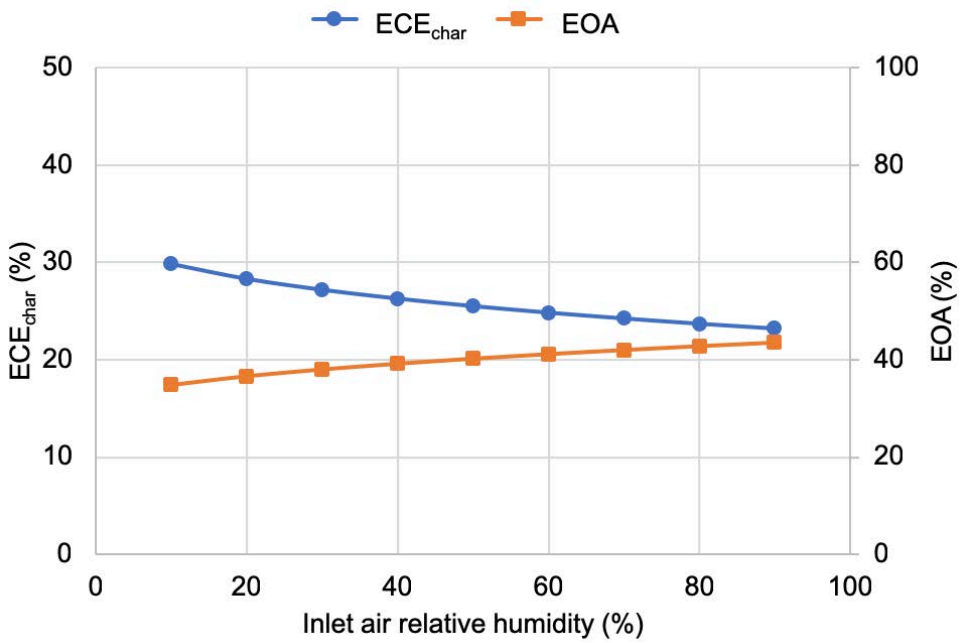

Figure 6 - 16 The reactor evaluation parameters with varying inlet air relative humidity in charging

The rise of the inlet air relative humidity reduces ECE_{char} and increases EOA. With respect to ECE_{char}, it reduces from 29.8% to about 23.1%. For the EOA, it increases from 34.8% to around 43.4%. The increase in inlet air relative humidity leads to a larger vapour pressure in the air. It increases adsorption volume W in the adsorbent, resulting in a larger water uptake at equilibrium state X_e. Since the rate of water uptake dX/dt is determined by the difference between the X_e and the actual water uptake X, the increase of equilibrium water uptake X_e leads to relatively lower rate of water uptake dX/dt and lower amount of moisture transfer. Although increasing the inlet air relative humidity is unfavourable to a charging process, the impact is relatively insignificant because the adsorbent temperature plays a dominant role in charging.

For a discharging process, Figure 6 - 17 depicts the $ECE_{dischar}$ and EOA with the inlet air relative humidity varying from 10% to 90%. Both parameters increase with the rising relative humidity from 1.7% to 11.9% for $ECE_{dischar}$ and from 42.1% to 52.1% for EOA. Since the mass transfer is initiated by the vapour pressure

difference between air and adsorbent, improving the inlet air relative humidity allows an increasing amount of moisture transfer.

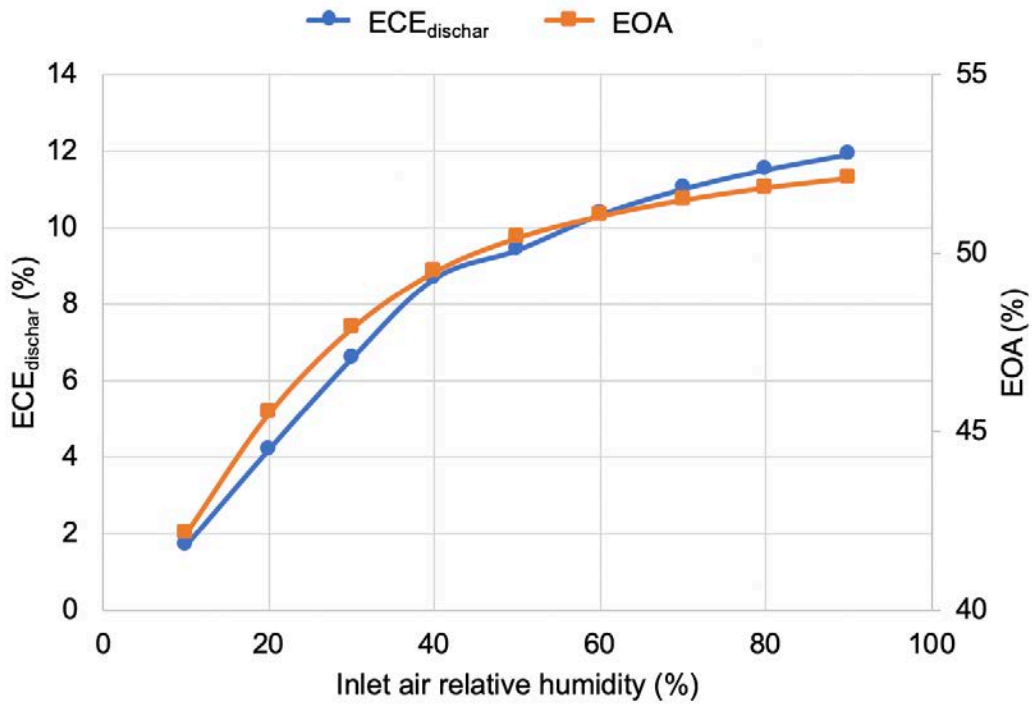

Figure 6 - 17 The reactor evaluation parameters with varying inlet air relative humidity in discharging

6.4.4 Impact of adsorbent particle diameter

To evaluate the impact of adsorbent particle diameter on evaluation parameters, analysis has been conducted on varying the particle diameter from 3.5 mm to 6 mm with other parameters remaining as the base conditions. The simulation results are shown in Figure 6 - 18.

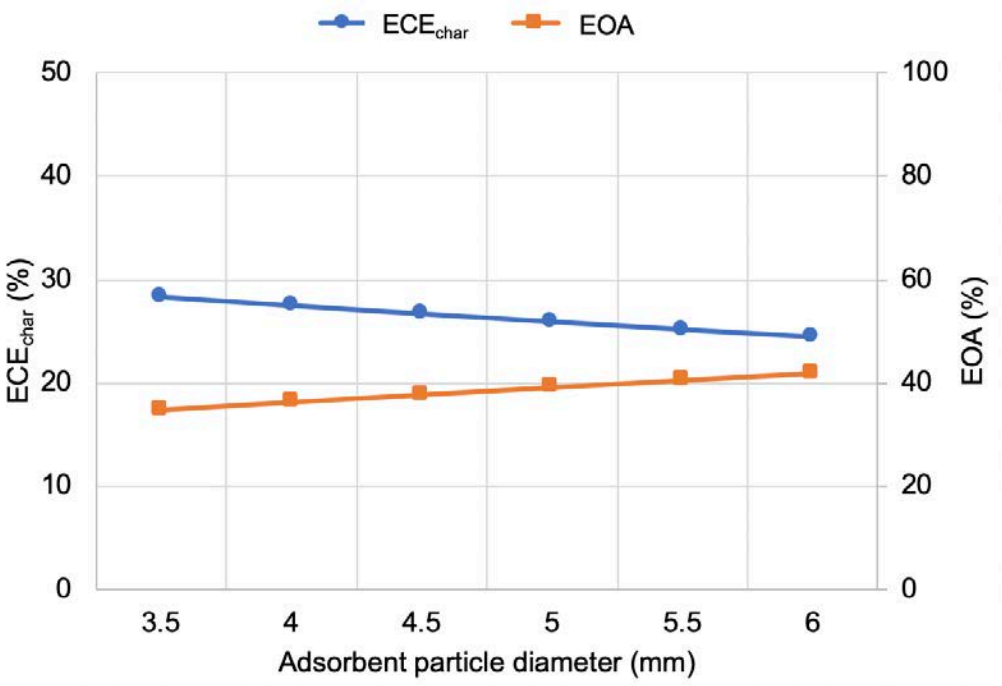

Figure 6 - 18 The reactor evaluation parameters with varying adsorbent particle diameter in charging

For charging, a larger particle diameter achieves a smaller ECE_{char} and a larger EOA. The ECE_{char} reduces from 28.3% at 3.5 mm to 24.4% at 6 mm. The EOA increases from 34.9% at 3.5 mm to 41.8% at 6 mm. This shows the reduction of the amount of moisture transfer with the increasing particle diameter. The particle diameters links to the mass transfer coefficient k_m, where the decrease of particle diameters achieves a larger k_m. The mass transfer coefficient k_m then contributes to a larger rate of water uptake dX/dt, promoting the moisture transfer. Besides the contribution to charging, a smaller particle diameter can achieve a more extensive discharging. As show in Figure 6 - 19, in the discharging analysis, the particle diameter at 3.5 mm achieves $ECE_{dischar}$ and EOA at 20.6% and 60.7%, respectively.

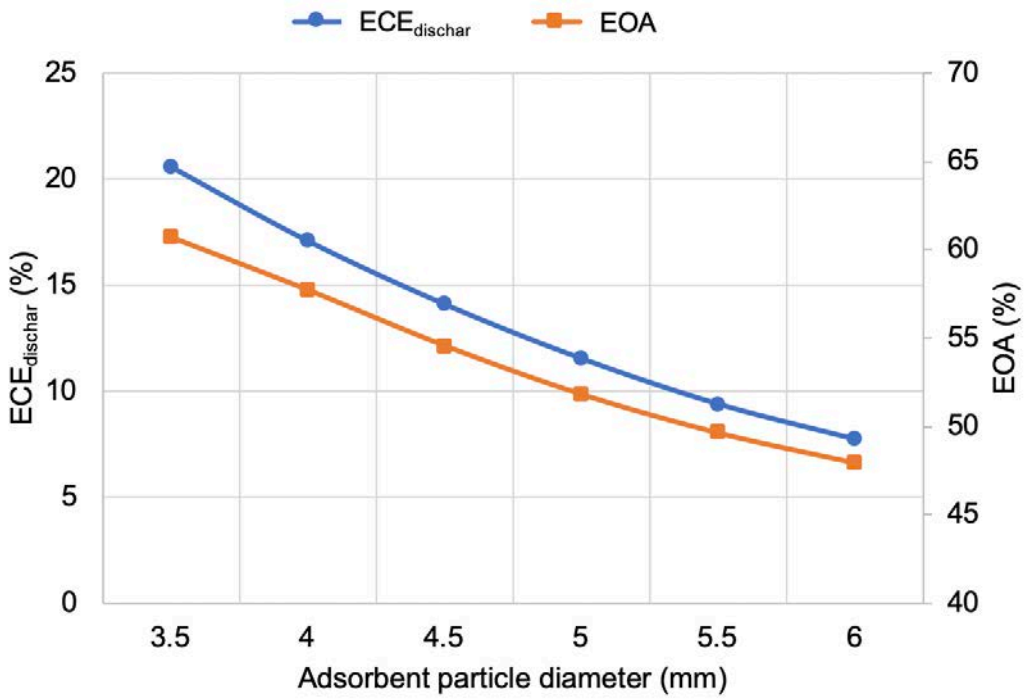

Figure 6 - 19 The reactor evaluation parameters with varying adsorbent particle diameter in discharging

6.4.5 Impact of reactor bed porosity

Reactor bed porosity provides the void fraction inside the reactor. When other parameters remain as the base conditions, analysis has been conducted by increasing the bed porosity from 0.3 to 0.7. Figure 6 - 20 depicts the evaluation parameters in charging. The ECE_{char} and EOA decrease drastically with the increasing bed porosity. The ECE_{char} drops from 26.7% at porosity of 0.3 to 0.5% at porosity of 0.7. The corresponding EOA decreases from 40.8% to 1.2%, respectively. The decrease of EOA shows an extensive amount of moisture has been extracted from the adsorbent. This is closely linked to the increase in air flows through the adsorbent. In detail, bed permeability has been increased when increasing the bed porosity value. According to the study, the permeability of bed porosity 0.6 is 23 times higher than that of the 0.3. Following the increase of permeability, air velocity has been improved accordingly. Therefore, under the same amount of charging duration, a relatively larger amount of air has travelled through the adsorbent, improving the moisture transfer. However, the increase of

air flow rate leads to the decrease of ECE_{char} by increasing the thermal energy input to the reactor.

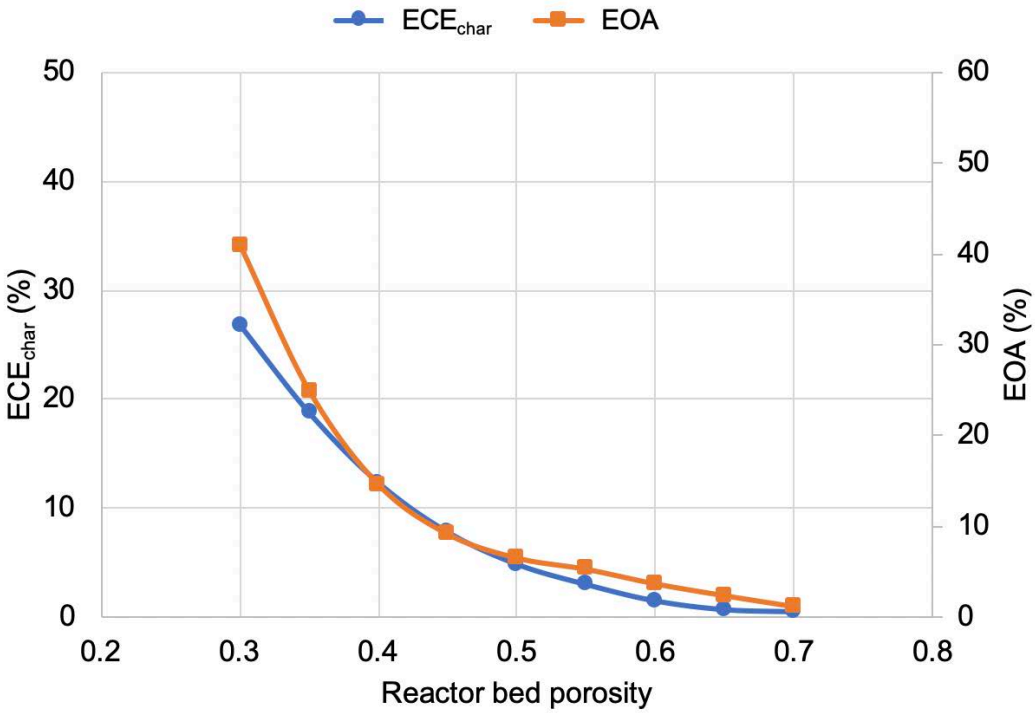

Figure 6 - 20 The reactor evaluation parameters with varying reactor bed porosity in charging

Figure 6 - 21 shows the evaluation parameters in discharging with increasing bed porosity. Unlike the charging analysis, both parameters remain almost constant in discharging. This is caused by the increase of air flow and decrease of mass transfer coefficient k_m. The increase of bed porosity leads to air flow rate increase. When air flow rate is relatively slow and the time for the mass transfer is relatively long, the air flow tends to become in equilibrium with the adsorbent. With the increase of air flow rate, the vapour pressure difference between the air and adsorbent becomes relatively larger which promotes the moisture transfer. However, the adsorbent temperature decreases with the increase of air flow rate because the heat transfers from the adsorbent to the air. This leads to the decrease of mass transfer coefficient k_m. In this analysis, the average mass transfer coefficient k_m has reduced by 26.7% with the porosity increasing from 0.3 to 0.7, which constrains the moisture transfer. In this analysis, the moisture

transfer elevation by the air flow and limitation from the mass transfer coefficient k_m has resulted in relatively stable evaluation parameters.

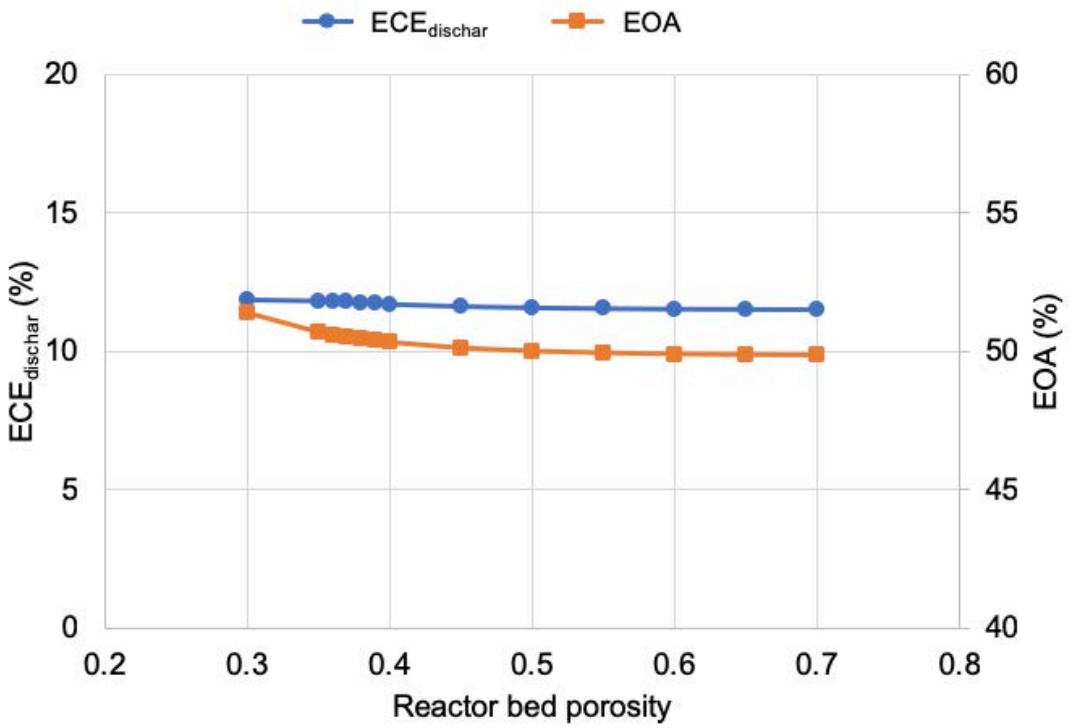

Figure 6 - 21 The reactor evaluation parameters with varying reactor bed porosity in discharging

6.4.6 Impact of charging and discharging duration

In addition to the parameters of air flow and solid adsorbent, the duration in charging and discharging can affect the evaluation parameters. In this study, the effect of charging duration has been investigated for the charging duration from 0.5 hour to 5.5 hours with other conditions remaining as the base conditions (Figure 6 - 22).

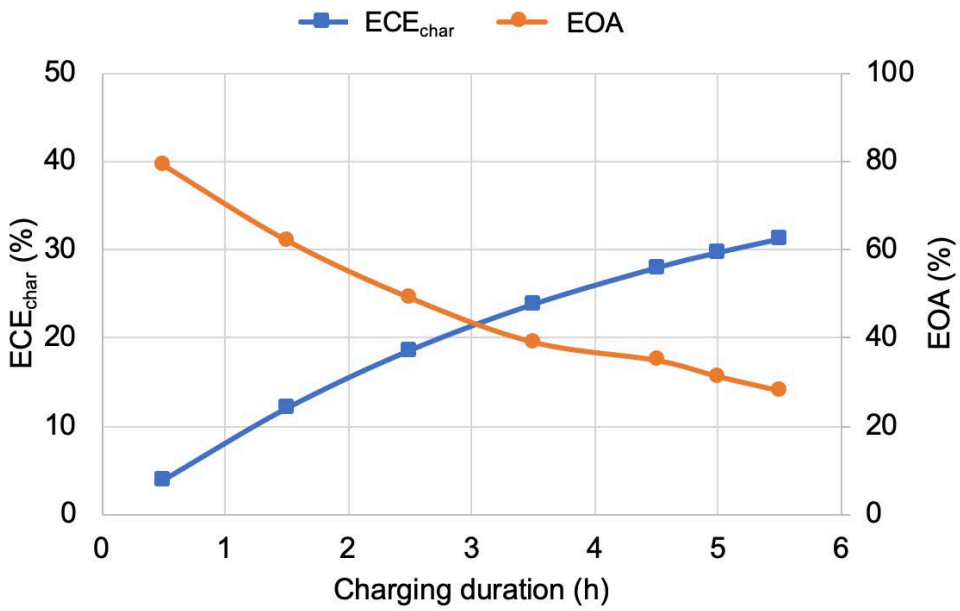

Figure 6 - 22 The reactor evaluation parameters with charging duration

The ECE_{char} increases from 3.9% for 0.5 hour to 31.1% for 5.5 hours. The EOA decreases from 89.4% for 0.5 hour to 28.1% for 5.5 hours. Besides the decrease of EOA, the change of EOA reduces with the increasing charging duration. The EOA reduces by 30.3% for charging duration from 0.5 hour to 2.5 hours and it reduces by 20.2% for charging duration from 2.5 hours to 4.5 hours. When the adsorbent reduces water uptake, a charging process requires increasing time consumption as the adsorbent approaches to the charging equilibrium.

Figure 6 - 23 depicts the rate of water uptake with the increase of charging duration along with the reactor bed length. Air travels through the reactor bed length and the peak rate of water uptake dX/dt for each duration has been marked in the figure. Dehydration occurs from the side of the inlet air to the exit. Therefore, with the charging time increases, the peak rate of water uptake moves along the bed length. However, for the time step of 1 hour, the distance of the dX/dt peaks (dash line in the figure) narrows when the charging time increases. This is because when the adsorbent is being dehydrated, it is losing vapour to the air flow, reducing the vapour pressure difference between the air and adsorbent. Therefore, it takes an increasing time consumption to proceed a charging process as the adsorbent becomes dehydrated.

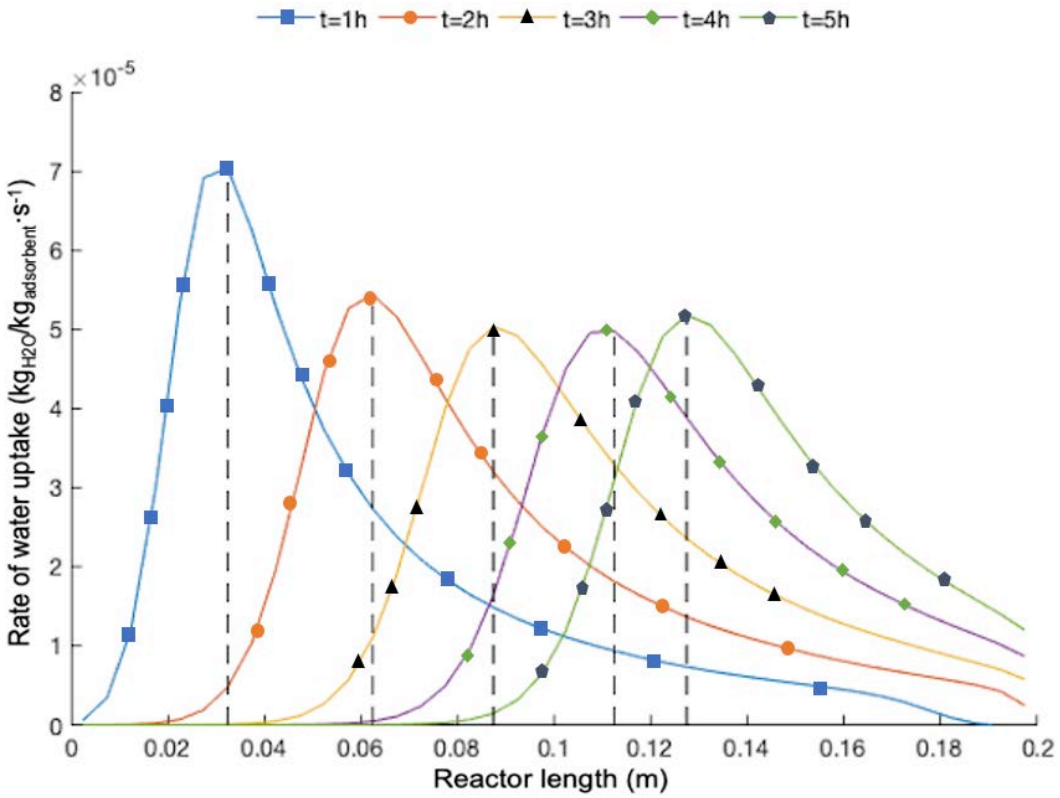

Figure 6 - 23 Rate of water uptake with the charging durations in the reactor

For the effect of discharging duration, Figure 6 - 24 depicts the evaluation parameters with the discharging duration increasing from 0.5 hour to 5.5 hours. In this analysis, both $ECE_{dischar}$ and EOA increase with the increase of discharging duration. Both parameters are nearly proportional to the discharging duration, because the inlet moisture is the main factor limiting the increase of the evaluation parameters in discharging. The adsorbent adsorbs the inlet water vapour until it achieves a certain amount of water uptake.

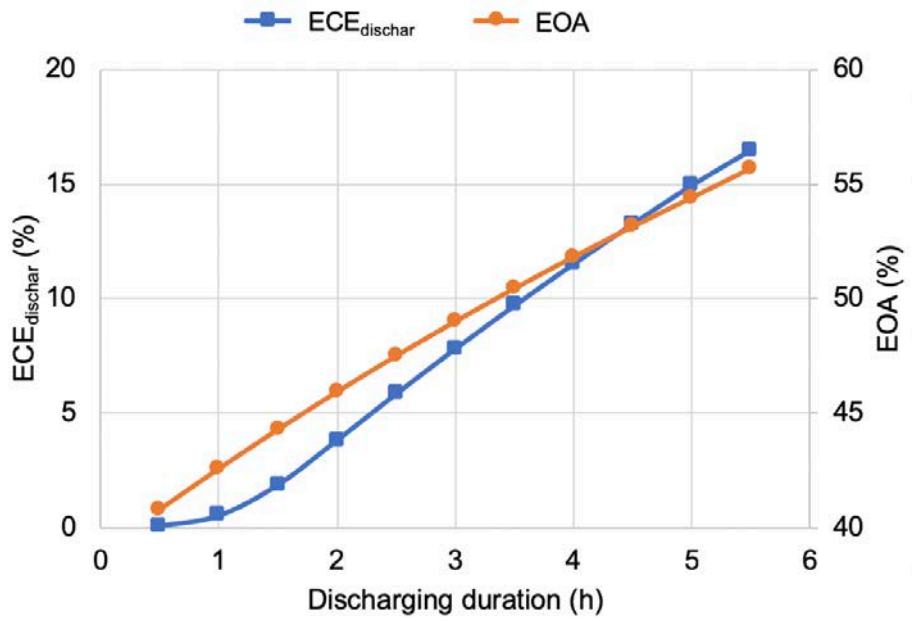

Figure 6 - 24 The reactor evaluation parameters with discharging duration

6.4.7 Interactions of the air and adsorbent parameters

Figure 6 - 25 shows the interactions of air and adsorbent parameters in charging and discharging processes. Parameters linked by the lines indicate a close correlation. The change of a parameter leads to the change of the other. A larger width of the lines indicates a relatively higher level of influence from one parameter to the other. For instance, the influence of bed porosity to permeability is relatively larger to the particle diameter.

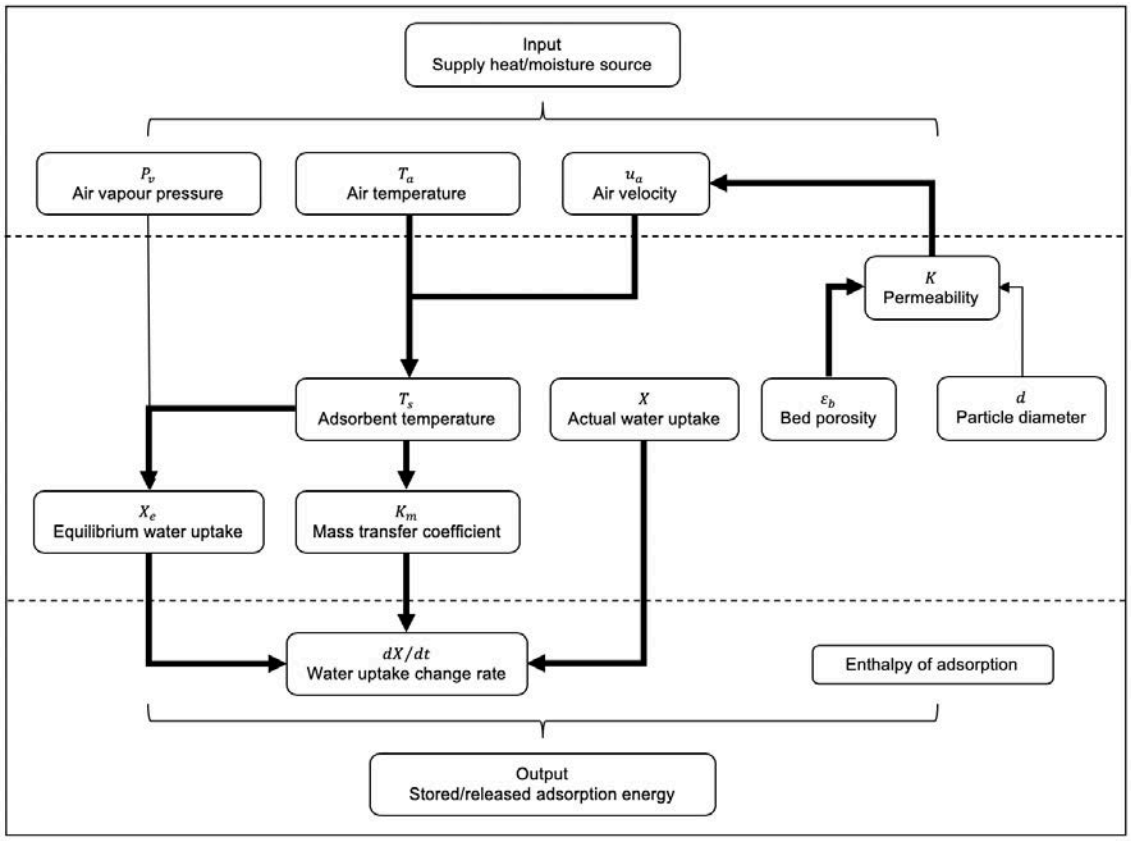

Figure 6 - 25 Interaction of parameters in charging and discharging

The interactions apply to both charging and discharging processes. With respect to a charging process, for example, the rise of adsorbent temperature T_s is initiated by the air temperature T_a. The T_s leads to the increase of mass transfer coefficient K_m and rate of water uptake change dX/dt, improving the mass transfer and allowing relatively more energy to be stored in the adsorbent. Meanwhile, the increase of T_s leads to the decrease of equilibrium water uptake X_e, contributing to the rise of dX/dt. Additionally, the actual water uptake X, determined by adsorbent initial condition and charging condition, affects the dX/dt during a charging process. For a discharging process, the air temperature T_a influences the adsorbent temperature T_s which can increase the mass transfer coefficient K_m and decrease the equilibrium water uptake X_{eq}. The mass transfer boosted by the increasing K_m and hindered by the decreasing X_{eq} ultimately results in the rate of water uptake dX/dt.

6.5 The three-phase reactor configuration effects and operation conditions on the evaluation indicators

Besides the investigation of air and adsorbent parameter's effect on the evaluation parameters, the study has conducted a configuration analysis on the three-phase reactor. The configuration study is to present and evaluate the three-phase reactor in both charging and discharging processes. The investigation includes geometric and operational parameters of the reactor including the integration of fins, fin pitches, reactor length and width, inlet air temperature and water flow rate. The evaluation indicators have been used for charging and discharging analysis, as given in Table 6 - 4.

Table 6 - 4 Evaluation indicators in the configuration analysis

Definition	Unit
Charging	
Time consumption for the EOA from 100% to 20%	Hour
ECE_{char}	%
Discharging	
Average outlet air temperature	°C
Average outlet water temperature	°C
EOA	%
$ECE_{dischar}$	%

The initial and operative conditions follow Table 6 - 3. Each evaluation includes a charging process and two discharging processes. The charging process starts from EOA at 100%, which is determined by the discharging base conditions. A charging process terminates when the EOA reaches 20% to store a relatively large amount of adsorption energy for the following discharging. The ECE_{char} and time consumption are the evaluation indicators in charging. For the first discharging process, the reactor operates in the air supply mode by using the reactor outlet air as the useful heat without water supply. For the second discharging process, the reactor operates in air and water supply mode by using air and water as useful heat. Each discharging process starts from the EOA at

20% with the operative conditions of Table 6 - 3 for 4 hours. The evaluation indicators in discharging are the average outlet air and water temperature, EOA at the end of discharging, and $ECE_{dischar}$.

6.5.1 The effect of fin pitches on the evaluation indicators

The effect of fin pitches has been studied by varying the fin pitch from 10 mm to 50 mm in charging and discharging processes. For charging, Figure 6 - 26 presents the ECE_{char} and time consumption of the fin pipe reactor under different fin pitches. According to Figure 6 - 26, smaller fin pitches leads to less time consumption and larger ECE_{char}, making the reactor more efficient in charging. From fin pitches of 50 mm to 10 mm, the ECE_{char} has been increased by 38.4% and the time consumption has been reduced by 37.1%. Reducing the fin pitches increases the number of fins in the reactor, improving the heat and mass transfer. The fins contribute to the increase of adsorbent temperature, rate of water uptake and mass transfer coefficient. Figure 6 - 27 depicts the overview of the fin pipe reactor temperature distribution in charging. It shows the fins direct the heat across the reactor, increasing the zeolite temperature significantly. Comparing with smooth pipe reactor, the average reactor temperature achieves 31% higher for the fin pipe reactor.

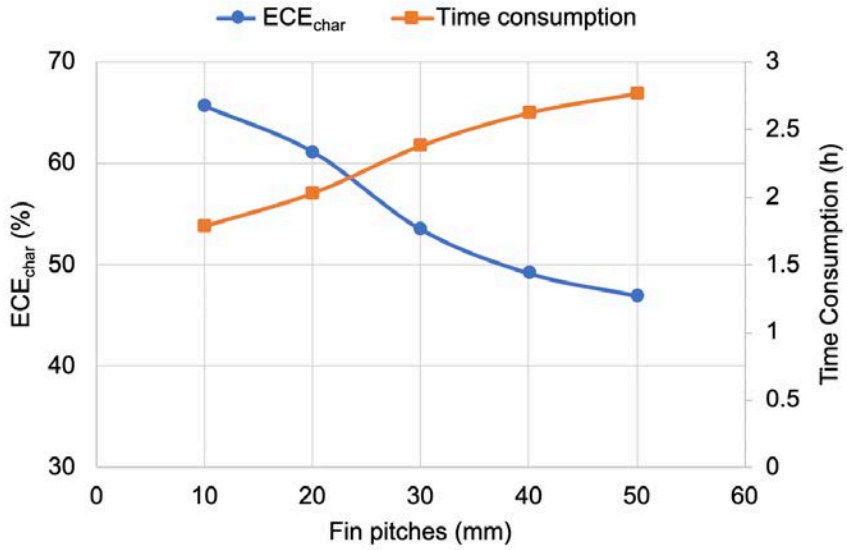

Figure 6 - 26 ECE_{char} and time consumption with varying fin pitches in charging

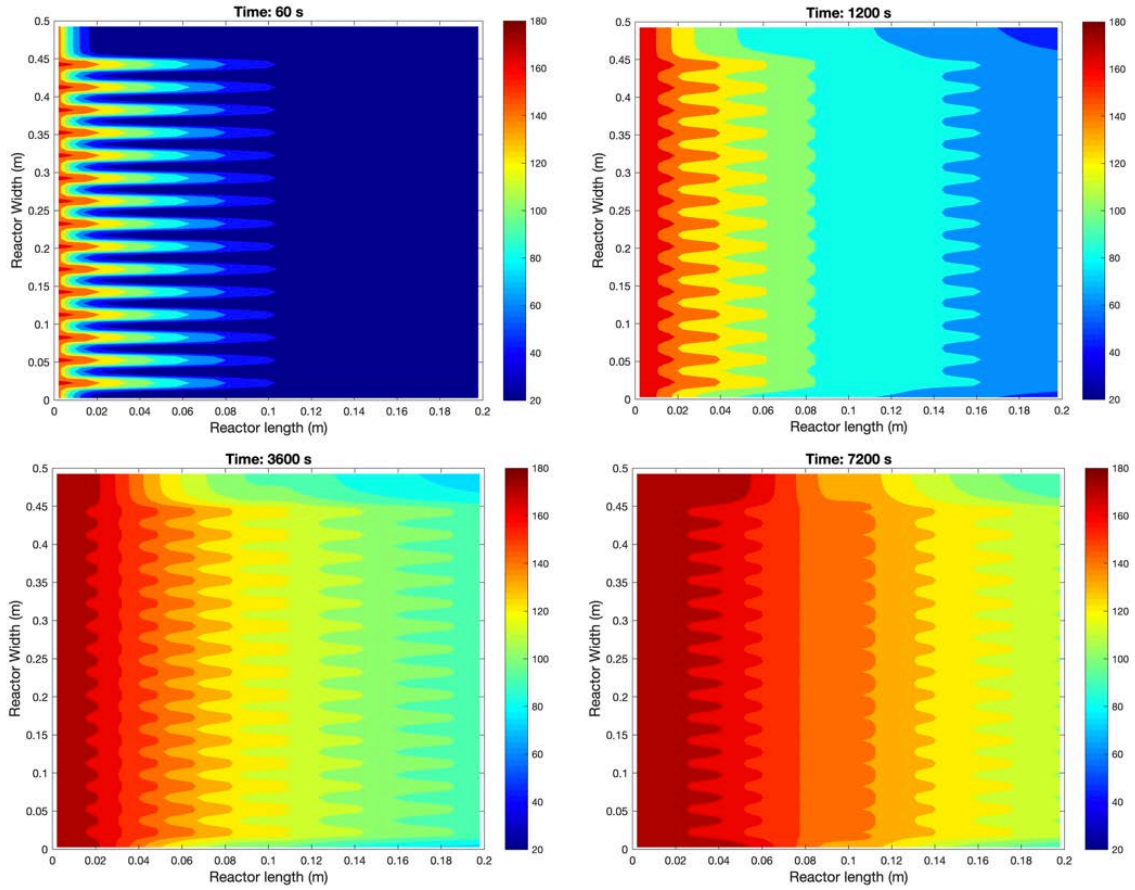

Figure 6 - 27 The fin pipe reactor temperature in charging

In terms of discharging, evaluation has been conducted for the reactor in air supply and air and water supply mode with varying fin pitches from 10 mm to 50 mm. Figure 6 - 28 gives the $ECE_{dischar}$ and EOA and Figure 6 - 29 shows the average outlet air and water temperature. Both $ECE_{dischar}$ and EOA are relatively higher in the air supply mode than the air and water supply mode. This is because without heat extraction of the water flow, the reactor temperature is higher in air supply mode which has enhanced the adsorption process. Relatively more moisture has been transferred to the zeolites, leading to a higher EOA and $ECE_{dischar}$. The water temperature increment is relatively small for the $ECE_{dischar}$ in air and water supply mode. For the air mode, when reducing the fin pitches from 50 mm to 10 mm, the $ECE_{dischar}$ and EOA reduce from 31.2% to 21.7% and from 53.1% to 50.9%, respectively. It shows that relatively less adsorption energy has been released when reducing the fin pitches, because reducing fin pitches leads to relatively smaller air outlet temperature. Since the inlet air temperature

can be lower than the adsorbent temperature, increasing the number of fins reduces the adsorbent temperature. When reducing the fin pitches, the adsorbent temperature is more likely to be affected by the initial conditions. As seen from Figure 6 - 29, for both air and air and water supply modes, the average outlet temperature increases with the increase of fin pitches. For the air and water supply mode, the water outlet increases from 20.3 °C at 10 mm fin pitch to 21.7 °C at 50 mm fin pitch. The reactor has achieved a relatively small outlet water temperature lift. This is mainly attributed to operational parameters such as inlet air temperature and flow rate. For the average outlet air temperature, the reactor achieves a relatively lower level than the air mode for the cooling effect of the water flow. The reactor with 50 mm fin pitch achieves the highest at 46.5 °C which gradually reduces with the fin pitches and achieves at 28.8 °C at 10 mm fin pitch.

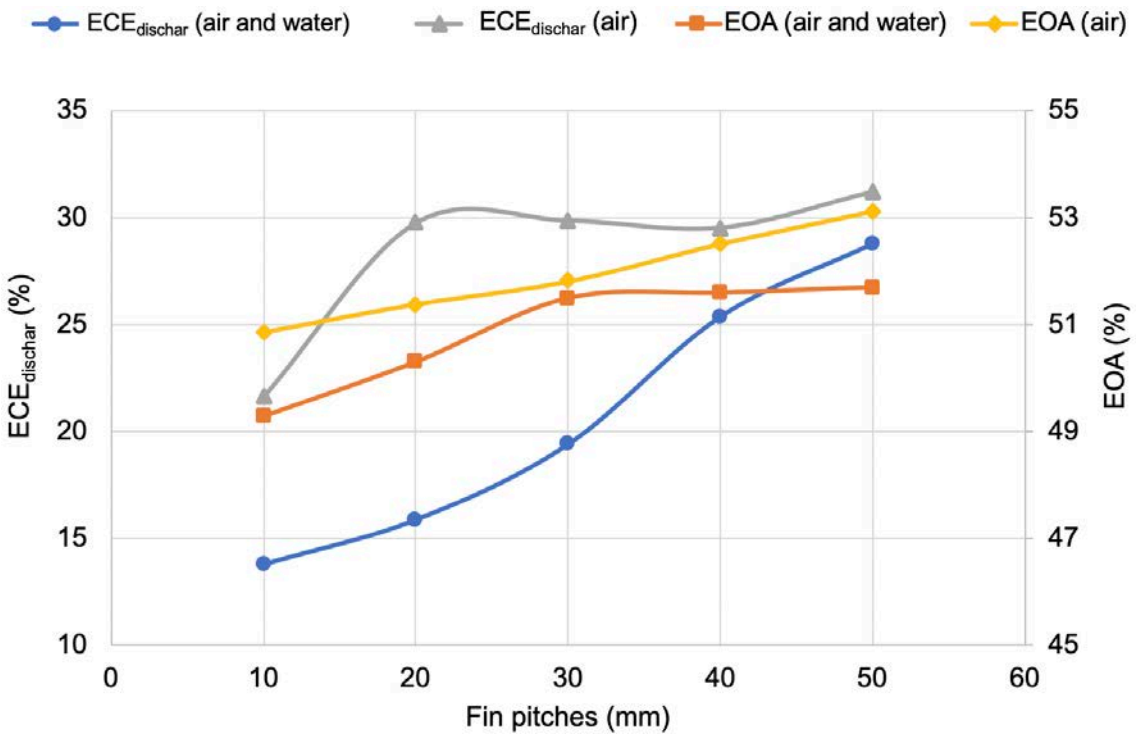

Figure 6 - 28 ECE$_{dischar}$ and EOA of the reactor with varying fin pitches in discharging in air supply mode and air and water supply mode

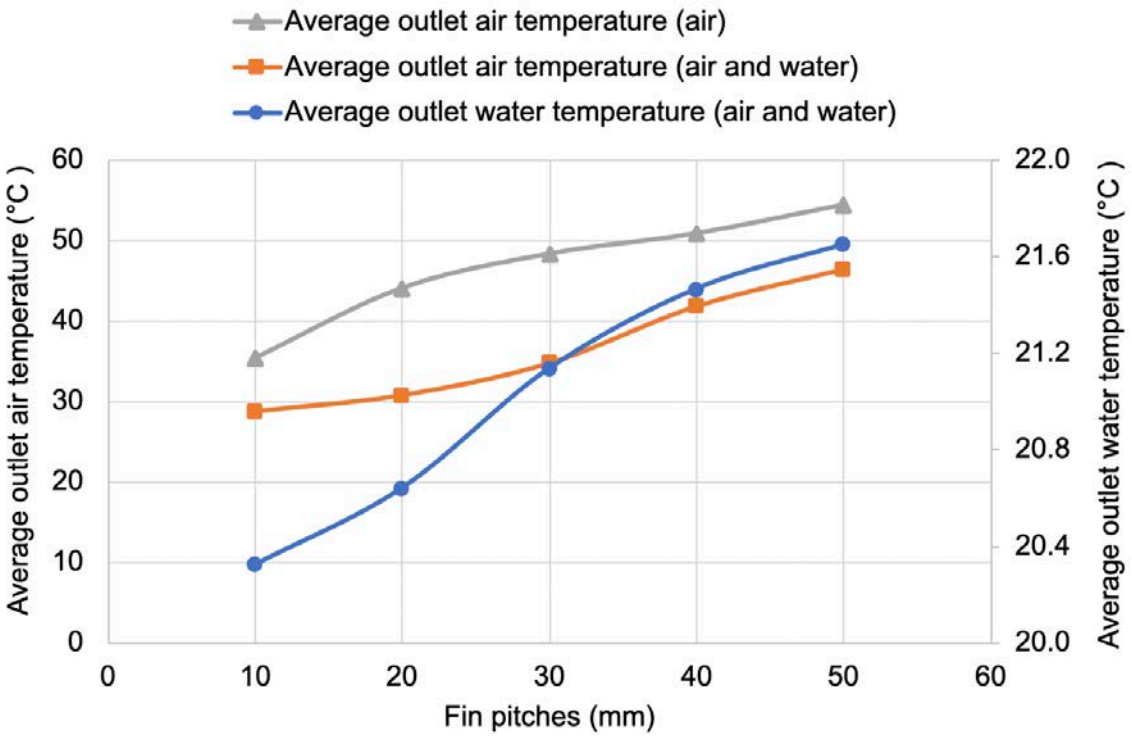

Figure 6 - 29 The average outlet air and water temperature with varying fin pitches in discharging in air supply mode and air and water supply mode

6.5.2 The effect of gap size on the evaluation indicators

The effect of varying the gap size has been evaluated with other parameters remaining as the initial conditions. According to the diameter of the zeolite particle, the gap size has been varying from 1 mm to 5 mm. Figure 6 - 30 illustrates the reactor ECE_{char} and time consumption with the varying gap size. The gap size increase has increased the thermal energy input of air and reduced the time consumption to reach the target EOA of 20% in charging. Increasing the gap size allows a relatively larger amount of air to travel through the reactor. It leads to higher temperature increase of the adsorbent and improves the mass transfer performance. As shown in the time consumption, the gap size of 5 mm has reduced the charging time by 30% comparing with gap size of 1 mm. For the ECE_{char}, the increase of gap size from 1 mm to 5 mm has reduced it from 55.8% to 47.1%.

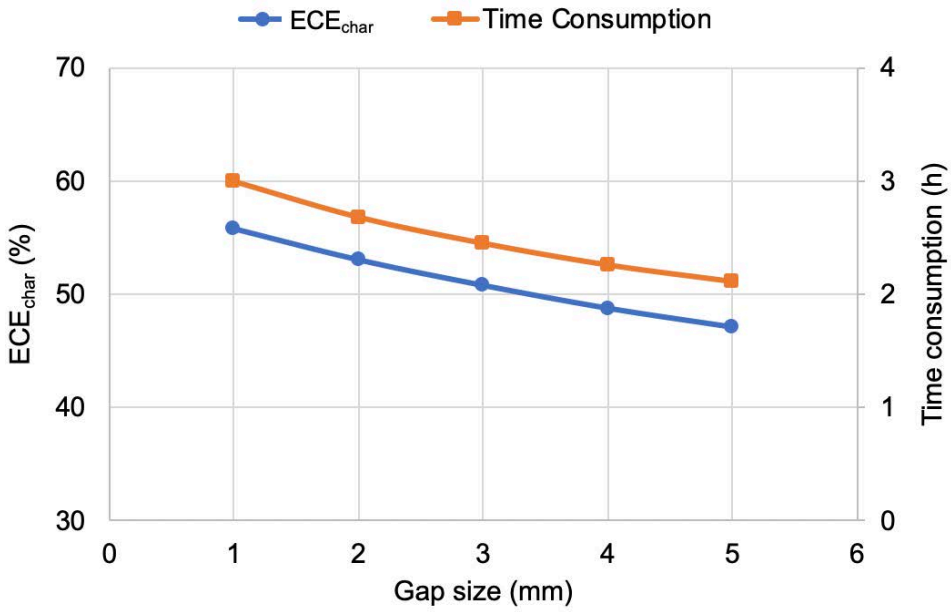

Figure 6 - 30 ECE$_{char}$ and time consumption with varying gap sizes in charging

For discharging, when the reactor operates in air supply mode and air and water supply mode, Figure 6 - 31 shows the average outlet air temperature with the varying gap sizes. For the air mode, the average outlet air temperature of the reactor increases with the increasing gap size and peaks at 53.4 °C with 2 mm before decreasing to 35.7 °C with 5 mm gap size. For the air and water supply mode, the reactor shows a similar trend in the air temperature profile and the water temperature reduces with the gap size increase. The 1 mm gap size achieves the average outlet water temperature at 21.5 °C, which reduces to 20.9 °C at 5 mm gap size. Figure 6 - 32 shows the ECE$_{dischar}$ and EOA with the varying gap size. The ECE$_{dischar}$ in air mode peaks at 31.1% at 2 mm gap size and drops to 18.6% at 5 mm gap size. In air and water mode, ECE$_{dischar}$ achieves the highest at 24.9% at 1 mm and reduces to 15.4% at 5 mm gap size. For the EOA, the reactor in air mode achieves a larger value at 54.6% at 5 mm gap size compared to the 51.7% in air and water mode with the same gap size. Increasing the gap size allows relatively more moisture to transfer to the adsorbent. This increases the water vapour pressure difference between the air and adsorbent which increases the EOA. However, the increasing gap size also enhances the cooling effect from the inlet air, reducing the adsorbent temperature and rate of water uptake. In this study, the gap size at 2 mm achieves the highest average

rate of water uptake at 6.97E-6 $kg_{H2O}/(kg_{zeolite}\cdot s)$ in discharging. Therefore, increasing the gap sizes leads to a larger EOA but an excessive gap size constrains the reactor achieving a relatively high output temperature.

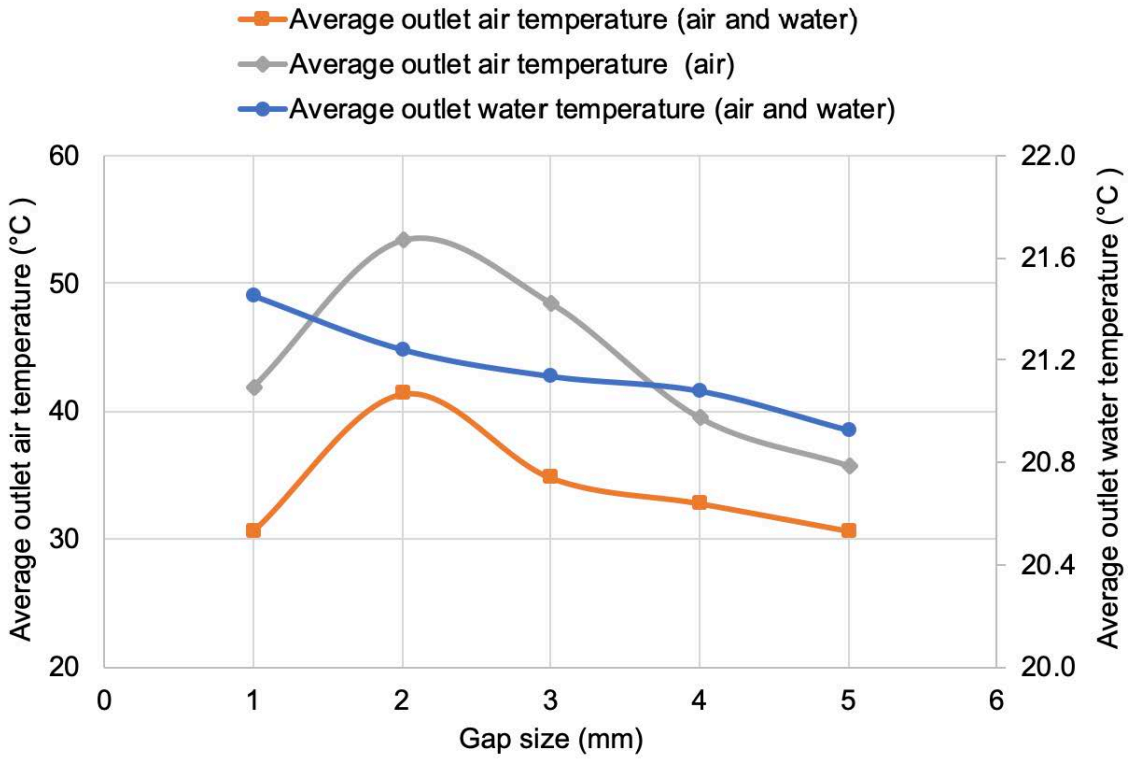

Figure 6 - 31 The average outlet air and water temperature with varying gap sizes in discharging in air mode and air and water mode

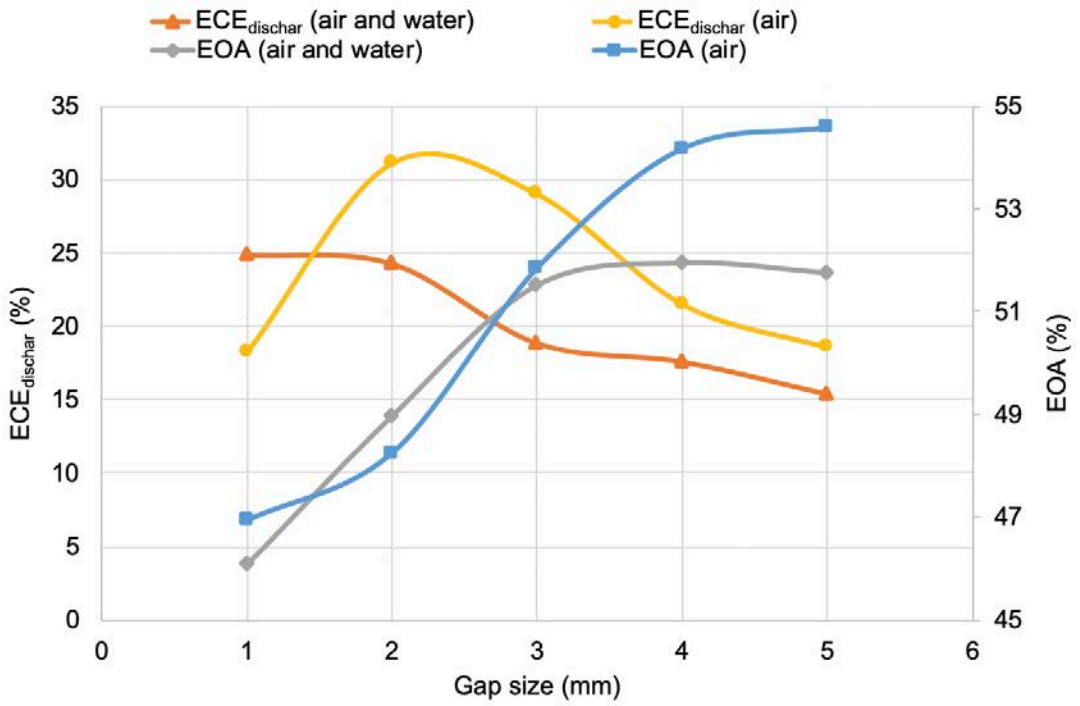

Figure 6 - 32 ECE$_{dischar}$ and EOA of the reactor with varying gap sizes in discharging in air supply mode and air and water supply mode

6.5.3 The effect of reactor width and length on the evaluation indicators

The effect of reactor bed length and width have been evaluated. The reactor bed length has been varying from 0.2 m to 0.5 m. Meanwhile, the corresponding bed width has been varying from 0.5 m to 0.2 m, as given in Table 6 - 5.

Table 6 - 5 The reactor configuration with varying bed length and width

Configuration	Reactor bed length (m)	Reactor bed width (m)
R1	0.20	0.50
R2	0.25	0.40
R3	0.30	0.33
R4	0.35	0.29
R5	0.40	0.25
R6	0.45	0.22
R7	0.50	0.20

The reactor charging performance with respect to the bed length and width configurations has been given in Figure 6 - 33. The time consumption increases and the ECE_{char} decreases with the increase of reactor bed length. For the configuration R5, the ECE_{char} has reduced to 30.4% and the time consumption has been increased to 5.4 hours. When increasing the reactor bed length, it increases the time for the air to travel across the reactor. This reduces the desorption moving from the air entrance to the exit.

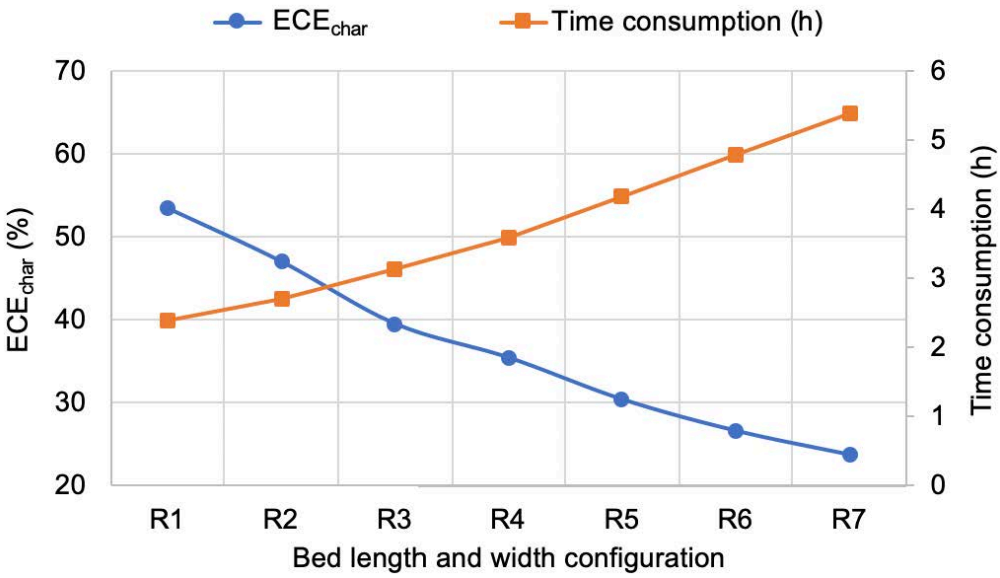

Figure 6 - 33 ECE_{char} and time consumption with varying bed length and width in charging

With respect to discharging, Figure 6 - 34 shows the average outlet air temperature of the reactor in air supply mode and air and water supply mode. Similar to the charging condition, for the air supply mode, the average outlet air temperature reduces with the increase of bed length. It decreases from 48.5 °C for R1 to 42.7 °C for R5. In discharging, since the water vapour pressure of air reduces along the bed length, the reaction intensity reduces with the increasing bed length. The adsorption heat is more likely to be retained in the reactor with the increasing bed length. The air temperature in air and water supply mode has presented a similar trend. For the water flow, increasing the bed length reduces the water flow heat contact area within the reactor for the reducing reactor bed

width. The water temperature reduces with the increasing bed length from 21.1 °C to 20.3 °C. Figure 6 - 35 shows the $ECE_{dischar}$ and EOA of the reactor in the air and air and water supply modes. Since the average rate of water uptake in discharging drops with the increasing reactor bed length, for the air supply mode from R1 to R7, the $ECE_{dischar}$ and EOA reduce from 29.9% to 5.2% and from 51.5% to 30.4%, respectively. For the air and water supply mode, the $ECE_{dischar}$ and EOA reduce to 5.2% and 30.4% at the bed length and width configuration R7.

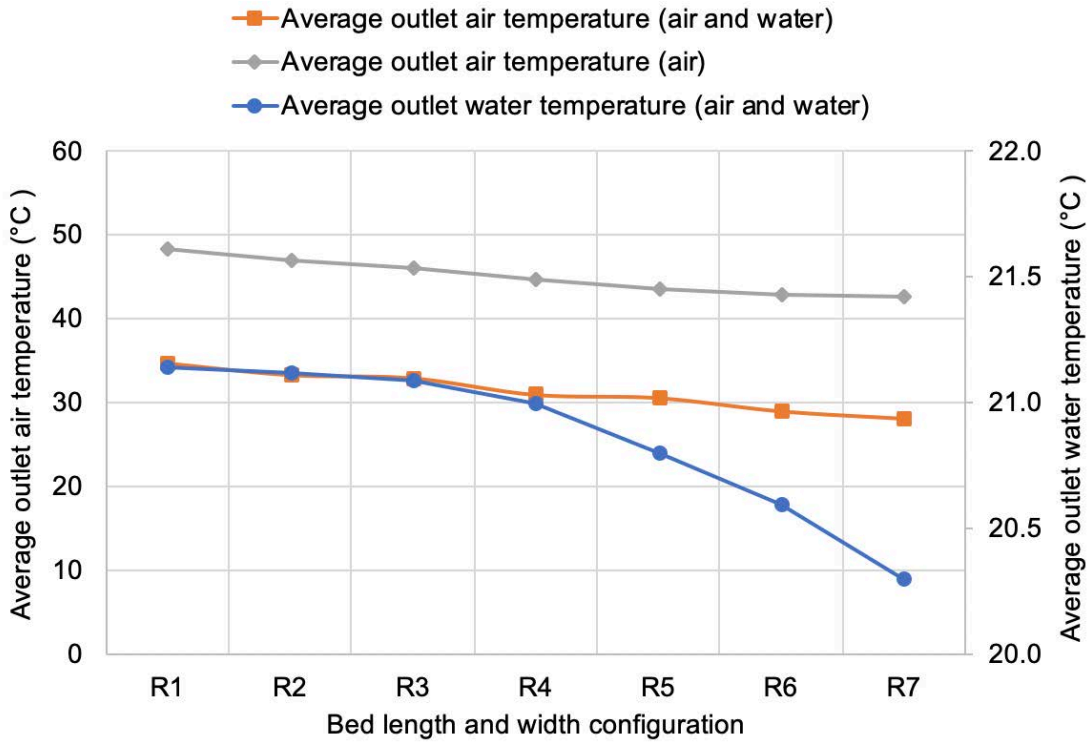

Figure 6 - 34 The average outlet air and water temperature with varying bed length and width in discharging in air supply and air and water supply mode

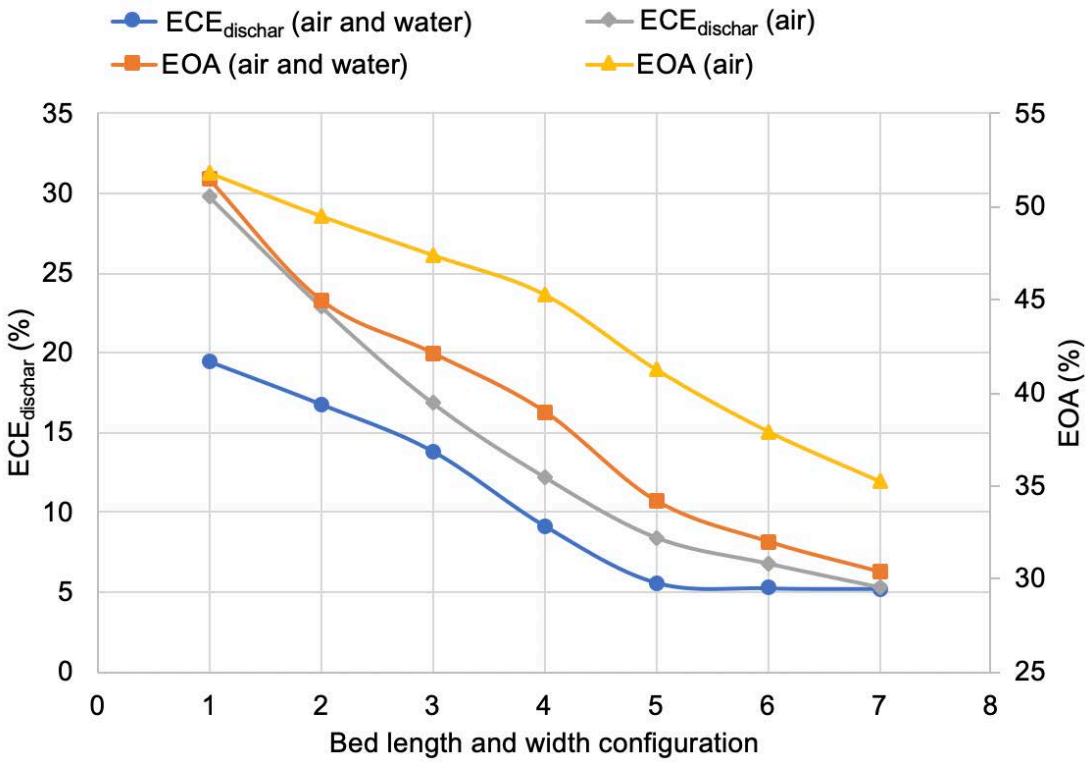

Figure 6 - 35 ECE$_{dischar}$ and EOA of the reactor with varying bed length and width in discharging in air supply and air and water supply mode

6.5.4 The effect of inlet air temperature on the evaluation indicators

The reactor discharging performance under varying inlet air temperature has been evaluated. Figure 6 - 36 shows the average outlet air and water profiles for the reactor in air supply and air and water supply mode. The reactor outlet air and water temperature increase with the increase of inlet air temperature. For air supply mode, the average outlet air temperature increases from 48.3 °C with inlet air at 20 °C to 71.9 °C with inlet air at 50 °C. Similarly, for the air and water supply mode, the average outlet air increases from 34.8 °C with inlet air at 20 °C to 58.4 °C with inlet air at 50 °C. The average outlet water has been increased from 21.1 °C to 25.1 °C with inlet air at 50 °C. For the reactor in air and water supply mode, the increase of the outlet air temperature becomes relatively smaller than that of the air supply mode, since an increasing part of the adsorption energy has been taken by the water flow.

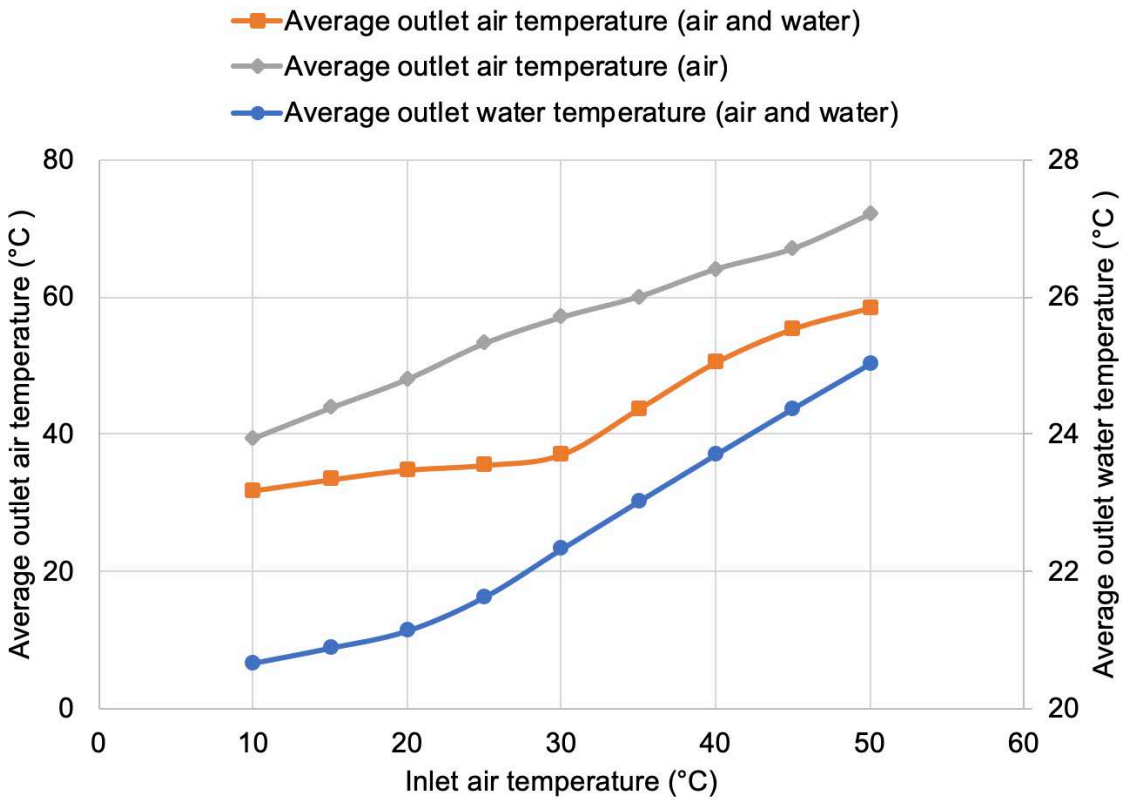

Figure 6 - 36 The average outlet air and water temperature with varying inlet air temperature in discharging in air supply and air and water supply mode

Figure 6 - 37 shows the $ECE_{dischar}$ and EOA of the reactor in discharging with the vary inlet air temperature. For the both modes, the $ECE_{dischar}$ increases with the increase of inlet air temperature. The air supply and air and water supply mode achieve the peak $ECE_{dischar}$ at 38.6% and 28.3% with the inlet air at 50 °C, respectively. The EOA for both modes increases with the inlet air temperature and then decreases with the inlet air at over 30 °C. The peak EOA for the air and air and water supply mode is 56.5% and 55.7%, respectively. The decreases of EOA under a relatively high inlet air temperature results from the reduction of the average rate of water uptake. The adsorbent rate of uptake reduces with the adsorbent at a higher temperature. For the air supply mode, the average rate of uptake reaches 5.33E-6 $kg_{H2O}/(kg_{zeolite}\cdot s)$ with the inlet air at 30 °C and reduces to 4.89E-6 $kg_{H2O}/(kg_{zeolite}\cdot s)$ with the inlet air at 50 °C.

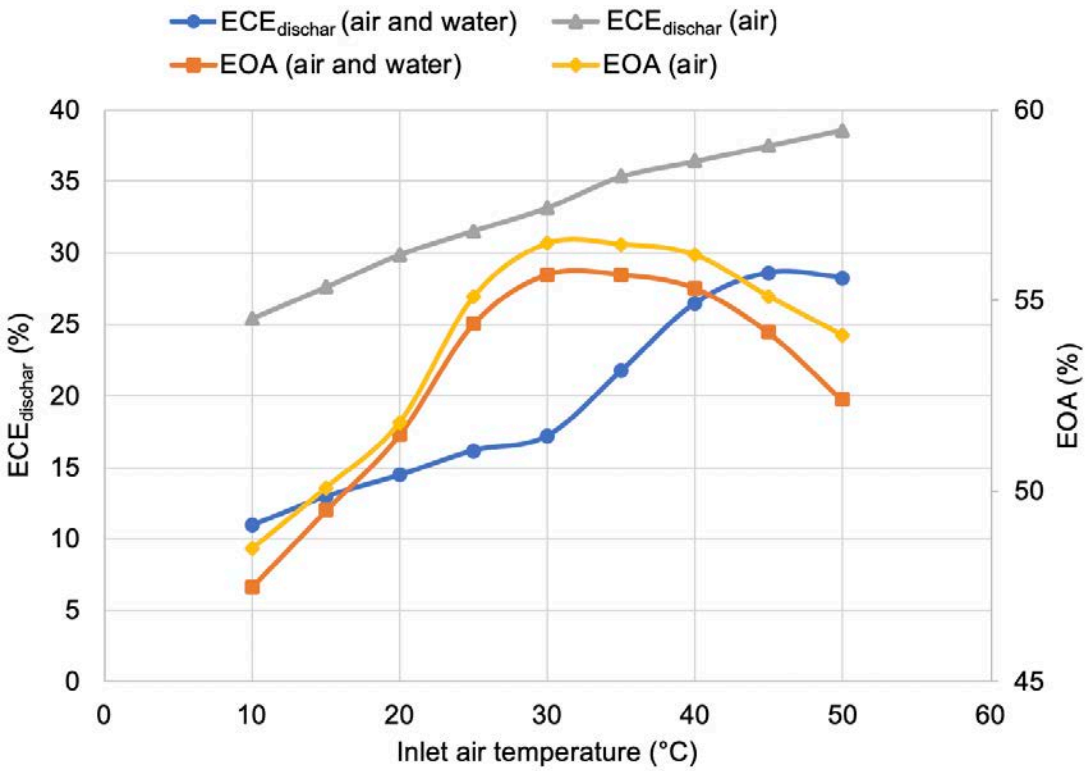

Figure 6 - 37 ECE$_{dischar}$ and EOA of the reactor with varying inlet air temperature in discharging in air supply and air and water supply mode

6.5.5 The effect of inlet air relative humidity on the evaluation indicators

Evaluation has been conducted on the effect of inlet air relative humidity on the reactor discharging performance in both air supply and air and water supply mode. Figure 6 - 38 shows the average outlet air and water temperature profiles. For the air supply mode, the average outlet air temperature has been lifted from 24.3 °C to 48.5 °C with the relative humidity increase from 15% to 95%. For the air and water supply mode, with the same relative humidity increase, the corresponding outlet air temperature increases from 22.4 °C to 34.8 °C. The increase in the inlet air relative humidity has a relatively significant effect on achieving a higher outlet air temperature. Figure 6 - 39 shows the ECE$_{dischar}$ and EOA of the reactor in the two supply modes. Both ECE$_{dischar}$ and EOA increase with the increase of inlet air relative humidity, because the increase of moisture content in the inlet air promotes the adsorption process. In the evaluation, in air supply mode, the average rate of water uptake increases from 4.38E-6

$kg_{H2O}/(kg_{zeolite}\cdot s)$ to 6.73E-6 $kg_{H2O}/(kg_{zeolite}\cdot s)$ with the inlet air relative humidity increasing from 55% to 95%.

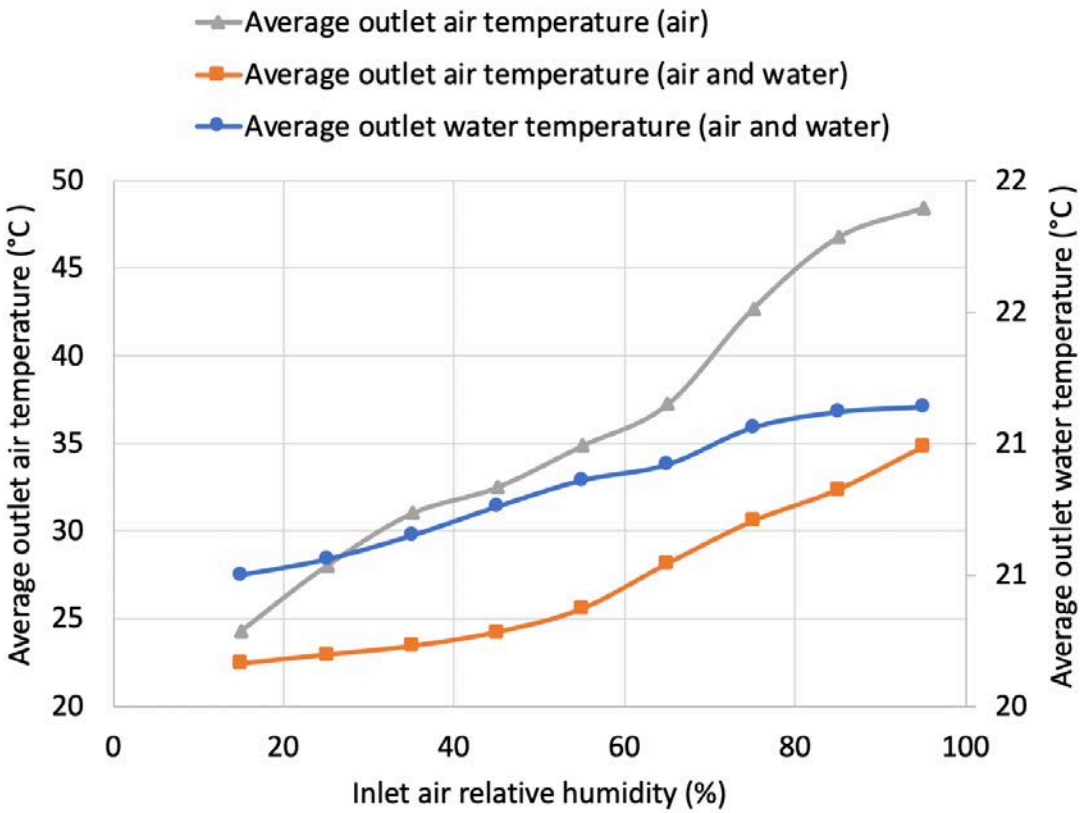

Figure 6 - 38 The average outlet air and water temperature with varying inlet air relative humidity in discharging in air supply and air and water supply mode

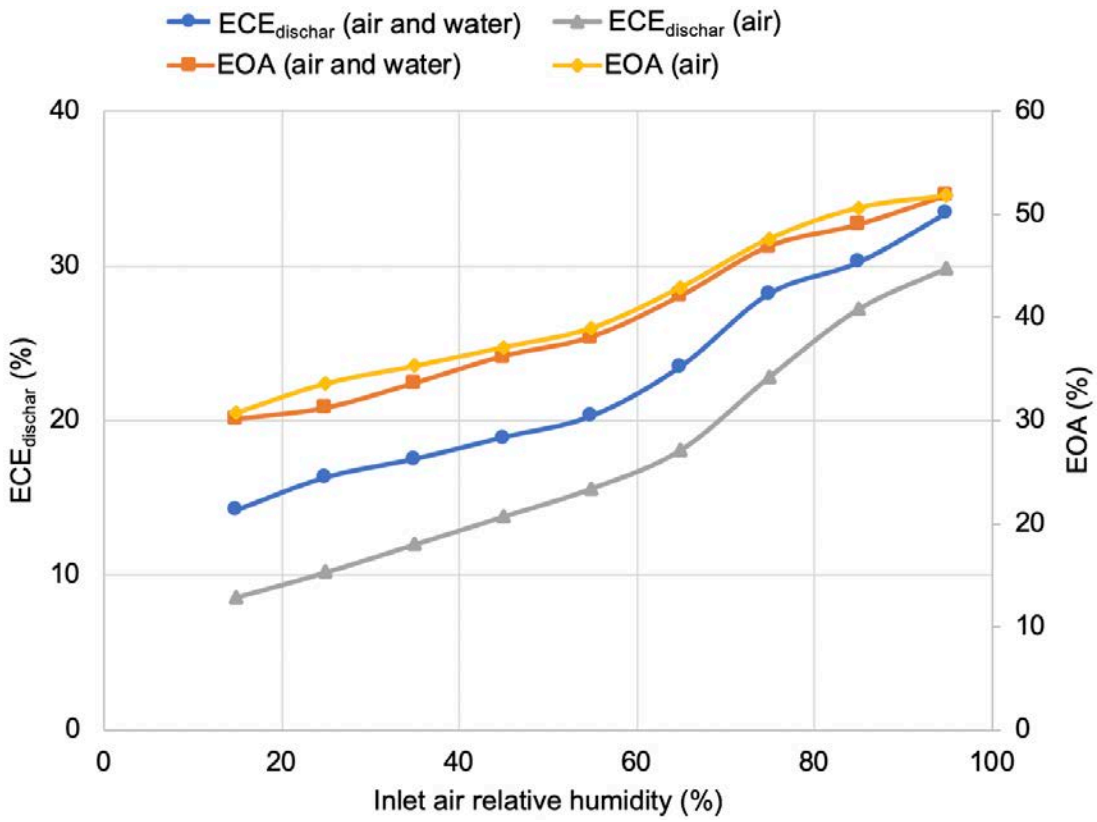

Figure 6 - 39 ECE$_{dischar}$ and EOA of the reactor with varying inlet air relative humidity in discharging in air supply and air and water supply mode

6.5.6 The effect of water flow rate on the evaluation indicators

The effect of water flow rate on the reactor evaluation parameters has been evaluated as shown in Figure 6 - 40 and Figure 6 - 41. The water flow rate has been varied from 0.02 L/min to 0.21 L/min. Both outlet air and water temperature reduce with increasing water flow rate due to the increasing cooling effect from the inlet water. For the outlet water temperature, it reduces from 21.6 °C at 0.12 L/min to 20.7 °C at 0.21 L/min. The outlet air temperature has witnessed a slight decrease from 34.81 °C at 0.12 L/min to 33.45 °C at 0.21 L/min. The ECE$_{dischar}$ and EOA achieve a relatively stable profile with the average ECE$_{dischar}$ at 19.5% and the average EOA at 51.5%.

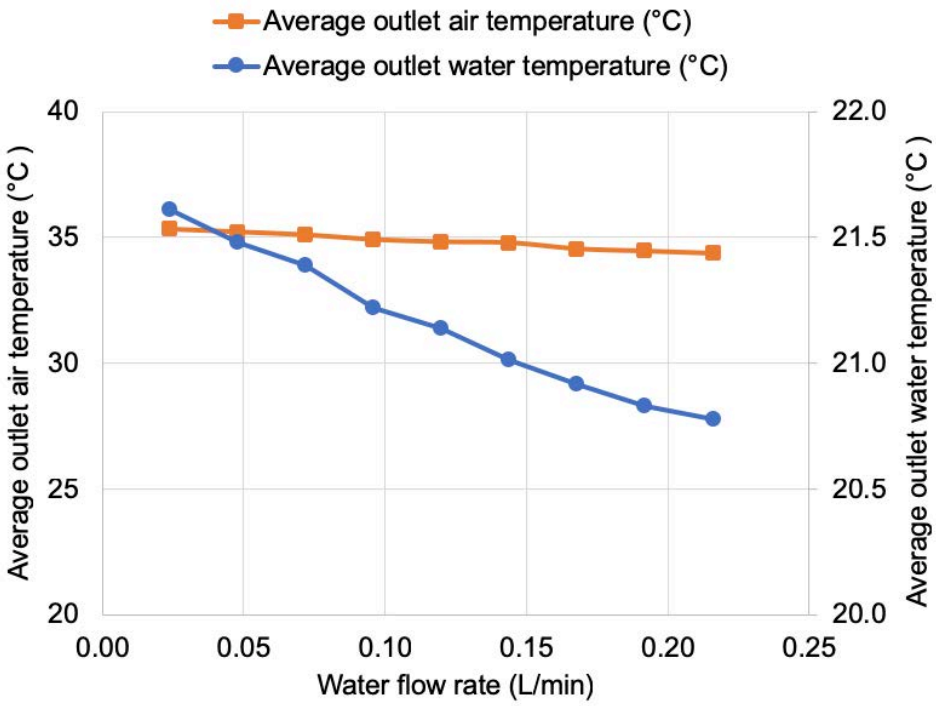

Figure 6 - 40 Average outlet air and water temperature for the reactor in discharging with varying water flow rates in air and water supply mode

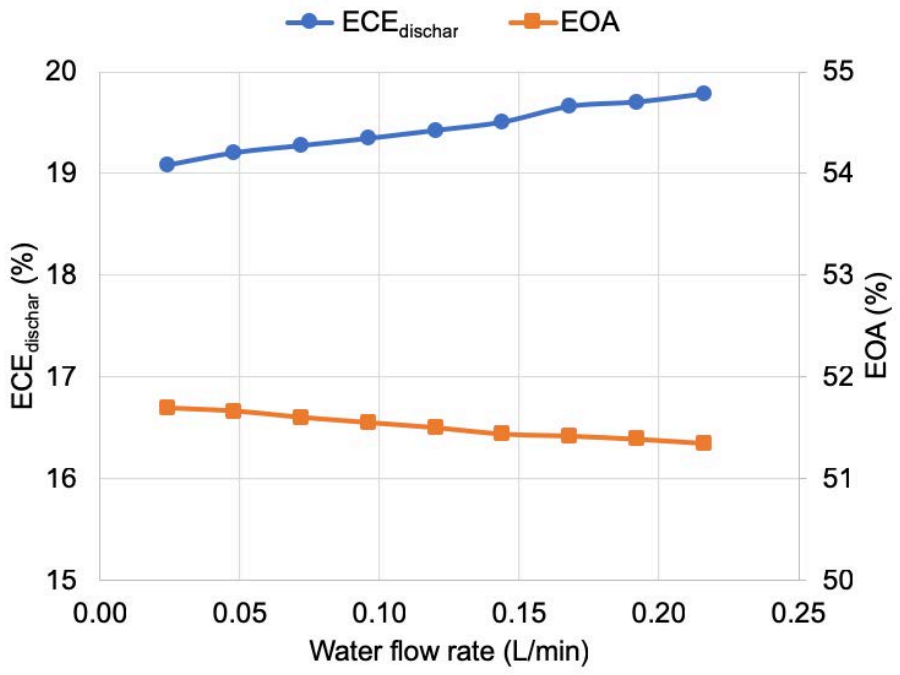

Figure 6 - 41 ECE$_{dischar}$ and EOA of the reactor with varying water flow rates in discharging in air and water supply mode

6.5.7 Reactor design considerations

This section presents the sizing and design considerations to obtain a reactor with relatively high evaluation indicators. The data produced in this study can serve as a decision-making tool for a designer with a specific design priority. This study has presented the reactor evaluation indicators in charging and discharging. For a charging process to achieve a specific EOA, it includes ECE_{char} and time consumption. For a discharging process, it covers the reactor in air supply and air and water supply mode, including air and water temperature, $ECE_{dischar}$, and EOA.

Figure 6 - 42 shows systematic design steps with a central consideration and the reactor performance indicators (Mohammadzadeh Kowsari et al. 2018). The design and decision-making steps can be suggested as follows.

- Step 1: Determine a central consideration for the thermochemical reactor.
- Step 2: Select the reactor bed length and width.
- Step 3: Determine the other reactor performance indicators in the charging and discharging process.
- Step 4: Evaluate an obtained performance indicator if it is located in the desirable range.
- Step 5: In the case of a performance indicator being undesirable, propose a corrected value and input into Figure 6 - 42 as the central consideration and then repeat the steps.

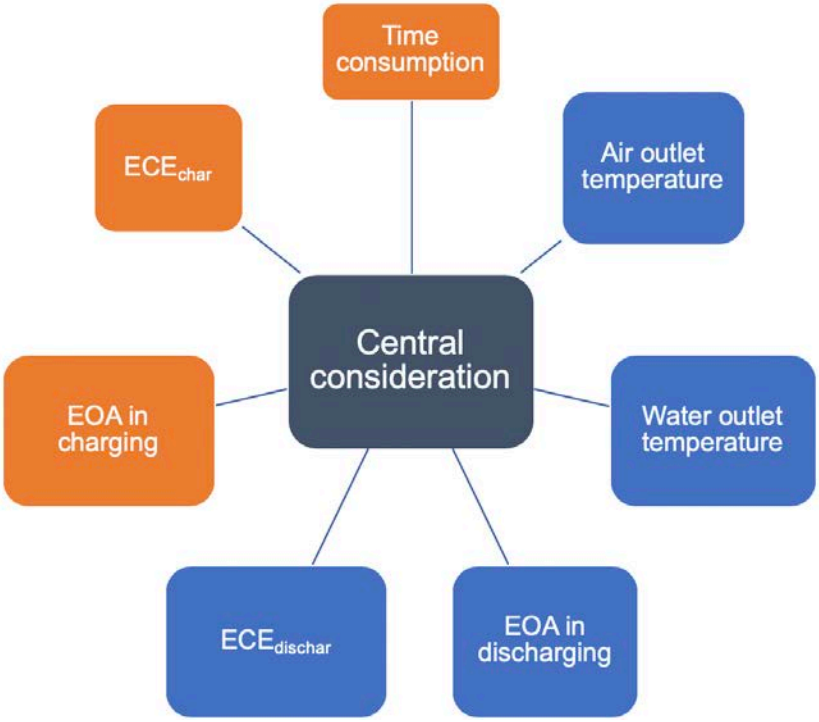

Figure 6 - 42 Schematic of a three-phase thermochemical reactor design considerations

Table 6 - 6 presents examples in application of the steps to determine the thermochemical reactor configurations. If selecting the highest EOA in discharging as the central consideration, the other reactor performance indicators can be obtained and the reactor configuration can be determined as listed in the first column of Table 6 - 6. However, if the average outlet air temperature is lower than the expectation, it can be input as the central consideration and repeat the process to determine the reactor configurations and evaluation indicators as the second and third column of Table 6 - 6. Similarly, if the lowest time consumption in charging is a critical consideration, it can be considered as the central consideration to obtain the reactor configuration and the evaluation indicators.

Table 6 - 6 An example of the reactor evaluation indicators according to the configurations and central consideration

Evaluation indicators		The central consideration			
		The highest EOA	The highest average outlet air temperature		The lowest time consumption in charging
The reactor geometry	Reactor bed length (m)	0.2	0.2	0.2	0.2
	Reactor bed width (m)	0.5	0.5	0.5	0.5
	Fin pitches (mm)	30	50	50	10
	Gap size (mm)	4	2	2.4	5
Evaluation indicators in charging	Time consumption (h)	2.5	2.7	2.7	**1.8**
	ECE_{char} (%)	49.2	53.1	51.2	65.6
Evaluation indicators in discharging	Air supply mode				
	$ECE_{dischar}$ (%)	21.5	31.1	32.1	21.7
	EOA (%)	**54.2**	48.3	49.1	50.9
	Average outlet air temperature in air supply mode (°C)	48.5	**53.4**	**54.2**	41.9
	Air and water supply mode				
	$ECE_{dischar}$ (%)	17.6	24.3	22.5	13.8
	EOA (%)	**51.9**	48.9	50.2	49.3
	Average outlet air temperature in air and water supply mode (°C)	34.8	**41.3**	**41**	30.6
	Average outlet water temperature in air and water supply mode (°C)	21.1	21.2	21.2	21.4

6.6 Sources of errors

Numerical analysis

- The boundary conditions are consistent during the numerical analysis. However, it can be transient in an experiment.
- There are errors because of the assumptions made in the numerical analysis.
- In the operations and configurations effect analysis, the study has analysed the effect of one variate keeping other parameters fixed. This method does not show how the interactions of the parameters affect the reactor performance.

6.7 Chapter summary

This chapter presents the investigation of a three-phase thermochemical reactor through the experimentally validated numerical model. The software Matlab has been used to solve the equations and provide the evaluation of the heat and mass transfer. Original measurements obtained from the experimental tests are used to validate the numerical model. Good agreement between the computing value and experimental measurements are obtained through the validation cases, including charging and discharging tests.

Followed by the validation, the chapter has presented the parameter sensitivity analysis, the effect of air and adsorbent parameters, and the reactor configuration study. The key outcomes of the chapter are summarised as follows.

- There is a fair agreement between the numerical and experimental values in the cases of charging and discharging with the root mean square percent error ranging from 6.02% to 12.78%.
- Reference diffusivity, heterogeneity factor and initial water uptake can affect the numerical calculation results significantly. The application of the parameters should be adjusted to produce convincing computing values.
- For the inlet air temperature, a higher inlet air temperature is desirable in charging. The inlet air below 100 °C can be ineffective as the simulation found

the EOA at 75.9%. In discharging, increasing the inlet air temperature increases output temperature but causes only a minor increase to the EOA. Therefore, a higher inlet air temperature in discharging is not cost-effective unless waste heat or heat recovery is available.

- The air mass flow rate is critical to a charging process but it can be less significant to the discharging process. In charging, when the air flow rate increases from 0.05 kg/s to 0.19 kg/s, the EOA reduces from 38.1%% to 11.2%. A higher air mass flow rate can be used to accelerate a charging process. However, an excessive value can cause unfavourable ECE_{char} with a slight change of EOA for the mass flow rate at over 0.08 kg/s. In discharging, increasing the air flow rate can reduce the adsorbent temperature and reduce the mass transfer coefficient. In this analysis, when increasing the air mass flow rate from 0.19 kg/s to 0.3 kg/s, the average adsorbent temperature reduces by 12 °C.
- The inlet air relative humidity is insignificant to the reactor's charging performance since the charging temperature plays a vital role. However, in discharging, a larger inlet air relative humidity leads to a larger EOA and $ECE_{dischar}$, especially for the relative humidity from 10% to 40%. The inlet relative humidity around 40% is suggested and the humidification methods can be investigated for the energy consumption and reactor's discharging performance.
- A smaller particle diameter is suggested as it leads to a larger mass transfer coefficient in both charging and discharging. It promotes the reactor's discharging performance but it has less impact on the charging process. In discharging, reducing the particle diameter from 6 mm to 3 mm increases the $ECE_{dischar}$ and EOA by 12.8% and 12.7%, respectively.
- In charging, a larger reactor bed porosity leads to the improvement of mass transfer. However, in discharging, it has less improvement since it reduces the adsorbent temperature. According to the analysis, the reactor bed porosity needs to be over 0.4 to achieve a relatively high mass transfer in charging. The bed porosity is closely linked to the packing of the adsorbent particles in

the reactor. In addition to randomly packing, the packing status can be further investigated for the reactor performance improvement.

- Regarding the charging and discharging duration, the increase of charging duration leads to a less improvement in moisture transfer as the adsorbent approaches to the charging equilibrium. However, the increase of discharging duration promotes the discharging process since the limiting factor is the inlet moisture content. This leads to the further investigations in effective humidification methods.

Regarding the configuration analysis, the study has investigated the fin pipe reactor under various reactor configurations and operations. Investigations in charging and discharging in air supply and water supply mode have been conducted. It covers the effect of fin pitches, gap size, reactor width and length, inlet air temperature and relative humidity, and inlet water flow rate. The results are summarised as follows.

- Integrating fins into the reactor increases the average adsorbent temperature by 31% compared with the smooth pipe reactor in charging.
- Reducing the fin pitches improves the charging performance by enhancing the heat transfer. However, in discharging, it makes the reactor more sensitive to the inlet air. In air supply mode discharging, when reducing the fin pitch from 50 mm to 10 mm, the average outlet air temperature drops from 54.6 °C to 35.5 °C and the $ECE_{dischar}$ reduces from 31.2% to 21.7%.
- In charging, increasing the gap size has a slight improvement to the reactor charging performance. In discharging, increasing the gap sizes enhances the cooling effect from the inlet air which reduces the adsorbent temperature. Gap size ranging from 2 mm to 3 mm is suggested for a relatively high $ECE_{dischar}$ and outlet temperature in both air supply and air and water supply modes.
- A smaller bed length or a smaller air travel path is desirable. When increasing the bed length from 0.2 m to 0.5 m, the charging time consumption has increased by 126% and the average outlet air temperature has reduced by 11.8% in the air supply and 19.2% in the water supply mode.

- Relevant considerations in the thermochemical reactor design and configuration have been discussed. A reactor design scheme has been proposed according to the evaluations in this chapter.

CHAPTER 7: CONCLUSIONS

7.1 Conclusions

The aim of the research is to develop and investigate a thermochemical reactor for residential building applications. The aim is successfully achieved through conducting the objectives as presented in Chapter 1. The main findings of the research are highlighted in this chapter.

The study has found that the thermochemical reactor requires improvements in structure optimisations, heat and mass transfer enhancements, improving the flexibility in discharging, operational condition investigations and reducing heat losses. The effective methods are reactor segmentations, adding air diffusers, creating air paths, inducing air flow into thermochemical materials, adjusting the reactor temperature and pressure, etc. Also, for the thermochemical materials, the study has found that further developments are needed to obtain suitable thermochemical material for the built environment. A material selection framework with selection criteria has been applied in the study.

Following the literature review, the study has conducted a theoretical study on a thermochemical reactor to serve as a foundation for the reactor and numerical model. It illustrates the principles of the heat and mass of a reactor in charging and discharging. According to the heat and mass conversions of the reactor, the study has proposed the energy conversion efficiency (ECE) and extent of adsorption (EOA) as the reactor evaluation parameters. It has also presented the enthalpy of adsorption of zeolites 13X, the LDF model for the adsorption kinetics and the Dubinin-Astakhov equation for zeolite 13X and water vapour adsorption.

To address the drawbacks of the thermochemical reactor, the study has proposed a three-phase thermochemical reactor. The reactor innovates in the trapezoid-shaped container for the robust material support and air gaps for air flow. It also features heat extraction of air and water flow. Fins have been integrated to

enhance heat and mass transfer. According to the reactor, the study has presented a numerical model to represent the reactor in charging and discharging. The numerical model involves heat and mass transfer of the air, solid adsorbent and water. Finite element method has been used in the calculation method and the software Matlab has been proposed to solve the equations.

To investigate the reactor under laboratory conditions and provide experimental data for the numerical model validation, the study has conducted the reactor experimental tests in charging and discharging. The findings of the experimental tests are concluded as follows.

- Integration of fins improves the reactor charging and discharging performance. In charging, the fin pipe reactor presents a significant increase in the thermochemical material temperature. In discharging, the outlet air temperature peaks at 77.2 °C, nearly 10 °C higher than the smooth pipe reactor. For the reactor in air and water supply mode, the fin pipe reactor presents the water temperature lift from 1.8 °C to 4 °C higher than the smooth pipe reactor.
- A higher inlet air temperature in charging improves the reactor performance. The tests have found that the material energy density has increased from 0.18 Wh/g to 0.21 Wh/g with the charging inlet air temperature increasing from 120 °C to 140 °C. With the charging at 180 °C, the discharging tests have shown an over 20 °C increase in the reactor temperature compared to the charging at 120 °C.
- The inlet air mass flow rate is critical to the reactor outlet air temperature in discharging tests, and adjustments of air mass flow should be made to obtain a desirable value. The tests have shown that the peak outlet air temperature has increased from 71.9 °C to 75.6 °C by increasing the air flow rate from 0.015 kg/s to 0.018 kg/s. However, it reduces to 67.6 °C when the air mass flow rate increases to 0.02 kg/s.

Following the experimental testing, the study has validated the numerical model by comparing the numerical calculations with the experimental measurements. It

has used Matlab to solve the equations and provide the evaluation results. A good agreement has been achieved with the root mean square percent error ranging from 6.02% to 12.78%. By using the validated numerical model, the study has presented the effect of air and adsorbent parameters on charging and discharging. The conclusions of the air and adsorbent parameter investigations are summarised as follows.

- Charging and discharging temperatures are critical to the reactor's performance. For charging, a relatively high charging temperature is suggested. For a future study, a heat source should be carefully adjusted to provide sufficient charging temperature. However, heat source such as the evacuated solar collector may not be able to achieve the charging temperature of zeolites. This shows the opportunity of investigations around a suitable heat source and a reactor's charging performance. For discharging, increasing the inlet air temperature achieves a higher outlet air temperature. This, however, only leads to a minor increase in the reactor's EOA and it can reduce the $ECE_{dischar}$. This study has found that increasing the inlet air temperature reduces the reactor temperature lift and limits the adsorption process. A relatively high inlet air temperature is unfavourable to the discharging process.
- The air mass flow rate is critical to a charging process but it can be less significant to the discharging process. Operation strategies of air mass flow should be focused on the charging process while excessive air mass flow rate in discharging may reduce the reactor outlet air temperature.
- The inlet relative humidity at around 40% is suggested in discharging as the discharging performance can be lifted greatly by increasing the inlet humidity from 10% to 40%. Relatively higher inlet air relative humidity is not as cost-effective as increasing energy input from the humidifier.
- A smaller particle diameter promotes the discharging but it has less impact on a charging process.
- For the bed porosity, it should be over 0.4 to achieve a relatively high mass transfer in charging. The reactor bed porosity shows less effect to the discharging performance.

- Key parameters are interlinked in evaluating the reactor performance. The study has presented the interactions of the air and adsorbent parameters in charging and discharging. It can serve as a tool to understand the change of a parameter to a charging or discharging process.

Additionally, the study has conducted a configuration study on the fin pipe reactor by investigating the reactor under various reactor configurations and operations. The conclusions of the configuration study are highlighted as follows.

- Reducing the fin pitches improves the charging performance but it makes the reactor become more sensible to the inlet air temperature in discharging.
- Increasing the gap size reduces the time consumption in charging slightly. However, it has an impact on the discharging performance. An excessive gap size of over 3 mm can reduce the outlet air and water temperature.
- The reactor with relatively smaller air travel path presents a superior performance in both charging and discharging. A reactor with relatively short air travel path is desirable.
- Finally, according to the evaluations, the study has proposed a reactor design scheme for the design of a three-phase thermochemical reactor to achieve a desirable output.

7.2 Future research challenges

Thermochemical energy storage has many advantages. To make it attractive for various applications in residential buildings, a thermochemical system should feature simple concept and configuration, be able to integrate with multiple heat sources, have high performance and low cost thermochemical materials, and high performance in system processes and operations. Through conducting the project, the future research challenges are summarised in this section.

A study in thermochemical energy storage as applied in buildings should address the challenges from the heat source. Regarding the achievable temperature, for using solar thermal as the heat source, it may not be easy to reach a desirable

charging temperature in the reactor. This study has investigated that using thermochemical material like the zeolites requires a relatively high charging temperature. Besides, a heat source can be variable depending on the location and time of the day. A thermochemical system should also consider the variation of the heat source in charging.

Thermochemical material is essential. Research is required to develop a suitable material with sufficient hydrothermal stability, low cost, high thermal conductivity and high energy density. Some composite materials have shown promising characteristics in water uptake capability, regeneration temperature and cyclability. Further research on the material pairs and characterisations would be meaningful and necessary. The development of new materials can be linked to heat sources in the built environment, not only the solar thermal energy. Additionally, a thermochemical energy storage system may feature more than one type of material for different charging and discharging scenarios.

The current study on the thermochemical reactor has revealed reactor development opportunities for future studies. A thermochemical reactor can be improved from different perspectives including the geometry design, the charging and discharging methods, the status of the thermochemical material in the reactor, etc. For the reactor geometry design, modifications can be conducted to promote the heat and mass transfer, such as increasing the contact area between the reactant materials. A reactor should also be efficient in charging and discharging. Innovative charging and discharging methods should be proposed. For a packed bed reactor using inlet heat air as the method of charging, it is energy intensive and time-consuming to regenerate the materials from the side of the air inlet to the outlet. Supplying the heat of charging into the materials for regeneration is critical. This also applies to the discharging using the humidified inlet air as the reaction front has to move from the moisture inlet to the outlet. Also, the status of the thermochemical material is key to a reactor in charging and discharging. The material status affects the bed porosity and air travel path, which further influences the heat and mass transfer in the charging and discharging process.

Most of the studies in literature have packed the thermochemical material randomly in the reactor. Furthermore, a study should look into the issue of heat losses and propose an approach to address the issue. The charging and discharging processes result in the heat accumulation in the reactor and the other system components. However, the heat will be lost if no action is taken, which hinders the system energy efficiency.

Water has been commonly used as the sorbate for building applications. The humidification methods are to be studied with the considerations of the discharging methods. Several humidification methods can be used in a study such as using ultrasonic humidifiers, bubble columns, spray humidifiers and evaporative humidifiers. The different methods can be suitable for specific discharging methods with different energy consumption. Additionally, to provide water as the sorbate in an adsorption process, liquid water can be supplied to the reactor. However, a reactor numerical model should be studied to provide the water behaviour in the reactor along with the related heat and mass transfer.

References

Abedin, A. H. and Rosen, M. A. (2012) 'Closed and Open Thermochemical Energy Storage: Energy- and Exergy-Based Comparisons'. *Energy* 41 (1), 83–92

Akhtar, F., Andersson, L., Ogunwumi, S., Hedin, N., and Bergström, L. (2014) 'Structuring Adsorbents and Catalysts by Processing of Porous Powders'. *Journal of the European Ceramic Society* [online] 34 (7), 1643–1666. available from <https://www.sciencedirect.com/science/article/pii/S0955221914000338> [14 August 2018]

van Alebeek, R., Scapino, L., Beving, M. A. J. M., Gaeini, M., Rindt, C. C. M., and Zondag, H. A. (2018) 'Investigation of a Household-Scale Open Sorption Energy Storage System Based on the Zeolite 13X/Water Reacting Pair'. *Applied Thermal Engineering* [online] 139, 325–333. available from <http://linkinghub.elsevier.com/retrieve/pii/S1359431117370436> [16 August 2018]

Allouche, Y., Varga, S., Bouden, C., and Oliveira, A. C. (2016) 'Validation of a CFD Model for the Simulation of Heat Transfer in a Tubes-in-Tank PCM Storage Unit'. *Renewable Energy*

Aristov, Y. I. (2007) 'New Family of Solid Sorbents for Adsorptive Cooling: Material Scientist Approach'. *Journal of Engineering Thermophysics* [online] 16 (2), 63–72. available from <http://link.springer.com/10.1134/S1810232807020026>

Aristov, Y. I., Restuccia, G., Tokarev, M. M., and Cacciola, G. (2000) 'Selective Water Sorbents for Multiple Applications, 10. Energy Storage Ability'. *Reaction Kinetics and Catalysis Letters* 69 (2), 345–353

Askalany, A., Henninger, S., and Ghazy, M. (2017) 'Effect of Improving Thermal Conductivity of the Adsorbent on Performance of Adsorption Cooling System'. *Applied Thermal* [online] available from <http://www.sciencedirect.com/science/article/pii/S135943111631434X> [20 January 2017]

Aydin, D. (2016) *Thermochemical Energy Storage Systems*. The University of

Nottingham

Aydin, D., Casey, S. P., Chen, X., and Riffat, S. (2016) 'Novel "Open-Sorption Pipe" Reactor for Solar Thermal Energy Storage'. *Energy Conversion and Management* 121, 321–334

Aydin, D., Casey, S. P., and Riffat, S. (2015) 'The Latest Advancements on Thermochemical Heat Storage Systems'. *Renewable and Sustainable Energy Reviews* [online] 41, 356–367. available from <http://dx.doi.org/10.1016/j.rser.2014.08.054>

Bales, C., Gantenbein, P., and Hauer, A. (2005) 'Thermal Properties of Materials for Thermo-Chemical Storage of Solar Heat'. *Report of IE Solar* [online] available from <https://www.w.iea-shc.org/data/sites/1/publications/task32-Thermal_Properties_of_Materials.pdf> [20 January 2017]

Bales, C., Gantenbein, P., Jaehnig, D., Kerskes, H., Essen, M. Van, Weber, R., and Zondag, H. (2008) '031 - Chemical and Sorption Storage – Results from IEA-SHC Task 32'. *Eurosun 2008* 1–8

Basdogan, Y. and Keskin, S. (2015) 'Simulation and Modelling of MOFs for Hydrogen Storage'. *CrystEngComm* [online] 17 (2), 261–275. available from <http://xlink.rsc.org/?DOI=C4CE01711K> [13 October 2017]

Bellos, E., Tzivanidis, C., Antonopoulos, K. A., and Daniil, I. (2016) 'The Use of Gas Working Fluids in Parabolic Trough Collectors – An Energetic and Exergetic Analysis'. *Applied Thermal Engineering*

Bertsch, F., Mette, B., Asenbeck, S., Kerskes, H., and Müller-Steinhagen, H. (2009) 'Low Temperature Chemical Heat Storage-an Investigation of Hydration Reactions'. *Effstock conference, Stockholm* 1–8

Beta, I. A., Böhlig, H., and Hunger, B. (2004) 'Structure of Adsorption Complexes of Water in Zeolites of Different Types Studied by Infrared Spectroscopy and Inelastic Neutron Scattering'. in *Physical Chemistry Chemical Physics*. held 2004

De Boer, R., Haije, W. G., Veldhuis, J. B. J., and Smeding, S. F. (2004) *Solid-Sorption Cooling with Integrated Thermal Storage: The Sweat Prototype*. [online] available from

<https://www.ecn.nl/docs/library/report/2004/rx04080.pdf> [22 November 2017]

De Boer, R., Smeding, S. F., Zondag, H. A., Krol, G., De Boer, Robert, Smeding, S., Zondag, H., and Krol, Guido (2014) *Development of a Prototype System for Seasonal Solar Heat Storage Using an Open Sorption Process*. [online] available from <https://www.ecn.nl/publications/PdfFetch.aspx?nr=ECN-M--14-009> [2 July 2017]

Bon, V. (2017) 'Metal-Organic Frameworks for Energy-Related Applications'. *Current Opinion in Green and Sustainable Chemistry* [online] 4, 44–49. available from <http://linkinghub.elsevier.com/retrieve/pii/S2452223616300657> [2 August 2017]

Brown, G. O., Hsieh, H. T., and Lucero, D. A. (2000) 'Evaluation of Laboratory Dolomite Core Sample Size Using Representative Elementary Volume Concepts'. *Water Resources Research*

Brunauer, S., Deming, L. S., Deming, W. E., and Teller, E. (1940) 'On a Theory of the van Der Waals Adsorption of Gases'. *Journal of the American Chemical Society*

Brunauer, S., Emmett, P. H., and Teller, E. (1938) 'Adsorption of Gases in Multimolecular Layers'. *Journal of the American Chemical Society*

Brunberg, E. A. (1980) 'The Tepidus System for Seasonal Heat Storage and for Cooling'. in *Int. Seminar on Thermochemical Energy Storage* [online] held 1980 at Stockholm, Sweden. available from <https://scholar.google.com/scholar?q=related:HxfmlvKa47AJ:scholar.google.com/&hl=zh-CN&as_sdt=0,5> [22 November 2017]

Burton, G. (2000) *Salters Advanced Chemistry Chemical Ideas*. London: Heinemann

Cabeza, L. F., Solé, A., and Barreneche, C. (2017) 'Review on Sorption Materials and Technologies for Heat Pumps and Thermal Energy Storage'. *Renewable Energy* [online] 110, 3–39. available from <http://ac.els-cdn.com/S0960148116308497/1-s2.0-S0960148116308497-

main.pdf?_tid=ad0675ee-5374-11e7-b733-00000aacb35e&acdnat=1497714804_295c5193acca2c6cf740a1da63958de3> [17 June 2017]

Canivet, J., Fateeva, A., Guo, Y., Coasne, B., and Farrusseng, D. (2014) 'Water Adsorption in MOFs: Fundamentals and Applications'. *Chem. Soc. Rev.* [online] 43 (16), 5594–5617. available from <http://xlink.rsc.org/?DOI=C4CS00078A> [13 October 2017]

Casey, S. P., Aydin, D., Elvins, J., and Riffat, S. (2017) 'Salt Impregnated Desiccant Matrices for "Open" Thermochemical Energy Conversion and Storage – Improving Energy Density Utilisation through Hygrodynamic & Thermodynamic Reactor Design'. *Energy Conversion and Management* [online] 142, 426–440. available from <http://ac.els-cdn.com/S0196890417302777/1-s2.0-S0196890417302777-main.pdf?_tid=983df180-5038-11e7-8d42-00000aacb35d&acdnat=1497359146_aa350c44ac5d880044c665d0a99e3f0c> [13 June 2017]

Casey, S. P., Aydin, D., Riffat, S., and Elvins, J. (2015) 'Salt Impregnated Desiccant Matrices for "open" Thermochemical Energy Storage—Hygrothermal Cyclic Behaviour and Energetic Analysis by Physical Experimentation'. *Energy & Buildings* [online] 92, 128–139. available from <http://ac.els-cdn.com/S0378778815000663/1-s2.0-S0378778815000663-main.pdf?_tid=9e87899e-4a1a-11e7-9ed1-00000aacb35e&acdnat=1496686564_6423cfde412e55108f2d9a8e6e950f06> [5 June 2017]

Casey, S. P., Elvins, J., Riffat, S., and Robinson, A. (2014) 'Salt Impregnated Desiccant Matrices for "open" Thermochemical Energy Storage - Selection, Synthesis and Characterisation of Candidate Materials'. *Energy and Buildings* 84, 412–425

ChemTube3D (2017) *HKUST-1 Metal Organic Framework Is Loaded* [online] available from <http://www.chemtube3d.com/solidstate/MOF-HKUST-1.html> [12 October 2017]

Chenari, B., Dias Carrilho, J., and Gameiro Da Silva, M. (2016) 'Towards

Sustainable, Energy-Efficient and Healthy Ventilation Strategies in Buildings: A Review'. in *Renewable and Sustainable Energy Reviews*. vol. 59. 1426–1447

Chiou, C. T. (2003) 'Fundamentals of the Adsorption Theory'. *Partition and Adsorption of Organic Contaminants in Environmental Systems* (October), 39–52

Chua, K. J., Chou, S. K., and Yang, W. M. (2010) 'Advances in Heat Pump Systems: A Review'. *Applied Energy* [online] 87 (12), 3611–3624. available from <http://linkinghub.elsevier.com/retrieve/pii/S030626191000228X> [14 June 2017]

Civan, F., Conference, T., Engineers, M., and Civan, F. (2011) *Porous Media Transport*.

Clark, R. J., Mehrabadi, A., and Farid, M. (2020) 'State of the Art on Salt Hydrate Thermochemical Energy Storage Systems for Use in Building Applications'. in *Journal of Energy Storage*.

Climate Change Act (2008) *Climate Change Act 2008*. Statute Law Database

Comissão Europeia (2019) '2030 Climate and Energy Framework'. *European Commission web-portal*

Committee on Climate Change (2019) *Reducing the UK's Emissions - Committee on Climate Change* [online] available from <https://www.theccc.org.uk/our-impact/reducing-the-uks-emissions/> [28 November 2019]

Cook, W. H. and Basmadjian, D. (1964) 'Correlation of Adsorption Equilibria of Pure Gases on Activated Carbon'. *The Canadian Journal of Chemical Engineering* [online] 42 (4), 146–151. available from <http://doi.wiley.com/10.1002/cjce.5450420403> [25 November 2019]

Cortés, F. B., Chejne, F., Carrasco-Marín, F., Moreno-Castilla, C., and Pérez-Cadenas, A. F. (2010) 'Water Adsorption on Zeolite 13X: Comparison of the Two m[1] F.B. Cortés, F. Chejne, F. Carrasco-Marín, C. Moreno-Castilla, A.F. Pérez-Cadenas, Water Adsorption on Zeolite 13X: Comparison of the Two Methods Based on Mass Spectrometry and Thermogravimetry, '. *Adsorption* 16 (3), 141–146

Courbon, E., D'Ans, P., Permyakova, A., Skrylnyk, O., Steunou, N., Degrez, M., and Frère, M. (2017) 'A New Composite Sorbent Based on SrBr2 and Silica Gel for Solar Energy Storage Application with High Energy Storage Density and Stability'. *Applied Energy* 190, 1184–1194

Cuypers, R., Maraz, N., Eversdijk, J., Finck, C., Henquet, E., Oversloot, H., Van 't Spijker, H., and De Geus, A. (2012) 'Development of a Seasonal Thermochemical Storage System'. *Energy Procedia* [online] 30, 207–214. available from <http://ac.els-cdn.com/S187661021201541X/1-s2.0-S187661021201541X-main.pdf?_tid=9b289fb2-5371-11e7-9aad-00000aab0f01&acdnat=1497713485_08d8ae77e0e66854b8e6df11bba254ba> [17 June 2017]

Daïan, J.-F. (2014a) *Equilibrium and Transfer in Porous Media 1: Equilibrium States* [online] London: Wiley. available from <https://onlinelibrary.wiley.com/doi/pdf/10.1002/9781118908884> [15 May 2018]

Daïan, J.-F. (2014b) *Equilibrium and Transfer in Porous Media 2: Transfer Laws* [online] London. available from <https://onlinelibrary.wiley.com/doi/pdf/10.1002/9781118931257> [15 May 2018]

Dash, J. G. (1975) *Films on Solid Surfaces: The Physics and Chemistry of Physical Adsorption* [online] Washington: Academic Press. available from <https://books.google.co.uk/books?hl=en&lr=&id=k5_RtvnCCLQC&oi=fnd&pg=PP1&dq=heat+of+adsorption,+chemical+adsorption,+physical+adsorption&ots=vF_ipSbM0T&sig=DI83Wph5LG5Lvw4FbzpYjFG-G-o#v=onepage&q=heat of adsorption%252C chemical adsorption%252C phys> [19 May 2017]

Demir, H., Mobedi, M., and Lkuä, S. (2008) 'A Review on Adsorption Heat Pump: Problems and Solutions'. *Renewable and Sustainable Energy Reviews* [online] 12, 2381–2403. available from <https://ac.els-cdn.com/S1364032107000998/1-s2.0-S1364032107000998-main.pdf?_tid=4a71b22a-d9cc-11e7-b9b3-00000aab0f26&acdnat=1512485891_e4e49b99ce8b2719f4e5ee9799b4e8

5f> [5 December 2017]

Dincer, I. and Rosen, M. (2011) *Thermal Energy Storage Systems and Applications* [online] United Kingdom: John Wiley & Sons. available from <https://books.google.co.uk/books?hl=en&lr=&id=EsfcWE5lX40C&oi=fnd&pg=PR17&dq=Dincer+I,+Rosen+M.+Thermal+Energy+Storage:+Systems+and+Applications+,+2002&ots=7XXq9MGxpy&sig=OyUKyD7XCfTItgA__xSkG0gqAR8> [18 January 2017]

Dolado, P., Lazaro, A., Marin, J. M., and Zalba, B. (2011) 'Characterisation of Melting and Solidification in a Real-Scale PCM-Air Heat Exchanger: Experimental Results and Empirical Model'. *Renewable Energy*

Donald A. N., and Adrian, B. (2013) *Convection in Porous Media* [online] London. available from <https://link.springer.com/content/pdf/10.1007%2F978-1-4614-5541-7.pdf> [15 May 2018]

Donkers, P. A. J., Sögütoglu, L. C., Huinink, H. P., Fischer, H. R., and Adan, O. C. G. (2017) *A Review of Salt Hydrates for Seasonal Heat Storage in Domestic Applications*. [online] available from <http://creativecommons.org/licenses/by/4.0/> [21 June 2017]

Donohue, M. D. and Aranovich, G. L. (1998) 'Classification of Gibbs Adsorption Isotherms'. *Advances in Colloid and Interface Science*

Druskea, M.-M., Fopah-Lele, A., Korhammera, K., Rammelberga, H., Wegscheidera, N., Rucka, W., and Schmidta, T. (2014) 'Developed Materials for Thermal Energy Storage: Synthesis and Characterisation'. in *The 6th International Conference on Applied Energy* [online] held 2014 at Taiwan. 96–99. available from <https://ac.els-cdn.com/S1876610214027453/1-s2.0-S1876610214027453-main.pdf?_tid=a02ef728-d51b-11e7-92e6-00000aab0f6c&acdnat=1511970208_02d8912149ede881c9151ae9b9ef97e4> [29 November 2017]

Dubinin, M. M. and Astakhov, V. A. (1971) 'Development of the Concepts of Volume Filling of Micropores in the Adsorption of Gases and Vapours by Microporous Adsorbents'. *Bulletin of the Academy of Sciences of the USSR*

Division of Chemical Science [online] 20 (1), 3–7. available from <http://link.springer.com/10.1007/BF00849307> [11 February 2019]

Eames, P., Dennis, L., Victoria, H., and Romanos, P. (2014) 'The Future Role of Thermal Energy Storage in the UK Energy System: An Assessment of the Technical Feasibility and Factors Influencing Adoption'. *Research Report (UKERC: London)*

Edem N'Tsoukpoe, K., Rammelberg, H. U., Fopah Lele, A., Korhammer, K., Watts, B. A., Schmidt, T., and Ruck, W. K. L. (2015) *A Review on the Use of Calcium Chloride in Applied Thermal Engineering*. [online] available from <http://ac.els-cdn.com/S1359431114008199/1-s2.0-S1359431114008199-main.pdf?_tid=89a87668-418d-11e7-bc2c-00000aab0f27&acdnat=1495746361_9216c9d61f757c6641275bf2503ed152> [25 May 2017]

Edem N 'tsoukpoe, K., Restuccia, G., Schmidt, T., and Py, X. (2014) 'The Size of Sorbents in Low Pressure Sorption or Thermochemical Energy Storage Processes'. *Energy* [online] 77, 983–998. available from <http://ac.els-cdn.com/S0360544214011621/1-s2.0-S0360544214011621-main.pdf?_tid=a57aa9b6-5109-11e7-a5d2-00000aab0f02&acdnat=1497448933_849d4b32c3c28b027b26e87fe15b23d1> [14 June 2017]

Ehrenmann, J., Henninger, S. K., and Janiak, C. (2011) 'Water Adsorption Characteristics of MIL-101 for Heat-Transformation Applications of MOFs'. *European Journal of Inorganic Chemistry* (4), 471–474

Elsayed, A., Elsayed, E., Al-Dadah, R., Mahmoud, S., Elshaer, A., and Kaialy, W. (2017) *Thermal Energy Storage Using Metal-Organic Framework Materials*. [online] available from <https://ac.els-cdn.com/S0306261916304342/1-s2.0-S0306261916304342-main.pdf?_tid=62d6e3e0-b19e-11e7-bd8e-00000aab0f26&acdnat=1508068128_4418bf424688bb696d37bb7cc631328c> [15 October 2017]

Ergun, S. (1952) 'Fluid Flow through Packed Columns'. *Chemical Engineering Progress*

van Essen, V. M., Cot Gores, J., Bleijendaal, L. P. J., Zondag, H. A., Schuitema, R., Bakker, M., and van Helden, W. G. J. (2009a) 'Characterisation of Salt Hydrates for Compact Seasonal Thermochemical Storage'. in *ASME 2009 3rd International Conference on Energy Sustainability, Volume 2* [online] held 2009. 825–830. available from <http://proceedings.asmedigitalcollection.asme.org/proceeding.aspx?articleid=1648078>

van Essen, V. M., Zondag, H. a., Gores, J. C., Bleijendaal, L. P. J., Bakker, M., Schuitema, R., van Helden, W. G. J., He, Z., and Rindt, C. C. M. (2009b) 'Characterisation of MgSO4 Hydrate for Thermochemical Seasonal Heat Storage'. *Journal of Solar Energy Engineering* 131 (4), 041014

van Essen, V. M., Zondag, H. a., Schuitema, R., van Helden, W. G. J., Rindt, C. C. M., Essen, V. M. Van, Zondag, H. a., Schuitema, R., Helden, W. G. J. Van, and Rindt, C. C. M. (2008) 'Materials for Thermochemical Storage : Characterisation of Magnesium Sulfate'. *Proceedings Eurosun* 4–9

European Commission (2019) *Energy Performance of Buildings* [online] available from <https://ec.europa.eu/energy/en/topics/energy-efficiency/energy-performance-of-buildings> [12 August 2019]

Fanchi, J. R. (2002) 'Measures of Rock-Fluid Interactions'. in *Shared Earth Modelling*.

Ferchaud, C., Zondag, H., Veldhuis, J., and Boer, R. de (2012) 'Study of the Reversible Water Vapour Sorption Process of MgSO4.7H2O and MgCl2.6H2O under the Conditions of Seasonal Solar Heat Storage'. *Journal of Physics: Conference Series* [online] 395 (1), 012069. available from <http://iopscience.iop.org.globalproxy.cvt.dk/1742-6596/395/1/012069>

Foo, K. Y. and Hameed, B. H. (2010) 'Insights into the Modelling of Adsorption Isotherm Systems'. in *Chemical Engineering Journal*.

Fopah-Lele, A., Kuznik, F., Osterland, T., and Ruck, W. K. L. (2016a) *Thermal Synthesis of a Thermochemical Heat Storage with Heat Exchanger Optimisation*. [online] available from <http://ac.els-cdn.com/S1359431115015069/1-s2.0-S1359431115015069-

main.pdf?_tid=07b4634a-569d-11e7-a64d-00000aab0f27&acdnat=1498061989_3e440a6e8879d38b8c720ccf6d059021> [21 June 2017]

Fopah-Lele, A., Rohde, C., Neumann, K., Tietjen, T., Rönnebeck, T., N'Tsoukpoe, K. E., Osterland, T., Opel, O., and Ruck, W. K. L. (2016b) 'Lab-Scale Experiment of a Closed Thermochemical Heat Storage System Including Honeycomb Heat Exchanger'. *Energy* [online] 114, 225–238. available from <http://www.sciencedirect.com/science/article/pii/S0360544216311124> [26 April 2017]

Fopah-Lele, A. and Tamba, J. G. (2017) 'A Review on the Use of SrBr2·6H2O as a Potential Material for Low Temperature Energy Storage Systems and Building Applications'. *Solar Energy Materials and Solar Cells* 164, 175–187

Fopah Lele, A., Edem N 'tsoukpoe, K., Osterland, T., Ed Eric Kuznik, F., and Ruck, W. K. L. (2015) 'Thermal Conductivity Measurement of Thermochemical Storage Materials'. *Applied Thermal Engineering* [online] 89, 916–926. available from <https://ac.els-cdn.com/S1359431115006377/1-s2.0-S1359431115006377-main.pdf?_tid=8a8ce0b6-da92-11e7-9960-00000aab0f6c&acdnat=1512571038_eb727aaed1c19b31a227632939e7420e> [6 December 2017]

Freni, A., Sapienza, A., Glaznev, I. S., Aristov, Y. I., and Restuccia, G. (2012) 'Experimental Testing of a Lab-Scale Adsorption Chiller Using a Novel Selective Water Sorbent "Silica Modified by Calcium Nitrate"'. *International Journal of Refrigeration* 35 (3), 518–524

Furukawa, H., Cordova, K. E., O'Keeffe, M., and Yaghi, O. M. (2013) 'The Chemistry and Applications of Metal-Organic Frameworks'. *Science* [online] 341 (6149). available from <http://science.sciencemag.org/content/341/6149/1230444> [2 August 2017]

Gaeini, M., van Alebeek, R., Scapino, L., Zondag, H. A., and Rindt, C. C. M.

(2018) ‘Hot Tap Water Production by a 4 kW Sorption Segmented Reactor in Household Scale for Seasonal Heat Storage’. *Journal of Energy Storage* [online] 17, 118–128. available from <https://doi.org/10.1016/j.est.2018.02.014>

Gallo, E., Lamberti, C., and Glatzel, P. (2013) ‘Dd Excitations in CPO-27-Ni Metal-Organic Framework: Comparison between Resonant Inelastic X-Ray Scattering and UV-Vis Spectroscopy’. *Inorganic Chemistry* 52 (10), 5633–5635

Gantenbein, P., Jaenig, D., Kerskes, H., Summer, K., and Van Essen, M. (2008) *Laboratory Tests of Chemical Reactions and Prototype Sorption Storage Units* [online] Borlange. available from <http://archive.iea-shc.org/publications/downloads/task32-b4.pdf> [12 June 2017]

Garg, H., Mullick, S., and Bhargava, V. (2012) *Solar Thermal Energy Storage* [online] Berlin: Springer Science & Business Media. available from <https://books.google.co.uk/books?hl=en&lr=&id=ut_qCAAAQBAJ&oi=fnd&pg=PR14&dq=Solar+thermal+energy+storage&ots=0iy_DeDore&sig=0BF02WcuYQga_T4Y0Tk3CFttkZ0> [6 February 2017]

Gartler, G., Jähnig, D., Purkarthofer, G., and Wagner, W. (2004) ‘Development of a High Energy Density Sorption Storage System Basic Principles of an Adsorption Heat Storage System’. in *Proceedings of the EuroSun Conference* [online] held 2004 at Freiburg, Germany. available from <http://download.aee-intec.at/0uploads/dateien7.pdf> [16 March 2017]

Gil, A., Medrano, M., Martorell, I., Lazaro, A., Dolado, P., Zalba, B., and Cabeza, L. F. (2010) ‘State of the Art on High Temperature Thermal Energy Storage for Power Generation. Part 1-Concepts, Materials and Modellisation’. *Renewable and Sustainable Energy Reviews* 14 (1), 31–55

Glasser, L. (2014) ‘Thermodynamics of Inorganic Hydration and of Humidity Control, with an Extensive Database of Salt Hydrate Pairs’. *Journal of Chemical & Engineering Data* [online] 59 (2), 526–530. available from <http://pubs.acs.org/doi/abs/10.1021/je401077x> [30 November 2017]

Glueckauf, E. (1955) ‘Theory of Chromatography: Part 10. - Formula for Diffusion into Spheres and Their Application to Chromatography’.

Transactions of the Faraday Society 51, 1540–1551

Glueckauf, E. and Coates, J. I. (1947) '241. Theory of Chromatography. Part IV. The Influence of Incomplete Equilibrium on the Front Boundary of Chromatograms and on the Effectiveness of Separation'. *Journal of the Chemical Society (Resumed)* [online] 1315. available from <http://xlink.rsc.org/?DOI=jr9470001315>

Gondre, D. (2017) *Numerical Modelling and Analysis of Heat and Mass Transfers in an Adsorption Heat Storage Tank : Influences of Material Properties , Operating Conditions and System Design on Storage Performances*.

Good, P., Zanganeh, G., Ambrosetti, G., Barbato, M. C., Pedretti, A., and Steinfeld, A. (2014) 'Towards a Commercial Parabolic Trough CSP System Using Air as Heat Transfer Fluid'. in *Energy Procedia*. held 2014

Gorbach, A., Stegmaier, M., and Eigenberger, G. (2004) 'Measurement and Modelling of Water Vapour Adsorption on Zeolite 4A—Equilibria and Kinetics'. *Adsorption* [online] 10 (1), 29–46. available from <http://link.springer.com/article/10.1023/B:ADSO.0000024033.60103.ff%5Cnhttp://link.springer.com/article/10.1023/B:ADSO.0000024033.60103.ff#page-1%5Cnhttp://link.springer.com/content/pdf/10.1023/B:ADSO.0000024033.60103.ff.pdf>

Gordeeva, L. G., Grekova, A. D., Krieger, T. A., and Aristov, Y. I. (2009) 'Adsorption Properties of Composite Materials (LiCl + LiBr)/Silica'. *Microporous and Mesoporous Materials* [online] 126 (3), 262–267. available from <http://www.sciencedirect.com/science/article/pii/S1387181109002960> [6 December 2017]

Guarino, F., Athienitis, A., Cellura, M., and Bastien, D. (2017) 'PCM Thermal Storage Design in Buildings: Experimental Studies and Applications to Solaria in Cold Climates'. *Applied Energy* 185, 95–106

Hassan, H. Z. and Mohamad, A. A. (2012) 'A Review on Solar Cold Production through Absorption Technology'. *Renewable and Sustainable Energy*

Reviews [online] 16 (7), 5331–5348. available from <http://linkinghub.elsevier.com/retrieve/pii/S1364032112003243> [28 July 2017]

Hauer, A. (2007) 'Sorption Theory for Thermal Energy Storage'. in *Thermal Energy Storage for Sustainable Energy Consumption* [online] Dordrecht: Springer Netherlands, 393–408. available from <http://link.springer.com/10.1007/978-1-4020-5290-3_24> [21 May 2017]

Helden, W. Van, Wagner, W., Schubert, V., and Krampe-Zadler, C. (2014) 'Experimental Tests on a Solid Sorption Prototype for Seasonal Solar Thermal Storage'. *Eurotherm Seminar #99: Advances in Thermal Energy Storage* 1–8

Hengyi Chemical (2018) *Zibo Hengyi Chemical Science and Technology Co., Ltd* [online] available from <https://zbhengyi.en.alibaba.com/productgrouplist-806185240/molecular_sieve.html?spm=a2700.icbuShop.74.2.67377be3uM8NoM> [26 February 2019]

Henner, K., Rebecca, W., Oitz, B., and Harald, D. (2014) 'Development of a Segmented Sorption Store within the Project "SolSpaces"'. in *International Conference on Solar Energy and Buildings* [online] held 2014 at Aix-les-Bains, France. available from <http://proceedings.ises.org/eurosun2014-proceedings.pdf> [23 June 2017]

Henninger, S. K., Ernst, S. J., Gordeeva, L., Bendix, P., Fröhlich, D., Grekova, A. D., Bonaccorsi, L., Aristov, Y., and Jaenchen, J. (2017) 'New Materials for Adsorption Heat Transformation and Storage'. *Renewable Energy* 110, 59–68

Henninger, S. K., Jeremias, F., Kummer, H., Schossig, P., and Henning, H. M. (2012) 'Novel Sorption Materials for Solar Heating and Cooling'. in *Energy Procedia*. held 2012. 279–288

Henninger, S. K., Schmidt, F. P., and Henning, H.-M. (2010) 'Water Adsorption Characteristics of Novel Materials for Heat Transformation Applications'. *Applied Thermal Engineering* [online] 30 (13), 1692–1702. available from <http://www.sciencedirect.com/science/article/pii/S1359431110001389>

[24 May 2017]

Hongois, S., Kuznik, F., Stevens, P., and Roux, J. J. (2011) 'Development and Characterisation of a New MgSO4-Zeolite Composite for Long-Term Thermal Energy Storage'. *Solar Energy Materials and Solar Cells* 95 (7), 1831–1837

Hui, L., N'Tsoukpoe, K. E., Lingai, L., Edem, N. K., Nolwenn, L. P., and Luo, L. (2011) 'Evaluation of a Seasonal Storage System of Solar Energy for House Heating Using Different Absorption Couples'. *Energy Conversion and Management* [online] 52 (6), 2427–2436. available from <http://dx.doi.org/10.1016/j.enconman.2010.12.049> [20 January 2017]

Huo, S.-H. and Yan, X.-P. (2012) 'Metal–Organic Framework MIL-100(Fe) for the Adsorption of Malachite Green from Aqueous Solution'. *Journal of Materials Chemistry* [online] 22 (15), 7449. available from <http://xlink.rsc.org/?DOI=c2jm16513a>

Hutson, N. D. and Yang, R. T. (1997) 'Theoretical Basis for the Dubinin-Radushkevitch (D-R) Adsorption Isotherm Equation'. *Adsorption* 3 (3), 189–195

IEA (2019) 'Global Energy & CO2 Status Report: Emissions'. *Iea.org* [online] 14. available from <https://www.iea.org/geco/emissions/>

IEA (2018) *World Energy Outlook 2018 Examines Future Patterns of Global Energy System at a T* [online] available from <https://www.iea.org/newsroom/news/2018/november/world-energy-outlook-2018-examines-future-patterns-of-global-energy-system-at-a-t.html> [12 August 2019]

IEA (2017) *Renewables 2017*. Paris

IEA (2016) *WEO-2016 Special Report: Energy and Air Pollution* [online] Paris. available from <www.iea.org/t&c/>

International Energy Agency (2012) *Technology Roadmap: Solar Heating and Cooling*.

International Renewable Energy Agency (2018) *Global Energy Tranformation*.

IPCC (2013) *Climate Change 2014: Mitigation of Climate Change* [online] vol. 23. Cambridge: Cambridge University Press. available from

<http://linkinghub.elsevier.com/retrieve/pii/S0959378013000770> [6 February 2017]

Jabbari-Hichri, A., Bennici, S., and Auroux, A. (2017) 'CaCl2-Containing Composites as Thermochemical Heat Storage Materials'. *Solar Energy Materials and Solar Cells* 172, 177–185

Jänchen, J., Ackermann, D., Stach, H., and Brösicke, W. (2004) 'Studies of the Water Adsorption on Zeolites and Modified Mesoporous Materials for Seasonal Storage of Solar Heat'. *Solar Energy* 76 (1–3), 339–344

Jänchen, J., Ackermann, D., Weiler, E., Stach, H., and Brösicke, W. (2005) 'Calorimetric Investigation on Zeolites, AlPO4's and CaCl2 Impregnated Attapulgite for Thermochemical Storage of Heat'. in *Thermochimica Acta*. held 2005. 37–41

Janchen, J., Herzog, T. H., Gleichmann, K., Unger, B., Brandt, A., Fischer, G., and Richter, H. (2015) 'Performance of an Open Thermal Adsorption Storage System with Linde Type A Zeolites: Beads versus Honeycombs'. *Microporous and Mesoporous Materials* [online] 207, 179–184. available from <http://ac.els-cdn.com/S138718111500030X/1-s2.0-S138718111500030X-main.pdf?_tid=5f1a0b72-5511-11e7-bef6-00000aab0f6c&acdnat=1497892055_10278515767a818b01723bdaa2669570> [19 June 2017]

Jänchen, J., Schumann, K., Thrun, E., Brandt, A., Unger, B., and Hellwig, U. (2012) 'Preparation, Hydrothermal Stability and Thermal Adsorption Storage Properties of Binderless Zeolite Beads'. *International Journal of Low-Carbon Technologies* [online] 7, 275–279. available from <https://oup.silverchair-cdn.com/oup/backfile/Content_public/Journal/ijlct/7/4/10.1093_ijlct_cts037/1/cts037.pdf?Expires=1495835118&Signature=K0vDr8PTNfUWc9X38b5b2gt2TmQDyFLhWBvEqtL8Sv7GDU-EFSju2cT6VANw80xug4Q~Urd8c2ieHLCdiTOMMXp2KFapazZY5~6~CIeoWiSUGGNglh> [25 May 2017]

Janiak, C. and Henninger, S. K. (2013) 'Porous Coordination Polymers as Novel Sorption Materials for Heat Transformation Processes'. *CHIMIA*

International Journal for Chemistry [online] 67 (6), 419–424. available from <http://openurl.ingenta.com/content/xref?genre=article&issn=0009-4293&volume=67&issue=6&spage=419> [13 October 2017]

Jarimi, H., Aydin, D., Yanan, Z., Ozankaya, G., Chen, X., and Riffat, S. (2019) 'Review on the Recent Progress of Thermochemical Materials and Processes for Solar Thermal Energy Storage and Industrial Waste Heat Recovery'. *International Journal of Low-Carbon Technologies* 14 (1), 44–69

Jenkins, H. D. B. (2008) 'Le Chatelier's Principle'. in *Chemical Thermodynamics at a Glance* [online] Oxford, UK: Blackwell Publishing Ltd, 160–163. available from <http://doi.wiley.com/10.1002/9780470697733.ch49> [27 May 2017]

Jeremias, F., Fröhlich, D., Janiak, C., and Henninger, S. K. (2014a) 'Water and Methanol Adsorption on MOFs for Cycling Heat Transformation Processes'. *New J. Chem.* [online] 38 (5), 1846–1852. available from <http://xlink.rsc.org/?DOI=C3NJ01556D>

Jeremias, F., Fröhlich, D., Janiak, C., and Henninger, S. K. (2014b) 'Advancement of Sorption-Based Heat Transformation by a Metal Coating of Highly-Stable, Hydrophilic Aluminium Fumarate MOF'. *RSC Adv.* [online] 4 (46), 24073–24082. available from <http://xlink.rsc.org/?DOI=C4RA03794D>

Jeremias, F., Khutia, A., Henninger, S. K., Janiak, C., Marrot, J., Férey, G., Stock, N., Mellot-Draznieks, C., Burghammer, M., Riekel, C., Jhung, S. H., and Férey, G. (2012) 'MIL-100(Al, Fe) as Water Adsorbents for Heat Transformation Purposes—a Promising Application'. *J. Mater. Chem.* [online] 22 (20), 10148–10151. available from <http://xlink.rsc.org/?DOI=C2JM15615F> [2 August 2017]

Jiang, L., Gao, J., Wang, L., Wang, R., Lu, Y., and Roskilly, A. P. (2017) 'Investigation on Performance of Multi-Salt Composite Sorbents for Multilevel Sorption Thermal Energy Storage'. *Applied Energy* 190, 1029–1038

Jiao, W. Z., Liu, Y. Z., and Qi, G. S. (2010) 'Gas Pressure Drop and Mass Transfer Characteristics in a Cross-Flow Rotating Packed Bed with Porous

Plate Packing'. *Industrial and Engineering Chemistry Research* 49 (8), 3732–3740

Jim Clark (2002) *An Introduction to Chemical Equilibria* [online] available from <http://www.chemguide.co.uk/physical/equilibria/introduction.html> [27 May 2017]

Johannes, K., Kuznik, F., Hubert, J.-L., Durier, F., and Obrecht, C. (2015) 'Design and Characterisation of a High Powered Energy Dense Zeolite Thermal Energy Storage System for Buildings'. *Applied Energy* [online] 159, 80–86. available from <http://ac.els-cdn.com/S0306261915010454/1-s2.0-S0306261915010454-main.pdf?_tid=64d4e5b0-5a74-11e7-a90b-00000aab0f27&acdnat=1498484341_15111906fe03a353a0c455ca374a558e> [26 June 2017]

De Jong, A. J., Trausel, F., Finck, C., Van Vliet, L., and Cuypers, R. (2014) 'Thermochemical Heat Storage - System Design Issues'. *Energy Procedia* [online] 48, 309–319. available from <http://dx.doi.org/10.1016/j.egypro.2014.02.036>

Kärger, J. (1996) 'Flow and Transport in Porous Media and Fractured Rock'. *Zeitschrift für Physikalische Chemie*

Kerskes, H., Mette, B., Bertsch, F., Asenbeck, S., and Drück, H. (2012) 'Chemical Energy Storage Using Reversible Solid/Gas-Reactions (CWS) – Results of the Research Project'. *Energy Procedia* 30, 294–304

Kim, H., Cho, H. J., Narayanan, S., Yang, S., Furukawa, H., Schiffres, S., Li, X., Zhang, Y. B., Jiang, J., Yaghi, O. M., and Wang, E. N. (2016) 'Characterisation of Adsorption Enthalpy of Novel Water-Stable Zeolites and Metal-Organic Frameworks'. *Scientific Reports* 6 (June 2015), 1–8

Krese, G., Koželj, R., Butala, V., and Stritih, U. (2018) 'Thermochemical Seasonal Solar Energy Storage for Heating and Cooling of Buildings'. *Energy and Buildings* [online] 164, 239–253. available from <https://doi.org/10.1016/j.enbuild.2017.12.057>

Küsgens, P., Rose, M., Senkovska, I., Fröde, H., Henschel, A., Siegle, S., and Kaskel, S. (2009) 'Characterisation of Metal-Organic Frameworks by Water Adsorption'. *Microporous and Mesoporous Materials* [online] 120 (3), 325–

330. available from <http://linkinghub.elsevier.com/retrieve/pii/S1387181108006100> [2 August 2017]

Kuwahara, F., Shirota, M., and Nakayama, A. (2001) 'A Numerical Study of Interfacial Convective Heat Transfer Coefficient in Two-Energy Equation Model for Convection in Porous Media'. *International Journal of Heat and Mass Transfer* [online] 44 (6), 1153–1159. available from <https://www.sciencedirect.com/science/article/pii/S0017931000001666> [13 August 2018]

Kuznik, F., David, D., Johannes, K., and Roux, J. J. (2011) 'A Review on Phase Change Materials Integrated in Building Walls'. in *Renewable and Sustainable Energy Reviews*. vol. 15 (1). 379–391

Kuznik, F., Gondre, D., Johannes, K., Obrecht, C., and David, D. (2019) 'Numerical Modelling and Investigations on a Full-Scale Zeolite 13X Open Heat Storage for Buildings'. *Renewable Energy* 132, 761–772

Kuznik, F., Johannes, K., and Obrecht, C. (2015) 'Chemisorption Heat Storage in Buildings: State-of-the-Art and Outlook'. *Energy and Buildings* [online] 106, 183–191. available from <http://dx.doi.org/10.1016/j.enbuild.2015.07.002>

Kuznik, F., Johannes, K., Obrecht, C., and David, D. (2018) 'A Review on Recent Developments in Physisorption Thermal Energy Storage for Building Applications'. *Renewable and Sustainable Energy Reviews* [online] 94 (November 2017), 576–586. available from <https://doi.org/10.1016/j.rser.2018.06.038>

Lahmidi, H., Mauran, S., and Goetz, V. (2006) 'Definition, Test and Simulation of a Thermochemical Storage Process Adapted to Solar Thermal Systems'. *Solar Energy* 80 (7), 883–893

Largitte, L. and Pasquier, R. (2016) 'A Review of the Kinetics Adsorption Models and Their Application to the Adsorption of Lead by an Activated Carbon'. *Chemical Engineering Research and Design* [online] 109, 495–504. available from <http://dx.doi.org/10.1016/j.cherd.2016.02.006>

Lele, A. F. (2015) *A Thermochemical Heat Storage System for Households:*

Thermal Transfers Coupled to Chemical Reaction Investigations.

Letcher, T. (2016) *Storing Energy: With Special Reference to Renewable Energy Sources*. Elsevier

Li, T. X., Xu, J. X., Yan, T., and Wang, R. Z. (2016) 'Development of Sorption Thermal Battery for Low-Grade Waste Heat Recovery and Combined Cold and Heat Energy Storage'. *Energy* [online] 107, 347–359. available from <http://ac.els-cdn.com/S0360544216303735/1-s2.0-S0360544216303735-main.pdf?_tid=f50ae8da-418a-11e7-a095-00000aacb35d&acdnat=1495745253_7daa635d55cd1795d63eda695e7fed01> [25 May 2017]

Liu, Y. (2006) 'Some Consideration on the Langmuir Isotherm Equation'. *Colloids and Surfaces A: Physicochemical and Engineering Aspects*

Lizana, J., Chacartegui, R., Barrios-Padura, A., and Valverde, J. M. (2017) 'Advances in Thermal Energy Storage Materials and Their Applications towards Zero Energy Buildings: A Critical Review'. in *Applied Energy*.

Marias, F., Neveu, P., Tanguy, G., and Papillon, P. (2014) *Thermodynamic Analysis and Experimental Study of Solid/Gas Reactor Operating in Open Mode*. [online] available from <https://ac.els-cdn.com/S0360544214001236/1-s2.0-S0360544214001236-main.pdf?_tid=a099ecfe-d5e3-11e7-b794-00000aacb35d&acdnat=1512056109_1ef59f45c70408693811958a23306480> [30 November 2017]

Mauran, S., Lahmidi, H., and Goetz, V. (2008) 'Solar Heating and Cooling by a Thermochemical Process. First Experiments of a Prototype Storing 60 KWh by a Solid/Gas Reaction'. *Solar Energy* [online] 82 (7), 623–636. available from <http://linkinghub.elsevier.com/retrieve/pii/S0038092X08000182> [16 March 2017]

Mette, B., Kerskes, H., and Druck, H. (2011) 'Process and Reactor Design for Thermo-Chemical Energy Stores'. in *ISES Solar World Congress* [online] held 2011 at Kassel. available from <http://forum.iea-shc.org/data/sites/1/publications/Task42-Process_and_Reactor_Design_for_Thermo-Chemical_Energy_Stores.pdf>

[20 December 2017]

Mette, B., Kerskes, H., and Drück, H. (2014a) ‘Experimental and Numerical Investigations of Different Reactor Concepts for Thermochemical Energy Storage’. *Energy Procedia* [online] 57, 2380–2389. available from <http://ac.els-cdn.com/S1876610214016130/1-s2.0-S1876610214016130-main.pdf?_tid=26337a8c-3fc7-11e7-8829-00000aab0f6b&acdnat=1495551203_86c5afc6d86017b5aefc8c1dc2c5abb0> [23 May 2017]

Mette, B., Kerskes, H., and Drück, H. (2012) ‘Concepts of Long-Term Thermochemical Energy Storage for Solar Thermal Applications – Selected Examples’. *Energy Procedia* [online] 30, 321–330. available from <http://linkinghub.elsevier.com/retrieve/pii/S1876610212015548> [26 April 2017]

Mette, B., Kerskes, H., Drück, H., and Müller-Steinhagen, H. (2014b) ‘Experimental and Numerical Investigations on the Water Vapour Adsorption Isotherms and Kinetics of Binderless Zeolite 13X’. *International Journal of Heat and Mass Transfer* [online] 71, 555–561. available from <http://www.sciencedirect.com/science/article/pii/S001793101301106X> [31 May 2017]

Mhimid, A. (1998) ‘Theoretical Study of Heat and Mass Transfer in a Zeolite Bed during Water Desorption: Validity of Local Thermal Equilibrium Assumption’. *International Journal of Heat and Mass Transfer* 41 (19), 2967–2977

Michel, B., Mazet, N., Mauran, S., Stitou, D., and Xu, J. (2012) ‘Thermochemical Process for Seasonal Storage of Solar Energy: Characterisation and Modelling of a High Density Reactive Bed’. *Energy* [online] 47 (1), 553–563. available from <http://www.sciencedirect.com/science/article/pii/S0360544212007074> [20 January 2017]

Michel, B., Mazet, N., and Neveu, P. (2016) ‘Experimental Investigation of an Open Thermochemical Process Operating with a Hydrate Salt for Thermal Storage of Solar Energy: Local Reactive Bed Evolution’. *Applied Energy*

[online] 180, 234–244. available from <http://ac.els-cdn.com/S0306261916310376/1-s2.0-S0306261916310376-main.pdf?_tid=f764aefe-56c0-11e7-823c-00000aab0f6b&acdnat=1498077424_128e3b16d58455b5b345f35a3478e6cb> [21 June 2017]

Michel, B., Mazet, N., and Neveu, P. (2014a) 'Experimental Investigation of an Innovative Thermochemical Process Operating with a Hydrate Salt and Moist Air for Thermal Storage of Solar Energy: Global Performance'. *Applied Energy* [online] 129, 177–186. available from <http://ac.els-cdn.com/S030626191400436X/1-s2.0-S030626191400436X-main.pdf?_tid=a6511cac-576d-11e7-bb45-00000aab0f01&acdnat=1498151592_6afcf1921827f17f7e62d6d3e9f8ff66> [22 June 2017]

Michel, B., Neveu, P., and Mazet, N. (2014b) 'Comparison of Closed and Open Thermochemical Processes, for Long-Term Thermal Energy Storage Applications'. *Energy* [online] available from <http://ac.els-cdn.com/S0360544214006641/1-s2.0-S0360544214006641-main.pdf?_tid=c32ce4da-569d-11e7-883c-00000aacb360&acdnat=1498062304_1e960e773d3a1ad20ec644ed944fcc63> [21 June 2017]

Mohammadzadeh Kowsari, M., Niazmand, H., and Tokarev, M. M. (2018) 'Bed Configuration Effects on the Finned Flat-Tube Adsorption Heat Exchanger Performance: Numerical Modeling and Experimental Validation'. *Applied Energy* 213 (October 2017), 540–554

Molenda, M., Stengler, J., Linder, M., and Wörner, A. (2013) 'Reversible Hydration Behaviour of CaCl2 at High H2O Partial Pressures for Thermochemical Energy Storage'. *Thermochimica Acta* 560, 76–81

Motsi, T., Rowson, N. A., and Simmons, M. J. H. (2009) *Adsorption of Heavy Metals from Acid Mine Drainage by Natural Zeolite*. [online] available from <https://ac.els-cdn.com/S0301751609000349/1-s2.0-S0301751609000349-main.pdf?_tid=be46a57e-bb23-11e7-a373-00000aacb35d&acdnat=1509114965_afa7042c046f92587105c41c98711f0

8> [27 October 2017]

Mugele, J. (2005) *Optimierung von Speichermaterialien Für Den Einsatz in Geschlossenen Thermochemischen Wärmespeichern Für Gebäudetechnische Anwendungen*. VDI-Verl

N'Tsoukpoe, K. E., Liu, H., Le Pierres, N., and Luo, L. (2009) 'A Review on Long-Term Sorption Solar Energy Storage'. *Renewable and Sustainable Energy Reviews* 13 (9), 2385–2396

N'Tsoukpoe, K. E., Mazet, N., and Neveu, P. (2016) 'The Concept of Cascade Thermochemical Storage Based on Multimaterial System for Household Applications'. *Energy and Buildings* [online] 129, 138–149. available from <http://dx.doi.org/10.1016/j.enbuild.2016.07.047>

N'Tsoukpoe, K. E., Le Pierrès, N., and Luo, L. (2013) 'Experimentation of a LiBr-H2O Absorption Process for Long-Term Solar Thermal Storage: Prototype Design and First Results'. *Energy* [online] 53, 179–198. available from <http://dx.doi.org/10.1016/j.energy.2013.02.023>

N'Tsoukpoe, Kokouvi Edem, Le Pierrès, N., and Luo, L. (2012) 'Experimentation of a LiBr-H2O Absorption Process for Long Term Solar Thermal Storage'. *Energy Procedia* 30, 331–341

N'Tsoukpoe, K. Edem, Pierrès, N Le, Luo, L., Le Pierrès, Nolwenn, and Luo, L. (2012) 'Numerical Dynamic Simulation and Analysis of a Lithium Bromide/Water Long-Term Solar Heat Storage System'. *Energy* [online] 37 (1), 346–358. available from <http://dx.doi.org/10.1016/j.energy.2011.11.020> [20 January 2017]

N'Tsoukpoe, K. E., Schmidt, T., Rammelberg, H. U., Watts, B. A., and Ruck, W. K. L. (2014) 'A Systematic Multi-Step Screening of Numerous Salt Hydrates for Low Temperature Thermochemical Energy Storage'. *Applied Energy* 124, 1–16

Nagel, T., Beckert, S., Böttcher, N., Gläser, R., and Kolditz, O. (2015) 'The Impact of Adsorbate Density Models on the Simulation of Water Sorption on Nanoporous Materials for Heat Storage'. *Energy Procedia* [online] 75, 2106–2112. available from <http://dx.doi.org/10.1016/j.egypro.2015.07.331>

National Library of Medicine (2015) *Cupric Chloride*.

Nic, M., Jirat, J., and Kosata, B. (2014) *Compendium of Chemical Terminology* [online] Oxford. available from <http://goldbook.iupac.org/index.html> [21 May 2017]

Nikolaev, K. M. and Dubinin, M. M. (1958) 'Concerning Adsorptional Properties of Carbon Adsorbents 3. A Study of Adsorption Isotherms of Gases and Vapours on Active Carbons over a Wide Interval of Temperatures, Including the Critical Region'. *Bulletin of the Academy of Sciences of the USSR Division of Chemical Science*

Oh, H. T., Lim, S. J., Kim, J. H., and Lee, C. H. (2017) 'Adsorption Equilibria of Water Vapour on an Alumina/Zeolite 13X Composite and Silica Gel'. *Journal of Chemical and Engineering Data* 62 (2), 804–811

Okhrimenko, L., Favergeon, L., Johannes, K., Kuznik, F., and Pijolat, M. (2017) 'Thermodynamic Study of MgSO4 – H2O System Dehydration at Low Pressure in View of Heat Storage'. *Thermochimica Acta* 656, 135–143

Okunev, B. N., Gromov, A. P., Heifets, L. I., and Aristov, Y. I. (2008) 'A New Methodology of Studying the Dynamics of Water Sorption/Desorption under Real Operating Conditions of Adsorption Heat Pumps: Modelling of Coupled Heat and Mass Transfer in a Single Adsorbent Grain'. *International Journal of Heat and Mass Transfer* [online] 51 (1–2), 246–252. available from <http://www.sciencedirect.com/science/article/pii/S001793100700292X> [6 December 2017]

Ooms, G., Van Santen, R. A., Jackson, R. A., and Catlow, C. R. A. (1988) 'The Relative Stability of Zeolite Frameworks'. *Studies in Surface Science and Catalysis* [online] 37 (C), 317–322. available from <http://dx.doi.org/10.1016/S0167-2991(09)60609-1>

Otterstedt, J.-E. and Brandreth, D. A. (1998) *Small Particles Technology* [online] Berlin: Springer. available from <https://books.google.co.uk/books?id=fbPbBwAAQBAJ&pg=PA197&lpg=PA197&dq=zeolite,+water+adsorption,+force+between+water+molecules+and+ions+of+zeolite&source=bl&ots=J2Eajzjhef&sig=Er28iiHBpDnEw-

w_nThnS7I9M9U&hl=en&sa=X&ved=0ahUKEwjX-NbkwZXUAhVLJsAKHSikC_AQ6A> [29 May 2017]

Paksoy, H. O. (2007) *Thermal Energy Storage for Sustainable Energy Consumption : Fundamentals, Case Studies and Design* [online] Cesme: Springer. available from <https://books.google.co.uk/books?hl=en&lr=&id=7MR0lR6sO14C&oi=fnd&pg=PA3&dq=Thermal+Energy+Storage+for+Sustainable+Energy+Consumption&ots=wWuNoBLCUA&sig=IscoF48urSA3MpCUx0mmjx5e2iY#v=onepage&q=Thermal Energy Storage for Sustainable Energy Cons> [19 May 2017]

Pardo, P., Deydier, A., Anxionnaz-Minvielle, Z., Rouge, S., Cabassud, M., and Cognet, P. (2014) 'A Review on High Temperature Thermochemical Heat Energy Storage'. *Renewable and Sustainable Energy Reviews* [online] 32, 591–610. available from <http://dx.doi.org/10.1016/j.rser.2013.12.014>

Paulik, J., Paulik, F., and Arnold, M. (1981) 'Dehydration of Magnesium Sulphate Heptahydrate Investigated by Quasi Isothermal-Quasi Isobaric TG'. *Thermochimica Acta* 50 (1–3), 105–110

Pinel, P., Cruickshank, C. A., Beausoleil-Morrison, I., and Wills, A. (2011) 'A Review of Available Methods for Seasonal Storage of Solar Thermal Energy in Residential Applications'. *Renewable and Sustainable Energy Reviews* [online] 15, 3341–3359. available from <http://ac.els-cdn.com/S136403211100150X/1-s2.0-S136403211100150X-main.pdf?_tid=d2e61304-49fc-11e7-bafc-00000aacb361&acdnat=1496673767_f5227eaefb5d2a8f92514dbec29ea2cf> [5 June 2017]

Poulopoulos, S. and Inglezakis, V. (2006) *Adsorption, Ion Exchange and Catalysis: Design of Operations and Environmental Applications* [online] available from <https://books.google.co.uk/books?hl=en&lr=&id=nbLp07ReR50C&oi=fnd&pg=PP1&dq=Adsorption,+Ion+Exchange+and+Catalysis:+Design+of+Operations+and+Environmental+Applications&ots=PBL0kai-2Q&sig=7kBVp9N-g_FAAIPSH5LlDhfqj1Y> [4 December 2017]

R. Welty, J., E. Wicks, C., E. Wilson, R., and Rorrer, G. (1970) *Fundamentals of Momentum, Heat and Mass Transfer* [online] vol. 13. available from <http://linkinghub.elsevier.com/retrieve/pii/0017931070900633>

Rahman, K. A., Loh, W. S., and Ng, K. C. (2013) 'Heat of Adsorption and Adsorbed Phase Specific Heat Capacity of Methane/Activated Carbon System'. in *Procedia Engineering*. held 2013. Elsevier Ltd, 118–125

Rebecca, W., Sebastian, A., Henner, K., and Harald, D. (2016) 'SolSpaces – Testing and Performance Analysis of a Segmented Sorption Store for Solar Thermal Space Heating'. *Energy Procedia* [online] 91, 250–258. available from <http://ac.els-cdn.com/S1876610216303125/1-s2.0-S1876610216303125-main.pdf?_tid=d8c80cc4-3fc4-11e7-910a-00000aacb360&acdnat=1495550214_22a57c3efbe2c714d34c3ada0bf0b26f> [23 May 2017]

Reichl, C., Lager, D., Englmair, G., Zettl, B., and Popovac, M. (2016) 'Fluid Dynamics Simulations for an Open-Sorption Heat Storage Drum Reactor Based on Thermophysical Kinetics and Experimental Observations'. *Applied Thermal Engineering* [online] 107, 994–1007. available from <http://ac.els-cdn.com/S135943111631033X/1-s2.0-S135943111631033X-main.pdf?_tid=20d1c692-576f-11e7-bcdb-00000aacb362&acdnat=1498152227_eb612b52c8e8213efb9148bab7a08d74> [22 June 2017]

Rezk, A., Al-Dadah, R., Mahmoud, S., and Elsayed, A. (2012) 'Characterisation of Metal Organic Frameworks for Adsorption Cooling'. *International Journal of Heat and Mass Transfer* 55 (25–26), 7366–7374

Richter, M., Bouché, M., and Linder, M. (2016) 'Heat Transformation Based on CaCl2H2O – Part A: Closed Operation Principle'. *Applied Thermal Engineering* [online] 102, 615–621. available from <https://ac.els-cdn.com/S1359431116303696/1-s2.0-S1359431116303696-main.pdf?_tid=ce47728a-e4c9-11e7-9810-00000aab0f26&acdnat=1513694286_a6a9a565bafcb3795f3a0849ea6aacd3> [19 December 2017]

Ristić, A., Logar, N. Z., Henninger, S. K., and Kaučič, V. (2012) 'The

Performance of Small-Pore Microporous Aluminophosphates in Low-Temperature Solar Energy Storage: The Structure-Property Relationship'. *Advanced Functional Materials* 22 (9), 1952–1957

Sahoo, D. K., Mishra, R., Singh, H., and Krishnamurthy, N. (2014) 'Determination of Thermodynamic Stability of Lanthanum Chloride Hydrates (LaCl3·xH2O) by Dynamic Transpiration Method'. *Journal of Alloys and Compounds* 588, 578–584

Scapino, L., Zondag, H. A., Van Bael, J., Diriken, J., and Rindt, C. C. M. (2017) 'Sorption Heat Storage for Long-Term Low-Temperature Applications: A Review on the Advancements at Material and Prototype Scale'. *Applied Energy* [online] 190, 920–948. available from <http://www.sciencedirect.com/science/article/pii/S0306261916319316> [26 April 2017]

Schreiber, H., Graf, S., Lanzerath, F., and Bardow, A. (2015) 'Adsorption Thermal Energy Storage for Cogeneration in Industrial Batch Processes: Experiment, Dynamic Modelling and System Analysis'. *Applied Thermal Engineering* 89, 485–493

Schumann, K., Unger, B., Brandt, A., Fischer, G., Richter, H., and Janchen, J. (2014) 'Preparation and Characterisation of Compact Binderless Zeolite Shapes with Faujasit and Linde Type A Structure'. *Chemie Ingenieur Technik*

Semprini, S., Lehmann, C., Beckert, S., Kolditz, O., Gläser, R., Kerskes, H., and Nagel, T. (2017) 'Numerical Modelling of Water Sorption Isotherms of Zeolite 13XBF Based on Sparse Experimental Data Sets for Heat Storage Applications'. *Energy Conversion and Management* 150 (August), 392–402

Shukla, A., Tiwari, G. N., and Sodha, M. S. (2008) 'Experimental Study of Effect of an Inner Thermal Curtain in Evaporative Cooling System of a Cascade Greenhouse'. *Solar Energy* 82 (1), 61–72

Siddiqui, M. U. and Said, S. A. M. (2014) 'A Review of Solar Powered Absorption Systems'. *Renewable and Sustainable Energy Reviews* [online] 42, 93–115. available from <http://ac.els-cdn.com/S1364032114008314/1-s2.0-S1364032114008314-main.pdf?_tid=0fa6b6ca-44c8-11e7-892e-

00000aab0f6c&acdnat=1496101350_5584106f4a24086727c0a72ea22ab971> [30 May 2017]

Sircar, S. and Hufton, J. R. (2000) 'Why Does the Linear Driving Force Model for Adsorption Kinetics Work?' *Adsorption* 6 (2), 137–147

Solé, A., Martorell, I., and Cabeza, L. F. (2015a) 'State of the Art on Gas-Solid Thermochemical Energy Storage Systems and Reactors for Building Applications'. *Renewable and Sustainable Energy Reviews* [online] 47, 386–398. available from <http://dx.doi.org/10.1016/j.rser.2015.03.077>

Solé, A., Miró, L., Barreneche, C., Martorell, I., and Cabeza, L. F. (2015b) 'Corrosion of Metals and Salt Hydrates Used for Thermochemical Energy Storage'. *Renewable Energy* 75, 519–523

Solmus, I., Andrew, D., Rees, S., Yamalı, C., Baker, D., and Kaftano Glu, B. (2012) 'Numerical Investigation of Coupled Heat and Mass Transfer inside the Adsorbent Bed of an Adsorption Cooling Unit'. *International Journal of Refrigeration* [online] 35, 652–662. available from <https://ac.els-cdn.com/S0140700711003070/1-s2.0-S0140700711003070-main.pdf?_tid=e0645c1e-a9e4-11e7-80ab-00000aacb35f&acdnat=1507218795_9f9ab18b2f816dbfa7dcfd0eb10eb655> [5 October 2017]

Srivastava, N. C. and Eames, I. W. (1998) 'A Review of Adsorbents and Adsorbates in Solid–Vapour Adsorption Heat Pump Systems'. *Applied Thermal Engineering* [online] 18 (9–10), 707–714. available from <http://linkinghub.elsevier.com/retrieve/pii/S1359431197001063>

Su, Y., Straathof, N. J. W., Hessel, V., and Noël, T. (2014) 'Photochemical Transformations Accelerated in Continuous-Flow Reactors: Basic Concepts and Applications'. in *Chemistry - A European Journal*. vol. 20 (34). 10562–10589

Sun, L. M., Ben Amar, N., and Meunier, F. (1995) 'Numerical Study on Coupled Heat and Mass Transfers in an Absorber with External Fluid Heating'. *Heat Recovery Systems and CHP* 15 (1), 19–29

Sun, M.-H., Huang, S.-Z., Chen, L.-H., Li, Y., Yang, X.-Y., Yuan, Z.-Y., and Su, B.-L. (2016) 'Applications of Hierarchically Structured Porous Materials

from Energy Storage and Conversion, Catalysis, Photocatalysis, Adsorption, Separation, and Sensing to Biomedicine'. *Chem. Soc. Rev.* [online] 45 (12), 3479–3563. available from <http://xlink.rsc.org/?DOI=C6CS00135A>

Tanh Jeazet, H. B., Koschine, T., Staudt, C., Raetzke, K., and Janiak, C. (2013) 'Correlation of Gas Permeability in a Metal-Organic Framework MIL-101(Cr)-Polysulfone Mixed-Matrix Membrane with Free Volume Measurements by Positron Annihilation Lifetime Spectroscopy (PALS)'. *Membranes* 3 (4), 331–353

Tatsidjodoung, P., Le Pierrès, N., Heintz, J., Lagre, D., Luo, L., and Durier, F. (2016) 'Experimental and Numerical Investigations of a Zeolite 13X/Water Reactor for Solar Heat Storage in Buildings'. *Energy Conversion and Management* [online] 108, 488–500. available from <http://ac.els-cdn.com/S0196890415010183/1-s2.0-S0196890415010183-main.pdf?_tid=55d8f0d6-576f-11e7-93ec-00000aacb35f&acdnat=1498152316_b409591bff48bd760035142f7b3d1f9d> [22 June 2017]

Tatsidjodoung, P., Le Pierres, N., and Luo, L. (2013) 'A Review of Potential Materials for Thermal Energy Storage in Building Applications'. *Renewable and Sustainable Energy Reviews* 18, 327–349

Thomas, W. J. and Crittenden, B. (1998) *Adsorption Technology and Design*.

Tian, B., Jin, Z., Wang, L., and Wang, R. (2012) 'Permeability and Thermal Conductivity of Compact Chemical and Physical Adsorbents with Expanded Natural Graphite as Host Matrix'. *Journal of Heat and Mass Transfer* [online] available from <http://www.sciencedirect.com/science/article/pii/S0017931012002591> [20 January 2017]

Trambouze, P. and Euzen, J.-P. (2004) *Chemical Reactors : From Design to Operation* [online] Paris: Editions Technip. available from <https://books.google.co.uk/books?id=UbhTAAAAMAAJ&dq=Trambouze%2C P%2C Euzen%2C J-P.%2C Chemical reactors. From design to operation%2C Technip&lr&source=gbs_book_other_versions> [20

December 2017]

Trausel, F., De Jong, A. J., and Cuypers, R. (2014) ‘A Review on the Properties of Salt Hydrates for Thermochemical Storage’. *Energy Procedia* [online] 48, 447–452. available from <http://dx.doi.org/10.1016/j.egypro.2014.02.053>

Ucar, M. and Pounder, B. (1982) ‘Heat-of-Adsorption Solar Thermal Energy Storage’. *Journal of Building Physics* [online] 6 (1), 48–58. available from <http://journals.sagepub.com/doi/10.1177/109719638200600104> [22 November 2017]

ul Qadir, N., Said, S. A. M., and Mansour, R. Ben (2017) *Modelling the Performance of a Two-Bed Solar Adsorption Chiller Using a Multi-Walled Carbon Nanotube/MIL-100(Fe) Composite Adsorbent*. [online] available from <https://ac.els-cdn.com/S0960148117302689/1-s2.0-S0960148117302689-main.pdf?_tid=ee385140-b19d-11e7-a1d1-00000aab0f27&acdnat=1508067932_6979dce2be9499dc3a92a442ef670102> [15 October 2017]

UN Environment and International Energy Agency (2017) *Global Status Report : Towards a Zero-Emission, Efficient, and Resilient Buildings and Construction Sector*.

University of Nebraska (2012) *Toxicology and Exposure Guidelines* [online] Nebraska. available from <https://ehs.unl.edu/documents/tox_exposure_guidelines.pdf> [29 November 2017]

Ürge-Vorsatz, D., Cabeza, L. F., Serrano, S., Barreneche, C., and Petrichenko, K. (2015) ‘Heating and Cooling Energy Trends and Drivers in Buildings’. in *Renewable and Sustainable Energy Reviews*. vol. 41. Elsevier Ltd, 85–98

Valdes-Parada, F. J., Ochoa-Tapia, J. A., and Alvarez-Ramirez, J. (2009) ‘Validity of the Permeability Carman-Kozeny Equation: A Volume Averaging Approach’. *Physica A: Statistical Mechanics and its Applications*

Vrdoljak, A. L. and Erfanifar, E. (2016) ‘Acute Toxicity and the Effects of Copper Sulphate (CuSO4.5H2O) on the Behaviour of the Grey Mullet (Mugil Cephalus)’. *Journal of Clinical Toxicology* [online] 06 (06). available from <https://www.omicsonline.org/conference-proceedings/euro-toxicology-

2016_posters-accepted-abstracts.digital> [29 November 2017]

Wakao, N. and Kagei, S. (1982) *Heat and Mass Transfer in Packed Beds* [online] Gordon and Breach Science Publishers. available from <https://books.google.co.ve/books?id=Ya5hzOgC05wC&hl=fr&source=gbs_navlinks_s> [13 August 2018]

Wang, K., Wu, J. Y., Wang, R. Z., and Wang, L. W. (2006) 'Effective Thermal Conductivity of Expanded Graphite-CaCl2 Composite Adsorbent for Chemical Adsorption Chillers'. *Energy Conversion and Management* 47 (13–14), 1902–1912

Wang, L. W., Wang, R. Z., and Oliveira, R. G. (2009) 'A Review on Adsorption Working Pairs for Refrigeration'. in *Renewable and Sustainable Energy Reviews*. vol. 13 (3). 518–534

Wang, S. and Peng, Y. (2010) 'Natural Zeolites as Effective Adsorbents in Water and Wastewater Treatment'. *Chemical Engineering Journal* [online] 156, 11–24. available from <https://ac.els-cdn.com/S1385894709007219/1-s2.0-S1385894709007219-main.pdf?_tid=313c2e20-bb22-11e7-b570-00000aab0f6b&acdnat=1509114299_a84b2a48c7cf95e68a6ca8db8f264e60> [27 October 2017]

Weber, R., Kerskes, H., and Drück, H. (2014) 'Development of a Combined Hot Water and Sorption Store for Solar Thermal Systems'. *Energy Procedia* [online] 48 (48), 464–473. available from <http://ac.els-cdn.com/S1876610214003178/1-s2.0-S1876610214003178-main.pdf?_tid=f455b786-5831-11e7-b77a-00000aab0f02&acdnat=1498235904_6c5c2430de702273702b869f2724295f> [23 June 2017]

Wright, P. A. (2008) *Microporous Framework Solids*.

Wu, W. D., Zhang, H., and Sun, D. W. (2009) 'Mathematical Simulation and Experimental Study of a Modified Zeolite 13X-Water Adsorption Refrigeration Module'. *Applied Thermal Engineering* [online] 29 (4), 645–651. available from <http://dx.doi.org/10.1016/j.applthermaleng.2008.03.037>

Wyttenbach, J., Bougard, J., Descy, G., Skrylnyk, O., Courbon, E., Frère, M.,

and Bruyat, F. (2018) ‘Performances and Modelling of a Circular Moving Bed Thermochemical Reactor for Seasonal Storage’. *Applied Energy* [online] 230 (August), 803–815. available from <https://doi.org/10.1016/j.apenergy.2018.09.008>

Xu, S. M., Zhang, L., Liang, J., and Du, R. (2007) ‘Variable Mass Energy Transformation and Storage (VMETS) System Using NH3-H2O as Working Fluid, Part 1: Modelling and Simulation under Full Storage Strategy’. *Energy Conversion and Management* 48 (1), 9–26

Xunzhang, P., Wenying, C., Clarke, L. E., Lining, W., and Guannan, L. (2017) ‘China’s Energy System Transformation towards the 2 °C Goal: Implications of Different Effort-Sharing Principles’. *Energy Policy*

Yang, R. T. (2003) *Adsorbents : Fundamentals and Applications*. Wiley-Interscience

Yu, N., Wang, R. Z., Li, T. X., and Wang, L. W. (2017) *Progress in Sorption Thermal Energy Storage*. Springer International Publishing, 541–572. available from <http://link.springer.com/10.1007/978-3-319-26950-4_28> [16 March 2017]

Yu, N., Wang, R. Z., Lu, Z. S., and Wang, L. W. (2015) ‘Study on Consolidated Composite Sorbents Impregnated with LiCl for Thermal Energy Storage’. *International Journal of Heat and Mass Transfer* 84, 660–670

Yu, N., Wang, R. Z., Lu, Z. S., Wang, L. W., and Ishugah, T. F. (2014) ‘Evaluation of a Three-Phase Sorption Cycle for Thermal Energy Storage’. *Energy* 67, 468–478

Yu, N., Wang, R. Z. Z., and Wang, L. W. W. (2013) ‘Sorption Thermal Storage for Solar Energy’. *Progress in Energy and Combustion Science* [online] 39 (5), 489–514. available from <http://linkinghub.elsevier.com/retrieve/pii/S0360128513000270> [16 March 2017]

Zamengo, M., Ryu, J., and Kato, Y. (2013) ‘Magnesium Hydroxide e Expanded Graphite Composite Pellets for a Packed Bed Reactor Chemical Heat Pump’. *Applied Thermal Engineering* [online] 61, 853–858. available from <http://ac.els-cdn.com/S1359431113003165/1-s2.0-S1359431113003165-

main.pdf?_tid=80ce0ec2-4a1b-11e7-8f6c-00000aacb362&acdnat=1496686944_3934062ea49d9c87afcd94fe63b9c354> [5 June 2017]

Zeng, C., Liu, S., Yang, L., Han, X., Song, M., and Shukla, A. (2019) 'Investigation of a Three-Phase Thermochemical Reactor through an Experimentally Validated Numerical Modelling'. *Applied Thermal Engineering* 162

Zettl, B., Englmair, G., and Steinmaurer, G. (2014) 'Development of a Revolving Drum Reactor for Open-Sorption Heat Storage Processes'. *Applied Thermal Engineering* [online] 70 (1), 42–49. available from <http://linkinghub.elsevier.com/retrieve/pii/S1359431114003330> [19 June 2017]

Zhai, X. Q., Qu, M., Li, Y., and Wang, R. Z. (2011) 'A Review for Research and New Design Options of Solar Absorption Cooling Systems'. *Renewable and Sustainable Energy Reviews* [online] 15 (9), 4416–4423. available from <http://linkinghub.elsevier.com/retrieve/pii/S136403211100356X> [28 July 2017]

Zhang, Y. N., Wang, R. Z., Zhao, Y. J., Li, T. X., Riffat, S. B., and Wajid, N. M. (2016) 'Development and Thermochemical Characterisations of Vermiculite/SrBr2 Composite Sorbents for Low-Temperature Heat Storage'. *Energy* [online] 115, 120–128. available from <http://www.sciencedirect.com/science/article/pii/S036054421631221X> [6 December 2017]

Zhao, Y. J., Wang, R. Z., Zhang, Y. N., and Yu, N. (2016) 'Development of SrBr2 Composite Sorbents for a Sorption Thermal Energy Storage System to Store Low-Temperature Heat'. *Energy* 115, 129–139

Zondag, Herbert, van Essen, M., Bleijendaal, L., Cot, J., Schuitema, R., and van Helden, W. (2008) *Comparison of Reactor Concepts for Thermochemical Storage of Solar Heat*. in [online] held 2008 at Berlin. available from <ftp://130.112.2.101/pub/www/library/report/2009/m09007.pdf> [29 November 2017]

Zondag, H. a, van Essen, V. M., Bleijendaal, L. P. J., Kikkert, B. W. J., and Bakker, M. (2010) ‘Application of MgCl2·6H2O for Thermochemical Seasonal Solar Heat Storage’. in *5th IRES Conference* [online] held 2010 at Berlin,. Energy research Centre of the Netherlands, 22–24. available from <ftp://www.nrg-nl.com/pub/www/library/report/2010/m10086.pdf%5Cnfiles/316/Zondag et al2.pdf> [20 November 2017]

Zondag, H., Kikkert, B., Smeding, S., Boer, R. de, and Bakker, M. (2013) ‘Prototype Thermochemical Heat Storage with Open Reactor System’. *Applied Energy* [online] 109, 360–365. available from <http://linkinghub.elsevier.com/retrieve/pii/S0306261913001013> [16 March 2017]

Appendix A - Details of the facilities used in the experiment

Facilities	Details	Picture
Fan	Air volume: 2000 m^3/h Pressure: 2000 Pa Power: 15 kW	
Air to air heat exchanger	Size: 500(W) * 500(L) * 360(H) Plate distance: 5 mm	
Humidifier	Humidification capacity: 6 kg/h Power: 5 kW	
Air duct valves	400 mm*300 mm (2 valves) 500 mm*150 mm (4 valves)	
Water tank	Size: 500 mm * 500 mm * 900 mm Insulation: 50 mm glass wool	
Water pump	Head: 36 m Maximum flow rate: 10 L/min	

Water loop valves	Diameter at 22 mm	
Temperature sensor	Manufacture: Sailing Technology Accuracy: 3%	
Humidity sensor	Manufacture: E+E Accuracy: 3%	
Pressure sensor	Manufacture: Setra Accuracy: 1%	
Air velocity sensor	Manufacture: E+E Accuracy: 3%	
Water flow meter	Manufacture: Sailing Technology Accuracy: 3%	
Frequency inverter	ABB ACS510-01-03A3-4 Power: 1.1 kW	
Data logger	Brand: Kunlun Tianchen Accuracy: 0.05%	

Electric cabinet	Control the air duct valves, water pump and fan.	
Insulation material	50 mm glass wool	
Stainless steel plates	201 stainless steel Thickness: 1.2 mm	-

Appendix B – Publications

Journal Publications

1. X. Han, S. Liu, **C. Zeng**, L. Yang, A. Shukla, Y. Shen, Investigating the Performance Enhancement of Copper Strips on Trapezoidal Thermochemical Reactor, Renewable Energy, November 2019
2. **C. Zeng**, S. Liu, L. Yang, X. Han, M. Song, A. Shukla, Investigation of a Three-phase Thermochemical Reactor through an Experimentally Validated Numerical Modelling, Applied Thermal Engineering, Aug 2019
3. **C. Zeng**, S. Liu, A. Shukla, B. Yang, Identifying the occupant's satisfaction and awareness for the performance of Eco houses in the United Kingdom, Journal of Building Engineering, March 2018
4. **C. Zeng**, S. Liu, A. Shukla, Adaptability research on Phase Change Materials based technologies in China, Renewable & Sustainable Energy Reviews, June 2017
5. **C. Zeng**, S. Liu, A. Shukla, A review on the air-to-air heat and mass exchanger technologies for building, Renewable & Sustainable Energy Reviews, November 2016

Conference Proceedings

6. L. Yang, **C. Zeng**, X. Han, M. Song, Y. Shen, A. Shukla, S. Liu, Feasibility Study of Thermochemical Energy Storage Applied in China, The 17th International Conference on Sustainable Energy Technologies, June 2018, Wuhan, China
7. **C. Zeng**, Y. Liu, X. Han, M. Song, A. Shukla, S. Liu, An experimental investigation of a thermochemical reactor for solar heat storage in buildings, 16th UK Heat Transfer Conference, September 2019, University of Nottingham, UK
8. **C. Zeng**, S. Liu, A. Shukla, L. Yang, X. Han, Configuration effects on the thermochemical reactor through numerical modelling, International Conference on Applied Energy, August 2019, Västerås, Sweden

Under review papers

9. **C. Zeng**, S. Liu, A. Shukla, L. Yang, X. Han, Y. Shen, Operational parameters study of a thermochemical reactor for residential use through a validated numerical modelling (Submit to Energy and Buildings, June 2020)

Contents lists available at ScienceDirect

Renewable Energy

journal homepage: www.elsevier.com/locate/renene

Investigating the performance enhancement of copper fins on trapezoidal thermochemical reactor

Xiaojing Han [a], Shuli Liu [a, b, *], Cheng Zeng [b], Liu Yang [a], Ashish Shukla [b], Yongliang Shen [a]

[a] School of Mechanical Engineering, Beijing Institute of Technology, Beijing, 100081, China
[b] School of Energy, Construction and Environment, Coventry University, Coventry, CV1 2HF, United Kingdom

Applied Thermal Engineering 162 (2019) 114223

Contents lists available at ScienceDirect

Applied Thermal Engineering

journal homepage: www.elsevier.com/locate/apthermeng

Investigation of a three-phase thermochemical reactor through an experimentally validated numerical modelling

Cheng Zeng[a], Shuli Liu[a,*], Liu Yang[b], Xiaojing Han[b], Ming Song[b], Ashish Shukla[a]

[a] Centre for Research in the Built and Natural Environment, Coventry University, Coventry CV1 2FB, UK
[b] School of Mechanical Engineering, Beijing Institute of Technology, China

Journal of Building Engineering 18 (2018) 281–291

Contents lists available at ScienceDirect

Journal of Building Engineering

journal homepage: www.elsevier.com/locate/jobe

Identifying the occupant's satisfaction and awareness for the performance of Eco houses in the United Kingdom

Cheng Zeng[a], Shuli Liu[a,*], Ashish Shukla[a], Benqiang Yang[b,**]

[a] School of Energy, Construction and Environment, Coventry University, Coventry CV1 2FB UK
[b] The State Key Laboratory of Power Transmission Equipment & System Security and New Technology, Chongqing University, 400044, China

Renewable and Sustainable Energy Reviews 73 (2017) 145–158

Contents lists available at ScienceDirect

Renewable and Sustainable Energy Reviews

journal homepage: www.elsevier.com/locate/rser

Adaptability research on phase change materials based technologies in China

Cheng Zeng[a], Shuli Liu[b,a,*], Ashish Shukla[a]

[a] School of Energy, Construction and Environment, Coventry University, Coventry CV1 2FB, UK
[b] School of Mechanical Engineering, Beijing Institute of Technology, Beijing, China

Renewable and Sustainable Energy Reviews 75 (2017) 753–774

Contents lists available at ScienceDirect

Renewable and Sustainable Energy Reviews

journal homepage: www.elsevier.com/locate/rser

A review on the air-to-air heat and mass exchanger technologies for building applications

Cheng Zeng, Shuli Liu*, Ashish Shukla

School of Energy, Construction and Environment, Coventry University, Coventry CV1 2HF, United Kingdom